Sources and Processes of Per- and Polyfluoroalkyl Substances in Snow and Ice on Svalbard



William Hartz

St Edmund Hall

University of Oxford

Thesis submitted for the degree of

Doctor of Philosophy

Trinity 2022

Abstract

Per- and polyfluoroalkyl substances (PFAS) are a group of persistent organic contaminants. Some are toxic and bioaccumulative, and pose a hazard to human and environmental health. This thesis aims to further understand the sources and environmental processes of PFAS in the Arctic terrestrial cryosphere. This was achieved by analysing PFAS in an ice core (spanning 2006 – 2019) from the remote Lomonosovfonna ice cap and surface snow samples collected seasonally (January – August 2019) on Svalbard (Norwegian Arctic). These samples were used to assess the levels, sources, and the significance of photochemical processes in the atmospheric transformations of PFAS. In addition, the extent of PFAS contamination from local sources in the settlement of Longyearbyen, Svalbard, was investigated. PFAS contamination is widespread in the remote Arctic, since more than 26 compounds were detected, including C_2 – C_{11} perfluoroalkyl carboxylic acids (PFCAs), perfluorohexane sulfonic acid (PFHxS) and perfluorooctane sulfonic acid (PFOS). In the Lomonosovfonna ice core, PFCAs are thought to come from the atmospheric degradation of fluorotelomer alcohols (FTOHs) and chlorofluorocarbon (CFC) replacement products such as hydrofluorocarbons (HFCs). High levels of trifluoroacetic acid (TFA) contribute to 71% of C_2 – C_{11} PFCAs in the ice core. Neither the ice core nor surface snow indicate that marine aerosols are a source of PFAS deposition in the Arctic. Hexafluoropropylene oxide dimer acid (HFPO-DA or GenX) and trifluoromethane sulfonic acid (TFMS) are widespread in surface snow, but the source of TFMS is unknown. During 24-hour daylight, the deposition fluxes of C_2 – C_{11} PFCAs, PFHxS, PFOS and HFPO-DA (GenX) were 2 – 38 times higher in surface snow. Several PFCAs, PFOS and HFPO-DA are found to correlate with solar radiation which indicates that photochemical processes likely contribute to the atmospheric formation of these PFAS. Further investigation suggests that bromine radicals are a significant additional oxidant for the degradation of precursors (e.g. FTOHs, HFCs) in the atmosphere during Arctic Springtime.

Acknowledgements

I am very grateful to have been able to do my DPhil as part of the DTP for Environmental Research in the Department of Earth Sciences and as a guest PhD candidate at the University Centre in Svalbard, Norway. Together, these have been an amazing learning and working environment. Firstly, I would like the thank my supervisors Marc Macias-Fauria and Stuart Robinson as well as my external supervisors Andy Hodson and Roland Kallenborn, who have also been instrumental to the project. Thank you for your help and input at all stages, and for making yourself available for guidance whenever and endless inspiring discussions about all kinds of things. Thank you Marc and Stuart, for believing in the synthetic chemist who turned up in your office 5.5 years ago and for always encouraging my ambitions. Thank you Roland for introducing me to organic trace analysis and bringing your wealth of experience to the project. And thank you Andy for, in particular, your support with fieldwork and having me join your AG-325 team and the fun times on Drønbreen.

This project also wouldn't have been possible, if it hadn't been for my collaboration with Leo Yeung, Maria Björnsdotter, Ingrid Ericson Jogsten, and Anna Kärrman at Örebro University. Many thanks for teaching me so much about PFAS analysis and having me to visit in 2019. Thank you, Leo, for your advice when completing this thesis, and to Maria for your work on the PFAS analysis, and to everyone for our great collaboration. Without our work together, I would have never had the opportunity to target so many compounds including the ultrashort chain PFAAs.

In addition, this project wouldn't have been possible without the support of Liz Thomas, Jack Humby, and Shaun Miller at the British Antarctic Survey. Many thanks to Liz for having me to visit BAS several times and our interesting discussions about all things ice cores, and to Jack for our work with the ion chromatography.

Thank you also to Chris Day in Earth Sciences for our work together on the stable water isotope analysis – it was always a pleasure doing these measurements. Many thanks also to Mona Edwards and Jack Longman for teaching me ion chromatography and ICP-MS.

I would also like to thank several science and maths teachers at school who inspired me by their subjects to follow Chemistry to University.

To numerous colleagues and friends at UNIS, Earth Sciences, and the DTP – many thanks also. In particular, I would like to thank colleagues in the UNIS logistics department for assistance with fieldwork preparation and lab space. In addition, a special thanks to Eivind, Erik, Julien, Leo and Veerle, for their herculean efforts in the field and assistance in the (cold!) lab, and without whom I wouldn't have had the chance to work on such diverse snow samples and of course the Lomonosovfonna ice core. A special thanks also to James, Liam, Endre and Jamie who introduced me to Svalbard and inspired me to work further there. And of course, a shout out also to the Svalbard folks – you know who you are, plus the WBN committee.

Lastly, I would like to thank my family, for their endless patience and support. I will be forever grateful for their help with early morning trips to Terminal 2, all kinds of ice logistics, and helpful advice all along the way.

“Sit back and think about them good ol' days,
The way we were raised and our Svalbard ways,
And we drove scooters and hit the breen,
And when they came back broke we fixed 'em,
We never thought that summer would come,
Amongst the glaciers and the midnight sun,
Things are different out there, that’s right,
But we sure did it good on the WB night,
See, if you really wanna fly across the sea,
To get off the road with belt and two skis,
Jump on in and together with friends,
We'll ride out far from where the Adventdal ends”

Contents

Chapter 1: Introduction 1
1.1 POPs and the Environment 2
1.2 PFAS 3
1.2.1 PFAS Structure and the C–F Bond 3
1.2.2 PFAS History and Manufacture 7
1.2.3 Physiochemical properties of PFAS 10
1.2.4 PFAS and humans 11
1.3 PFAS in the Arctic 11
1.3.1 Evidence for marine transport to the Arctic. 11
1.3.2 Evidence for atmospheric transport to the Arctic 12
1.4 Svalbard 24
1.4.1 PFAS in Svalbard Biota 25
1.4.2 Setting and Climate 26
1.4.3 Local Sources of PFAS on Svalbard 28
1.4.4 Snow Science on Svalbard 30
1.5 Ice Cores 32
1.5.1 Ice cores as a deposition record of POPs 32
1.5.2 Svalbard Ice Cores 34
1.5.3 Lomonosovfonna 37
1.6 Aims and Objectives 39
1.7 References 41
Chapter 2: Per- and Polyfluoroalkyl Substances (PFAS): an Ice Core Perspective 49
2.1 Abstract 50
2.2 Introduction 51
2.3 Literature 51
2.4 Description of Ice Core Records 52
2.5 Discussion 53
2.5.1 PFAS detected and Levels 53
2.5.2 PFCA Even:Odd Molar Ratios and Precursor Sources 56
2.5.3 PFCA Source Distribution Profiles 58
2.5.4 Further discussion and limitations 62
2.6 Conclusion 63
2.7 References 65

Chapter 3: Materials and Methods 67

3.1 Abstract 68
3.2 Snow Sampling 69
3.2.1 Field Sampling and Sample Preparation 69
3.3 Ice Core Drilling and sample preparation 71
3.3.1 Ice core drilling 71
3.3.2 Ice core sampling preparation 72
3.4 Ice Core Dating & Ice Core Chemistry Analyses 74
3.5 PFAS analysis 75
3.5.1 Extraction and instrument analysis 75
3.5.2 Quality Assurance and Quality Control 76
3.6 Hybrid Single-Particle Lagrangian Integrated Trajectory Model Analysis (HYSPLIT) 76
3.7 References 78

Chapter 4: Levels and Distribution Profiles of Per- and Polyfluoroalkyl Substances (PFAS) in a High Arctic Svalbard Ice Core 79

4.1 Abstract 81
4.2 Introduction 82
4.3 Materials and Methods 85
4.3.1 Ice Core Drilling and Dating 85
4.3.2 Sample Preparation and PFAS Analysis 86
4.3.3 Ice Core Dating and Data Treatment 87
4.4 Results and Discussion 88
4.4.1 Fluxes and Concentrations of PFAS on Lomonosovfonna 88
4.4.2 Chemical Sources of PFCAs to Lomonosovfonna 91
4.4.3 Chemical Sources of PFSAs to Lomonosovfonna 96
4.4.4 Temporal Trends in PFAS Deposition 98
4.4.5 Marine environment as a source of PFAS 100
4.4.6 Air mass source regions 101
4.4.7 Redistribution of PFAS during melt 103
4.5 Conclusion 106
4.6 References 109
4.7 Supporting Information 113

Chapter 5: Levels and seasonal trends of $C_1 – C_4$ perfluoroalkyl acids and the discovery of trifluoromethane sulfonic acid in surface snow in the Arctic 141

5.1 Abstract 143
5.2 Introduction 144
5.3 Materials and Methods 147
5.3.1 Chemicals and Reagents 147
5.3.2 Sample Collection 147
5.3.3 Sample Preparation and Analysis 151
5.3.4 Statistical Analysis 153
5.3.5 Quality Assurance and Quality Control 153
5.3.6 Air Mass Trajectories and Solar Radiation 154
5.4 Results and Discussion 155
5.4.1 $C_1 – C_4$ PFAAs in Surface Snow 155
5.4.2 Seasonal Variation of TFA, PFPrA, and PFBA in Surface snow 157
5.4.3 Discovery of TFMS at Foxfonna Ice Cap 159
5.5 References 162
5.6 Supporting Information 165

Chapter 6: Levels and Seasonal Variations of Per- and Polyfluoroalkyl Substances (PFAS) in Surface Snow in the Arctic 173

6.1 Abstract 175
6.2 Introduction 176
6.3 Materials and Methods 179
6.3.1 Target Analysis 179
6.3.2 Sample Collection 179
6.3.3 Sample Extraction and PFAS analysis 182
6.3.4 Data Treatment 183
6.4 Results and Discussion 184
6.4.1 Concentrations and fluxes of PFAS in Surface Snow 184
6.4.2 Comparison of surface snow with the Lomonosovfonna 2019 ice core 187
6.4.3 Seasonal variations of PFAS in Surface Snow in Longyearbyen 191
6.4.4 Seasonal variations of PFAS in Surface Snow on Foxfonna 192
6.5 References 200
6.6 Supporting Information 202

Chapter 7: Arctic Springtime Atmospheric Degradation of Per- and Polyfluoroalkyl Substance (PFAS) Precursors driven by Bromine Radicals 225

7.1 Abstract 227
7.2 Introduction 228
7.3 Results and Discussion 231
7.3.1 Evidence for bromine radical driven degradation of precursors in Snow from Foxfonna 231
7.3.2 Evidence for bromine radical driven degradation in the 2019 Lomonosovfonna Ice Core 233
7.3.3 Environmental Implications 235
7.4 Materials and Methods 237
7.4.1 Target Analytes 237
7.4.2 Ice Core Drilling and Analysis 237
7.4.3 Surface Snow Sampling 238
7.4.4 Data Treatment 238
7.5 References 240
7.6 Supporting Information 244

Chapter 8: Discussion and Outlook 249

8.1 Discussion and Conclusion 250
8.2 Outlook 252
8.3 References 257

List of Abbreviations

ALC	Annual Layer Counting
AMDE	Atmospheric Mercury Depletion Event
CFC	Chlorofluorocarbon
ECF	Electrochemical Fluorination
GWP	Global Warming Potential
K_{OW}	n-Octanol-Water Partition Coefficient
LOD	Limit Of Detection
LOQ	Limit Of Quantification
m.a.s.l.	Metres Above Sea Level
MQL	Method Quantification Limit
NO_x	$NO + NO_2$
ODE	Ozone Depletion Event
pKa	Acid Dissociation Constant
POPs	Persistent Organic Pollutants
SI	Supporting Information
S_N2	Bimolecular Nucleophilic Substitution
SSML	Sea Surface Microlayer
UV	Ultraviolet
weq	Water Equivalent
Σ_xPFAS	Total Concentrations of x PFAS

All PFAS abbreviations can be found in Chapter 1, Tables 1 – 4

Chapter 1

Introduction

1.1 POPs and the Environment 2
1.2 PFAS 3
1.2.1 PFAS Structure and the C–F Bond 3
1.2.2 PFAS History and Manufacture 7
1.2.3 Physiochemical properties of PFAS 10
1.2.4 PFAS and humans 11
1.3 PFAS in the Arctic 11
1.3.1 Evidence for marine transport to the Arctic. 11
1.3.2 Evidence for atmospheric transport to the Arctic. 12
1.4 Svalbard 24
1.4.1 PFAS in Svalbard Biota 25
1.4.2 Setting and Climate 26
1.4.3 Local Sources of PFAS on Svalbard 28
1.4.4 Snow Science on Svalbard 30
1.5 Ice Cores 32
1.5.1 Ice cores as a deposition record of POPs 32
1.5.2 Svalbard Ice Cores 34
1.5.3 Lomonosovfonna 37
1.6 Aims and Objectives 39
1.7 References 41

1.1 POPs and the Environment

The environmental impact of persistent organic pollutants (POPs) was first brought to public attention in 1962 by Rachel Carson's book 'Silent Spring'.[1] This book detailed the environmental impacts of pesticides and ultimately contributed to the creation of the Environmental Protection Agency (EPA) and the ban on dichlorodiphenyltrichloroethane (DDT) in the United States.[2] 42 years later, twelve POPs were largely banned under the United Nations treaty, the Stockholm Convention, in 2004.[3] The initial twelve POPs, or the 'Dirty Dozen', included pesticides like DDT, but also industrial chemicals like polychlorinated biphenyls (PCBs) and other organic contaminants produced unintentionally (e.g. waste incineration).

However, the magnitude and diversity of global chemical manufacture means that a further 17 groups of POPs have been added to the Stockholm Convention since it entered into force.[3] Additional pollutants can be proposed for inclusion in the treaty, provided there is evidence, or potential, to show that they are persistent, bioaccumulative and toxic (PBT), as well as being able to undergo long-range transport in the environment (Stockholm Convention, Annex D). For example, (i) a persistent compound with a half-life greater than 2 months in water, (ii) a bioaccumulation factor greater than 5,000 in aquatic organisms (or $\log K_{OW} > 5$), (iii) with adverse human/environmental health effects, (iv) that is able to undergo long-range atmospheric transport (for example, it has an atmosphere lifetime greater than 3 days), would be suitable for proposal for inclusion in the treaty.

Three such compounds that have been successfully added to the treaty include perfluorooctanesulfonic acid (PFOS, in 2009), perfluorooctanoic acid (PFOA, in 2018) and perfluorohexanesulfonic acid (PFHxS, on 6th June 2022).[3] The motivating factors for their addition in the Treaty included: (i) high stability and environmental persistence, (ii) significant

bioaccumulating properties, (iii) carcinogenic properties and other adverse health effects such as thyroid disease, and (iv) evidence for their presence in air, water, sediment, and biota in the remote Arctic environment. These three POPs are part of a broader family of their own called Per- and Polyfluoroalkyl Substances (PFAS). In recent years, they have also been referred to as 'Forever Chemicals'[4] and have been brought to broader public attention in the film 'Dark Waters' featuring Mark Ruffalo.[5] The presence of these 'Forever Chemicals' in the Arctic, raises the question of how these contaminants have become widespread in the Arctic environment. This thesis aims to understand the sources and processes that transport PFAS to the Arctic, using snow and ice core records.

1.2 PFAS

1.2.1 PFAS Structure and the C–F Bond

In 2018, the United Nations Environment Program published a list of over 4,700 PFAS.[6] This is considerably more than PCBs (209 compounds) or DDT (2 compounds). In 2021, the definition of PFAS was broadened to encompass any fluorinated substance with at least one fully fluorinated methyl or methylene group (i.e. $-CF_3$ or $-CF_2-$).[7] This broad definition now encompasses many compounds. As of August 2021, the US EPA toxicity database now lists 10,776 different PFAS.[8] Whilst a large focus of research has been on perfluoroalkyl acids (PFAAs), such as perfluoroalkyl carboxylic acids (PFCAs) and perfluoroalkyl sulfonic acids (PFSAs),[9] PFAS are a diverse group of chemicals. Typically, they consist of a per- or polyfluorinated organofluorine chain with a head group of varying chemical functionality. A non-exhaustive list of PFAS is shown, alongside abbreviations, and chemical structures in Tables 1 – 4. In the following chapters, these PFAS are often referred to by their abbreviations. These tables also include examples of four fluoropolymers;

PTFE (Teflon), FEP, PFA and ETFE, (which together with other tetrafluoroethylene copolymers made up 70 – 75% of global consumption of fluoropolymers in 2015).[10]

Table 1. CFC replacement products referred to in this thesis

Abbreviation	Name	Generic Formula Example	Example
HFCs	Hydrofluorocarbons	$C_nF_{2n+1}(CHF)_xCH_yF_z$ $C_nF_{2n+1}(CHF)_x(CF_2)_yF$ (x = 0 – 2, y = 0 – 3, z = 0 – 3)	HFC-134a (CF_3CH_2F)
HCFCs	Hydrochlorofluorocarbons	$C_nF_{2n+1}CHFCl$ $C_nF_{2n+1}CH_xCl_y$ (x = 1 – 2, y = 1 – 2)	HCFC-123 (CF_3CCl_2H)
HFEs	Hydrofluoroethers	$C_nF_{2n+1}O(CH_2)_xH$ (x = 1 – 2)	HFE-236ea2 ($CF_3CFHOCF_2H$)
HFOs	Hydrofluoroolefins	$C_nF_{2n+1}CF=CH_xF_y$ (x = 0 – 2, y = 0 – 2)	HFO-1234yf ($CF_3CF=CH_2$)

Table 2. Neutral PFAS compounds referred to in this thesis

Abbreviation	Name	Structure
-	**Perfluorosulfonamides**	
FBSA	Perfluorobutane Sulfonamide	$CF_3(CF_2)_3SO_2NH_2$
FHxSA	Perfluorohexane Sulfonamide	$CF_3(CF_2)_5SO_2NH_2$
FOSA	Perfluorooctane Sulfonamide	$CF_3(CF_2)_7SO_2NH_2$
FASAs	N-alkyl perfluoroalkane sulfonamide	
MeFBSA	N-Methyl Perfluorobutane Sulfonamide	$CF_3(CF_2)_3SO_2NH_2$
MeFHxSA	N-Methyl Perfluorohexane Sulfonamide	$CF_3(CF_2)_5SO_2NH_2$
MeFOSA	N-Methyl Perfluorooctane Sulfonamide	$CF_3(CF_2)_7SO_2NH_2$
EtFOSA	N-Ethyl Perfluorooctane Sulfonamide	$CF_3(CF_2)_7SO_2NH_2$
FOSEs	**N-alkyl perfluoroalkane sulfonamido ethanols**	
MeFBSE	N-Methyl Perfluorobutane Sulfonamidoethanol	$CF_3(CF_2)_3SO_2N(CH_3)(CH_2CH_2OH)$
MeFOSE	N-Methyl Perfluorooctane Sulfonamidoethanol	$CF_3(CF_2)_7SO_2N(CH_3)(CH_2CH_2OH)$
EtFOSE	N-Ethyl Perfluorooctane Sulfonamidoethanol	$CF_3(CF_2)_7SO_2N(CH_3)(CH_2CH_2OH)$
FTOHs	**Fluorotelomer alcohols**	
4:2 FTOH	4:2 Fluorotelomer Alcohol	$CF_3(CF_2)_3(CH_2)_2OH$
6:2 FTOH	6:2 Fluorotelomer Alcohol	$CF_3(CF_2)_5(CH_2)_2OH$
8:2 FTOH	8:2 Fluorotelomer Alcohol	$CF_3(CF_2)_7(CH_2)_2OH$
10:2 FTOH	10:2 Fluorotelomer Alcohol	$CF_3(CF_2)_9(CH_2)_2OH$
12:2 FTOH	12:2 Fluorotelomer Alcohol	$CF_3(CF_2)_{11}(CH_2)_2OH$
FTAs	**Fluorotelomer acrylate**	
6:2 FTA	6:2 Fluorotelomer Acrylate	$CF_3(CF_2)_5(CH_2)_2OC(O)CHCH_2$
8:2 FTA	8:2 Fluorotelomer Acrylate	$CF_3(CF_2)_7(CH_2)_2OC(O)CHCH_2$
Other		
POSF	Perfluorooctane Sulfonyl Fluoride	$CF_3(CF_2)_7SO_2F$

Table 3. Per- and polyfluoroalkyl acids referred to in this thesis

Abbreviation	Name	Structure
PFCAs	**Perfluoroalkyl carboxylic acids**	
TFA	Trifluoroacetic Acid	CF_3CO_2H
PFPrA	Perfluoropropanoic Acid	$CF_3CF_2CO_2H$
PFBA	Perfluorobutanoic Acid	$CF_3(CF_2)_2CO_2H$
PFPeA	Perfluoropentanoic Acid	$CF_3(CF_2)_3CO_2H$
PFHxA	Perfluorohexanoic Acid	$CF_3(CF_2)_4CO_2H$
PFHpA	Perfluoroheptanoic Acid	$CF_3(CF_2)_5CO_2H$
PFOA	Perfluorooctanoic Acid	$CF_3(CF_2)_6CO_2H$
PFNA	Perfluorononanoic Acid	$CF_3(CF_2)_7CO_2H$
PFDA	Perfluorodecanoic Acid	$CF_3(CF_2)_8CO_2H$
PFUnDA	Perfluoroundecanoic Acid	$CF_3(CF_2)_9CO_2H$
PFDoDA	Perfluorododecanoic Acid	$CF_3(CF_2)_{10}CO_2H$
PFTrDA	Perfluorotridecanoic Acid	$CF_3(CF_2)_{11}CO_2H$
PFTeDA	Perfluorotetradecanoic Acid	$CF_3(CF_2)_{12}CO_2H$
PFHxDA	Perfluorohexadecanoic Acid	$CF_3(CF_2)_{14}CO_2H$
PFOcDA	Perfluorooctadecanoic Acid	$CF_3(CF_2)_{18}CO_2H$
PFSAs	**Perfluoroalkyl sulfonic acids**	
TFMS	Trifluoromethane Sulfonic Acid	CF_3SO_3H
PFEtS	Perfluoroethane Sulfonic Acid	$CF_3CF_2SO_3H$
PFPrS	Perfluoropropane Sulfonic Acid	$CF_3(CF_2)_2SO_3H$
PFBS	Perfluorobutane Sulfonic Acid	$CF_3(CF_2)_3SO_3H$
PFPeS	Perfluoropentane Sulfonic Acid	$CF_3(CF_2)_4SO_3H$
PFHxS	Perfluorohexane Sulfonic Acid	$CF_3(CF_2)_5SO_3H$
PFHpS	Perfluoroheptane Sulfonic Acid	$CF_3(CF_2)_6SO_3H$
PFOS	Perfluorooctane Sulfonic Acid	$CF_3(CF_2)_7SO_3H$
PFNS	Perfluorononane Sulfonic Acid	$CF_3(CF_2)_8SO_3H$
PFDS	Perfluorodecane Sulfonic Acid	$CF_3(CF_2)_9SO_3H$
PFDoDS	Perfluorododecane Sulfonic Acid	$CF_3(CF_2)_{12}SO_3H$
PFECHS	Perfluoroethylcyclohexane Sulfonic Acid	$(CF_3CF_2)C_6F_{10}SO_3H$
PFECAs	**Perfluoroalkyl ether carboxylic acids**	
HFPO-DA (GenX)	Hexafluoropropylene Oxide Dimer Acid	$CF_3(CF_2)_2OCH(CF_3)CO_2H$
ADONA	3H-Perfluoro-3-[(3-Methoxy-Propoxy)Propanoic Acid]	$CF_3O(CF_2)_3OCHFCF_2CO_2H$
PFESAs	**Perfluoroalkyl ether sulfonic acids**	
6:2 Cl-PFESA	6:2 Chlorinated Polyfluorinated Ether Sulfonic Acid	$ClCF_2(CF_2)_5O(CF_2)_2SO_3H$
8:2 Cl-PFESA	8:2 Chlorinated Polyfluorinated Ether Sulfonic Acid	$ClCF_2(CF_2)_7O(CF_2)_2SO_3H$
FTSAs	**Fluorotelomer sulfonic acids**	
4:2 FTSA	4:2 Fluorotelomer Sulfonic Acid	$CF_3(CF_2)_3(CH_2)_2SO_3H$
6:2 FTSA	6:2 Fluorotelomer Sulfonic Acid	$CF_3(CF_2)_5(CH_2)_2SO_3H$
8:2 FTSA	8:2 Fluorotelomer Sulfonic Acid	$CF_3(CF_2)_7(CH_2)_2SO_3H$
FTUCAs	**Fluorotelomer Unsaturated Carboxylic Acid**	
6:2 FTUCA	6:2 Fluorotelomer Unsaturated Carboxylic Acid	$CF_3(CF_2)_4CFCHCO_2H$
8:2 FTUCA	8:2 Fluorotelomer Unsaturated Carboxylic Acid	$CF_3(CF_2)_6CFCHCO_2H$
FTCAs	**Fluorotelomer Carboxylic Acid**	
6:2 FTCA	6:2 Fluorotelomer Carboxylic Acid	$CF_3(CF_2)_5CH_2CO_2H$
8:2 FTCA	8:2 Fluorotelomer Carboxylic Acid	$CF_3(CF_2)_7CH_2CO_2H$

Table 4. Examples of fluoropolymers

Abbreviation	**Name**	**Structure**
PTFE (Teflon)	Polytetrafluoroethylene	$(CF_2CF_2)_n$
FEP	Fluorinated ethylene propylene	$(CF_2CF_2)_n(CF_2CFCF_3)_m$
PFA	Perfluoroalkoxy alkanes	$(CF_2CF_2)_n(CF_2CFOCF_3)_m$
ETFE	Ethylene tetrafluoroethylene	$(CH_2CH_2CF_2CF_2)_n$

Part of the industrial success of PFAS can be attributed to the unique and industrially desirable chemistry of the C–F bond. This has made organofluorine chemistry a success in several industries such as materials, pharmaceuticals and agrochemicals.[11] Fluorine is the most electronegative element on the periodic table ($\chi = 4$). As a result, its bonding with carbon has a larger electrostatic than covalent component ($C^{\delta+}$–$F^{\delta-}$) and fluorine's three lone pairs of electrons are closely held (unlike, for example, oxygen).[12] Hence, the C–F bond has limited electron sharing, but a large electrostatic attraction between carbon and fluorine, and this results in the strongest single bond in organic chemistry (441.0 KJ/mol).[12] Fluorine is often substituted for hydrogen in C–H bonds for industrial and pharmaceutical purposes, owing to similar bond lengths and carbon hybridisation/geometric preferences. However, this can have significant changes in a molecule's properties (e.g. pK_a's). Fluoride, from the C–F bond, does not produce a good leaving group during chemical reactions (e.g. S_N2).[13] Despite the significant partial positive charge on the carbon ($C^{\delta+}$), the strength of C–F bonds makes such reactions undesirable and hence resistant to direct attack from nucleophiles. As a result, compounds based on aliphatic organofluorine chemistry (i.e., the vast majority of PFAS) are resistant to a variety of chemical conditions and moreover natural processes in the biotic and abiotic environment do not readily degrade them. Indeed, the rebranding of PFAS as 'Forever Chemicals' reflects the 'F–C' (*forever-chemical*) bond on which they are built.[14] Very few natural compounds with C–F bonds are known to exist (e.g. CFH_2CO_2H), and

molecules with -CF_3 or -CF_2- groups are not known in nature.[11]

The success of PFAS in industrial applications has relied on the chemically resistant perfluorinated aliphatic chain. A perfluorinated chain is equivalent to a hydrocarbon chain, however all C–H bonds have been substituted by C–F bonds to create -CF_3 and/or -CF_2- groups. Compounds with perfluorinated chains are almost chemically inert, non-wetting, and have very high-temperature ratings.[15] This has made PFAS useful in numerous applications including firefighting foams, food handling equipment (e.g. teflon), medical equipment, oil additives as well as fire retardant, and water and stain resistant textiles (e.g. clothing and furnishings).

1.2.2 PFAS History and Manufacture

In 1928, CCl_2F_2 was synthesised by General Motors Corporation chemists McNary, Midgley and Henne.[16] The refrigerant was reported in 1930 at a meeting of the American Chemical Society, by Midgley breathing in CCl_2F_2 and then exhaling it to put out a candle.[17] Later in the 1930s it was commercialised as Freon-12, alongside several other Freons. This included Freon-22 ($CHClF_2$), which was used in the synthesis of tetrafluoroethylene (C_2F_4). In 1938, DuPont chemist Roy Plunkett discovered that an old cylinder of C_2F_4 had polymerised as a result of high pressures and cold temperatures.[18] He found the resulting substance to be chemically inert and resistant to high temperatures. He had discovered PTFE (later commercialised as 'Teflon' in 1948),[19] one of the first PFAS. However, it wasn't until the Manhattan project during World War II,[20] that organofluorine chemistry was scaled up to synthesise coolants, lubricants, and fluoropolymers to assist in the production of two atomic bombs. This was required to handle the highly reactive UF_6. Indeed, one of the major manufacturing techniques for PFAS was invented during this project – electrochemical fluorination (ECF). However, this technique was not declassified until 1949 when it was commercialised by Minnesota Mining and Manufacturing Company (3M).[21]

From 1949 – 2002, 3M used ECF to produce perfluorooctane sulfonyl fluoride (POSF, $CF_3(CF_2)_7SO_2F$) as a starting material for other PFAS. This was done by applying a voltage across a solution of $CH_3(CH_2)_7SO_2F$ dissolved in hydrogen fluoride. In this reaction, all C–H bonds are substituted for C–F bonds to produce POSF. POSF can then be used as a starting material to produce, for example: (i) PFOS, by hydrolysis of POSF, (ii) MeFOSA and EtFOSA, by reaction of POSF with methyl/ethyl amine and then (iii) MeFOSE and EtFOSE by further reaction with ethylene glycol carbonate. PFOA can also be produced by ECF of $CH_3(CH_2)_7C(O)F$, followed by hydrolysis. ECF production of POSF has a low yield (34 – 40%). Final products of 3M ECF PFOS contained PFSA impurities of chain lengths C_4 – C_{12} including both linear and branched isomers.[22] 3M ECF PFOS contained 70% linear-PFOS. Similarly, 3M ECF PFOA contained impurities of chain lengths C_6 – C_{12} with both linear and branched isomers. 3M ECF PFOA contained 78% linear-PFOA.

An alternative synthesis for PFAS by telomerization was first reported in 1949 by Haszeldine, but was not commercialised until 1975.[23] Telomerisation involves the production of PFAS in C_2 units. C_2F_4 is reacted with IF_5 to produce CF_3CF_2I. Perfluoroalkyl radicals ($CF_3CF_2^{\bullet}$) are then photochemically produced, reacted with C_2F_4 via telomerisation, and terminated with I_2 to produce perfluoroalkyl iodides (PFAIs, $CF_3CF_2(CF_2CF_2)_xI$). These are then reacted with C_2H_4 to produce n:2 fluorotelomer iodides (n:2 FTIs, $CF_3CF_2(CF_2CF_2)_xCH_2CH_2I$), which like POSF, are the starting material for further PFAS production (e.g. FTOHs, via hydrolysis). Due to the nature of the telomerisation process, a variety of linear isomers with even chain lengths are produced. POSF production continues in Europe and Asia (albeit regulated by the Stockholm Convention).[24] Production of fluorotelomer-based PFAS via telomerisation also continues.

Chlorofluorocarbon (CFCs) replacement products came into use in the 1990s as a result of

the Montreal Protocol in 1989.[25] CFCs have been used in various domestic and industrial uses such as refrigerants since the 1930s. However, in 1974 it was discovered that the breakdown of CFCs in the stratosphere produced Cl radicals which damaged the ozone layer causing higher harmful UV radiation at the earth's surface. Indeed, in 1995, Frank Sherwood Rowland, Mario Molina and Paul Crutzen were awarded the Nobel Prize in Chemistry for this discovery.[26] CFC replacement products included numerous hydrofluorocarbons (HFCs), hydrochlorofluorocarbons (HCFCs), hydrofluoroethers (HFEs), and hydrofluoroolefins (HFOs). Whilst few CFCs themselves were defined as PFAS, many of their aforementioned replacement products are.

Like CFCs, HCFCs are similar to CFCs but contain C–H bonds which make HCFC vulnerable to degradation. This reduces their atmospheric lifetimes compared to CFCs, which limits their transport to the stratosphere.[27] One such HCFC is HCFC-123 (CF_3CCl_2H) which replaced CFC-11 and since 1989 has been used a refrigerant. HFCs are similar to HCFCs, but without C–Cl bonds. HFC-134a (CF_3CH_2F) is one of the most significant CFC replacement products (of CFC-12) and has been used in, for example, air conditioning units.[28] HFEs are similar to HFCs but contain ether linkages. For example, HFE-236ea2, also known as desflurane ($CF_3CFHOCF_2H$), is used as a general anaesthetic.[29] However, HFCs, HCFCs and HFEs have been found to have high global warming potentials (GWP).[29,30] To this address, HFOs are being increasingly used as a result of the 2019 Kigali amendment to the Montreal Protocol to phase out the use of HFCs.[31] HFOs are similar to HFCs but contain double bonds. For example, HFO-1234yf ($CF_3CF=CH_2$) is being used as a propellant and is planned to replace HFC-134a in air conditioning units. Whilst the examples given here of HFCs, HCFC, HFEs and HFOs are two or three carbon species, these CFC replacement products are known to have been manufactured in a diversity of different compounds of chain lengths as high as 6 carbons.[32]

1.2.3 Physiochemical properties of PFAS

Table 5. Physicochemical properties of several PFAS[33–36]

PFAS	pK_a	Vapour Pressure	Solubility in water
TFA (acid)	0.23	10,570 Pa	miscible
TFA (salt)	-	-	625,000
PFOA (acid)	-0.16 – 3.8	5 Pa	3400
PFOS (acid)	-6.0 – -2.6	15 Pa	67
PFOS (salt)	-	3.3×10^{-4} Pa	680
8:2 FTOH	-	22.7 Pa	3.00
MeFOSA	-	10.4 Pa	0.000092
MeFOSE	-	0.015 Pa	0.000067

The perfluoroalkyl chain can inductively stabilise the negative charge of the conjugate bases of PFCAs and PFSAs. PFOS has a $pK_a < -2.6$ and PFOA < 3.8 (Table 5). This promotes high water solubility and low vapour pressures and as a result, they exist as their conjugates bases in water (i.e. anionic form). In their protonated form, they have low water solubility and high vapour pressures. However, PFCAs and PFSAs exist as the carboxylate and sulfonate, respectively, since the conditions for them to exist in the protonated form are not common in the environment.[33] However, neutral PFAS such as FTOHs and FOSEs have high vapour pressures and are volatile.[35] Likewise, HFCs have even higher vapour pressures and exist as gases.[37] As a result, direct emissions of PFCAs and PFSAs tend to be released in runoff into the ocean/rivers (i.e. dissolved in the aqueous phase) whereas direct emissions of neutral PFAS, and HFCs and related compounds, tend to be gas phase emissions into the atmosphere. These physical and chemical properties have enabled PFAS to become widespread through oceanic and atmospheric processes, including to the Arctic. Nonetheless, the mechanisms for these processes are still not well understood.

1.2.4 PFAS and humans

Some of the most significant research into the human health effects from PFAS exposure, particularly PFOA, come from communities living in the Ohio River Valley in the United States. It was in this area that DuPont's Washington Works Chemical Plant contaminated the local environment leading to elevated levels of PFOA local residents. This story has been popularised in the 2019 film 'Dark Waters'.[5] Local residents with elevated PFOA levels were found to have higher instances of testicular and kidney cancer.[38] Further epidemiological studies have also linked exposure to some PFAS with reduced responses to vaccines, lower birth weights, thyroid disease, increased cholesterol levels and liver damage.[39]

1.3 PFAS in the Arctic

PFAS can be released into the environment during manufacture, for example by ECF and telomerisation. Alternatively, PFAS can be released during use and disposal, for example, firefighting forms and landfill leachate. At this point, PFAS can undergo processes which enable its long-range transport (over 1000 kms). As a result of this, PFAS has been detected ubiquitously in the environment, including in the Arctic.[40] For PFAS, three main mechanisms have been found to exist for their transport to the Arctic. These include (i) long-range transport through ocean currents, (ii) marine aerosols, and (iii) the long-range transport of volatile neutral PFAS (so called precursors) followed by their atmospheric degradation and subsequent deposition. Local sources of PFAS in the Arctic can also be significant.

1.3.1 Evidence for marine transport to the Arctic.

Several studies have identified long-range oceanic transport of PFAS to the Arctic Ocean.[41–44] Discharge from terrestrial sources can be transported in rivers and runoff to coastal waters.[45] PFAS

can then enter global ocean currents and become ubiquitous in both surface waters and within the water column down to several hundred metres. These processes typically take decades to occur and have contributed to the detection of PFAS in the Arctic Ocean.[41,43]

Once in surface waters, PFAS can become redistributed to the terrestrial environment far from their primary source via marine aerosols. Since PFAAs are highly surface-active compounds, it can be that they readily form part of the sea surface micro layer (SSML). Bubble bursting from wave action at the sea surface enables organic compounds and marine salts to be transported into the atmosphere in marine aerosols.[46] These aerosols can then be deposited in the terrestrial environment by wet and dry deposition. McMurdo et al. found in a laboratory-based experiment that PFOA would be enriched in aerosols significantly relative to a parent water body.[47] A recent study by Sha et al. found that several PFAS correlated with Na^+, a marine aerosol tracer, in atmospheric samples collected on quartz fibre filters from Andøya in the mainland Norwegian Arctic.[48] Further laboratory experiments and modelling by Johansson et al. found that the Arctic Ocean would not be a source of PFOA enriched aerosols.[49] Instead, they found that the northern Pacific and Atlantic Oceans would be possible sources to coastal areas of Europe and parts of North America, but less so the Arctic. Snowpits and ice cores investigating several years of PFAS accumulation on the Devon Ice Cap in Arctic Canada found that marine aerosols were not a significant source of PFAS deposition, since no correlations were found between PFAS and Na^+ ions.[50–52] Field evidence for PFAS atmospheric transport in marine aerosols to and within the Arctic is limited.

1.3.2 Evidence for atmospheric transport to the Arctic.

The high solubility and low volatility of PFCAs and PFSAs in the environment means that they are unable to undergo direct long-range atmospheric transport to the Arctic, as was found to be the

case for PCBs. However, other PFAS, which are sufficiently volatile, can undergo long-range atmospheric transport to the Arctic atmosphere. This includes neutral PFAS such as FTOHs, FOSEs and FASAs as well as CFC replacement products such as HFCs, HCFCs, HFEs and HFOs.

Table 6. Five studies reporting the atmospheric concentrations of neutral PFAS in the Arctic (pg/m3)

Location	**North American Arctic (>60°N)**	**European Arctic (>60°N)**	**Canadian Arctic**	**Canadian Arctic**	**Svalbard**
Time	July – August 2010	August 2007	July 2005	July - August 2004	September 2011 - September 2012
Site	Ocean	Ocean	Ocean	Terrestrial	Terrestrial
n	8	8	20	10	45
4:2 FTOH	n.a.	<LOD	n.a.	n.a.	n.a.
6:2 FTOH	3	22	2.6	1.97	5.1
8:2 FTOH	120	15	11	7.96	10
10:2 FTOH	17	3.6	6.3	0.35	2
12:2 FTOH	7.7	1.4	n.a.	n.a.	0.8
MeFBSA	0.54	2.5	n.a.	n.a.	0.6
MeFOSA	0.1	2.7	n.a.	n.a.	0.3
EtFOSA	0.57	0.88	n.a.	5.54	0.2
MeFBSE	1.7	1.7	n.a.	3.7	0.6
MeFOSE	0.13	0.97	8.3	7.35	0.2
EtFOSE	0.1	1.4	1.9	<LOD	0.1
6:2 FTA	0.14	2.6	n.a.	n.a.	0.1
8:2 FTA	8.6	1.8	n.a.	n.a.	0.1
10:2 FTA	4.3	0.1	n.a.	n.a.	n.a.
Reference	Cai et al.[53]	Dreyer et al.[54]	Shoeib et al.[55]	Stock et al.[56]	Xie et al.[57]

Table 6 summarises the results of five studies that have investigated the levels of FTOHs, FASAs, FOSEs and FTAs in the atmosphere over both ocean and land. Consistently at both European and North American Arctic sites, FTOHs dominated the neutral PFAS detected and 8:2 FTOH was often the most abundant neutral PFAS. This also indicates that FTOHs, FASAs, FOSEs and FTAs are all capable of long-range atmospheric transport to the Arctic atmosphere.

Furthermore, for those studies measuring both particle-bound and gas phase neutral PFAS, they found that the gas phase was most prominent, particularly for FTOHs.[55]

HFCs, HCFC, HFEs and HFOs also contribute a source of neutral PFAS to the Arctic atmosphere. However, only HFCs and HCFCs are currently part of routine monitoring and the only site doing so in the Arctic is the Zeppelin Observatory, Ny-Ålesund, Svalbard (Norwegian Arctic).[58] Regardless, like HFCs and HCFCs, the atmospheric lifetimes of HFEs and HFOs are sufficient for long-range atmospheric transport to the Arctic (Table 8). The limiting factor for their atmospheric lifetimes is photochemical degradation by hydroxyl (OH) radicals. Indeed, this provides an oxidation pathway for neutral PFAS (FTOHs, HFCs, etc) to form PFCAs and PFSAs. Since PFCAs and PFSAs will be readily removed from the atmosphere by wet and dry deposition, this degradation process is able to deliver PFCAs and PFSAs to the remote Arctic. Herein, this mechanism is discussed.

HFCs,[59] HCFCs,[60] HFEs,[61] HFOs,[62] FTOHs,[63–66] FASAs,[67] FOSEs,[68] and FTAs[69] (so called precursors) have all been identified to degrade to PFCAs, initiated by OH radicals. Many of these degradations were found to be purely gas phase processes. Since FTOHs have the highest atmospheric concentrations of the longer chain precursors, the degradation of FTOHs are herein discussed further. The removal of FTOHs from the atmosphere by photolysis is insignificant since alcohols do not absorb the UV wavelengths present in sunlight,[70] and fluorination is expected to only decrease the wavelengths that fluorinated alcohol absorbs at.[71] Ellis et al. calculated the removal of 8:2 FTOH by wet deposition and dry deposition had atmospheric lifetimes of 2.5×10^6 years and 8.4 years, respectively.[72] Hence, the reaction of FTOHs with OH radicals (to form PFCAs) is expected to be the major pathway for the removal of FTOHs from the atmosphere. Ellis et al. conducted a study investigating the degradation products of 4:2 FTOH, 6:2 FTOH and 8:2

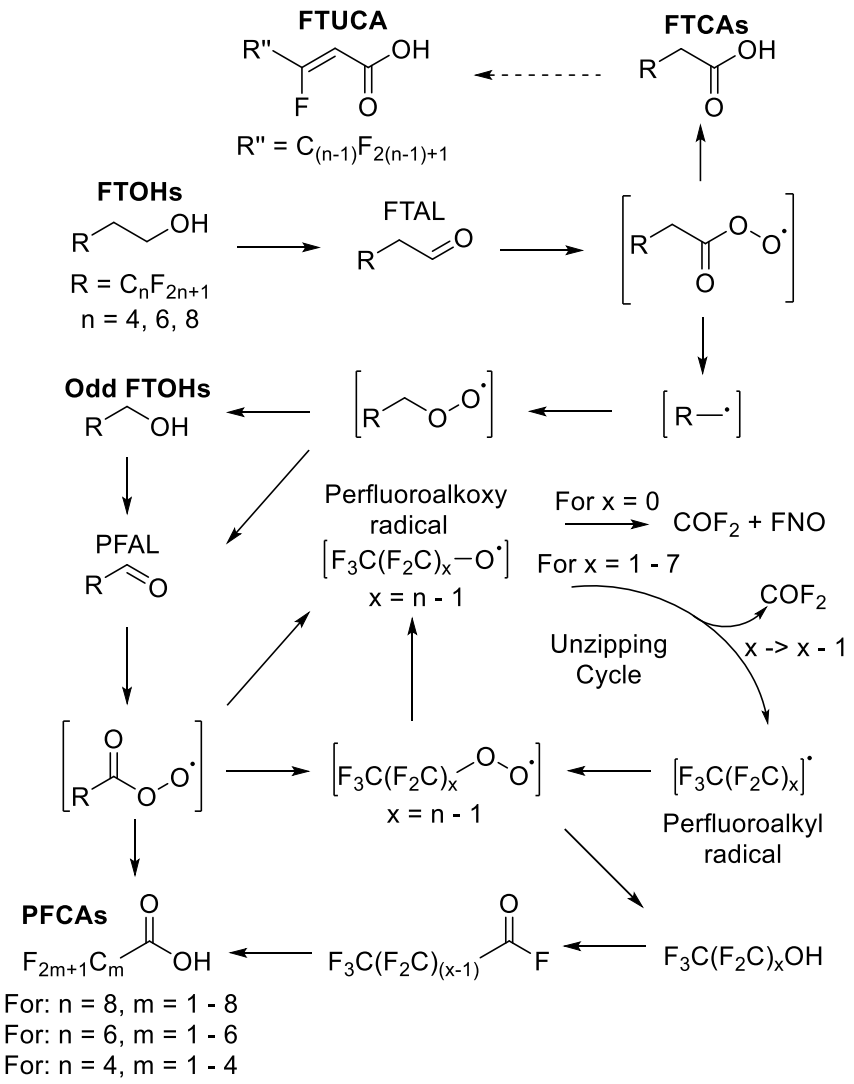
FTOH individually in a smog chamber with chlorine radicals.[64] Chlorine radicals were chosen as they were easier to generate and react with FTOHs in the same manner as OH radicals. Each FTOH degraded to produce a PFCA with an intact perfluorinated chain (i.e. 8:2 FTOH yielded PFNA). Further analysis (by LC/MS-MS) found each FTOH produced a homologous series of PFCAs of shorter chain lengths than the chosen FTOH reagent. For example, the reaction of 8:2 FTOH produced a homologous series of PFCAs from TFA to PFNA (i.e. C_2 – C_9 PFCAs), with the majority of PFCAs being PFOA and PFNA (Table 7).

As can be seen in Table 7, 8:2 FTOH reacted to produce a homologous series of PFCAs of equal or shorter perfluorinated chain length than itself. Moreover, PFNA and PFOA were the dominant PFCAs and were produced in broadly equal quantities (0.95:1 molar ratio for PFOA:PFNA). Hence, it can be hypothesised that if PFNA and PFOA occur in equal quantities in environmental matrices fed solely by atmospheric sources, then this would support the argument that OH radical mediated atmospheric degradation of 8:2 FTOH is occurring. It would also be expected that a similar observation would exist for 6:2 FTOH and 10:2 FTOH (for PFHxA:PFHpA and PFDA:PFUnDA ratios, respectively). In contrast, for Eurasian emissions the PFOA:PFNA ratios will be higher (7 – 15:1), than the broadly equal quantities of PFOA and PFNA observed in the degradation of 8:2 FTOH.[73] Furthermore, it was found during the degradation of FTOHs that a large proportion of the degradation products would be FTCAs, and that only the n:2 FTOH could yield the corresponding n:2 FTCA. Hence, detection of an n:2 FTCA in the environment could indicate atmospheric oxidation of the terminal alcohol of the respective n:2 FTOH. This laboratory degradation study was conducted in the absence of NO_x species (NO_x = NO + NO_2). It was concluded that increased NO_x concentrations would decrease the yield of PFCAs, such as in urban air, which is typically polluted with NO_x. However, in the Arctic atmosphere and over oceans,

NO_x levels will be lower, and FTOH degradation will not be suppressed.[74] The homologous series of C_2 – C_{n+1} PFCAs observed for the degradation of an n:2 FTOH was explained by an 'unzipping'[75] cycle whereby perfluoroalkoxy radicals are able to shorten their chain lengths through loss of COF_2 (Scheme 1). The formation of PFCAs via an unzipping cycle is also known to occur for FASAs[67] and FOSEs[68] via formation of a perfluoroalkyl radical (Scheme 1). FTOH degradation is thought to happen on the time scale of weeks to months depending on season, latitude, and NO_x abundance.[74] Modelling by Wallington et al. found that PFOA atmospheric concentrations over the Arctic Ocean would be approximately 15 – 20 times higher during July compared to January in the Arctic.[76]

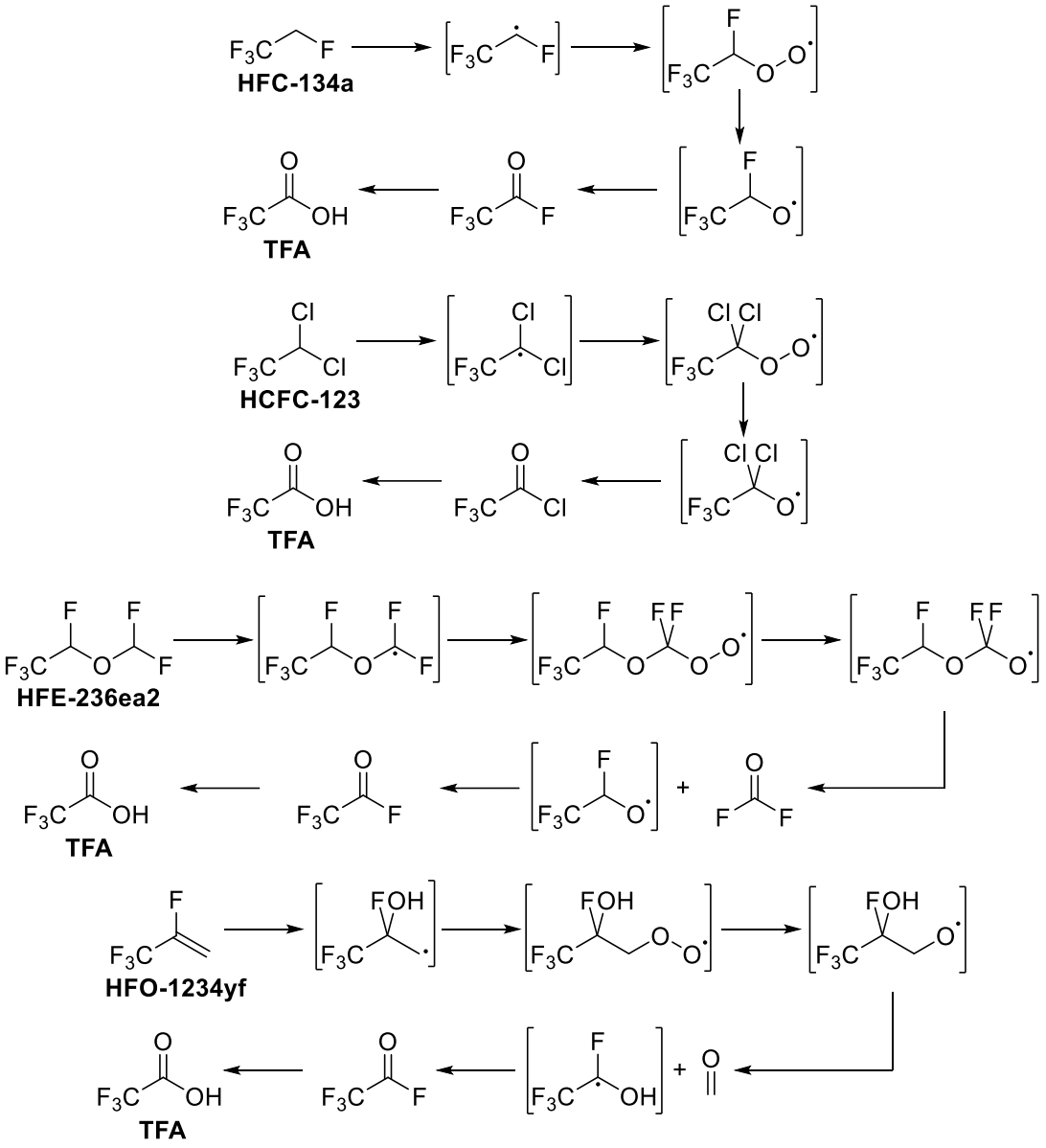
Table 7. Table adapted from the study by Ellis et al.[64] outlining the oxidation of 4:2 FTOH, 6:2 FTOH and 8:2 FTOH in a smog chamber experiment. (x) – Corresponding analyte detected. [a]Unwanted CO_2 could have formed from reactions with the chamber wall and this number indicates the upper limit of the yield observed.

Product	4:2 FTOH	6:2 FTOH	8:2 FTOH	C mass balance, 8:2 FTOH (%)
Perfluorinated acids				
PFNA			x	1.6
PFOA			x	1.5
PFHpA		x	x	0.32
PFHxA		x	x	0.24
PFPeA	x	x	x	0.10
PFBA	x	x	x	<0.1
PFPA	x	x	x	<0.1
TFA	x	x	x	<0.1
Fluorotelomer acids				
8:2 FTCA			x	26
6:2 FTCA		x		
4:2 FTCA	x			
Telomer Aldehydes				
8:2 FTAL			x	6
6:2 FTAL		x		
4:2 FTAL	x			
Perfluoroaldehydes				
C8 PFAL			x	21
C6 PFAL		x		
C4 PFAL	x			
Odd Telomer Alcohols				
8:1 FTOH			x	3.9
6:1 FTOH		x		
4:1 FTOH	x			
Unreacted FTOH				
8:2 FTOH			x	6
Single Carbon Products				
COF_2	x	x	x	22
CF_3OH	x	x	x	2.6
CO_2	x	x	x	<21[a]
			Total:	91 – 112



Scheme 1. Summary of the mechanism for the degradation of FTOHs as reported by Ellis et al.[64] FTCAs will eliminate HF to form FTUCAs (dashed arrow).[77]

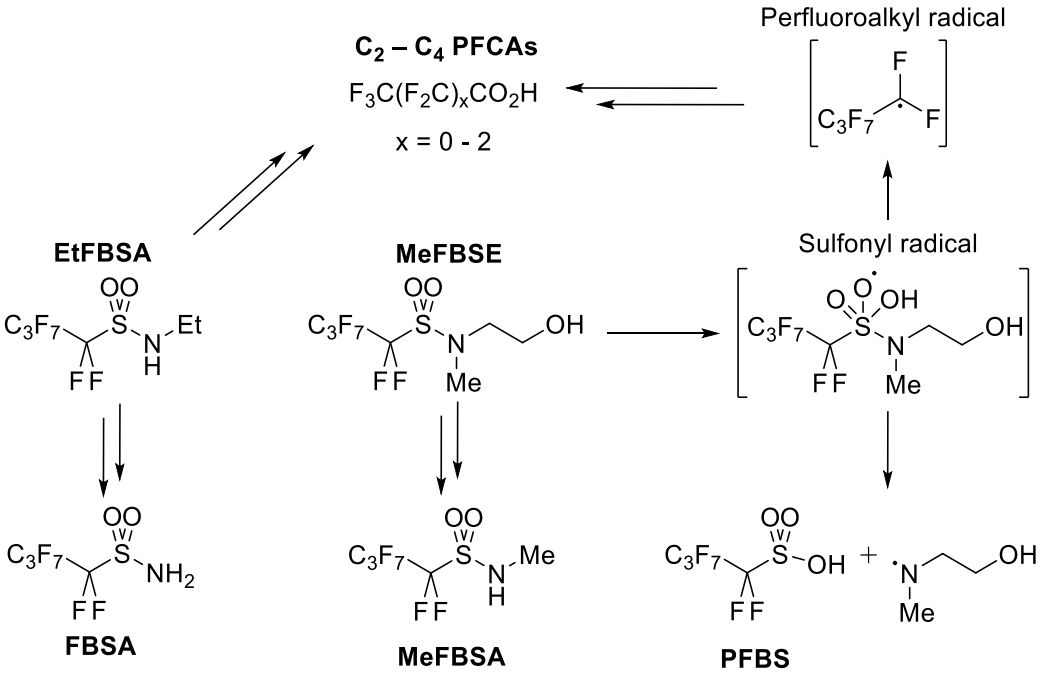
The degradation of HFCs and related compounds is simpler than the degradation of longer chain neutral PFAS, but it is fundamentally the same process. The degradation of the aforementioned HFCs, HCFCs, HFEs and HFOs (see examples Table 1) are all known to degrade in the presence of OH radicals to the shortest PFCA, TFA (Scheme 2). Nonetheless, the degradation of longer chain HFCs, HCFCs, HFEs and HFOs likely also involves an unzipping cycle via a perfluoroalkoxy radical (as for FTOHs) and form a homologues series of PFCAs.



Scheme 2. Mechanism for the formation of TFA from HFC-134a, HCFC-123, HFE-236ea2 and HFO-1234yf[78–80]

Only one study has found evidence for the atmospheric formation of a PFSA from FASAs, FOSEs, or other atmospheric precursors. D'Eon et al. found that PFBS could form from the degradation of MeFBSE (Scheme 3). This was thought to occur by the direct attack of OH radicals at the sulfur centre to form a sulfonyl radical. At this stage, the S–C bond can break to form the

respective perfluorocarbon centred radical or the S–N bond can break to form the respective PFSA, in this case PFBS. Note that the perfluoroalkyl radical is still able to degrade further to a homologous series of PFCAs through an unzipping cycle (see Scheme 1), whereas the PFSA has reached its final degradation product at this stage. For example in Scheme 3, the degradation of MeFBSE produces C_2 – C_4 PFCAs, and only the C_4 PFSA is produced in contrast (PFBS).[68] After 50% consumption of MeFBSE, it was found that concentrations of C_2 – C_4 PFCAs were 10 times higher than that of PFBS. This indicated the preference for cleavage of the C–S bond over the S–N bond.



Scheme 3. Evidence for the formation of PFCAs, PFSAs and perfluorosulfonamides according to D'Eon et al.[68] and Martin et al.[67] Double arrows represent the summation of several steps.

D'Eon et al. also found that MeFBSE was able to have its nitrogen associated functionality degraded.[68] In this case, the alcohol functionality (–CH_2CH_2OH) was removed by OH radicals to form MeFBSA (Scheme 3). In another study by Martin et al., tenuous evidence was found for the

formation of FBSA from EtFBSA – i.e. radical degradation had removed the ethyl chain from the nitrogen.[67] However, this observation could not be excluded as an analytical artifact. Nonetheless, these two, albeit limited observations, contribute to the possibility for the atmospheric formation of non-alkylated perfluorosulfonamides (e.g. FBSA, FHxSA and FOSA) from FASAs and FOSEs.

Table 8. Atmospheric lifetimes of precursors with respect to OH radical degradation

Precursor	**Lifetime with respect to OH radical degradation**	**References**
FTOHs	20 – 80 days	Ellis et al.,[72] Piekarz et al.[81]
FASAs	20 – 50 days	Martin et al.[67]
FOSEs	2 days	D'Eon et al.[68]
FTAs	1 day	Butt et al.[69]
HFCs	13 – 40 years	Derwent et al.[82]
HCFCs	1 – 6 years	Derwent et al.[82]
HFEs	3 – 50 years	Burkholder et al.[83]
HFOs	10 – 24 days	Hurley et al.,[80] Young et al.[62]

As a result of these numerous studies into the degradation of neutral PFAS, it has been possible to calculate atmospheric lifetimes for the precursors with respect to atmospheric OH radical mediated degradation (Table 8). However, this table should only be treated as a rough guide. This is because the actual lifetimes will vary seasonally and geographically, depending on the atmospheric OH radical concentrations and temperature, as well as the specific nature of the precursor in question. The shorter atmospheric lifetime of FOSEs can be attributed to the vulnerability of H-abstraction by OH radicals of the hydrogen α to the hydroxyl group and hence majority of OH radicals will attack this part of the molecule. Nonetheless, this process is known to form the respective FASA (e.g. MeFBSA from MeFBSE, Scheme 3), which have significantly longer atmospheric lifetimes.[67,68] HFOs can also react with O_3 owing to their double bond(s) and this was also considered as another removal pathway for HFOs. However, HFOs' lifetimes with respect to ozonolysis was found to be 2 – 25 years,[62,80] and therefore reaction with OH radicals

was considered to be a more important reaction pathway. The fast reaction of HFOs with OH radicals compared to HFCs, HCFCs and HFEs could be due to the vulnerability of its double bond(s) to addition with OH radicals. Finally, thermolysis of fluoropolymers (e.g. PTFE) during high-temperature applications (e.g. combustion engines) can also result in the atmospheric emission of PFCAs and their precursors.[84]

Once PFCAs and PFSAs have formed in the atmosphere, they will be readily deposited by wet and dry deposition. The most compelling evidence for this was from Taniyasu et al.[85] They measured sequentially each single mm of rainfall during several precipitation events at locations on mainland Japan and 1000 km off the Pacific coast. For $C_4 - C_{12}$ PFCAs, FOSA and PFOS, they found that fluxes typically decreased with each additional mm of rainfall and that the first mm of rainfall contained the largest proportion of individual PFAS. They determined that for a 5 mm rainfall event, approximately 75% of the PFAS had been deposited after 3 mm of precipitation. Their results found that PFAS would be effectively scavenged by wet deposition. Further work by Pike et al. demonstrated that PFAS concentrations in rainfall were partly dependent on the sampling sites' proximity to point sources.[86] However, in the Arctic, particularly at high elevation locations on glaciers, the majority of precipitation will fall as snow, instead of rain. Wang et al. measured the concentrations of several PFAS in snow on 15 high elevation glaciers on the Tibetan Plateau (3500 to 6500 m.a.s.l.).[87] The total concentrations were found to vary with latitude and the PFAS homologue profile varied spatially depending on the sampling site's proximity to urban areas, as well as prevailing weather conditions (westerly winds versus monsoon) and the different sources associated with these. Moreover, this study demonstrated that snowfall will also effectively deposit PFAS, and that sampling surface snow offers a route to understanding the atmospheric processes for PFAS.

The atmospheric lifetimes of several PFAS with respect to wet and dry deposition have been calculated. As mentioned previously, the atmospheric lifetime of 8:2 FTOH with respect to wet deposition and dry deposition is >8.4 years. However, the atmospheric lifetime of PFCAs and PFSAs (i.e. precursor degradation products) will be on the order of days. PFOA was calculated to have an atmospheric lifetime of 12 days with respect to wet and dry deposition (as well as 8:2 FTCA).[76] TFA was assumed to have an atmospheric lifetime similar to that of HNO_3 of 9 days with respect to wet deposition.[78] Regardless, these atmospheric lifetimes should only be considered as a rough guide and would expect to vary depending on atmospheric conditions.

In summary, several precursors have been identified in the Arctic atmosphere and are known to undergo OH radical initiated degradation to PFAAs. Upon formation, these will readily be removed from the atmosphere by rain and snowfall. Measurements of rain and surface snow found that it was possible to investigate PFAS atmospheric processes and sources using these matrices. It is unclear what the relative significance of the different PFAS long-range transport mechanisms that exist is to the import of PFAS to the Arctic (e.g. ocean currents vs atmospheric degradation of precursors). However, four studies investigating the presence of PFAS in ocean waters all noted that atmospheric processes contributed to PFAS input in the Arctic Ocean.[41–44] One recent study by Joerss et al. found that the Arctic could indeed be a net exporter of some PFAS compounds through ocean currents in the Fram Strait between Svalbard and Greenland.[41] Those PFAS undergoing net transport out of the Arctic were thought to come from atmospheric sources, highlighting the importance of atmospheric sources and processes in the overall input of PFAS into the Arctic. The far-reaching accumulation of PFAS in the Arctic has been best documented in the archipelago of Svalbard (Norwegian Arctic), where is has been detected in over 20 species. Nonetheless, little is known about the long-range sources of PFAS to the Archipelago.

1.4 Svalbard



Figure 1. Map of Svalbard showing major settlements (red) and established ice core drilling sites (blue). Insert: Svalbard's position within the northern hemisphere

1.4.1 PFAS in Svalbard Biota

Svalbard (Figure 1) is likely the most studied location in the Arctic for PFAS in biota. PFAS have been detected in species throughout the food webs in the archipelago. This includes multiple mammals such as the beluga whale (*Delphinapterus leucas*),[88] Atlantic walrus (*Odobenus rosmarus rosmarus*),[89] harbour seal (*Phoca vitulina*),[90] ringed seal (*Pusa hispida*),[91] Svalbard reindeer (*Rangifer tarandus platyrhynchus*),[92] polar bear (*Ursus maritimus*),[93–96] and arctic fox (*Vulpes lagopus*);[97,98] several species of birds including barnacle goose (*Branta leucopsis*),[99] black guillemot (*Cepphus grille*),[100] northern fulmars (*Fulmarus glacialis*),[101] glaucus gull (*Larus hyperboreus*),[100,102,103] ivory gull (*Pagophila eburnea*),[104,105] snow bunting (*Plectrophenax nivealis*),[106] and black-legged kittiwake (*Rissa tridactyla*);[107,108] several further marine species including sea ice amphipod (*Gammarus wilkitzkii*),[100] great spider crab (*Hyas araneus*),[109] zooplankton (mostly North Atlantic copepod, *Calanus spp*),[109] as well as several species of fish including wolffish (*Anarhichas lupus*),[109] polar cod (*Boreogadus saida*),[100] Atlantic cod (*Gadus morhua*),[110] sculpin (*Myoxocephalus scorpius*)[109] and beaked redfish (*Sebastes mentella*).[110]

Many of these species measured for PFAS have been collected in remote parts of the archipelago. Furthermore, PFAS contamination extends to both the terrestrial and marine food webs at all levels, as well as to both migratory and non-migratory species. The levels of PFSAs detected in these studies tended to be larger than PFCAs, and PFOS, PFOA and PFNA were the most frequently detected PFAS. PFHxS, PFOS, and C_8 – C_{11} PFCAs were ubiquitously detected in Svalbard's polar bears, indicating a high exposure and the significant bioaccumulative ability of these PFAS.[93–96] Three species had significantly higher average levels of PFAS than the others: polar bear (Σ_{6-13}PFAS = 336 – 486 ng/g in blood plasma),[93–95] Arctic fox (Σ_{11-13}PFAS = 120 – 185 ng/g in liver)[97,98] and glaucus gull (Σ_{7-10}PFAS = 75 – 235 ng/g in plasma).[102,103] In contrast,

the lowest levels were found in zooplankton (Σ_{14}PFAS = 0.34 – 2.0 ng/g whole body).[109] To put these values in perspective, the blood plasma concentrations of local residents (not factory workers) living within 3 km of a factory manufacturing PFAS by ECF in China was on average Σ_4PFAS = 136 ng/g (range: 37.4 – 774 ng/g).[111] Whilst for these residents direct exposure to PFAS from dust in their living and working environments was found to be important to their exposure to PFAS, clearly this input mechanism does not exist for polar bears, Arctic foxes and glaucous gulls on Svalbard. The high concentrations observed in these species were found to be caused by PFAS exposure in their diet from bioaccumulation because of their high trophic level.[112] In addition, effective long-range transport mechanisms for PFAS from populated and industrialised areas to the remote Arctic environment must nonetheless exist in order to expose these food webs to PFAS.

1.4.2 Setting and Climate

In order to understand the long-range and local sources of PFAS in Svalbard, it is necessary to understand its climate and human population. Svalbard is an archipelago (61,000 km^2) in the European Arctic spanning from 74° to 81°N (Figure 1). It is surrounded by the Arctic Ocean, North Atlantic Ocean and Barents Sea, and stands at the southerly extent of the Arctic sea ice front.[113,114] Glaciation on the archipelago covers approximately 57% of the land area, and seasonal snow covers the entire archipelago during winter.[115] There are four main settlements, all located on the west coast of Spitsbergen, the largest island in the Archipelago. These are Ny-Ålesund in Kongsfjord (30 – 110 inhabitants) and in Isfjord; Barentsburg (approximately 450 inhabitants), Pyramiden (<10 inhabitants), and Longyearbyen (approximately 2,400 inhabitants). All settlements have had coal mines, but only Longyearbyen and Barentsburg are still active. Tourism is also important to the local economy in Longyearbyen and receives up to 100,000 tourists annually by cruise ship and plane.[116]

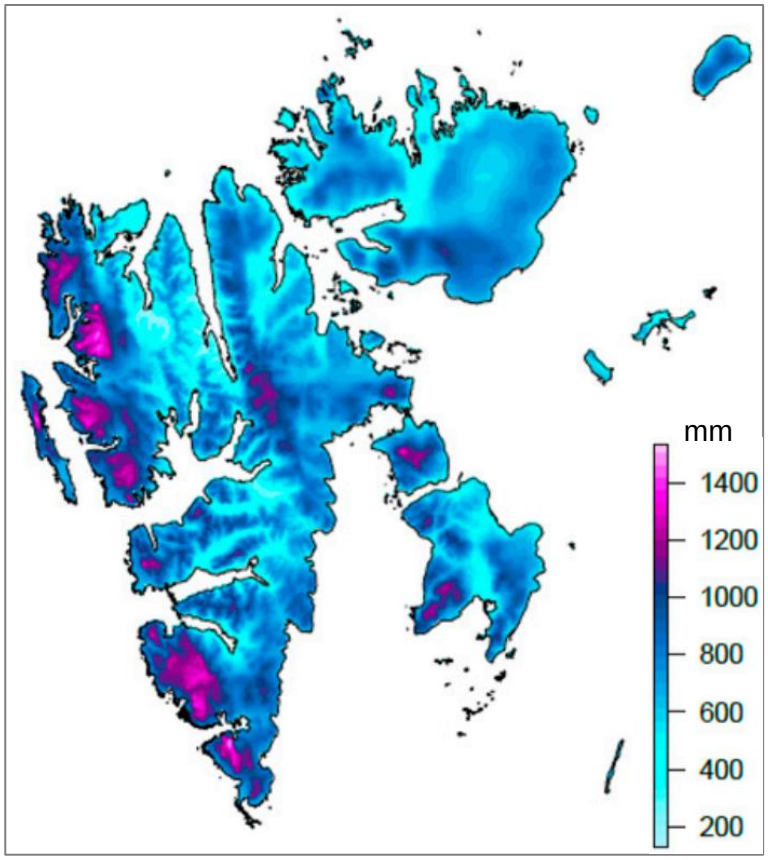


Figure 2. Modelled mean annual precipitation (1971 – 2000). Figure from Førland et al.[117]

The climate is highly variable owing to its position at the interface between the West Spitsbergen Current, which brings warm Atlantic water to the west of the archipelago, and the Barents Sea to the east which has seasonal sea ice cover.[118,119] Atmospheric circulation is balanced by the Icelandic Low and Siberian High pressures and as a result, the North Atlantic cyclone track brings mild mid-latitude air masses to the archipelago. This is most significant during winter when temperatures are much more variable.[120,121] During the 1971 – 2000 climate normal period the mean annual air temperatures at the Svalbard Airport were coldest during December – February (–13.9°C) and March – May (–9.6°C), and averaged –5.9 °C overall. Annual precipitation averaged 196 mm at the station and was one of the lowest measured on Svalbard.[122] However, precipitation is spatially highly variable (Figure 2)[117] and has increased in recent decades.[123]

Nonetheless, precipitation is predominantly solid,[121] however the proportion of rain is increasing.[124] During 1991 – 2020, Svalbard experienced temperature increases of 1.1 – 2.7 °C per decade. This is 2 – 2.5 times the average increase in the Arctic, and 5 – 7 times the average globally.[125] The archipelago also experiences large changes in seasonal light. In Longyearbyen, the sun is below the horizon from late-October to mid-February each year (known as the Polar night) and the sun is continuously above the horizon from mid-April – late August each year (24-hour daylight).

During the autumn to winter period, Svalbard prominently receives air masses from Eurasia. Hence, the long-range transport of pollutants from Eurasia will be enhanced during this time.[126] Indeed, the long-range transport of polyaromatic hydrocarbons (PAHs) is known to be enhanced during winter.[127]

1.4.3 Local Sources of PFAS on Svalbard

Despite effective long-range transport mechanisms existing for PFAS through oceanic and atmospheric processes, input from local sources in the Arctic cannot be dismissed. In Svalbard, significant local sources from landfill and firefighting training sites (FFTS) have been found in Longyearbyen and Ny-Ålesund.[109,128,129] In Longyearbyen, Ali et al. found high levels of PFAS in runoff from the FFTS (Σ_{14}PFAS = 57.4 ± 4.0 ng L^{-1}), where aqueous film forming foams (AFFF) are regularly used for firefighting training purposes. PFOS (35%) had the largest mass contribution in runoff followed by: PFHxS (22%), PFHxA (18%), PFOA (11%), PFHpA (6%) and 6:2 FTSA (3%). A landfill site in Longyearbyen was also analysed. This landfill site was most active during 1991 – 2007. After this period, most local waste was transported to mainland Europe for incineration and the site has been used primarily for non-degradable waste (e.g. concrete, steel, etc). In leachate from this landfill (Σ_{14}PFAS = 643 ± 84 ng L^{-1}), PFOS also had the highest mass

contribution (48%) followed by $C_6 – C_{11}$ PFCAs (43%) including PFOA (20%). Knutsen et al. also found similar PFAS levels in the leachate from the same landfill (Σ_{23}PFAS = 540 ng/L) and that PFOS (30%) had the largest mass contributions as well as $C_6 – C_{11}$ PFCAs (47%) including PFOA (22%).[130] Downstream of these sites in Adventfjord (Chapter 3, Figure 1), PFOS was the dominant PFAS (63–93% of Σ_{14}PFAS), whereas in the Longyearbyen river (and a river close by to Longyearbyen) $C_9 – C_{14}$ PFCAs were the dominant PFAS (37–59%). This indicated that the aforementioned point sources, as well as diffuse sources in the settlement of Longyearbyen, were important to the PFAS exposure of the marine food web in the local fjord. The percentage of linear isomers of PFOS from the FFTS runoff (69 ± 1%), landfill leachate (73 ± 1%), and the Longyearbyen river (74 ± 1%) indicated an electrochemical fluorination (ECF) source. Local sources of PFAS in Longyearbyen likely contributed to PFAS in the local marine food web.[109] However, it is unclear what the geographical extent of PFAS contamination from Longyearbyen into the marine and terrestrial environments might be, as well as the relative importance of local sources compared to PFAS input from long-range ocean currents and long-range atmospheric processes.

Besides Longyearbyen and Ny-Ålesund, local sources of PFAS have been identified in Barentsburg.[106,128] Warner et al. compared PFAS levels and distribution profiles in snow bunting (*Plectrophenax nivalis*) using eggs collected from nests in Longyearbyen, Barentsburg and Pyramiden (Figure 1). Snow bunting eggs were considered useful for investigating the spatial extent of PFAS from local point sources in the terrestrial environment owing to the limited range of these birds. It was concluded that local sources of PFAS in the active settlements of Barentsburg and Longyearbyen had contributed to higher levels of PFAS in the snow bunting eggs. Whereas, long-range atmospheric processes, such as the atmospheric degradation of FTOHs, were more

important for snow buntings' PFAS exposure in Pyramiden. Pyramiden was abandoned in 1998, and there has been limited activities there since. Together these observations suggest that local sources of PFAS are limited in the settlement of Pyramiden and that long-range sources are more important.

Apart from the three studies discussed thus far,[109,128,129] there have been only two further studies into PFAS in Svalbard abiota.[131,132] In contrast, there have been over 20 studies into PFAS in Svalbard's biota. Atmospheric monitoring of 12 PFAS at the Zeppelin Observatory in Ny-Ålesund is the only long-term work into measuring PFAS in the Archipelago.[132] However, the number of compounds is limited, and sampling only measures the particle bound component of the atmosphere. Hence, sampling precipitation offers the opportunity to understanding PFAS processes at a variety of locally contaminated and remote locations. For example, use of seasonal snow sampling and multiyear glacier ice core records could used to understand seasonal variations and long-term remote deposition of PFAS on Svalbard.

1.4.4 Snow Science on Svalbard

In the past two decades, extensive research has been undertaken to investigate the chemistry of the Svalbard snowpack. These include investigations into sources, seasonal trends, diurnal variations, spatial variations, atmospheric processes, and melt processes of black carbon, elemental carbon, water-insoluble organic carbon, dissolved organic carbon, trace metals, halogens, mercury, microbiology, water stable isotopes and major ions (Ca^{2+}, K^{+}, Na^{+}, Mg^{2+}, NH_4^{+}, SO_4^{2-}, Br^{-}, Cl^{-}, methanesulfonic acid (MSA), and NO_3^{-}), as well as organic contaminants such as pesticides, PCBs, PAHs and personal care products.[133–142] Ny-Ålesund has been largely the centre of this work. This research has also been complemented by several ice cores from Svalbard, providing >1000-year records, and atmospheric monitoring at the Zeppelin Observatory above the settlement of Ny-

Ålesund, which has been active since 1990.[143,144] As a result, a large body of knowledge about the Svalbard snowpack now exists. This has made a significant contribution towards understanding the sources and processes of several chemical species in the Arctic snowpack and Arctic atmosphere. However, unlike the aforementioned chemical species, no such systematic study has been undertaken to understand the sources and processes of PFAS in the Svalbard snow or glacier ice.

Sporadic sampling of snow by three studies that investigated PFAS sources in abiota in Svalbard found that surface snow had been influenced by local sources of PFAS.[109,128,145] Kwok et al. found that surface snow on Longyearbreen glacier (4 km from the centre of Longyearbyen) had lower PFAS levels than those samples collected in Longyearbyen settlement.[145] It was concluded that local sources had influenced PFAS levels in surface snow in the settlement, in addition to that from long-range atmospheric transport processes. Skaar et al. measured surface snow at Lake Linnévatnet (9 km west of Barentsburg).[128] Since these snow samples were aged by melt and metamorphosis, it was thought that PFAS profiles had been affected by this and this would explain the non-detectable PFBA in these samples. This observation was in agreement with Codling et al. and Plassmann et al., who found that (more soluble) short-chain PFCAs would be preferentially eluted out of the snowpack.[146,147] Kwok et al. conducted sampling in May 2006 and Skaar et al. in June 2015.[128,145] It is therefore difficult to draw any conclusions about seasonal trends or further source apportioning using these results from snow on Svalbard. However, Ademollo et al. found higher PFAS levels in surface water in Kongsfjord in June 2016 compared to March 2017, but it was not clear what processes contributed to this.[131] Research focus thus far has been on identifying local sources of PFAS using snow samples, however no investigation has been done into the spatial and seasonal variations of PFAS in snow, or reported the levels of

atmospheric deposition of PFAS in the remote environment on Svalbard.

1.5 Ice Cores

1.5.1 Ice cores as a deposition record of POPs

The first continuous surface to bedrock ice core was drilled at Camp Century on the Greenland ice cap in 1966.[148] Since the analysis of water stable isotopes in this core, ice cores have been considered one of the most valuable paleoclimate archives. For example, ice core records have provided a unique record of atmospheric gases, such as CO_2 and methane, covering approximately 800,000 years. As such, the completion of drilling at Vostok in Antarctica in 1998 gave an ice core which is now central to our understanding of the earth's climate.[149]

Organic contaminants, subject to long-range atmospheric transport, can travel from industrialised/populated regions to become deposited on glacier surfaces during precipitation (wet deposition). Contaminants can also become deposited through processes such as condensation or particle-bound atmospheric transport (dry deposition). Decomposition of organic contaminants when frozen in ice is likely to be slow (in comparison to other matrices). Hence, ice core records from glaciers and ice caps offer a route to understanding the historical deposition and atmospheric processes of POPs and other contaminants. Furthermore, these ice cores are often retrieved from remote high-altitude sites, ideal for investigating the background atmospheric processes of contaminants – above the atmospheric boundary layer and far from local sources.

In more recent decades, atmospheric monitoring of several POPs and organic contaminants has been established in the Arctic, for example at Alert in Canada and at the Zeppelin Observatory on Svalbard.[143] Atmospheric monitoring of contaminants provides the opportunity to have a higher sampling resolution (typically 48 hours – 2 weeks per sample for organic contaminants) compared

to ice core records. This data can then be used to investigate specific transport events or seasonal trends, for example. This is a significant advantage with respect to long-term atmospheric monitoring over ice core records. However, many organic contaminants only become part of routine long-term monitoring many years after the environmental impact of these contaminants has been identified. For example, peak emissions of PCBs were in the 1970s, but it wasn't until 2000 that PCBs became part of long-term monitoring (and measurements had not been affected by contamination during sampling).[150] Instead, ice cores can be used to retrospectively investigate the atmospheric deposition of a chosen contaminant. Furthermore, an ice core provides a record of contaminant deposition, and not just what is present in the atmosphere at a particular site. This is important to distinguish, since contaminants that actually become deposited have the potential to enter the ecosystem, whereas those in the atmosphere don't necessarily undergo deposition into the environment. Atmospheric monitoring also varies in consistency between measurements of the gaseous component of the contaminant and the particle-bound fraction (collected on filters).[151] This is important, as the atmospheric processes for particle bound and non-particle bound components may be different. Ice cores can also distinguish between particle bound and non-particle bound components provided filters are used during extraction.[152] Furthermore, nearby settlements, as well as the infrastructure required for long-term atmospheric monitoring, may also mean that the monitoring site does not reflect a background location. Nonetheless, ice core records are not without problems in providing an atmospheric signal since post-depositional processes can damage the atmospheric record. For example, meltwater percolation could modify the vertical distribution of contaminants.[152] In addition, post-depositional chemical transformations of contaminants in the snowpack could change the levels and distribution profile of the target analytes in the ice core.[153] Atmospheric deposition records of contaminants in ice cores may also be

influenced by seasonal and year-to-year variations in accumulation at the drilling site on the glacier. As a result, some ice cores have chosen to report the deposition of contaminants in flux (mass per unit area per year) rather than simply by concentration (mass per unit volume of melted of ice core).[154]

Ice cores have become a useful tool for investigating the atmospheric processes and historical deposition of several contaminants around the world. Ice core records from the European Alps,[155] Canadian Arctic,[52] Himalayas,[156] Svalbard[157] and Antarctica[158] have been used to investigate organic contaminants including PCBs,[159] brominated flame retardants,[160] pesticides[161] and PFAS.[162] More information on the ice core records for PFAS are discussed in Chapter 2.

1.5.2 Svalbard Ice Cores

Ice core drilling on Svalbard was establish during 1965 – 1987 by scientists from the former U.S.S.R. Japanese scientists drilling from 1992 – 1999 established the drilling site at Holtedahlfonna.[163] Since 1997, international teams have drilled notable ice cores from Lomonosovfonna (in 1997 and 2009)[164,165] and Holtedahlfonna (in 2005).[166] None of these reached close to full depth apart from the Lomonosovfonna core in 1997 (121.6 m). The most significant paleoclimate records for Svalbard have come from these three cores, and all of Svalbard ice core records span <1300 years.

Snow accumulation rates on Svalbard are much higher compared to Greenland or Antarctica[167] (0.58 ± 0.13 m water equivalent per year for the 2009 Lomonosovfonna ice)[165] but are lower than most alpine drilling sites.[168] As with ice core records from Greenland and Antarctica, ice cores on Svalbard have been dated using annual layer counting (ALC) and reference horizons.[164] Reference horizons are one-off events that provide a 'tie point' to a known date and are typically recorded in the geochemistry of the ice core. They can be anthropogenic or natural

events. In Svalbard, thermonuclear bombing testing (causing a peak in tritium deposition in 1963) and the Chernobyl disaster in May 1987 (causing a peak in ^{137}Cs) provide reference horizons from anthropogenic events.[164] Peaks in sulfate ions, caused by known past volcanic eruptions can also provide a natural reference horizon.[165] These can be complemented by identifying associated (and geochemically unique) tephra shards such as those produced by the Laki (1783)[169] and Grímsvötn (1903)[170] eruptions. Since Svalbard is situated downwind of Iceland, volcanic activity in Iceland will be effectively transported to Svalbard, providing a useful tool for dating in Svalbard ice cores. Nonetheless, more precise dating can be achieved by ALC. ALC relies on seasonal variations in, for example, water stable isotope ratios (δD, $\delta^{18}O$) and major ions (e.g. Na^+).[165] Seasonal temperature variations typically cause precipitation in summer to be isotopically enriched with heavier stable water isotopes, whereas in winter precipitation will be isotopically lighter. These seasonal variations cause peaks and troughs which correspond to annual layers in the core. Similarly, in winter/spring there will be a greater sea ice extent around Svalbard, which reduces the deposition of marine aerosols (containing Na^+) as a result of a 'cap' on the ocean. In summer, this will be reduced and therefore an increased deposition of Na^+ is expected. Together, ALC and the aforementioned reference horizons have been vital to dating the two recent ice cores from Lomonosovfonna in 1997 and 2009.[164,165]

Due to Svalbard's relative proximity to Eurasia, the archipelago provides an opportunity to study the long-range transport of contaminants. As discussed previously in *1.4.2 - Setting and Climate*, Svalbard receives air masses whose source regions often originate over Eurasia. Analysis of pollen in an ice core from Lomonosovfonna suggested that Eurasia was the primary source of pollen deposition in Svalbard, since the quantities and taxa indicated sources in Fennoscandia (i.e. not North America).[171] Furthermore, comparisons between pesticide deposition in two Svalbard

ice cores showed that Austfonna (740 m.a.s.l.) had a greater detection frequency and higher levels of several pesticides compared to an ice core from Holtedahlfonna (1150 m.a.s.l., figure 1).[166] When comparing the same 10-year period in both records, 74% of air masses to Austfonna originated were found to originate from Eurasia compared to just 45% for Holdahlfonna (calculated using Hybrid Single-Particle Lagrangian Integrated Trajectory model, HYSPLIT).[172] These results indicated that both sites were influenced by Eurasian air mass sources, and that even short distances (approximately 200 km) within the Arctic may affect deposition levels. Both sites were thought to have been influenced predominantly by long-range atmospheric transport and not local sources.

A comprehensive study of major ions in the seasonal snowpack of 22 sites on seven glaciers on Svalbard concluded that sites above 600 – 700 m.a.s.l. would be less impacted by local sources.[133] Hence, drilling sites above this elevation will be more representative of a regional signal. The study identified Holtedahlfonna and Lomonosovfonna as the optimal sites to investigate long-range contaminant deposition on Svalbard. Indeed, ice cores from these two sites have previously been used to investigate the long-range atmospheric deposition of PCBs,[159] brominated flame retardants,[160] pesticides,[166] black carbon[173] and elemental carbon.[174] However, all established ice core drilling sites will likely be experiencing increased summer meltwater percolation in the coming decades due to increasing summer temperatures across the archipelago.[125] This will disrupt the atmospheric record. The effects of summer melt on Svalbard's ice core records have been well researched. Wendl et al. and Iizuka et al. used a stratigraphic melt index and chemical melt proxy to quantify the effects of melt on Svalbard ice cores.[165,175] The stratigraphic melt index uses the physical constraints of the melt features within the ice core to quantify historical melt, whereas the chemical melt proxy uses the preferential percolation of Mg^{2+}

relative Na^+ to quantify melt (by calculating $\log([Na^+]/[Mg^{2+}])$ values).

1.5.3 Lomonosovfonna

Lomonosovfonna is one of the highest elevation glacier plateaus on Svalbard. It has a large area above 1000 m.a.s.l. and an accumulation area of about 600 km^2. Several glaciers drain this accumulation down to sea level. The first comprehensive paleoclimate record from a Svalbard ice core was reported by Isaksson et al. for the 1997 ice core, drilled almost to bedrock (121.6 m of 126 m) on Lomonosovfonna.[164] Prior to the 1997 core, the best-preserved record was from the 1976 ice core (200 m), drilled at another location on the plateau, which was dated back approximately 900 years based on accumulation rates in the upper part of the core.[176] The upper 36 m of the 1997 core was dated back to 1920 (77 years) using ALC and a reference horizon from the peak in thermonuclear bomb testing in 1963. Further work by Divine et al. dated the entire core back to 770 ± 150 AD.[144]

After the 1997 core, a new record was drilled on Lomonosovfonna in 2009. The 2009 core created a new baseline for ice core geochemistry and paleoclimate records on Svalbard.[165,173] The core was originally planned to be drilled at the same site as the 1997 ice core. However, due to the opening of a crevasse at the 1997 site, it could not be certain that the record at the 1997 site had not been affected by this. Hence, a new site was selected 4.6 km to the south. Both sites have a cupola shape. The 2009 site (1202 m.a.s.l.) has a slightly lower elevation than the 1997 site (1250 m.a.s.l.), but both sites are the two highest established drilling sites on Svalbard, and are well above the equilibrium line at around 720 m.a.s.l.[177] The new core in 2009 was drilled to 149.5 m, but the drill got stuck, and did not reach bedrock at around 200 m depth. The core was dated back to 1222 ± 10 AD using the 1963 tritium peak, major volcanic eruptions, ^{210}Pb decay, ALC, and glacier flow models.[165] A parallel core to 37 m depth (1957 – 2009), was also drilled for organic

contaminant analysis. Both the 1997 and 2009 records suffered from melt which disrupted the water stable isotope and major ion records. Nonetheless, an atmospheric signal was preserved. For the 1997 core, Pohjola et al. found that ions like NO_3^- and SO_4^{2-} were influenced most by meltwater percolation but were still found to typically be preserved within the annual layer.[178] However, Moore et al. concluded that percolation could sometimes extend up to 8 annual layers.[179] As a result, Wendl et al. often considered interpretations from the 2009 ice core on a decadal scale.[165] Regardless of meltwater percolation, all studies were able to extract a meaningful atmospheric record from Lomonsovfonna.

The 1997 core had a mean borehole temperature of –2.8°C.[164] The 2009 borehole measurements had somewhat warmer temperatures between –1.7°C and –4.3°C in the upper 42 m. The firn extends to a depth of approximately 20 m, and more recent measurements found that the temperature at 10 m is now 0°C year-round. Furthermore, by the end of the ablation season, the upper 10 m of firn/snowpack will be isothermal.[180] Nonetheless, between 1957 – 2018, runoff from the 2009 site has been minimal.[181] In comparison to other sites on Svalbard, Lomonosovfonna likely preserves the best possible ice core records due to its high elevation and position further east (i.e. lower summer temperatures) compared to other sites. Several studies have taken advantage of this to investigate the historical deposition of black carbon,[173] aromatic acids[182] and PCBs[159] in the 2009 ice cores. The Holtedahlfonna ice core has also been analysed for brominated flame retardants.[160] However, in a study comparing the two sites, it was found that Lomonosovfonna was better exposed to tropospheric processes and that it provided a broader regional climate signal.[183] Since the recent drilling of the cores from Holtedahlfonna and Lomonosovfonna, several shallow cores (5 – 15 m) have been drilled at these sites to investigate other physical and chemical parameters in these glaciers.[184–186] Regularly drilling shallow cores provides the opportunity to

build on current knowledge, extend existing records, investigate the most recent atmospheric processes, and collect larger masses of ice for chemical analyses. In addition, this can all be conducted at lower cost compared to previous deeper drilling campaigns.

1.6 Aims and Objectives

This thesis aims to provide a deeper understanding of the long-range atmospheric processes of PFAS in the Arctic through two field studies. Svalbard has been selected as the study site because of well-established infrastructure for polar logistics and limited knowledge of PFAS atmospheric processes in this Arctic region. Whilst a large body of knowledge has been established for the processes of PFAS in biota, little is known about the long-range sources that contribute to PFAS input in the archipelago. Using a new ice core record from Lomonosovfonna and surface snow samples, this project has used this complementary approach to investigate the atmospheric sources and processes of PFAS in the European Arctic. Whilst the ice core record allowed for a retrospective investigation into >10 years of PFAS accumulation in the remote Arctic, the surface snow sampling was used to inspect individual precipitation events and the seasonal atmospheric processes that contributed to the PFAS observed.

In particular, this thesis aims to use an ice core from Lomonosovfonna (discussed in Chapter 4) to:

(i) Establish the atmospheric deposition fluxes of PFAS in the remote environment on Svalbard and how these compare to existing Arctic records

(ii) Identify atmospheric precursors and other atmospheric processes that contribute to PFAS deposition in the Arctic

(iii) Identify air mass source regions

(iv) Understand the possible redistribution of PFAS during summer meltwater percolation in the Svalbard snowpack/glacier firn

In addition, using surface snow samples, collected seasonally from January – August (discussed in Chapters 5 and 6), this thesis aims to:

(i) Investigate the levels and seasonal variations of PFAS deposition in the Arctic

(ii) Understand the extent of PFAS contamination from local sources

(iii) Identify possible atmospheric precursors and other atmospheric processes that contribute to PFAS deposition

Lastly, this thesis aims to investigate evidence for bromine radical initiated precursor degradations in the Arctic atmosphere, by bringing these two datasets together alongside major ion data (discussed in Chapter 7). However, first this thesis undertakes a review using existing PFAS ice core records to understand this contaminants' atmospheric sources and processes, and identify gaps in existing knowledge for future research. (Chapter 2). This is followed by an overview of the methods used by this thesis (Chapter 3), more details of which can be found in Chapters 4 – 7.

1.7 References

1. Carson, R. *Silent Spring*. (Houghton Mifflin, 1962).
2. Glausiusz, J. Better Planet: Can A Maligned Pesticide Save Lives? *Discover Magazine* 34 (2007).
3. Stockholm Convention. http://www.pops.int/.
4. Roberts, S. Like a Forever Chemical. (2020).
5. Haynes, T. *Dark Waters*. (Focus Features, 2019).
6. *Toward a new comprehensive global database of per- and polyfluoroalkyl substances (PFASs)*. (2018).
7. Wang, Z. *et al.* A New OECD Definition for Per- And Polyfluoroalkyl Substances. *Environ. Sci. Technol.* **55**, 15575–15578 (2021).
8. CompTox Chemicals Dashboard. https://comptox.epa.gov/dashboard/chemical-lists/PFASSTRUCTv4.
9. Wang, Z., DeWitt, J. C., Higgins, C. P. & Cousins, I. T. A Never-Ending Story of Per- and Polyfluoroalkyl Substances (PFASs)? *Environ. Sci. Technol.* **51**, 2508–2518 (2017).
10. Henry, B. J. *et al.* A critical review of the application of polymer of low concern and regulatory criteria to fluoropolymers. *Integr. Environ. Assess. Manag.* **14**, 316–334 (2018).
11. Hiyama, T. & Yamamoto, H. Biologically Active Organofluorine Compounds. *Organofluor. Compd.* 137–182 (2000) doi:10.1007/978-3-662-04164-2_5.
12. O'hagan, D. Understanding organofluorine chemistry. An introduction to the C–F bond. *Chem. Soc. Rev.* **37**, 308–319 (2008).
13. Chambers, R. D. *Fluorine in Organic Chemistry*. (Blackwell Publishing Ltd, 2004).
14. Allen, J. G. These toxic chemicals are everywhere — even in your body. And they won't ever go away. *The Washington Post* (2018).
15. Posner, S. Perfluorinated Compounds: Occurrence and Uses in Products. *Handb. Environ. Chem.* **17**, 25–39 (2012).
16. Okazoe, T. Overview on the history of organofluorine chemistry from the viewpoint of material industry. *Proc. Jpn. Acad. Ser. B. Phys. Biol. Sci.* **85**, 276 (2009).
17. Midgley, T. & Henne, A. L. Organic Fluorides as Refrigerants. *Ind. Eng. Chem.* **22**, 542–545 (1930).
18. Pluckett, R. J. Tetrafluoroethylene polymers. (1939).
19. Banks, R. E. & Tatlow, J. C. Synthesis of C-F bonds: the pioneering years, 1835 – 1940. *J. Fluor. Chem.* **33**, 71–108 (1986).
20. Goldwhite, H. The Manhattan Project. *J. Fluor. Chem.* **33**, 109–132 (1986).
21. Simons, J. H. Production of Fluorocarbons: I. The Generalized Procedure and its Use with Nitrogen Compounds. *J. Electrochem. Soc.* **95**, 47 (1949).
22. Benskin, J. P., De Silva, A. O. & Martin, J. W. Isomer profiling of perfluorinated substances as a tool for source tracking: a review of early findings and future applications. *Rev. Environ. Contam. Toxicol.* **208**, 111–160 (2010).
23. Haszeldine, R. N. The reactions of fluorocarbon radicals. Part I. The reaction of iodotrifluoromethane with ethylene and tetrafluoroethylene. *J. Chem. Soc.* 2856–2861 (1949) doi:10.1039/JR9490002856.
24. Carloni, D. *Perfluorooctane Sulfonate (PFOS) Production and Use: Past and Current Evidence*. https://www.researchgate.net/publication/267995130_Perfluorooctane_Sulfonate_PFOS_Production_and_Use_Past_and_Current_Evidence_Prepared_for_UNIDO (2009).
25. Velders, G. J. M., Andersen, S. O., Daniel, J. S., Fahey, D. W. & McFarland, M. The importance of the Montreal Protocol in protecting climate. *Proc. Natl. Acad. Sci. U. S. A.* **104**, 4814–4819 (2007).
26. Van Houten, J. A century of chemical dynamics traced through the nobel prizes. 1995: Paul Crutzen, Sherwood Rowland, and Mario Molina. *J. Chem. Educ.* **79**, 1182 (2002).
27. Reizian-Fouley, A., Dat, Y. & Rault, S. Chlorofluorocarbon CFCs, Potential Alternative HCFCs and HFCs, and Related Chlorinated Compounds: Mass Spectral Study, Part II. *Ecotoxicol. Environ. Saf.* **36**, 197–204 (1997).
28. Montzka, S. A. *et al.* Recent trends in global emissions of hydrochlorofluorocarbons and hydrofluorocarbons: Reflecting on the 2007 adjustments to the montreal protocol. *J. Phys. Chem. A* **119**, 4439–4449 (2015).
29. Vollmer, M. K. *et al.* Modern inhalation anesthetics: Potent greenhouse gases in the global atmosphere. *Geophys. Res. Lett.* **42**, 1606–1611 (2015).
30. Hodnebrog *et al.* Global warming potentials and radiative efficiencies of halocarbons and related compounds: A comprehensive review. *Rev. Geophys.* **51**, 300–378 (2013).
31. Polonara, F., Kuijpers, L. J. M. & Peixoto, R. A. Potential impacts of the Montreal Protocol Kigali Amendment to the choice of refrigerant alternatives. *Int. J. Heat Technol.* **35**, S1–S8 (2017).

32. Wilson, D. P., Singh, R. R., Basu, R. S., Swan, E. L. & Nalewajek, D. Azeotrope-like mixtures of pentafluoropropane and hydrofluorocarbon having 3-6 carbon atoms useful as heat-transfer agents and/or refrigerants. (1997).
33. Rayne, S. & Forest, K. Perfluoroalkyl sulfonic and carboxylic acids: A critical review of physicochemical properties, levels and patterns in waters and wastewaters, and treatment methods. *J. Environ. Sci. Heal. Part A* **44**, 1145–1199 (2009).
34. Xie, Z. *et al.* Neutral poly- and perfluoroalkyl substances in air and seawater of the North Sea. *Environ. Sci. Pollut. Res.* **20**, 7988–8000 (2013).
35. Smith, J. W. N. *et al. Environmental fate and effects of poly-and perfluoroalkyl substances (PFAS)*. (2016).
36. *Dictionary of Organic Compounds*. (Chapman and Hall, 1982).
37. Fermeglia, M., Bertucco, A. & Patrizioi, D. Thermodynamic properties of pure hydrofluorocarbons by a perturbed hard-sphere-chain equation of state. *Chem. Eng. Sci.* **52**, 1517–1527 (1997).
38. Barry, V., Winquist, A. & Steenland, K. Perfluorooctanoic acid (PFOA) exposures and incident cancers among adults living near a chemical plant. *Environ. Health Perspect.* **121**, 1313–1318 (2013).
39. Fenton, S. E. *et al.* Per- and Polyfluoroalkyl Substance Toxicity and Human Health Review: Current State of Knowledge and Strategies for Informing Future Research. *Environ. Toxicol. Chem.* **40**, 606–630 (2021).
40. Giesy, J. P. & Kannan, K. Global Distribution of Perfluorooctane Sulfonate in Wildlife. *Environ. Sci. Technol.* **35**, 1339–1342 (2001).
41. Joerss, H. *et al.* Transport of Legacy Perfluoroalkyl Substances and the Replacement Compound HFPO-DA through the Atlantic Gateway to the Arctic Ocean - Is the Arctic a Sink or a Source? *Environ. Sci. Technol.* **54**, 9958–9967 (2020).
42. Benskin, J. P. *et al.* Perfluoroalkyl Acids in the Atlantic and Canadian Arctic Oceans. *Environ. Sci. Technol* **46**, 35 (2012).
43. Yeung, L. W. *et al.* Vertical Profiles, Sources, and Transport of PFASs in the Arctic Ocean. *Environ. Sci. Technol.* **51**, 6735–6744 (2017).
44. Cai, M. *et al.* Occurrence of Perfluoroalkyl Compounds in Surface Waters from the North Pacific to the Arctic Ocean. *Environ. Sci. Technol.* **46**, 661–668 (2012).
45. Yamazaki, E. *et al.* Emission, Dynamics and Transport of Perfluoroalkyl Substances from Land to Ocean by the Great East Japan Earthquake in 2011. *Environ. Sci. Technol.nviron* **46**, 11421–11428 (2015).
46. De Leeuw, G. *et al.* Production flux of sea spray aerosol. *Rev. Geophys.* **49**, 2001 (2011).
47. McMurdo, C. J. *et al.* Aerosol enrichment of the surfactant PFO and mediation of the water--air transport of gaseous PFOA. *Environ. Sci. Technol.* **42**, 3969–74 (2008).
48. Sha, B. *et al.* Sea Spray Aerosol (SSA) as a Source of Perfluoroalkyl Acids (PFAAs) to the Atmosphere: Field Evidence from Long-Term Air Monitoring. *Environ. Sci. Technol.* **56**, 228–238 (2022).
49. Johansson, J. H. *et al.* Global transport of perfluoroalkyl acids via sea spray aerosol. *Environ. Sci. Process. Impacts* **21**, 635–649 (2019).
50. Young, C. J. *et al.* Perfluorinated Acids in Arctic Snow: New Evidence for Atmospheric Formation. **41**, (2007).
51. MacInnis, J. J. *et al.* Emerging investigator series: a 14-year depositional ice record of perfluoroalkyl substances in the High Arctic. *Environ. Sci. Process. Impacts* **19**, 22–30 (2017).
52. Pickard, H. M. *et al.* Continuous non-marine inputs of per- and polyfluoroalkyl substances to the High Arctic: a multi-decadal temporal record. *Atmos. Chem. Phys.* **18**, 5045–5058 (2018).
53. Cai, M. *et al.* Polyfluorinated compounds in the atmosphere along a cruise pathway from the Japan Sea to the Arctic Ocean. *Chemosphere* **87**, 989–997 (2012).
54. Dreyer, A., Weinberg, I., Temme, C. & Ebinghaus, R. Polyfluorinated Compounds in the Atmosphere of the Atlantic and Southern Oceans: Evidence for a Global Distribution. *Environ. Sci. Technol.* **43**, 6507–6514 (2009).
55. Shoeib, M., Harner, T. & Vlahos, P. Perfluorinated chemicals in the arctic atmosphere. *Environ. Sci. Technol.* **40**, 7577–83 (2006).
56. Stock, N. L., Furdui, V. I., Muir, D. C. G. & Mabury, S. A. Perfluoroalkyl Contaminants in the Canadian Arctic: Evidence of Atmospheric Transport and Local Contamination. *Environ. Sci. Technol.* **41**, 3529–3536 (2007).
57. Xie, Z. *et al.* Neutral Poly-/perfluoroalkyl Substances in Air and Snow from the Arctic. *Sci. Rep.* **5**, 8912 (2015).
58. EBAS. http://ebas-data.nilu.no/.
59. Young, C. J., Hurley, M. D., Wallington, T. J. & Mabury, S. A. Atmospheric chemistry of CF3CF2H and

CF3CF2CF2CF2H: Kinetics and products of gas-phase reactions with Cl atoms and OH radicals, infrared spectra, and formation of perfluorocarboxylic acids. *Chem. Phys. Lett.* **473**, 251–256 (2009).
60. Wallington, T. J. *et al.* The Environmental Impact of CFC Replacements-HFCs and HCFCs. *Environ. Sci. Technol.* **28**, (1994).
61. Oyaro, N., Sellevåg, S. R. & Nielsen, C. J. Atmospheric chemistry of hydrofluoroethers: Reaction of a series of hydrofluoroethers with OH radicals and Cl atoms, atmospheric lifetimes, and global warming potentials. *J. Phys. Chem. A* **109**, 337–346 (2005).
62. Young, C. J., Hurley, M. D., Wallington, T. J. & Mabury, S. A. Atmospheric chemistry of perfluorobutenes (CF3CF=CFCF3 and CF3CF2CF=CF2): Kinetics and mechanisms of reactions with OH radicals and chlorine atoms, IR spectra, global warming potentials, and oxidation to perfluorocarboxylic acids. *Atmos. Environ.* **43**, 3717–3724 (2009).
63. Hurley, M. D. *et al.* Atmospheric Chemistry of 4:2 Fluorotelomer Alcohol (CF3(CF2)3CH2CH2OH): Products and Mechanism of Cl Atom Initiated Oxidation. *J. Phys. Chem. A* **108**, 5635–5642 (2004).
64. Ellis, D. A. *et al.* Degradation of fluorotelomer alcohols: a likely atmospheric source of perfluorinated carboxylic acids. *Environ. Sci. Technol.* **38**, 3316–21 (2004).
65. Sulbaek Andersen, M. P. *et al.* Atmospheric chemistry of 4:2 Fluorotelomer alcohol (n-C4F9CH2CH2OH): Products and mechanism of Cl atom initiated oxidation in the presence of NO x. *J. Phys. Chem. A* **109**, 1849–1856 (2005).
66. Styler, S. A., Myers, A. L. & Donaldson, D. J. Heterogeneous photooxidation of fluorotelomer alcohols: A new source of aerosol-phase perfluorinated carboxylic acids. *Environ. Sci. Technol.* **47**, 6358–6367 (2013).
67. Martin, J. W., Ellis, D. A., Mabury, S. A., Hurley, M. D. & Wallington, T. J. Atmospheric chemistry of perfluoroalkanesulfonamides: kinetic and product studies of the OH radical and Cl atom initiated oxidation of N-ethyl perfluorobutanesulfonamide. *Environ. Sci. Technol.* **40**, 864–72 (2006).
68. D'eon, J. C., Hurley, M. D., Wallington, T. J. & Mabury, S. A. Atmospheric chemistry of N-methyl perfluorobutane sulfonamidoethanol, C4F9SO2N(CH3)CH2CH2OH: kinetics and mechanism of reaction with OH. *Environ. Sci. Technol.* **40**, 1862–8 (2006).
69. Butt, C. M., Young, C. J., Mabury, S. A., Hurley, M. D. & Wallington, T. J. Atmospheric Chemistry of 4:2 Fluorotelomer Acrylate [C4F9CH2CH2OC(O)CH═CH2]: Kinetics, Mechanisms, and Products of Chlorine-Atom- and OH-Radical-Initiated Oxidation. *J. Phys. Chem. A* **113**, 3155–3161 (2009).
70. Calvert, J. G. & Pitts, J. N. *Photochemistry*. (John Wiley, 1966).
71. Schneider, W. F., Wallington, T. J., Minschwaner, K. & Stahlberg, E. A. Atmospheric Chemistry of CF3OH: Is Photolysis Important? *Environ. Sci. Technol.* **29**, 247–250 (1995).
72. Ellis, D. A. *et al.* Atmospheric lifetime of fluorotelomer alcohols. *Environ. Sci. Technol.* **37**, 3816–20 (2003).
73. Armitage, J. M., Macleod, M. & Cousins, I. T. Comparative assessment of the global fate and transport pathways of long-chain perfluorocarboxylic acids (PFCAs) and perfluorocarboxylates (PFCs) emitted from direct sources. *Environ. Sci. Technol.* **43**, 5830–5836 (2009).
74. Yarwood, G. *et al.* High-resolution atmospheric modeling of fluorotelomer alcohols and perfluorocarboxylic acids in the North American troposphere. *Environ. Sci. Technol.* **41**, 5756–5762 (2007).
75. Hurley, M. D. *et al.* Atmospheric chemistry of perfluorinated carboxylic acids: Reaction with OH radicals and atmospheric lifetimes. *J. Phys. Chem. A* **108**, 615–620 (2004).
76. Wallington, T. J. *et al.* Formation of C7F15COOH (PFOA) and other perfluorocarboxylic acids during the atmospheric oxidation of 8:2 fluorotelomer alcohol. *Environ. Sci. Technol.* **40**, 924–30 (2006).
77. Loewen, M., Halldorson, T., Wang, F. & Tomy, G. Fluorotelomer carboxylic acids and PFOS in rainwater from an urban center in Canada. *Environ. Sci. Technol.* **39**, 2944–2951 (2005).
78. Kotamarthi, V. R. *et al.* Trifluoroacetic acid from degradation of HCFCs and HFCs: A three-dimensional modeling study. *J. Geophys. Res. Atmos.* **103**, 5747–5758 (1998).
79. Sulbaek Andersen, M. P., Nielsen, O. J., Karpichev, B., Wallington, T. J. & Sander, S. P. Atmospheric chemistry of isoflurane, desflurane, and sevoflurane: Kinetics and mechanisms of reactions with chlorine atoms and oh radicals and global warming potentials. *J. Phys. Chem. A* **116**, 5806–5820 (2012).
80. Hurley, M. D., Ball, J. C. & Wallington, T. J. Atmospheric chemistry of the Z and E isomers of CF3CF=CHF; Kinetics, mechamsms, and products of gas-phase reactions with Cl atoms, OH radicals, and O3. *J. Phys. Chem. A* **111**, 9789–9795 (2007).
81. Piekarz, A. M., Primbs, T., Field, J. A., Barofsky, D. F. & Simonich, S. Semivolatile Fluorinated Organic Compounds in Asian and Western U.S. Air Masses. *Environ. Sci. Technol.* **41**, 8248–8255 (2007).
82. Derwent, R. G., Volz-Thomas, A. & Prather, M. J. *Tropospheric OH and HCFC/HFC Lifetimes*. (1989).
83. Burkholder, J. B., Cox, R. A. & Ravishankara, A. R. Atmospheric Degradation of Ozone Depleting

Substances, Their Substitutes, and Related Species. *Chem. Rev.* **115**, 3704–3759 (2015).
84. Ellis, D. A., Mabury, S. A., Martin, J. W. & Muir, D. C. G. Thermolysis of fluoropolymers as a potential source of halogenated organic acids in the environment. *Nature* **412**, 321–324 (2001).
85. Taniyasu, S., Yamashita, N., Yamazaki, E., Petrick, G. & Kannan, K. The environmental photolysis of perfluorooctanesulfonate, perfluorooctanoate, and related fluorochemicals. *Chemosphere* **90**, 1686–1692 (2013).
86. Pike, K. A., Edmiston, P. L., Morrison, J. J. & Faust, J. A. Correlation Analysis of Perfluoroalkyl Substances in Regional U.S. Precipitation Events. *Water Res.* **190**, 116685 (2021).
87. Wang, X., Chen, M., Gong, P. & Wang, C. Perfluorinated alkyl substances in snow as an atmospheric tracer for tracking the interactions between westerly winds and the Indian Monsoon over western China. *Environ. Int.* **124**, 294–301 (2019).
88. Villanger, G. D. *et al.* Perfluoroalkyl substances (PFASs) in white whales (Delphinapterus leucas) from Svalbard – A comparison of concentrations in plasma sampled 15 years apart. *Environ. Pollut.* **263**, 114497 (2020).
89. Scotter, S. E. *et al.* Contaminants in Atlantic walruses in Svalbard part 1: Relationships between exposure, diet and pathogen prevalence. *Environ. Pollut.* **244**, 9–18 (2019).
90. Routti, H., Lydersen, C., Hanssen, L. & Kovacs, K. M. Contaminant levels in the world's northernmost harbor seals (Phoca vitulina). *Mar. Pollut. Bull.* **87**, 140–146 (2014).
91. Routti, H., Gabrielsen, G. W., Herzke, D., Kovacs, K. M. & Lydersen, C. Spatial and temporal trends in perfluoroalkyl substances (PFASs) in ringed seals (Pusa hispida) from Svalbard. *Environ. Pollut.* **214**, 230–238 (2016).
92. Roos, A. M. *et al.* Perfluoroalkyl substances in circum-ArcticRangifer: caribou and reindeer. *Environ. Sci. Pollut. Res.* **29**, 23721–23735 (2022).
93. Tartu, S. *et al.* Diet and metabolic state are the main factors determining concentrations of perfluoroalkyl substances in female polar bears from Svalbard. *Environ. Pollut.* **229**, 146–158 (2017).
94. Bytingsvik, J. *et al.* Perfluoroalkyl substances in polar bear mother–cub pairs: A comparative study based on plasma levels from 1998 and 2008. *Environ. Int.* **49**, 92–99 (2012).
95. Tartu, S. *et al.* Choose Your Poison—Space-Use Strategy Influences Pollutant Exposure in Barents Sea Polar Bears. *Environ. Sci. Technol.* **52**, 3211–3221 (2018).
96. Smithwick, M. *et al.* Circumpolar study of perfluoroalkyl contaminants in polar bears (Ursus maritimus). *Environ. Sci. Technol.* **39**, 5517–23 (2005).
97. Aas, C. B., Fuglei, E., Herzke, D., Yoccoz, N. G. & Routti, H. Effect of Body Condition on Tissue Distribution of Perfluoroalkyl Substances (PFASs) in Arctic Fox (Vulpes lagopus). *Environ. Sci. Technol.* **48**, 11654–11661 (2014).
98. Routti, H. *et al.* Emission Changes Dwarf the Influence of Feeding Habits on Temporal Trends of Per- and Polyfluoroalkyl Substances in Two Arctic Top Predators. *Environ. Sci. Technol.* **51**, 11996–12006 (2017).
99. Hitchcock, D. J. *et al.* Potential Effect of Migration Strategy on Pollutant Occurrence in Eggs of Arctic Breeding Barnacle Geese (Branta leucopsis). *Environ. Sci. Technol.* **53**, 5427–5435 (2019).
100. Haukås, M., Berger, U., Hop, H., Gulliksen, B. & Gabrielsen, G. W. Bioaccumulation of per- and polyfluorinated alkyl substances (PFAS) in selected species from the Barents Sea food web. *Environ. Pollut.* **148**, 360–371 (2007).
101. Knudsen, L. B. *et al.* Halogenated organic contaminants and mercury in northern fulmars (Fulmarus glacialis): levels, relationships to dietary descriptors and blood to liver comparison. *Environ. Pollut.* **146**, 25–33 (2007).
102. Verreault, J. *et al.* Perfluorinated Alkyl Substances in Plasma, Liver, Brain, and Eggs of Glaucous Gulls (Larus hyperboreus) from the Norwegian Arctic. *Environ. Sci. Technol.* **39**, 7439–7445 (2005).
103. Melnes, M., Gabrielsen, G. W., Herzke, D., Sagerup, K. & Jenssen, B. M. Dissimilar effects of organohalogenated compounds on thyroid hormones in glaucous gulls. *Environ. Res.* **158**, 350–357 (2017).
104. Lucia, M. *et al.* Circumpolar contamination in eggs of the high-Arctic ivory gull *Pagophila eburnea*. *Environ. Toxicol. Chem.* **34**, 1552–1561 (2015).
105. Lucia, M., Strøm, H., Bustamante, P., Herzke, D. & Gabrielsen, G. W. Contamination of ivory gulls (Pagophila eburnea) at four colonies in Svalbard in relation to their trophic behaviour. *Polar Biol.* **40**, 917–929 (2017).
106. Warner, N. A. *et al.* Snow buntings (Plectrophenax nivealis) as bio-indicators for exposure differences to legacy and emerging persistent organic pollutants from the Arctic terrestrial environment on Svalbard. *Sci. Total Environ.* **667**, 638–647 (2019).
107. Blévin, P. *et al.* Perfluorinated substances and telomeres in an Arctic seabird: Cross-sectional and longitudinal

approaches. *Environ. Pollut.* **230**, 360–367 (2017).
108. Jouanneau, W. *et al.* A Bad Start in Life? Maternal Transfer of Legacy and Emerging Poly- And Perfluoroalkyl Substances to Eggs in an Arctic Seabird. *Environ. Sci. Technol.* **2022**, 6102 (2021).
109. Ali, A. M. *et al.* The fate of poly- And perfluoroalkyl substances in a marine food web influenced by land-based sources in the Norwegian Arctic. *Environ. Sci. Process. Impacts* **23**, 588–604 (2021).
110. Kowalczyk, J., Flor, M., Karl, H. & Lahrssen-Wiederholt, M. Perfluoroalkyl substances (PFAS) in beaked redfish (Sebastes mentella) and cod (Gadus morhua) from arctic fishing grounds of Svalbard. *Food Addit. Contam. Part B* **13**, 34–44 (2019).
111. Fu, J. *et al.* Elevated levels of perfluoroalkyl acids in family members of occupationally exposed workers: the importance of dust transfer. *Sci. Reports 2015 51* **5**, 1–7 (2015).
112. Conder, J. M., Hoke, R. A., De Wolf, W., Russell, M. H. & Buck, R. C. Are PFCAs bioaccumulative? A critical review and comparison with regulatory criteria and persistent lipophilic compounds. *Environ. Sci. Technol.* **42**, 995–1003 (2008).
113. Rogers, J. C., Yang, L. & Li, L. The role of Fram Strait winter cyclones on sea ice flux and on Spitsbergen air temperatures. *Geophys. Res. Lett.* **32**, 1–4 (2005).
114. Aagaarda, K., Foldvik, A. & Hillman, S. R. The West Spitsbergen Current: Disposition and water mass transformation. *J. Geophys. Res. Ocean.* **92**, 3778–3784 (1987).
115. Nuth, C. *et al.* Decadal changes from a multi-temporal glacier inventory of Svalbard. *Cryosphere* **7**, 1603–1621 (2013).
116. Roura, R. M. *The footprint of Polar tourism : Tourist behaviour at cultural heritage sites in Antarctica and Svalbard*. vol. 7 (Barkhuis, 2011).
117. Førland, E. J. *et al.* Measured and Modeled Historical Precipitation Trends for Svalbard. *J. Hydrometeorol.* **21**, 1279–1296 (2020).
118. Carmack, E. *et al.* Toward Quantifying the Increasing Role of Oceanic Heat in Sea Ice Loss in the New Arctic. *Bull. Am. Meteorol. Soc.* **96**, 2079–2105 (2015).
119. Aagaard, K. & Greisman, P. Toward new mass and heat budgets for the Arctic Ocean. *J. Geophys. Res.* **80**, 3821–3827 (1975).
120. Førland, E. J., Hanssen-Bauer, I. & Nordli, P. Ø. *Climate statistics and longterm series of temperature and precipitation at Svalbard and Jan Mayen*. *Rapport 21/97 – Report Series of the Norwegian Meteorological Institute* (1997).
121. Eckerstorfer, M. & Christiansen, H. The "High Arctic Maritime Snow Climate" in Central Svalbard. *Arctic, Antarct. Alp. Res.* **43**, 11–21 (2018).
122. Vikhamar Schuler, D., Førland, E. J., Lutz, J. & Gjelten, H. M. *Evaluation of downscaled reanalysis and observations for Svalbard -- Background report for Climate in Svalbard 2100*. www.klimaservicesenter.no (2019).
123. Wickström, S., Jonassen, M. O., Vihma, T. & Uotila, P. Trends in cyclones in the high-latitude North Atlantic during 1979–2016. *Q. J. R. Meteorol. Soc.* **146**, 762–779 (2020).
124. Bintanja, R. & Andry, O. Towards a rain-dominated Arctic. *Nat. Clim. Chang. 2017 74* **7**, 263–267 (2017).
125. Isaksen, K. *et al.* Exceptional warming over the Barents area. *Sci. Reports 2022 121* **12**, 1–18 (2022).
126. Tunved, P., Ström, J. & Krejci, R. Arctic aerosol life cycle: Linking aerosol size distributions observed between 2000 and 2010 with air mass transport and precipitation at Zeppelin station, Ny-Ålesund, Svalbard. *Atmos. Chem. Phys.* **13**, 3643–3660 (2013).
127. Drotikova, T., Dekhtyareva, A., Kallenborn, R. & Albinet, A. Polycyclic aromatic hydrocarbons (PAHs) and their nitrated and oxygenated derivatives in the Arctic boundary layer: seasonal trends and local anthropogenic influence. *Atmos. Chem. Phys* **21**, (2021).
128. Skaar, J. S., Ræder, E. M., Lyche, J. L., Ahrens, L. & Kallenborn, R. Elucidation of contamination sources for poly- and perfluoroalkyl substances (PFASs) on Svalbard (Norwegian Arctic). *Environ. Sci. Pollut. Res.* **26**, 7356–7363 (2019).
129. Kwok, K. Y. *et al.* Transport of Perfluoroalkyl substances (PFAS) from an arctic glacier to downstream locations: Implications for sources. *Sci. Total Environ.* **447**, 46–55 (2013).
130. Knutsen, H., Mæhlum, T., Haarstad, K., Slinde, G. A. & Arp, H. P. H. Leachate emissions of short- and long-chain per- and polyfluoralkyl substances (PFASs) from various Norwegian landfills. *Environ. Sci. Process. Impacts* **21**, 1970–1979 (2019).
131. Ademollo, N. *et al.* Occurrence, distribution and pollution pattern of legacy and emerging organic pollutants in surface water of the Kongsfjorden (Svalbard, Norway): Environmental contamination, seasonal trend and climate change. *Mar. Pollut. Bull.* **163**, 111900 (2021).

132. Wong, F. *et al.* Assessing temporal trends and source regions of per- and polyfluoroalkyl substances (PFASs) in air under the Arctic Monitoring and Assessment Programme (AMAP). *Atmos. Environ.* **172**, 65–73 (2018).
133. Barbaro, E. *et al.* Measurement report: Spatial variations in ionic chemistry and water-stable isotopes in the snowpack on glaciers across Svalbard during the 2015-2016 snow accumulation season. *Atmos. Chem. Phys.* **21**, 3163–3180 (2021).
134. Hermanson, M. H., Isaksson, E., Divine, D., Teixeira, C. & Muir, D. C. G. Atmospheric deposition of polychlorinated biphenyls to seasonal surface snow at four glacier sites on Svalbard, 2013–2014. *Chemosphere* **243**, 125324 (2020).
135. Koziol, K. A., Moggridge, H. L., Cook, J. M. & Hodson, A. J. Organic carbon fluxes of a glacier surface: A case study of Foxfonna, a small Arctic glacier. *Earth Surf. Process. Landforms* **44**, 405–416 (2019).
136. Vecchiato, M. *et al.* Fragrances and PAHs in snow and seawater of Ny-Ålesund (Svalbard): Local and long-range contamination. *Environ. Pollut.* **242**, 1740–1747 (2018).
137. Bertò, M. *et al.* Variability in black carbon mass concentration in surface snow at Svalbard. *Atmos. Chem. Phys* **21**, 12479–12493 (2021).
138. Spolaor, A. *et al.* Diurnal cycle of iodine, bromine, and mercury concentrations in Svalbard surface snow. *Atmos. Chem. Phys.* **19**, 13325–13339 (2019).
139. Spolaor, A. *et al.* Source, timing and dynamics of ionic species mobility in the Svalbard annual snowpack. *Sci. Total Environ.* **751**, 141640 (2021).
140. Spolaor, A. *et al.* Investigation on the Sources and Impact of Trace Elements in the Annual Snowpack and the Firn in the Hansbreen (Southwest Spitsbergen). *Front. Earth Sci.* **8**, 664 (2021).
141. Zdanowicz, C. *et al.* Elemental and water-insoluble organic carbon in Svalbard snow: A synthesis of observations during 2007-2018. *Atmos. Chem. Phys.* **21**, 3035–3057 (2021).
142. Grzesiak, J. *et al.* Microbial community development on the surface of Hans and Werenskiold Glaciers (Svalbard, Arctic): a comparison. *Extremophiles* **19**, 885–897 (2015).
143. Platt, S. M. *et al.* Atmospheric composition in the European Arctic and 30 years of the Zeppelin Observatory, Ny-Ålesund. *Atmos. Chem. Phys* **22**, 3321–3369 (2022).
144. Divine, D. *et al.* Thousand years of winter surface air temperature variations in Svalbard and northern Norway reconstructed from ice core data. *Polar Res.* **30**, (2011).
145. Kwok, K. Y. *et al.* Transport of Perfluoroalkyl substances (PFAS) from an arctic glacier to downstream locations: Implications for sources. *Sci. Total Environ.* **447**, 46–55 (2013).
146. Codling, G. *et al.* The fate of per- and polyfluoroalkyl substances within a melting snowpack of a boreal forest. *Environ. Pollut.* **191**, 190–198 (2014).
147. Plassmann, M. M. *et al.* Laboratory Studies on the Fate of Perfluoroalkyl Carboxylates and Sulfonates during Snowmelt. *Environ. Sci. Technol* **45**, 6872–6878 (2011).
148. Hansen, B. L. & Langway, J. C. C. Deep core drilling in ice and core analysis at Camp Century, Greenland, 1961-1966. *Antarct. J. United States* **1**, 207–208 (1966).
149. Petit, J. R. *et al.* Climate and atmospheric history of the past 420,000 years from the Vostok ice core, Antarctica. *Nature* **399**, 429–436 (1999).
150. Ubl, S., Scheringer, M. & Hungerbühler, K. Relationships between Atmospheric Transport Regimes and PCB Concentrations in the Air at Zeppelin, Spitsbergen. *Environ. Sci. & Technol.* **51**, 9784–9791 (2017).
151. Wong, F. *et al.* Assessing temporal trends and source regions of per- and polyfluoroalkyl substances (PFASs) in air under the Arctic Monitoring and Assessment Programme (AMAP). *Atmos. Environ.* **172**, 65–73 (2018).
152. Pavlova, P. A. *et al.* Polychlorinated Biphenyls in a Temperate Alpine Glacier: 1. Effect of Percolating Meltwater on their Distribution in Glacier Ice. *Environ. Sci. Technol.* **49**, 14085–14091 (2015).
153. Matykiewiczová, N., Klánová, J. & Klán, P. Photochemical degradation of PCBs in snow. *Environ. Sci. Technol.* **41**, 8308–8314 (2007).
154. Garmash, O. *et al.* Deposition History of Polychlorinated Biphenyls to the Lomonosovfonna Glacier, Svalbard: A 209 Congener Analysis. *Environ. Sci. Technol.* **47**, 12064–12072 (2013).
155. Pavlova, P. A. *et al.* Polychlorinated biphenyls in glaciers. 1. Deposition history from an Alpine ice core. *Environ. Sci. Technol.* **48**, 7842–7848 (2014).
156. Wang, X. *et al.* Accumulation of Perfluoroalkyl Compounds in Tibetan Mountain Snow: Temporal Patterns from 1980 to 2010. *Environ. Sci. Technol.* **48**, 173–181 (2014).
157. Hermanson, M. H. *et al.* Current-use and legacy pesticide history in the Austfonna ice cap, Svalbard, Norway. *Environ. Sci. Technol.* **39**, 8163–8169 (2005).
158. Giannarelli, S. *et al.* Chemosphere Paleo-environmental record of polycyclic aromatic hydrocarbons and polychlorobiphenyls at the peripheral site GV7 in Victoria Land (East. *Chemosphere* **174**, 390–398 (2017).

159. Garmash, O. *et al.* Deposition history of polychlorinated biphenyls to the lomonosovfonna glacier, Svalbard: A 209 congener analysis. *Environ. Sci. Technol.* **47**, 12064–12072 (2013).
160. Hermanson, M. H. *et al.* Deposition history of brominated flame retardant compounds in an ice core from Holtedahlfonna, Svalbard, Norway. *Environ. Sci. Technol.* **44**, 7405–7410 (2010).
161. Villa, S., Vighi, M., Maggi, V. & Finizio, A. Historical Trends of Organochlorine Pesticides in an Alpine Glacier. *J. Atmos. Chem.* **46**, 295–311 (2003).
162. Kirchgeorg, T., Dreyer, A., Gabrielli, P., Gabrieli, J. & Thompson, L. G. Seasonal accumulation of persistent organic pollutants on a high altitude glacier in the Eastern Alps. *Environ. Pollut.* **218**, 804–812 (2016).
163. Kotlyakov, V. M., Arkhipov, S. M., Henderson, K. A. & Nagornov, O. V. Deep drilling of glaciers in Eurasian Arctic as a source of paleoclimatic records. *Quat. Sci. Rev.* **23**, 1371–1390 (2004).
164. Isaksson, E. *et al.* A new ice-core record from Lomonosovfonna, Svalbard: viewing the 1920-97 data in relation to present climate and environmental conditions. *J. Glaciol.* **47**, 335–245 (2001).
165. Wendl, I. A., Eichler, A., Isaksson, E., Martma, T. & Schwikowski, M. 800-year ice-core record of nitrogen deposition in Svalbard linked to ocean productivity and biogenic emissions. *Atmos. Chem. Phys* **15**, 7287–7300 (2015).
166. Ruggirello, R. M. *et al.* Current use and legacy pesticide deposition to ice caps on Svalbard, Norway. *J. Geophys. Res. Atmos.* **115**, (2010).
167. Alley, R. B. & Bentley, C. R. Ice-Core Analysis on the Siple Coast of West Antarctica. *Ann. Glaciol.* **11**, 1–7 (1988).
168. Mariani, I. *et al.* Temperature and precipitation signal in two Alpine ice cores over the period 1961-2001. *Clim. Past* **10**, 1093–1108 (2014).
169. Kekonen, T., Moore, J., Perämäki, P. & Martma, T. The Icelandic Laki volcanic tephra layer in the Lomonosovfonna ice core, Svalbard. *Polar Res.* **24**, 33–40 (2005).
170. Wastegård, S. & Davies, S. M. An overview of distal tephrochronology in northern Europe during the last 1000 years. *J. Quat. Sci.* **24**, 500–512 (2009).
171. Hicks, S. & Isaksson, E. Assessing source areas of pollutants from studies of fly ash, charcoal, and pollen from Svalbard snow and ice. *J. Geophys. Res. Atmos.* **111**, (2006).
172. Stein, A. F. *et al.* NOAA's HYSPLIT Atmospheric Transport and Dispersion Modeling System. *Bull. Am. Meteorol. Soc.* **96**, 2059–2077 (2015).
173. Osmont, D. *et al.* An 800-year high-resolution black carbon ice core record from Lomonosovfonna, Svalbard. *Atmos. Chem. Phys.* **18**, 12777–12795 (2018).
174. Ruppel, M. M. *et al.* Increase in elemental carbon values between 1970 and 2004 observed in a 300-year ice core from Holtedahlfonna (Svalbard). *Atmos. Chem. Phys.* **14**, 11447–11460 (2014).
175. Iizuka, Y., Igarashi, M., Kamiyama, K., Motoyama, H. & Watanabe, O. Ratios of Mg2+/Na+ in snowpack and an ice core at Austfonna ice cap, Svalbard, as an indicator of seasonal melting. *J. Glaciol.* **48**, 452–460 (2002).
176. Gordiyenko, F. G., Kotlyakov, V. M., Punning, Y.-K. M. & Vairmäe, R. Polar Geography Study of a 200-m core from the lomonosov ice plateau on spitsbergen and the paleoclimatic implications. (2008) doi:10.1080/10889378109388695.
177. Van Pelt, W. J. J. *et al.* Simulating melt, runoff and refreezing on Nordenskiöldbreen, Svalbard, using a coupled snow and energy balance model. *Cryosphere* **6**, 641–659 (2012).
178. Pohjola, V. A. *et al.* Effect of periodic melting on geochemical and isotopic signals in an ice core from Lomonosovfonna, Svalbard. *J. Geophys. Res. Atmos.* **107**, ACL 1-1 (2002).
179. Moore, J. C., Grinsted, A., Kekonen, T. & Pohjola, V. Separation of melting and environmental signals in an ice core with seasonal melt. *Geophys. Res. Lett.* **32**, 1–4 (2005).
180. Marchenko, S., Pohjola, V., Pettersson, R., Van Pelt, W. & Reijmer, C. Thermal conductivity of firn at Lomonosovfonna, Svalbard, derived from subsurface temperature measurements. *Cryosph.* **13**, 1843–1859 (2019).
181. Van Pelt, W. *et al.* A long-term dataset of climatic mass balance, snow conditions, and runoff in Svalbard (1957-2018). *Cryosphere* **13**, 2259–2280 (2019).
182. Grieman, M. M., Aydin, M., Isaksson, E., Schwikowski, M. & Saltzman, E. S. Aromatic acids in an Arctic ice core from Svalbard: A proxy record of biomass burning. *Clim. Past* **14**, 637–651 (2018).
183. Beaudon, E. *et al.* Lomonosovfonna and Holtedahlfonna ice cores reveal east–west disparities of the Spitsbergen environment since AD 1700. *J. Glaciol.* **59**, 1069–1083 (2013).
184. Marchenko, S. *et al.* A plot-scale study of firn stratigraphy at Lomonosovfonna, Svalbard, using ice cores, borehole video and GPR surveys in 2012–14. *J. Glaciol.* **63**, 67–78 (2017).

185. Spolaor, A. *et al.* Sea ice dynamics influence halogen deposition to Svalbard. *Cryosphere* **7**, 1645–1658 (2013).
186. Burgay, F. *et al.* First discrete iron(II) records from Dome C (Antarctica) and the Holtedahlfonna glacier (Svalbard). *Chemosphere* **267**, 129335 (2021).

Chapter 2

Per- and Polyfluoroalkyl Substances (PFAS): an Ice Core Perspective

This chapter reviews and compares findings from existing PFAS ice core records

2.1 Abstract 50
2.2 Introduction 51
2.3 Literature 51
2.4 Description of Ice Core Records 52
2.5 Discussion 53
2.5.1 PFAS detected and Levels 53
2.5.2 PFCA Even:Odd Molar Ratios and Precursor Sources 56
2.5.3 PFCA Source Distribution Profiles 58
2.5.4 Further discussion and limitations 62
2.6 Conclusion 63
2.7 References 65

This chapter was conceptualised and written by William F. Hartz.

2.1 Abstract

Six published ice core records from the Canadian Arctic, the European Alps and the Himalayas show that ice cores can provide multiyear deposition records that can be used to understand the atmospheric transport processes of PFAS. These ice core records are reviewed here to provide context to the data generated from Svalbard in this thesis. Perfluoroalkyl carboxylic acids (PFCAs) were widely detected in these high-altitude records. This suggested that atmospheric processes contribute to widespread global deposition of PFCAs. Fluorotelomer alcohols (FTOHs) were identified as possible atmospheric precursors to C_6 – C_{11} PFCAs in the Canadian Arctic. In the European Alps, FTOHs were also possible atmospheric precursors, however upward transport of PFCAs from local PFAS sources in the surrounding valleys may have also contributed. Apart from 4:2 FTOH, FTOHs were not found to be an important precursor to PFCAs in the Himalayas. The PFCA distribution profile for the Himalayan cores was distinctively different compared to the European and Canadian Arctic cores. This suggested that an alternative emission source in Asia (or different time span of the records) may have contributed to this difference. The PFCA distribution profile also suggested that the European Alps and Devon Ice Cap, Canada, shared a common PFAS source. The median concentrations of several PFCAs on the Devon Ice Cap were higher than on some Eurasian sites. This suggested that atmospheric processes in the Arctic may enhance PFCA formation, but it was unclear why. More work is required to understand and verify this. Perfluorooctane sulfonic acid (PFOS) was detected in the Devon Ice Cap core and several other records, but it was unclear what precursor, or other atmospheric process, might enable the remote deposition of PFOS. C_2 and C_3 PFCAs were only measured in two ice cores but at significantly higher levels compared to PFOA and PFOS. This review identifies the need for future ice core studies at new locations to understand the atmospheric processes PFOS and C_1 – C_3

perfluoroalkyl acids (PFAAs), and what processes might contribute to possibly higher PFCA deposition in the Arctic. Furthermore, sampling surface snow over several months, would enable investigation into sub-annual (i.e. seasonal) trends in PFAS deposition. This might be potentially important, given the photochemical processes identified in this review.

2.2 Introduction

Per- and polyfluoroalkyl substances (PFAS) are a wide-ranging group of organofluorine compounds.[1] Many PFAS are persistent, toxic and bioaccumulative,[2–4] and have been found ubiquitously in the environment.[5] Existing research has found that atmospheric precursors can degrade in the atmosphere to form perfluoroalkyl carboxylic acids (PFCAs) and perfluoroalkyl sulfonic acids (PFSAs), which are both types of perfluoroalkyl acids (PFAAs). These precursors include fluorotelomer alcohols (FTOHs),[6,7] *N*-alkylated perfluoroalkane sulfonamides (FASAs),[8] perfluoroalkane sulfonamido ethanols (FOSEs),[9]and chlorofluorocarbon (CFC) replacement products.[10–13] Since PFAAs will readily be removed from the atmosphere by wet deposition,[14] ice cores can serve as useful tool to understanding the historic atmospheric deposition of PFAS over several years. This review uses six ice cores from the Canadian Arctic, the European Alps and the Himalayas to assess PFAS levels and distribution profiles as well as the atmospheric processes (e.g. precursor degradation) that could have contributed to PFAS deposition on these glaciers.

2.3 Literature

The ice cores reviewed here all (i) provided a continuous multiyear record of PFAS accumulation, (ii) were analysed for more than one PFAS, (iii) were dated using at least annual layer counting with $\delta^{18}O$, (iv) were retrieved from an established ice coring site, and (v) were published in a peer-review journal prior to submission of this thesis (23rd July 2022). These screening factors ensured: (i) a long-term continuous record of PFAS deposition, (ii) the possibility to investigate PFAS

distribution profiles within a single core, (iii) that sequential annual layers had broadly been identified, (iv) that the ice core was retrieved from a site known to produce ice core reliable records, and (v) a high quality of PFAS analysis. Six ice cores from five publications were identified for this review (Table 1), and three studies did not fulfil these criteria.[15–17]

2.4 Description of Ice Core Records

Table 1. Summary of existing PFAS ice core records

	Location	Abbreviation	PFAS detected	Coordinates	Altitude (m)	Dates	Years	Depth (m)	Date Drilled	Study
European Alps	Colle Gnifetti	CG08	$C_4 – C_{14}$ PFCAs, PFOS	45.93°N, 7.88°E	4455	1996 - 2007	11	10	August 2008	Kirchgeorg et al., 2013[18]
	Alto dell'Ortles	AO09	$C_4 – C_{14}$ PFCAs, PFOS	46.51°N, 10.54°E	3830	2005 - 2009	4	10	June 2009	Kirchgeorg et al., 2016[19]
Canadian Arctic	Devon Ice Cap	Dv15	$C_2 – C_{14}$, C_{16}, C_{18} PFCAs, PFBS, PFHpS, PFOS, FOSA	75.2°N, 82.7°W	2175	1977 - 2015	38	15.5	May 2015	Pickard et al., 2018[20] Pickard et al., 2020[21]
	Mt Oxford Icefield	Ox17	$C_2 – C_4$ PFCAs	82.19°N, 72.96°W	1784	1967 - 2017	50	16.5	May 2017	Pickard et al., 2020[21]
Himalayas	Mt Muztagata	Mz99	C_5, C_6, $C_8 – C_{12}$ PFCAs, PFOS	38.28°N, 75.10°E	6300	1980 - 1999	19	22.4	September 1999	Wang et al., 2014[22]
	Mt Zuoqiupu	Zq07	C_4, C_5, C_6, $C_8 – C_{10}$ PFCAs	29.21°N, 96.92°E	5600	1996 - 2007	11	30	May 2007	Wang et al., 2014[22]

The ice cores included in this review had been drilled during 1999 – 2017 and had records that spanned the years 1967 – 2017. They were drilled in the Canadian Arctic, the European Alps and the Himalayas. All ice cores were drilled at high elevation sites, relative to the region they were collected from. This offered the possibility to understand regional atmospheric processes over local signals. All ice cores were relatively shallow (10 – 30 m). Depending on the accumulation at each

site, the cores were able to cover 4 – 50 years of deposition, and hence the focus was on atmospheric process in the most recent years. Ice cores with the longest timespans from the Canadian Arctic were compared with global PFAS emission records.[20,21] In contrast, shorter records, with a higher time resolution were used to investigate seasonality in PFAS deposition.[19] All ice cores targeted PFAAs, and they are known to be the atmospheric degradation products of precursors.[6] All cores targeted C_4 – C_{11} PFCAs and PFOS, apart from the Ox17 core which only records C_2 – C_4 PFCAs. All publications discussed that melt water percolation could have disturbed the PFAS deposition records. The atmospheric sources and processes of PFAS for these six cores, are herein investigated.

2.5 Discussion

2.5.1 PFAS detected and Levels

Table 2. PFAS Detection Frequencies in all 6 ice cores

	CG08	**AO09**	**Dv15**	**Ox17**	**Mz99**	**Zq07**
TFA			100%	96%		
PFPrA			100%	100%		
PFBA	100%	100%	97%	100%	0%	50%
PFPeA	92%	95%	76%		100%	33%
PFHxA	100%	95%	100%		80%	17%
PFHpA	100%	100%	100%		0%	0%
PFOA	100%	100%	100%		100%	100%
PFNA	100%	100%	100%		60%	25%
PFDA	100%	100%	100%		70%	33%
PFUnDA	92%	100%	92%		50%	0%
PFDoDA	100%	95%	14%		60%	0%
PFTrDA	77%	62%	5%		0%	0%
PFTDA	62%	71%	0%		0%	0%
PFHxDA			0%			
PFOcDA			0%			
PFBS		0%	5%		0%	0%
PFPeS		0%				
PFHxS		0%	0%		0%	0%
PFHpS		0%	5%		0%	0%
PFOS	23%	57%	100%		100%	0%
PFDS		0%	0%		0%	0%

The detection frequencies between these six ice cores show that PFAS is widespread in glaciers in the Canadian Arctic, European Alps and Himalayas (Table 2). Many of these cores have been retrieved from high altitude remote locations and this would suggest that the atmospheric processes of PFAS have enabled this contaminant to become globally distributed. Long-range atmospheric processes could be through the atmospheric degradation of precursors whereas short-range atmospheric processes could be from nearby sources. For example, in the European Alps, settlements in the valleys are known to be able to act as a local seasonal source of contaminants to high altitude glaciers through convective mixing.[23]

PFOA, one of the major PFAS produced, was detected ubiquitously in all sections of all ice cores that targeted this compound. Hence, PFOA input into high altitude glaciated areas in Canadian Arctic, European Alps and Himalayas has been constant for several years, indeed up to several decades at some locations. This suggests that an effective mechanism(s) exists for the atmospheric deposition of PFOA. PFNA, which is also a major PFCA degradation product of 8:2 FTOH, was also detected in all ice cores that targeted this compound.

PFOS was also detected in every core (that targeted this analyte), apart from the Zq07 ice core (Himalayas). The lack of detection of PFOS in the Zq07 record (1996 – 2007) was thought to be due to the decline of atmospheric PFOS emissions (and/or its precursors).[22] This could be corroborated by Pickard et al. who found that deposition of FOSA (a manufacturing product of PSOF and a possible atmospheric precursor of PFOS) had significantly decreased on the Devon Ice Cap after 2000.[20] However, PFOS deposition continued after this date on the Devon Ice Cap, despite 3M phasing out the production of POSF by electrochemical fluorination (ECF).[24] The lack of detection of PFOS in the Zq07 ice core could be instead due to the relatively high detection limit for PFOS (25 pg/L compared to 1.3 pg/L for the Devon Ice Cap core). Hence it is possible

that PFOS deposition still occurred at Zq07, albeit below detection limit.

PFBA was detected in all ice cores apart from the Mz99 core. The presence of PFBA in the Zq07 core was attributed to the atmospheric degradation of 4:2 FTOH, with precursor emissions coming from the Indian subcontinent. The lack of detection of PFBA in the Mz99 core (1980 – 1999) was attributed to the lack of PFAS emissions with C_4 chemistry during the time span of this core.[22]

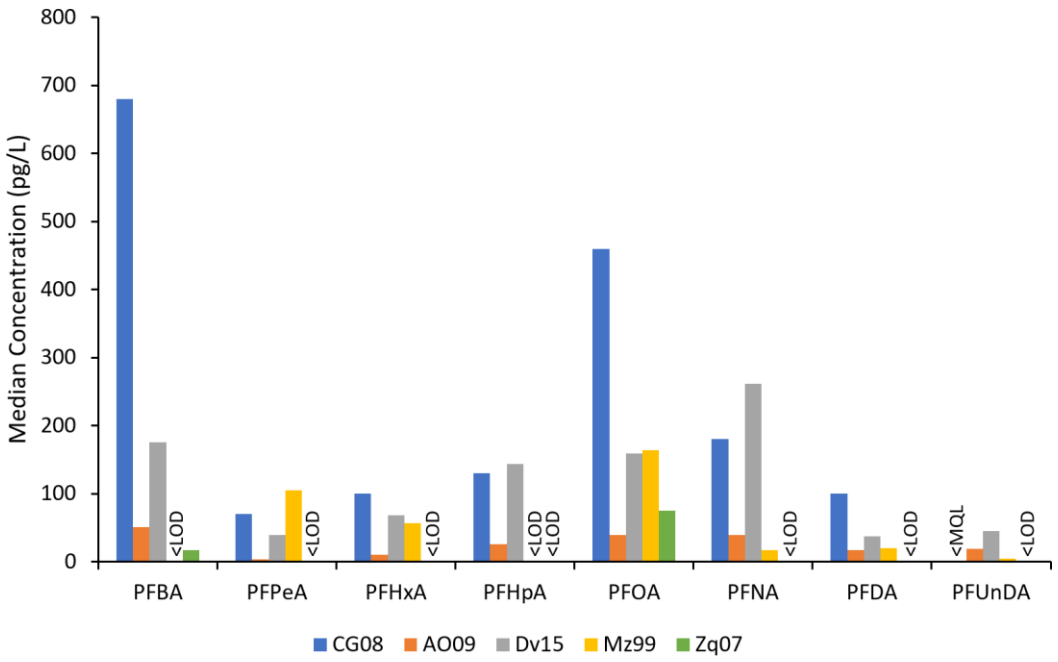


Figure 1. Median Concentrations in C_4 – C_{11} PFCAs in the CG08, AO09, Dv15, Ox17, Mz99 and Zq07 ice cores. <LOD = below the limit of detection, <MQL = below the limit of quantification.

The median concentrations of C_4 – C_{11} PFCAs (Figure 1) were typically lower in the AO09 and Zq07 ice cores, and typically highest in Dv15 and CG08 cores. However, it would be expected that the Arctic ice core from the Devon Ice Cap would have the lowest median PFCA concentrations, due to its remoteness from possible PFAS sources. It is unclear what processes have contributed to the Dv15 core often having higher median concentrations than some Alpine and Himalayan sites. Variations in median concentrations between these 6 cores could be due to:

(i) proximity to nearby PFAS sources, (ii) the varying source profiles at each site, (iii) differences in PFAS emissions due to the varying time spans covered by each core, (iv) seasonal variations in snow accumulation at each site, and (v) variations in the oxidative capacity of the atmosphere at each site. It cannot be excluded that variations in PFAS analytical methodology between the studies may have affected the accuracy of some results. Nonetheless, variations in the oxidative capacity (e.g. from OH radicals) of the atmosphere would be expected to affect the rate at which PFAS precursor degradation products are formed. Hence, higher than expected PFCA median concentrations on the Devon Ice Cap could be due to a higher oxidative capacity of the Arctic atmosphere during summer. Modelling has suggested that PFOA formation from 8:2 FTOH in the Arctic atmosphere in the summer is higher than other parts of the world (e.g. European Alps and Himalayas) due to low NO_x concentrations.[25] Indeed, the median concentration of PFNA (the major PFCA degradation product of 8:2 FTOH) was highest in the Devon Ice Cap core. For the CG08 core, the higher median concentrations of PFBA and PFOA could be due to the upward transport of PFAS from nearby sources in the valleys surrounding the site. This process was also thought to affect the PFAS deposition in the AO09 core.[19] It can also be that high winds in winter, which are known to remove 7 – 41% of the winter snow accumulation at Colle Gnifetti, would remove snow with a possibly lower PFAA content. As such the CG08 core is largely consisting of summer accumulation, which possibly had a higher PFAS content and this inflated the PFAS concentrations in the core.[18]

2.5.2 PFCA Even:Odd Molar Ratios and Precursor Sources

Since FTOHs make up a large proportion of long chain precursors (≥ 6 carbons) in the atmosphere (e.g. Chapter 1, Table 5), it is worth investigating if they are able to provide an atmospheric precursor source for PFCA formation.[26] Even-odd pairs of PFCAs were used to calculate their

molar ratios (for TFA:PFPrA, PFBA:PFPeA, PFHxA:PFHpA, PFOA:PFNA and PFDA:PFUnDA). This was to investigate if FTOHs could be possible precursor sources of PFCAs (for 2:2 FTOH, 4:2 FTOH, 6:2 FTOH, 8:2 FTOH and 10:2 FTOH, respectively). If even:odd PFCA molar ratios are between 0.5 and 2, this could indicate a possible FTOH source.[27] Table 3 shows the percentage of core sections whereby the molar ratios were found to be between 0.5 and 2.

Table 3. Percentage of Even:Odd ratios between 0.5 and 2

	CG08	**AO09**	**Dv15**	**Ox17**	**Mz99**	**Zq07**
TFA:PFPrA	-	-	36%	6%	-	-
PFBA:PFPeA	0%	0%	0%	-	0%	100%
PFHxA:PFHpA	100%	29%	78%	-	0%	0%
PFOA:PFNA	36%	83%	94%	-	0%	0%
PFDA:PFUnDA	100%	100%	72%	-	0%	0%

Of the two Arctic ice cores analysed for TFA and PFPrA, neither had high enough percentages to suggest 2:2 FTOH was a source. No ice cores had PFBA:PFPrA ratios between 0.5 and 2 (all 0%), except for the Zq07 core (100 %), suggesting a 4:2 FTOH precursor source for this core. Indeed, this core was thought to be most influenced by air masses containing 4:2 FTOH from the Indian subcontinent.[22] Li et al. found on average that this precursor was the most abundant neutral PFAS in the atmosphere in India (of 14 neutral PFAS measured).[28] However, no other Himalayan ice core had even:odd ratios between 0.5 and 2, suggesting that 6:2 FTOH, 8:2 FTOH and 10:2 FTOH were not significant precursor sources. Furthermore, the lack of detection of PFHpA (the major PFCA degradation product of 6:2 FTOH), and low detection frequencies of PFNA (the major PFCA degradation product of 8:2 FTOH) in the Himalayan cores is in contrast to the other cores. This suggests that a significantly different precursor source profile (or otherwise) exists for C_6 – C_{11} PFCAs in these two Himalayan ice cores. This is likely due to different time spans of these two cores (i.e. the Mz99 core spanned 1980 – 1999 and the Zq07 core

1996 – 2007) and exposure to different emission sources in this part of Asia. Indeed, the continuous detection of PFOA, but complete lack of detection of PFHpA for these two cores, suggests an atmospheric process which does not involve a radical mediated unzipping process. This unzipping cycle would produce a complete range of PFCAs of varying chain lengths and is known to exist during the degradation of FTOHs, FASAs and FOSEs.[6,8,9]

The two cores from the European Alps were inconsistent in indicating 6:2 FTOH and 8:2 FTOH as possible atmospheric precursors, suggesting that these FTOHs only made-up part of the sources for C_6 – C_9 PFCAs in these cores. For example, in the CG08 core, the high median concentration of PFOA (Figure 1) could indicate a PFOA input from sources in the valley, which then raises the PFOA:PFNA ratio greater than 2.[29] In contrast, the PFHxA:PFHpA and PFOA:PFNA molar ratios for the Dv15 core indicated that 6:2 FTOH and 8:2 FTOH were significant sources of C_6 – C_9 PFCAs in the Canadian Arctic. All cores outside of the Himalayas had high percentages of core sections with PFDA:PFUnDA molar ratios between 0.5 and 2, suggesting that 10:2 FTOH was a precursor source at these sites.

Kirchgeorg et al. suggested that PFOS deposition in the CG08 and AO09 cores could occur from the atmospheric degradation of PFOS precursors or from particle-bound transport of PFOS to the glaciers.[18,19] However, no study was able to provide evidence to suggest an atmospheric transport mechanism for PFOS for the ice cores in this review.

2.5.3 PFCA Source Distribution Profiles

The percentage mass contribution for individual C_4 – C_{11} PFCAs is plotted for five of the cores in Figure 2. Both the Himalayan cores had a similar distribution profile of C_4 – C_{11} PFCAs. Wang et al. suggested that the Mz99 core had been influenced by European sources,[22] however its PFCA distribution profile does not reflect that of the CG08 or AO09 cores from the European Alps.

Instead, the Mz99 PFCA distribution profile could be due to Asian sources or due to the earlier time span recorded by the Mz99 core. Regardless, PFOA had the most significant mass contribution of PFCAs in the Himalayan cores (42 – 59%). There was a large similarity in the PFCA distribution profile for the Dv16 and AO09 cores. However, it was unclear what processes contributed to the Dv16 core having consistently higher median concentrations of C_4 – C_{11} PFCAs compared to the AO09 core (Figure 1). Regardless, the similarity between these two records, and also to some extent the CG08 core, suggests that the Devon Ice Cap has been influenced by European sources of PFCA precursors.

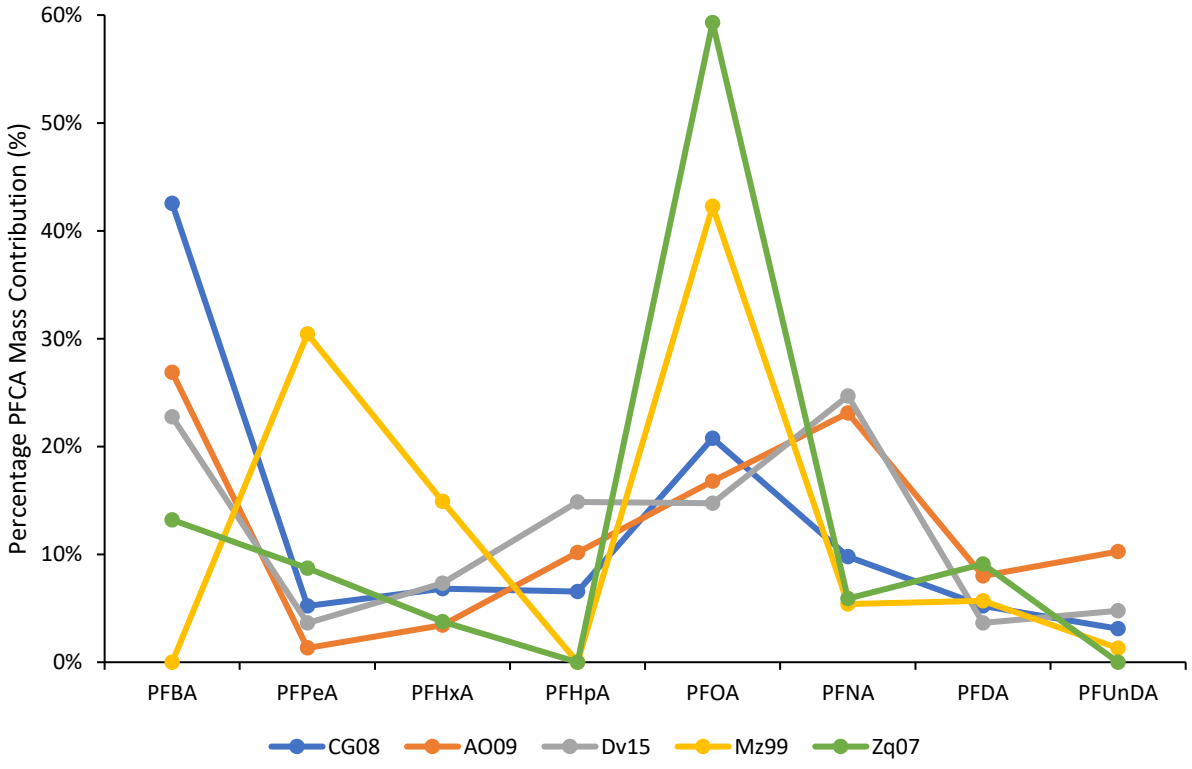


Figure 2. The percentage mass contribution of individual PFCAs to C_4 – C_{11} PFCAs in the CG08, AO09, Dv15, Mz99 and Zq07 ice cores

All cores had a relatively large contribution of PFBA (13 – 43%) apart from the Mz99 core.

As discussed previously, this was thought to be a result of the lower emissions of PFAS with C_4 chain lengths during the time span of this ice core (1980 – 1999). For the remaining ice cores, each publication suggested various sources including direct emissions from local sources, particle-bound transport, atmospheric degradation of CFC replacement products and atmospheric degradation of other precursors such as FTOHs. Regardless of the source, the phasing out of PFAS with C_8 chain lengths and increased emissions of CFC replacement products will likely influence the atmospheric deposition of C_2 – C_4 PFCAs in future PFAS ice core records.[21]

2.5.4 Temporal Trends

Ice cores offer a unique perspective to assess temporal trends in atmospheric deposition on timescales and locations not possible for long term atmospheric monitoring. Figure 3 shows to historical deposition of PFBA, PFOA and PFOS in these ice core records. For PFBA, all cores outside of the Himalayas show increasing concentrations after 1995 – 2000. This likely reflects an increasing shift to C_4 based chemistry as well as the increased use of hydrofluorocarbons, and other CFC replacement products, after the introduction of the Montreal Protocol in 1989.[30] PFOA shows broadly consistent concentrations in Arctic and Himalayan records since the late 1980s. It is difficult to establish whether the efforts to reduce PFOA precursors (i.e. 8:2 FTOH)[31] and other emission sources have had an effect due to limited PFOA ice core records after 2008. Whilst temporal trends are limited and unclear for PFOS, measurable deposition in ice cores has existed since 1977. The studies reporting PFAS records in the AO09, Zq07, Dv15 and Ox17 cores all commented that summer meltwater percolation might have somewhat influenced the PFAS temporal records.

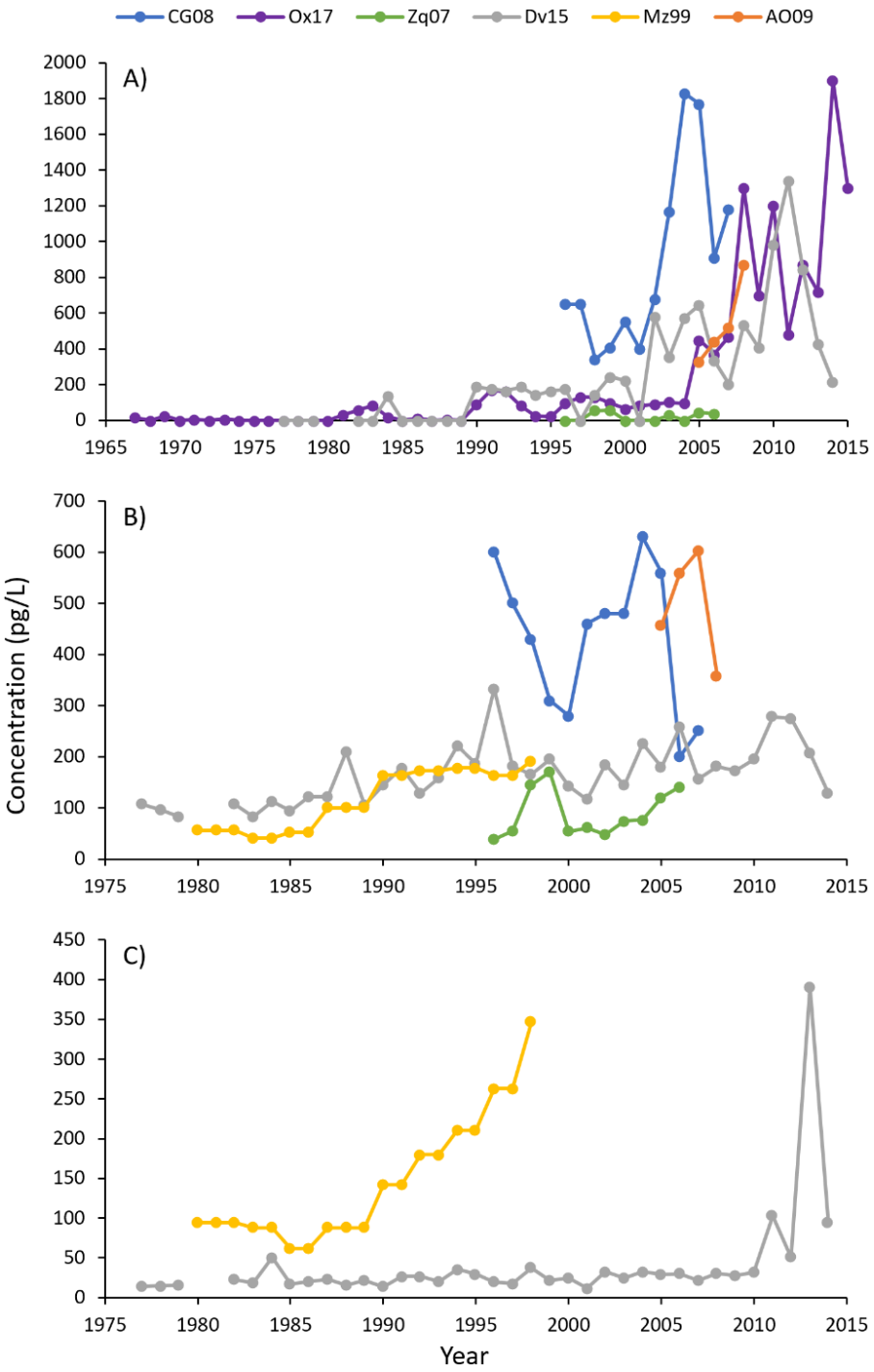


Figure 3. Yearly concentrations of A) PFBA, B) PFOA and C) PFOS in the CG08, AO09, Dv15, Ox17, Mz99 and Zq07 cores. For PFBA, those sections with concentrations <LOD/<MQL were substituted with zero values (and the Mz99 core was excluded for this reason also). For PFOS only the Dv15 and Mz99 cores had values >MQL.

2.5.5 Further discussion and limitations

This review is limited by a shortage of publications reporting more geographically widespread PFAS analysis in ice cores, as well as variations in the time span of each of the ice core records. For example, it is hard to draw conclusions about the sources of PFAS for the Mz99 core, due to differences in the time span of the core compared to the Zq07, CG08 and AO09 cores. Several locations have yet to report PFAS deposition records from ice cores. In particular, no records have yet been published from Antarctica or anywhere in the southern hemisphere.[15] Svalbard has been identified as a good location to study the long-range atmospheric deposition of organic contaminants,[32] however no such record from Svalbard was used in this review. Kwok et al. analysed two ice cores from the Longyearbreen glacier, which is 3.5 km from the centre of the Longyearbyen settlement, however limited information on the dating of these cores was provided and no $\delta^{18}O$ record was reported.[16] Furthermore, the Longyearbreen glacier is unable to produce a continuous multiyear ice core record since vast parts of the glacier have been in negative mass balance for several years and it is not an established ice coring site.[33] Hence the results from the Longyearbreen glacier were excluded from this study. Future ice core records for PFAS might look at the possibilities for new sites in Svalbard, the Russian Arctic, South America, and Antarctica. This would be with the intent to understand more about PFAS atmospheric processes in the Arctic and southern hemisphere.

Future studies should carefully consider the possible influences of melt percolation on their ice core record, given the high solubility of PFAAs.[34] Melt water percolation is known to affect the deposition record of organic contaminants.[35] In the Dv15 and CG08 cores, PFAS were investigated for correlations with Na^+ ions, however no significant correlations were found. This indicated that marine aerosols were not a significant source of PFAS to these ice cores since Na^+

ions can be considered as a marine aerosol proxy. Nonetheless, major ions were found to provide a useful tool in further understanding PFAS sources, and future studies could include major ion analyses to assist in source elucidation.

Future research might also consider redrilling an ice core from Mt Muztagata to be able to compare the past two decades with the existing cores. Given the implications of the Montreal Protocol and associated recent amendments (e.g. Kigali amendment), future ice cores should consider including analysis of C_2 and C_3 PFCAs, which have already been found at high levels in two Arctic ice cores compared to longer chain PFAAs (e.g. PFOA and PFOS).[21] In addition, as PFOA and PFOS are phased out, future studies should aim to include replacement products (e.g. GenX) to test if these might also be transported by atmospheric processes. Nonetheless, many of the drilling sites referred to in this review are likely subject to increased summer melt in the future. Regardless, more work needs to be done to establish whether existing international regulation has been sufficient in limiting PFAS deposition to remote regions (e.g. limited recent records for PFOA and PFOS in Figure 3). Together this highlights the importance of retrieving new records in the coming years and the establishment of new locations where meltwater percolation is likely limited.

2.6 Conclusion

In summary, these six ice core records have provided useful year-on-year PFAS atmospheric deposition records in the European Alps, the Canadian Arctic and the Himalayas. FTOHs were identified as possible atmospheric precursors to C_6 – C_{11} PFCAs in the Canadian Arctic, and somewhat also in the European Alps. However, the sources of these PFCAs in the Himalayan ice core records were likely coming from an alternative source, possibly due to variations in the time spans of the cores and differences in PFAS emissions in southern Asia. C_4 –

C_{11} PFCAs were detected at all sites (except for PFHpA in the Himalayan cores), indicating that atmospheric processes contribute to widespread deposition of PFCAs. The median concentrations of $C_4 – C_{11}$ PFCAs on the Devon Ice Cap in the Canadian Arctic were higher than some Himalayan and Alpine sites, suggesting that atmospheric processes in the Arctic may enhance PFCA deposition, although it was unclear why this might be. Despite the detection of PFOS in several ice cores, including on the Devon Ice Cap in the Canadian Arctic, no study was able to identify a precursor source or other atmospheric processes that might contribute to remote PFOS atmospheric deposition.

2.7 References

1. Wang, Z. *et al.* A New OECD Definition for Per- And Polyfluoroalkyl Substances. *Environ. Sci. Technol.* **55**, 15575–15578 (2021).
2. Frömel, T. & Knepper, T. P. Biodegradation of Fluorinated Alkyl Substances. in *Reviews of environmental contamination and toxicology* vol. 208 161–177 (2010).
3. Conder, J. M., Hoke, R. A., De Wolf, W., Russell, M. H. & Buck, R. C. Are PFCAs bioaccumulative? A critical review and comparison with regulatory criteria and persistent lipophilic compounds. *Environ. Sci. Technol.* **42**, 995–1003 (2008).
4. Jensen, A. A. & Leffers, H. Emerging endocrine disrupters: perfluoroalkylated substances. *Int. J. Androl.* **31**, 161–169 (2008).
5. Giesy, J. P. & Kannan, K. Global Distribution of Perfluorooctane Sulfonate in Wildlife. *Environ. Sci. Technol.* **35**, 1339–1342 (2001).
6. Ellis, D. A. *et al.* Degradation of fluorotelomer alcohols: a likely atmospheric source of perfluorinated carboxylic acids. *Environ. Sci. Technol.* **38**, 3316–21 (2004).
7. Sulbaek Andersen, M. P. *et al.* Atmospheric chemistry of 4:2 Fluorotelomer alcohol (n-C4F9CH2CH2OH): Products and mechanism of Cl atom initiated oxidation in the presence of NO x. *J. Phys. Chem. A* **109**, 1849–1856 (2005).
8. Martin, J. W., Ellis, D. A., Mabury, S. A., Hurley, M. D. & Wallington, T. J. Atmospheric chemistry of perfluoroalkanesulfonamides: kinetic and product studies of the OH radical and Cl atom initiated oxidation of N-ethyl perfluorobutanesulfonamide. *Environ. Sci. Technol.* **40**, 864–72 (2006).
9. D'eon, J. C., Hurley, M. D., Wallington, T. J. & Mabury, S. A. Atmospheric chemistry of N-methyl perfluorobutane sulfonamidoethanol, C4F9SO2N(CH3)CH2CH2OH: kinetics and mechanism of reaction with OH. *Environ. Sci. Technol.* **40**, 1862–8 (2006).
10. Young, C. J., Hurley, M. D., Wallington, T. J. & Mabury, S. A. Atmospheric chemistry of CF3CF2H and CF3CF2CF2CF2H: Kinetics and products of gas-phase reactions with Cl atoms and OH radicals, infrared spectra, and formation of perfluorocarboxylic acids. *Chem. Phys. Lett.* **473**, 251–256 (2009).
11. Wallington, T. J. *et al.* The Environmental Impact of CFC Replacements-HFCs and HCFCs. *Environ. Sci. Technol.* **28**, (1994).
12. Oyaro, N., Sellevåg, S. R. & Nielsen, C. J. Atmospheric chemistry of hydrofluoroethers: Reaction of a series of hydrofluoroethers with OH radicals and Cl atoms, atmospheric lifetimes, and global warming potentials. *J. Phys. Chem. A* **109**, 337–346 (2005).
13. Young, C. J., Hurley, M. D., Wallington, T. J. & Mabury, S. A. Atmospheric chemistry of perfluorobutenes (CF3CF=CFCF3 and CF3CF2CF=CF2): Kinetics and mechanisms of reactions with OH radicals and chlorine atoms, IR spectra, global warming potentials, and oxidation to perfluorocarboxylic acids. *Atmos. Environ.* **43**, 3717–3724 (2009).
14. Taniyasu, S. *et al.* Does wet precipitation represent local and regional atmospheric transportation by perfluorinated alkyl substances? *Environ. Int.* **55**, 25–32 (2013).
15. Garnett, J. Investigating the occurrence and accumulation of perfluoroalkylated substances and other persistent organic pollutants in snow and ice of the Earth's Polar regions. (2020).
16. Kwok, K. Y. *et al.* Transport of Perfluoroalkyl substances (PFAS) from an arctic glacier to downstream locations: Implications for sources. *Sci. Total Environ.* **447**, 46–55 (2013).
17. Hermanson, M. H., Leonards, P., Isaksson, E. & Schwikowski, M. Burdens and inputs of perflourinated compounds in the Lomonosovfonna Ice Core, Svalbard (2009). in *6th SETAC World Conference/SETA Europe 22nd Annual Meeting* (2012).
18. Kirchgeorg, T. *et al.* Temporal variations of perfluoroalkyl substances and polybrominated diphenyl ethers in alpine snow. *Environ. Pollut.* **178**, 367–374 (2013).
19. Kirchgeorg, T., Dreyer, A., Gabrielli, P., Gabrieli, J. & Thompson, L. G. Seasonal accumulation of persistent organic pollutants on a high altitude glacier in the Eastern Alps. *Environ. Pollut.* **218**, 804–812 (2016).
20. Pickard, H. M. *et al.* Continuous non-marine inputs of per- and polyfluoroalkyl substances to the High Arctic: a multi-decadal temporal record. *Atmos. Chem. Phys.* **18**, 5045–5058 (2018).
21. Pickard, H. M. *et al.* Ice Core Record of Persistent Short-Chain Fluorinated Alkyl Acids: Evidence of the Impact From Global Environmental Regulations. *Geophys. Res. Lett.* **47**, (2020).
22. Wang, X. *et al.* Accumulation of Perfluoroalkyl Compounds in Tibetan Mountain Snow: Temporal Patterns from 1980 to 2010. *Environ. Sci. Technol.* **48**, 173–181 (2014).

23. Schwikowski, M. *et al.* Post-17th-Century Changes of European Lead Emissions Recorded in High-Altitude Alpine Snow and Ice. *Environ. Sci. Technol.* **38**, 957–964 (2004).
24. Wang, Z., Cousins, I. T., Scheringer, M. & Hungerbühler, K. Fluorinated alternatives to long-chain perfluoroalkyl carboxylic acids (PFCAs), perfluoroalkane sulfonic acids (PFSAs) and their potential precursors. *Environ. Int.* **60**, 242–248 (2013).
25. Wallington, T. J. *et al.* Formation of C7F15COOH (PFOA) and other perfluorocarboxylic acids during the atmospheric oxidation of 8:2 fluorotelomer alcohol. *Environ. Sci. Technol.* **40**, 924–30 (2006).
26. Dreyer, A., Weinberg, I., Temme, C. & Ebinghaus, R. Polyfluorinated Compounds in the Atmosphere of the Atlantic and Southern Oceans: Evidence for a Global Distribution. *Environ. Sci. Technol.* **43**, 6507–6514 (2009).
27. MacInnis, J. J. *et al.* Emerging investigator series: a 14-year depositional ice record of perfluoroalkyl substances in the High Arctic. *Environ. Sci. Process. Impacts* **19**, 22–30 (2017).
28. Li, J. *et al.* Perfluorinated compounds in the asian atmosphere. *Environ. Sci. Technol.* **45**, 7241–7248 (2011).
29. Armitage, J. M., Macleod, M. & Cousins, I. T. Comparative assessment of the global fate and transport pathways of long-chain perfluorocarboxylic acids (PFCAs) and perfluorocarboxylates (PFCs) emitted from direct sources. *Environ. Sci. Technol.* **43**, 5830–5836 (2009).
30. Velders, G. J. M., Andersen, S. O., Daniel, J. S., Fahey, D. W. & McFarland, M. The importance of the Montreal Protocol in protecting climate. *Proc. Natl. Acad. Sci. U. S. A.* **104**, 4814–4819 (2007).
31. Wang, Z., Cousins, I. T., Scheringer, M., Buck, R. C. & Hungerbühler, K. Global emission inventories for C4-C14 perfluoroalkyl carboxylic acid (PFCA) homologues from 1951 to 2030, Part I: Production and emissions from quantifiable sources. *Environ. Int.* **70**, 62–75 (2014).
32. Isaksson, E. *et al.* Ice cores from Svalbard—useful archives of past climate and pollution history. *Phys. Chem. Earth, Parts A/B/C* **28**, 1217–1228 (2003).
33. Hagen, J. O., Kohler, J., Melvold, K. & Winther, J.-G. Glaciers in Svalbard: mass balance, runoff and freshwater flux. *Polar Res.* **22**, 145–159 (2003).
34. Wang, Z. *et al.* Using COSMOtherm to predict physicochemical properties of poly- and perfluorinated alkyl substances (PFASs). *Environ. Chem.* **8**, 389–398 (2011).
35. Pavlova, P. A. *et al.* Polychlorinated Biphenyls in a Temperate Alpine Glacier: 1. Effect of Percolating Meltwater on their Distribution in Glacier Ice. *Environ. Sci. Technol.* **49**, 14085–14091 (2015).

Chapter 3

Materials and Methods

3.1 Abstract 68
3.2 Snow Sampling 69
3.2.1 Field Sampling and Sample Preparation 69
3.3 Ice Core Drilling and sample preparation 71
3.3.1 Ice core drilling 71
3.3.2 Ice core sampling preparation 72
3.4 Ice Core Dating & Ice Core Chemistry Analyses 74
3.5 PFAS analysis 75
3.5.1 Extraction and instrument analysis 75
3.5.2 Quality Assurance and Quality Control 76
3.6 Hybrid Single-Particle Lagrangian Integrated Trajectory Model Analysis (HYSPLIT) 76
3.7 References 78

3.1 Abstract

In this chapter, an overview of the field and analytical methods used this thesis is provided; detailed analytical methods are described in each data chapter. Surface snow samples were collected during January – August 2019 on Svalbard with the aim to collect samples as soon as possible after a precipitation event (i.e. event-focused sampling). In addition, a 12.3 m ice core from the Lomonosovfonna ice cap, Svalbard was also drilled (which spanned the years 2006 – 2019). Both the snow samples and the ice core were melted, extracted, and analysed for PFAS, largely with the same methods. A total of 45 PFAS analytes were targeted using supercritical fluid chromatography (SFC) tandem mass spectrometry (MS/MS) and ultra-performance liquid chromatography (UPLC) MS/MS. The Hybrid Single-Particle Lagrangian Integrated Trajectory model (HYSPLIT) was used to inspect for geographic source regions for the ice core and calculate solar radiation fluxes for each of the precipitation events sampled (i.e. for the surface snow samples). Major ions analysis of both the snow and ice core samples was performed using ion chromatography. These results were used to assist in source elucidation. In addition, this data, together with the water stable isotope data, were used for annual layer counting (ALC) to date the ice core. Herein, these methods are reported, and further details are also provided in Chapters 4 – 7.

3.2 Snow Sampling

3.2.1 Field Sampling and Sample Preparation

During January – August 2019, 32 surface snow samples were collected from several locations around Svalbard. This was with the intent of understanding local and long-range atmospheric processes of PFAS, as well as investigating seasonal variations in PFAS deposition. During this time period, the weather forecast (www.yr.no) was monitored for upcoming precipitation events. After the end of each targeted precipitation event, snow sampling was undertaken as soon as reasonably possible. This was to ensure that snow had been collected as fresh as possible and that post-depositional effects (e.g. revolatilisation losses and melt) had been minimised. However, in some cases, sampling was not possible for some days due to bad weather. Nonetheless, this approach meant that each surface snow sample represented an individual precipitation event. Further details of the locations and times of sampling are outlined in the methods sections of Chapters 5 and 6.

The upper 0 – 5 cm of snow was sampled into a precleaned barrel using a precleaned aluminium shovel. The volume of the barrel (>33 litres) allowed for a large surface area to be sampled (typically around 1.8 m^2). This ensured that snow sampling was representative of the precipitation event. The barrel was then sealed and transported back to the University Centre in Svalbard (UNIS) in Longyearbyen. Here, the barrel was stored in the fridge (5 °C) to allow the snow to melt and then bottled into precleaned polypropylene containers. In addition, a sample for major ion analyses was also collected. Melted snow samples were then stored in the fridge, until PFAS extraction. Precleaning of the sampling equipment and storage containers was done by washing with soapy water followed by several rinses with Milli-Q water and then methanol. Precise details are described in Chapters 5 and 6.

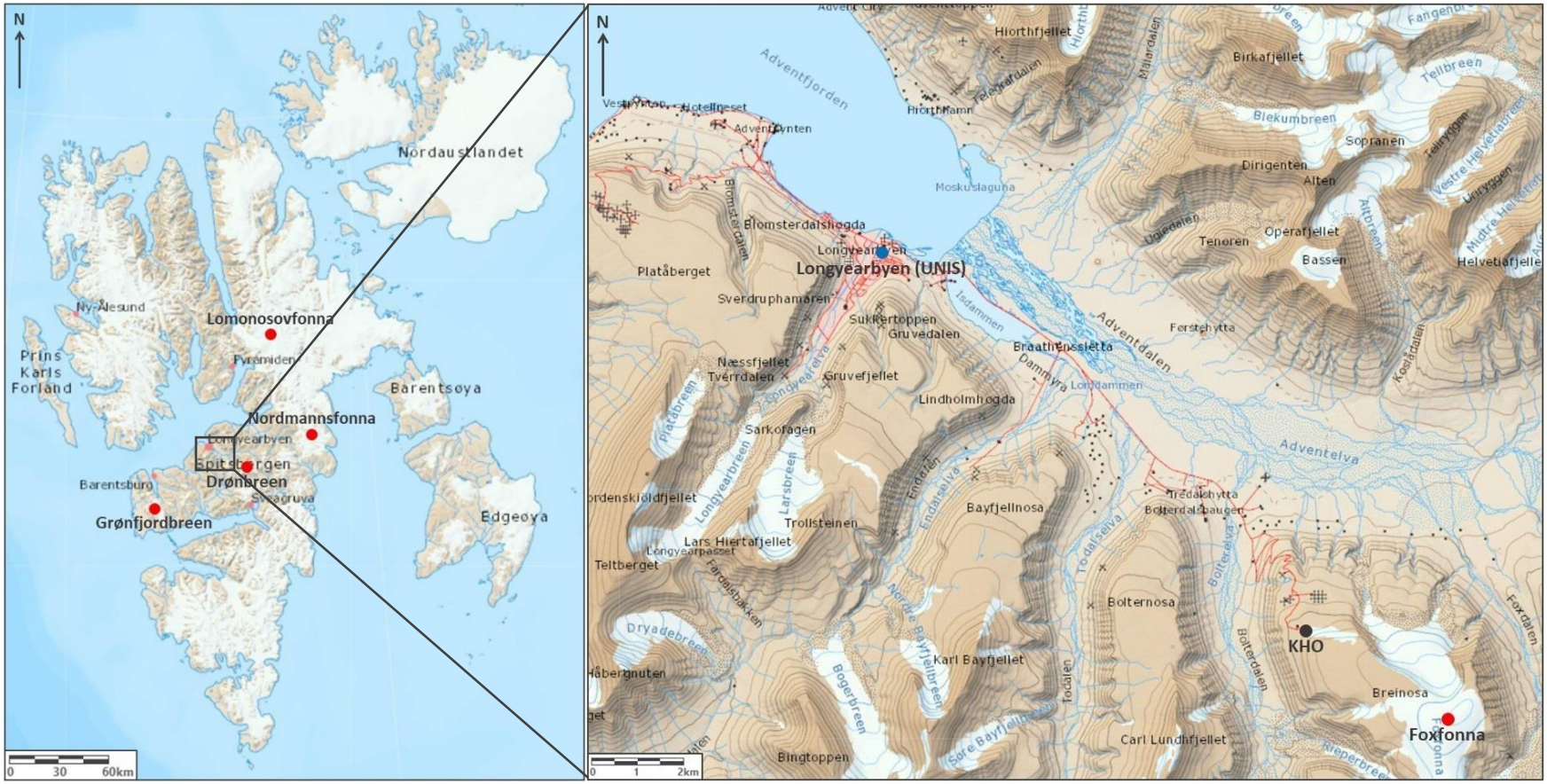


Figure 1. Map showing the sampling locations for surface snow sampling in this thesis. A 12.3 m ice core was also drilled at Lomonosovfonna.

3.3 Ice Core Drilling and sample preparation

3.3.1 Ice core drilling



Figure 2. Tent camp on Lomonosovfonna during ice core drilling in April 2019 (the drill site, 180 m away, is not shown here). Photo: Eirik Rolland Enger

During 2nd – 7th April 2019, a 6-day expedition with three people went to the 2009 Lomonosovfonna drill site (78°49.454'N, 17°26.193'E, 1198 m.a.s.l.). On the copula, a field camp was established 180 m downwind of the desired drilling location. Over 4 days during this period, a 12.27 m ice core (14.0 cm diameter) was drilled using a Kovacs Mark V core barrel and SideWinder (Kovacs Enterprise, LLC, Roseburg, OR, USA). Before travelling to Lomonosovfonna, trials with the drilling equipment were undertaken to allow for the field team to familiarise themselves with the drilling rig. During drilling of the snowpack/shallow firn on

Lomonosovfonna, the depth screws were set fully retracted and core dogs were set less aggressively. During drilling of deeper firn (approximately >7 m depth), the depth screws were set to partially protrude and core dogs were set most aggressively. After 7 m, the sidewinder was used to drill and assist with lowering and raising the core barrel. Prior to this depth, manual drilling was undertaken by hand. Wide blades were used throughout drilling. A generator was used to power the electric drill in the sidewinder and the generator was set up 25 m downwind in a snowpit of approximately 1 m deep.

After drilling, individual core sections (4.5 – 63.5 cm, average 35 cm) were sealed into airtight low-density polyethylene lay flat tubing. All 103.5 kg of samples were then carefully packed and transported back to UNIS by snowmobile. Here, they were stored frozen (-20 °C) until cutting and processing.

3.3.2 Ice core sampling preparation

Ice core sections were cut and processed in a cold room (-20 °C) as follows. Prior to cutting, each core section was unpacked and then weighed and measured in length to calculate the density. At this point, each core section was backlit to note melt features in the core. Next, each core section was cut on a precleaned aluminium surface according to Figure 3. Subsamples for water isotope analysis were collected close to the edge, whereas subsamples for major ions were taken from an inner section. The large central inner section of the core was used for PFAS analysis, and this section was no closer than 1 cm to the outer surface of the ice core (and a maximum of 2.7 cm). Core sections were handled throughout using nitrile gloves. Exterior sections not included in analyses were repacked into polyethylene bags for future analyses (shaded in grey in Figure 3).

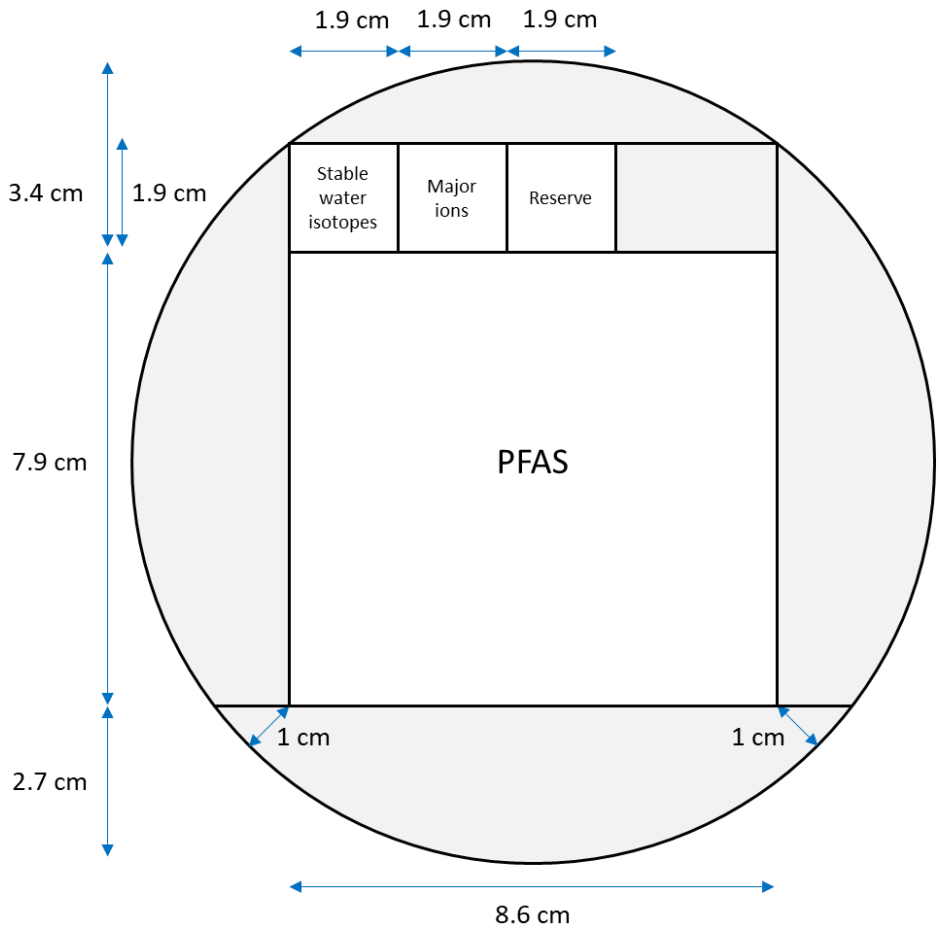


Figure 3. Cutting Scheme for the ice core indicating which sample were analysed for PFAS, stable water isotopes and major ions. Grey shaded sections were archived.

In addition to the cutting scheme, 1 cm was removed from the upper and lower ends of each core section. Overall, this approach ensured that potential contamination of the outer surfaces of the core during drilling, transport, and storage was removed. Subsamples for major ion and stable water isotope analysis were collected at a 5 cm resolution along the length of the core. Subsections for PFAS analysis were cut such that each section was at least 2 kg. In total, 17 sections for PFAS analysis were collected, as well as 205 subsamples for major ion analysis and 209 subsamples for water stable isotopes.

Prior to cutting, each core section was backlit, and clear/bubbly melt features appeared as more transparent when compared to the porous firn. Each core section was logged using the methods described by Wendl et al. for the Lomonosovfonna 2009 core.[1] In summary, the length of each melt feature was first measured, and this was multiplied by the percentage of the cross-sectional area of the core affected. This gave an effective melt layer thickness (cm). The results of this can be seen in the appendix of Chapter 4.

3.4 Ice Core Dating & Ice Core Chemistry Analyses

Measurements of the water stable isotopes and major ions were undertaken, such that annual layer counting (ALC) could be used for dating the ice core. Oxygen and hydrogen stable isotope ratios ($\delta^{18}O$ and δD) of the melted ice were analysed using isotope ratio mass spectrometry. Ion chromatography was used to measure the major ion concentrations. The cations targeted were Na^+, K^+, Mg^{2+} and Ca^{2+}. The anions targeted were methanesulfonic acid (MSA), Cl^-, Br^-, NO_3^- and SO_4^{2-}. Details of the instrument analyses for major ions and water stable isotopes are reported in Chapter 4.

Stable isotope ratios and some ionic species showed seasonal variations. $[Na^+]/[Cl^-]$ also showed seasonality, and this was used alongside $\delta^{18}O$ to undertake ALC. It was thought that $[Na^+]/[Cl^-]$ showed cycles appropriate for ALC due to seasonal acid displacement of Cl^- in aged marine aerosols (with strong acids e.g. HNO_3) to form gaseous HCl.[2] Therefore marine aerosols were possibly seasonally depleted in Cl^- relative to Na^+. As well as ALC, a peak in non-sea-salt sulfate ($nssSO_4^{2-}$) was identified as the 2011 Grímsvötn volcanic eruption in Iceland, and used as a reference horizon.[3,4] This approach found 12 complete annual layers. Therefore, it was concluded that the core spanned 2006 – 2019. A ±2 year error was applied to this owing to the possible misassignment of annual layers (see Figure S2 in the appendix of Chapter 4).

3.5 PFAS analysis

3.5.1 Extraction and instrument analysis

The melted snow and ice core samples were extracted and analysed for 45 PFAS target analytes (Chapter 5, Table S1). Samples were extracted using weak anion exchange solid-phase extraction (Oasis® WAX, Waters Corporation, Milford, USA) following the ISO25101 method, albeit with some modifications. After extraction, a neutral fraction and anionic fraction were eluted from the cartridges and the elutes analysed by SFC-MS/MS and UPLC-MS/MS. The extraction and instrument methods were identical for both the surface snow samples and ice core samples, apart from one additional step in the extraction of the snow samples. Owing to visible particles in the surface snow samples from one of the sampling sites, all surface snow samples were filtered using glass fibre filters before extraction. This was to reduce the possibility that extraction cartridges would become blocked during extraction. To ensure method consistency, this was done to all snow samples. Filters were later extracted with methanol, and extracts combined with the melted snow sample prior to extraction. Full details of the extraction methods for the surface snow samples and ice core are described in Chapters 4, 5 and 6.

SFC-MS/MS and UPLC-MS/MS instruments were used to analyse the target analytes. Isotope dilution was used for quantification with mass labelled standards. Liquid chromatography (LC) for analysis of PFAS is well established, however use of SFC for analysis is a relatively new technique.[5] In this thesis, SFC was used for separation of C_1 – C_4 PFAAs. This was because SFC produced narrower peaks in the chromatogram for these compounds compared to LC separation and there was no need to change the column on the LC instrument. SFC has several other advantages including shorter run times and less solvent usage compared to LC.[5] Further details of the instrument set ups are described in Chapters 4 – 6.

Concentrations of PFAS were reported (as mass per unit volume of melted snow/ice) Where necessary, these were converted to fluxes as a mass per unit area per year (for the ice core) or a mass per unit area per precipitation event (for the surface snow samples).

3.5.2 Quality Assurance and Quality Control

Full details of the Quality Assurance and Quality Control (QAQC) for the snow and ice core analysis can be found in Chapters 4 – 6. In these chapters, details about the limits of detection/quantification, extraction efficiencies and repeatability, and mass-labelled standards are documented. Furthermore, steps taken during snow sampling and ice core drilling in the field, as well as during snow and ice core sample preparation, to remove and reduce the possibilities of contamination during these steps are also discussed. The procedure and results for blank samples are also included in these chapters.

3.6 Hybrid Single-Particle Lagrangian Integrated Trajectory Model Analysis (HYSPLIT)

Hybrid Single-Particle Lagrangian Integrated Trajectory Model (HYSPLIT) can be used to investigate air mass sources and process.[6] Since each surface snow sample was collected after a precipitation event, a backward air mass trajectory could be calculated using HYSPLIT for each precipitation event. As the majority of PFAS will be deposited at the start of the precipitation event,[7] the backward air mass trajectory was timed to end at the onset of the precipitation event at the sampling site. A 6-day backwards airmass trajectory was used, since this is the atmospheric half-life of TFA with respect to wet and dry deposition.[8] The onset of the precipitation event could be established by inspecting meteorological data from a local weather station. A value for the total solar radiation that each air mass had been subject to, which represented the precipitation event, was also calculated. This calculation was done by summing the downward short-wave radiation at each hourly point on the trajectory.

For the ice core, a similar approach was undertaken. For the 12 complete annual layers that the ice core recorded (2007 – 2018), daily backward air mass trajectories, of again 6 days in length, were calculated. This resulted in 4383 daily backward air mass trajectories which ended at the Lomonosovfonna drilling site. These trajectories were plotted together on a trajectory frequency plot, whereby the number of trajectory intersections in each 1-degree grid cell was given as a percentage of the total number of trajectories. The results were used to access the predominant air mass source regions, as well as in four seasonal plots to access any seasonal variations in air mass source regions.

The National Centre for Environmental Prediction's Global Data Assimilation System (GDAS) model was used for the meteorological input data. Further details of the HYSPLIT analysis are described for the ice core in Chapter 4 and for the surface snow samples in Chapters 5 and 6.

3.7 References

1. Wendl, I. High resolution records of black carbon and other aerosol constituents from the Lomonosovfonna 2009 ice core. (Paul Scherrer Institut and University of Bern, 2014).
2. Wang, X. *et al.* The role of chlorine in global tropospheric chemistry. *Atmos. Chem. Phys.* **19**, 3981–4003 (2019).
3. Burgay, F. *et al.* First discrete iron(II) records from Dome C (Antarctica) and the Holtedahlfonna glacier (Svalbard). *Chemosphere* **267**, (2021).
4. Karasiński, G. *et al.* Lidar Observations of Volcanic Dust over Polish Polar Station at Hornsund after Eruptions of Eyjafjallajökull and Grímsvötn. *Acta Geophys.* **62**, 316–339 (2014).
5. Yeung, L. W. Y., Stadey, C. & Mabury, S. A. Simultaneous analysis of perfluoroalkyl and polyfluoroalkyl substances including ultrashort-chain C2 and C3 compounds in rain and river water samples by ultra performance convergence chromatography. *J. Chromatogr. A* **1522**, 78–85 (2017).
6. Stein, A. F. *et al.* NOAA's HYSPLIT Atmospheric Transport and Dispersion Modeling System. *Bull. Am. Meteorol. Soc.* **96**, 2059–2077 (2015).
7. Taniyasu, S. *et al.* Does wet precipitation represent local and regional atmospheric transportation by perfluorinated alkyl substances? *Environ. Int.* **55**, 25–32 (2013).
8. Kotamarthi, V. R. *et al.* Trifluoroacetic acid from degradation of HCFCs and HFCs: A three-dimensional modeling study. *J. Geophys. Res. Atmos.* **103**, 5747–5758 (1998).

Chapter 4

Levels and Distribution Profiles of Per- and Polyfluoroalkyl Substances (PFAS) in a High Arctic Svalbard Ice Core

William F. Hartz,[a,b] Maria K. Björnsdotter,[c,d] Leo W. Y. Yeung,[d] Andrew Hodson,[b,e] Elizabeth R. Thomas,[f] Jack D. Humby,[f] Chris Day,[a] Ingrid Ericson Jogsten,[d] Anna Kärrman,[d] Roland Kallenborn[g,h]

In review at Science of the Total Environment, submitted November 2022

4.1 Abstract 81
4.2 Introduction 82
4.3 Materials and Methods 85
4.3.1 Ice Core Drilling and Dating 85
4.3.2 Sample Preparation and PFAS Analysis 86
4.3.3 Ice Core Dating and Data Treatment 87
4.4 Results and Discussion 88
4.4.1 Fluxes and Concentrations of PFAS on Lomonosovfonna 88
4.4.2 Chemical Sources of PFCAs to Lomonosovfonna 91
4.4.3 Chemical Sources of PFSAs to Lomonosovfonna 96
4.4.4 Temporal Trends in PFAS Deposition 98
4.4.5 Marine environment as a source of PFAS 100
4.4.6 Air mass source regions 101
4.4.7 Redistribution of PFAS during melt 103
4.5 Conclusion 106
4.6 References 109
4.7 Supporting Information 113

This chapter was conceptualised by William F. Hartz, who also undertook the fieldwork, sample preparation, PFAS sample extraction, data interpretation and writing as well as assisting with ion chromatography. PFAS elution preparation, instrument analysis, and data processing was led by Maria K. Björnsdotter and ion chromatography analysis by Jack Humby. Maria K. Björnsdotter, Jack Humby and Chris Day wrote part of the methods in the Supporting Information. All co-authors have assisted in editing of the manuscript.

[a]Department of Earth Sciences, University of Oxford, South Parks Road, Oxford, OX1 3AN, United Kingdom

[b]Department of Arctic Geology, University Centre in Svalbard (UNIS), NO-9171, Longyearbyen, Svalbard, Norway

[c]Institute of Environmental Assessment and Water Research (IDAEA-CSIC), C/Jordi Girona, 18-26, 08034 Barcelona, Catalonia, Spain

[d]Man-Technology-Environment Research Centre (MTM), Örebro University, SE-701 82 Örebro, Sweden

[e]Department of Environmental Sciences, Western Norway University of Applied Sciences, NO-6851, Sogndal, Norway

[f]Ice Dynamics and Paleoclimate, British Antarctic Survey, High Cross, Cambridge, CB3 0ET, United Kingdom

[g]Faculty of Chemistry, Biotechnology and Food Sciences (KBM), Norwegian University of Life Sciences (NMBU), NO-1432 Ås, Norway

[h]Department of Arctic Technology, University Centre in Svalbard (UNIS), NO-9171, Longyearbyen, Svalbard, Norway

4.1 Abstract

Per- and polyfluoroalkyl substances (PFAS) are a group of persistent organic contaminants of which some are toxic and bioaccumulative. Several PFAS can be formed from the atmospheric degradation of precursors such as fluorotelomer alcohols (FTOHs) as well as hydrochlorofluorocarbons (HFCs) and other ozone-depleting chlorofluorocarbon (CFC) replacement compounds. Svalbard ice cores have been shown to provide a valuable record of long-range atmospheric transport of contaminants to the Arctic. This study uses a 12.3 m ice core from the remote Lomonosovfonna ice cap on Svalbard to understand the atmospheric deposition of PFAS in the Arctic. A total of 45 PFAS compounds were targeted, of which 26 were detected, using supercritical fluid chromatography (SFC) tandem mass spectrometry (MS/MS) and ultra-performance liquid chromatography (UPLC) MS/MS. C_2 to C_{11} perfluoroalkyl carboxylic acids (PFCAs) were detected continuously in the ice core and their fluxes ranged from 2.5 – 8200 ng m^{-2} yr^{-1} (9.51 – 16,500 pg L^{-1}). Trifluoroacetic acid (TFA) represented 71% of the total mass of C_2 – C_{11} PFCAs in the ice core and had increasing temporal trends in deposition. The distribution profile of PFCAs suggested that FTOHs were likely the atmospheric precursor to C_8 – C_{11} PFCAs, whereas C_2 – C_6 PFCAs had alternative sources, such as HFCs and other CFC replacement compounds. Perfluorooctanesulfonic acid (PFOS) was also widely detected in 82% of ice core subsections, and its isomer profile (81% linear) indicated an electrochemical fluorination manufacturing source. Comparisons of PFAS concentrations with a marine aerosol proxy showed that marine aerosols were insignificant for the deposition of PFAS on Lomonosovfonna. Comparisons with a melt proxy showed that TFA and PFOS were mobile during meltwater percolation. This indicates that seasonal snowmelt and runoff from post-industrial accumulation on glaciers could be a significant seasonal source of PFAS to ecosystems in Arctic fjords.

4.2 Introduction

Per- and polyfluoroalkyl substances (PFAS) are a diverse group of organofluorine compounds, used in a variety of industrial and consumer applications.[1] However, many PFAS are persistent, toxic and bioaccumulative.[2–4] Research has been particularly focused on perfluoroalkyl acids (PFAAs), including perfluoroalkyl carboxylic acids (PFCAs) and perfluoroalkyl sulfonic acids (PFSAs). The ubiquitous detection of PFAAs and other PFAS in the environment, including Arctic biota and abiota confirms the high environmental mobility of PFAS.[5]

The low volatility and high solubility of PFCAs and PFSAs do not promote direct long-range atmospheric transport from industrialized or populated areas to remote regions, such as the Arctic.[6] However, several mechanisms for long-range transport of PFAS to the Arctic have been proposed and investigated. One such mechanism is through long-range ocean currents, whereby ocean currents distribute PFAS from source regions to remote Arctic marine environments.[7,8] Marine aerosols have also been identified as PFAS carriers for long-range transport.[9] The long-range atmospheric transport of volatile precursor PFAS, followed by their atmospheric degradation to PFAAs and subsequent deposition has also been identified.[10,11] However, the relative significance of each transport mechanism is unclear.

Several volatile neutral PFAS have been identified as atmospheric precursors to PFAS degradation products. These include fluorotelomer alcohols (FTOHs), N-alkylated perfluoroalkane sulfonamides (FASAs), perfluoroalkane sulfonamido ethanols (FOSEs), and fluorotelomer acrylates (FTAs), several of which have been identified in the Arctic atmosphere, including in Svalbard (Norwegian Arctic).[12–16] These studies found FTOHs dominated the mass of precursors detected and that the most abundant precursor targeted was 8:2 FTOH.

Several studies have undertaken laboratory experiments to investigate the atmospheric

chemistry of precursors including FTOHs,[10,17] FASAs,[18] FOSEs,[19] and FTAs.[20] All found that these precursors would be able to degrade via a gaseous radical-mediated process to a suite of equal or shorter chain PFCAs aided by an unzipping cycle. Once PFAAs have formed in the atmosphere, they will be effectively scavenged by wet deposition.[21] Hence during precipitation, the vast majority of PFAAs will be removed from the atmosphere and undergo deposition.[22,23]

Whilst trifluoroacetic acid (TFA) and shorter chain PFAAs can form from the degradation of longer chain precursors such as FTOHs,[10] these short-chain PFAAs can have additional more significant atmospheric precursors. For example, hydrofluorocarbons (HFCs),[24] hydrochlorofluorocarbons (HCFCs),[25] hydrofluoroethers (HFEs),[26] and hydrofluoroolefins (HFOs)[27] have been identified as atmospheric precursors to TFA and other short-chain PFAAs. HFCs, HCFCs, HFEs, and HFOs were introduced as replacement products for ozone-depleting chlorofluorocarbons (CFCs) in the 1990s. CFCs were previously used as cooling agents but were banned in 1989 after the introduction of the Montreal protocol.[28] However, TFA has been found ubiquitously in surface snow, including in the Arctic,[29] and environmental levels are increasing.[30,31] Trifluoromethanesulfonic acid (TFMS) was also recently detected ubiquitously in surface snow in the Arctic, however, the study was not able to assign a source (Chapter 5).[29]

Ice cores can provide a record of several years of snow accumulation and hence a route to understanding PFAS atmospheric sources and transformation processes. Remote ice cores spanning several years have already been used to elucidate atmospheric sources of PFAS on the Devon Ice Cap and Mt Oxford icefield in the Canadian Arctic.[30,32] Unlike long-term atmospheric monitoring studies, ice cores can help to retrospectively investigate atmospheric processes and deposition. Svalbard (Norwegian Arctic) is known to receive contaminated air masses from Eurasia and has several established sites for ice core research.[33] Lomonosovfonna is the highest

elevation site (1198 m.a.s.l.) in the Svalbard Archipelago (Section 1.5.3, Chapter 1) and is sufficiently remote and high elevation to capture predominantly long-range processes.[34,35] A study of 22 sites on Svalbard glaciers identified Lomonosovfonna as an optimal site to investigate long-range pollution deposition.[36] As observed elsewhere in the Arctic, local sources of PFAS have also been identified in Svalbard, including firefighting training and landfill sites in Longyearbyen and Ny-Ålesund.[37–39]

This study uses a 12.3 m ice core (spanning 2006 to 2019) from Lomonosovfonna to investigate the long-range atmospheric deposition of PFAS to the Arctic. By targeting 45 different PFAS analytes, this study aims to understand the sources and processes for PFAS deposition on Lomonosovfonna. This study (i) compares annual PFAS fluxes with other remote Arctic ice cores, (ii) elucidates PFAS precursor sources or otherwise (iii) compares PFAS concentrations with a marine aerosol proxy, (iv) investigates air mass source regions, and (v) investigates the redistribution of PFAS during meltwater percolation. To the best of our knowledge, this work reports the first remote ice core in the European Arctic to be analyzed for neutral and ultra-short chain PFAS, as well as several other PFAS.

4.3 Materials and Methods

4.3.1 Ice Core Drilling and Dating

In April 2019, a 12.3 m ice core (2006 – 2019), diameter 14.0 cm, was drilled on Lomonosovfonna (78°49.454'N, 17°26.193'E, 1198 m.a.s.l., Figure 1) using a Kovacs Mark V core barrel and SideWinder (Kovacs Enterprise, LLC, Roseburg, OR, USA). The ice core was transported to the University Centre in Svalbard (UNIS) in Longyearbyen by snowmobile and stored at -20°C prior to analysis. Further information on the characteristics of the site is described in the supporting information (page S1).



Figure 1. Map showing the location of the Lomonosovfonna ice core drilling site. Insert: Location of Svalbard in the northern hemisphere. The map was reproduced from TopoSvalbard, Norwegian Polar Institute.

4.3.2 Sample Preparation and PFAS Analysis

A total of 45 different PFAS analytes were targeted as follows. PFAAs targeted were C_2 – C_{14}, C_{16}, and C_{18} PFCAs, and C_1 – C_{10} and C_{12} PFSAs. Fluorotelomers targeted were 4:2 FTSA, 6:2 FTSA, 8:2 FTSA, 6:2 FTUCA and 8:2 FTUCA. Further anionic target analytes included 6:2 Cl-PFESA, 8:2 Cl-PFESA, HFPO-DA (GenX), and ADONA. In total, 9 neutral compounds were also targeted: FBSA, MeFBSA, FHxSA, MeFHxSA, FOSA, MeFOSA, EtFOSA, MeFOSE and EtFOSE. C_2 – C_3 PFCAs and C_1 – C_3 PFSAs were measured by supercritical fluid chromatography (SFC) tandem mass spectrometry (MS/MS) system. All other compounds were measured by ultra-performance liquid chromatography (UPLC) MS/MS. A full list of names, abbreviations and instrument methods are described in Table S1.

In the cold lab (-20°C), the outer surfaces of the ice core (1.0 – 2.3 cm) were carefully removed and discarded to avoid possible contamination from drilling, handling, transport, and storage. Subsamples for water stable isotopes and major ions were collected at a 5 cm resolution. Subsections for PFAS analysis (n = 17) were sampled sequentially, such that each section was at least 2 kg, into sterile polyethylene whirltop bags, which were then stored frozen at -20°C. Immediately prior to extraction, ice core samples were melted and bottled into precleaned polypropylene containers. Samples were extracted by weak anion exchange solid-phase extraction following the ISO25101 method with some modifications.[40] Full details of the chemicals and reagents, sample extraction, instrument analysis, quality control and quality assurance, MQLs (method quantification limits), Hybrid Single-Particle Lagrangian Integrated Trajectory model

(HYSPLIT) analysis, major ion analysis and water stable isotope analysis can be found in the supporting information (pages S1 – S8).

4.3.3 Ice Core Dating and Data Treatment

An age-depth relationship for the ice core was established using a multi-proxy approach including (i) seasonal variations in the stable isotope ratio $\delta^{18}O$, (ii) seasonal variations in the $[Na^+]/[Cl^-]$ ratio, and (iii) a peak in non-sea-salt sulfate ($nssSO_4^{2-}$) at 404.5 cm water equivalent (weq) assigned to be the 2011 Grímsvötn volcanic eruption in Iceland.[41,42] As such, 12 complete annual layers were observed, and the annual layers were counted from 2019 back to 2006 ±2 years (Figure S1).

PFAS analyte concentrations are reported in pg L^{-1}. In order to remove the effects of annual accumulation variability (measured to be 26 – 75 cm weq for 2007 – 2018 from this ice core), annual flux values were also calculated. Analyte concentrations (in pg L^{-1}) were first converted into ng $year^{-1}$. This was then divided by the cross-sectional area of the ice core (0.0154 m^2) to give a flux value in ng m^{-2} yr^{-1}. The values for the Na^+ concentrations and melt proxy $\log([Na^+]/[Mg^{2+}])$ for each PFAS subsection of the ice core, were calculated by averaging across the 5 cm subsamples (n = 7 – 19) for each of the PFAS subsections. Spearman rank correlation coefficients (r) were used to calculate correlations. Tests for statistical significance were performed using a two-tailed Student's t-test (p).

4.4 Results and Discussion

4.4.1 Fluxes and Concentrations of PFAS on Lomonosovfonna

In summary, all C_2 – C_{11} PFCAs were detected continuously throughout the whole core which spanned 2006 - 2019 (n = 17). There was also widespread detection of FBSA, FOSA, PFHxS, and PFOS, as well as C_{12} and C_{13} PFCAs (all greater than 50% >MQL). C_{14} and C_{15} PFCAs, PFBS, PFPeS, 6:2 FTSA, 6:2 FTUCA, 8:2 FTUCA and 5 neutral PFAS (MeFBSA, FHxSA, EtFOSA, MeFOSE and EtFOSE) were also detected, albeit at a lesser occurrence (with detection less than 50% >MQL). C_{18} PFCA, C_2, C_3, C_7, C_9, C_{10}, and C_{12} PFSAs, 4:2 FTSA, 8:2 FTSA, PFECHS, 4 PFAS with ether functionality (6:2 Cl-PFESA, 8:2 Cl-PFESA, ADONA and HFPO-DA i.e. GenX) and 2 neutral PFAS (MeFHxSA and MeFOSA) were not detected throughout the entire core. Herein, fluxes (ng m^{-2} yr^{-1}) and concentrations (pg L^{-1}) are reported. Further information on detection, concentrations, and fluxes can be found in Tables S7 – S12.

For C_2 – C_{11} PFCAs, fluxes ranged from 2.5 - 8200 ng m^{-2} yr^{-1} (9.51 – 16,500 pg L^{-1}). Fluxes of these PFCAs increased greatly toward shorter chain lengths (Figure 2). Indeed, TFA represented 71% of the mass of C_2 – C_{11} PFCAs detected in the core. Longer chain lengths contributed significantly less mass: PFPrA (16%), PFBA (6%), PFPeA (2%), PFHxA (1%), PFHpA (1%) and C_8 – C_{11} PFCAs (each <1%). Of the PFSAs targeted, only PFBS, PFPeS, PFHxS, and PFOS were detected. PFOS was the dominant PFSA, detected in 82% of the subsections with fluxes ranging from 1.7 – 70 ng m^{-2} yr^{-1} (<MQL – 195 pg L^{-1}). PFHxS was detected in 65% of the subsections and its fluxes ranged from 0.12 – 1.0 (<MQL – 28.3 pg L^{-1}). PFBS was detected in 24% of the subsections (<MQL – 28.4 pg L^{-1}). 6:2 FTSA was also detected in 41% of subsections (<MQL – 14.1 pg L^{-1}). Both 6:2 FTUCA and 8:2 FTUCA were detected in 35% and 6% of subsections, respectively (<MQL – 194 pg L^{-1}). Of the 9 targeted neutral compounds, 7 were

detected. The most notable of these were FBSA and FOSA, which were detected in 82% and 59% of subsections.

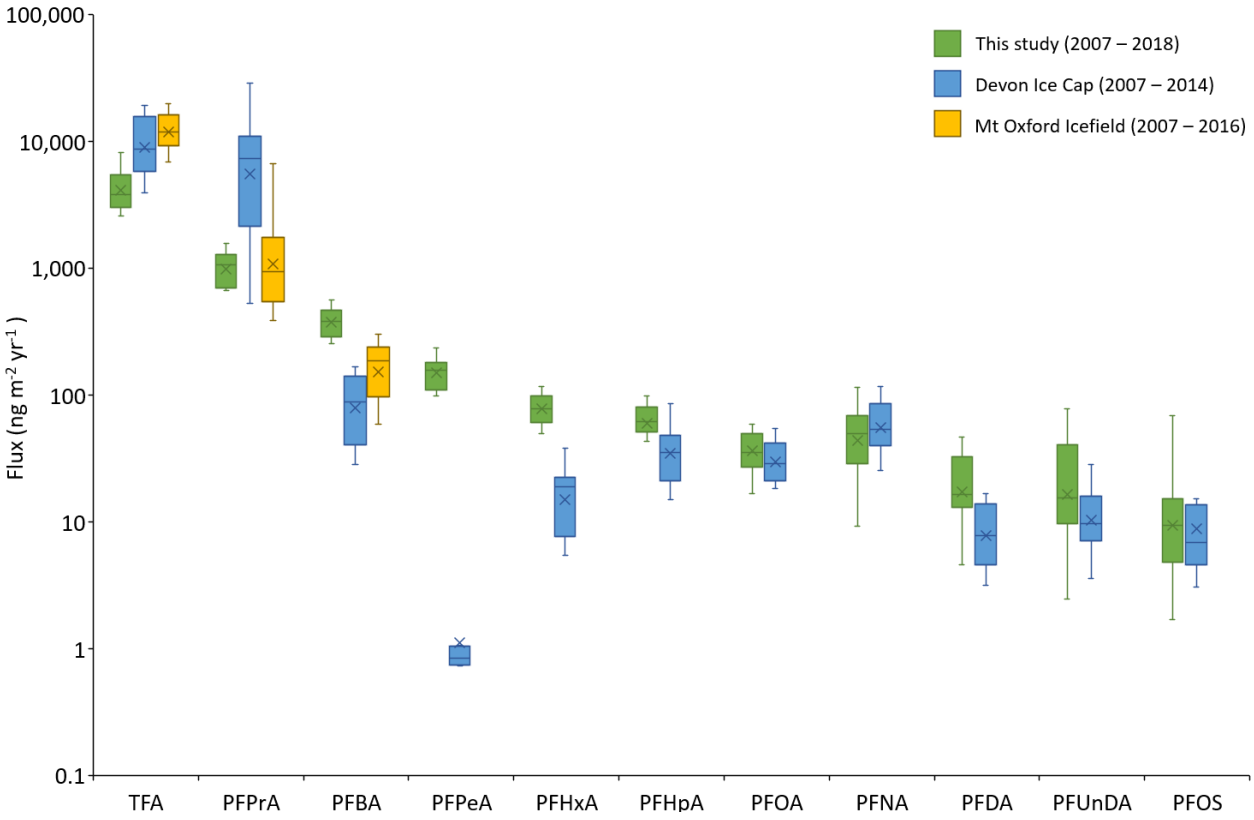


Figure 2. Fluxes (ng m^{-2} yr^{-1}) of C_2 – C_{11} PFCAs and PFOS in Arctic ice cores from Lomonosovfonna (2007 – 2018, this study), Devon Ice Cap (2007 – 2014)[30,32] and the Mt Oxford icefield (2007 – 2016).[30] Cross = mean, horizontal line = median.

Prior to this study, two other remote Arctic ice cores have been analyzed for PFAS. One of these is from the Devon Ice Cap in the Canadian Arctic and has targeted 23 PFAS including a range of PFCAs and PFSAs.[30,32] The second is from the Mt Oxford icefield in the Canadian Arctic which has targeted C_2 – C_4 PFCAs.[30] Both the Devon Ice Cap and Lomonosovfonna ice cores had widespread detection of C_2 – C_{11} PFCAs. Another study has measured several PFAS in an ice core from the Longyearbreen glacier on Svalbard.[43] However, owing to the proximity of this site to a

number of significant PFAS sources in Longyearbyen settlement (4 – 10 km),[38,39] it would be inappropriate to use this record to understand the background atmospheric processes of PFAS in the Arctic. Furthermore, Longyearbreen is not an established site for multiyear ice core records on Svalbard and its high equilibrium line altitude (~615 m.a.s.l. in 2004) casts doubt on the potential to retrieve reliable multiyear ice core records from this glacier.[44] An overview comparing the fluxes of C_2 – C_{11} PFCAs and PFOS on Lomonosovfonna (2007 – 2018, this study), Devon Ice Cap (2007 – 2014)[30,32], and Mt Oxford Ice Cap (2007 – 2016)[30] can be seen in Figure 2. For measurements below the limit of detection, fluxes were calculated using half the limit of detection (which was only for some measurements of PFOS on Lomonosovfonna and PFPeA on the Devon Ice Cap). Herein, the comparisons between fluxes and detection frequencies refer to these time periods.

The fluxes of TFA and PFPrA were typically lower on Lomonosovfonna compared to the Devon Ice Cap and Mt Oxford icefield. In contrast, the fluxes of PFBA were higher on Lomonosovfonna, compared to the Devon Ice Cap and Mt Oxford icefield. For C_5 – C_{11} PFCAs, measured only on the Devon Ice Cap, fluxes were similar or higher on Lomonosovfonna. C_5 – C_7 PFCAs were higher on Lomonosovfonna – fluxes of PFPeA, PFHxA, and PFHpA were on average 56, 4.6 and 1.6 times greater. The fluxes of PFDA and PFUnDA were also 2.3 and 2.0 times higher on Lomonosovfonna compared to the Devon Ice Cap. PFDoDA and PFTrDA were detected much more frequently in the Lomonosovfonna ice core (82% and 88%, respectively) compared to the Devon Ice Cap core (13% and 0%, respectively), despite similar detection limits around 2 – 4 pg L^{-1} for both ice cores. In contrast, the cores have similar fluxes of PFOA, PFNA and PFOS. United States Environmental Protection Agency (EPA) drinking water health advisory levels were

consistently exceeded for both ice cores for PFOA, and sometimes exceeded for PFOS, despite their remote Arctic locations.

FOSA fluxes remained low with 0.37 – 4.6 ng m^{-2} yr^{-1} (<MQL – 9.56 pg L^{-1}) on Lomonosovfonna and <MQL – 2.97 ng m^{-2} yr^{-1} (<MQL – 1.5 pg L^{-1}) on the Devon Ice Cap. This is most likely as a result of the phasing out of the production of perfluorooctane sulfonyl fluoride (POSF) by 3M between 2000 and 2002.[32]

The variability in fluxes between the three sites might be explained by the differences in each site's proximity to various sources and/or the differences in seasonal variations in accumulation on these glaciers. It is known that the deposition of some PFAAs in the Arctic is highly seasonal, with increased deposition during months with 24-hour daylight (Chapter 5).[29] Hence, increased accumulation in the winter months might underrepresent the relative atmospheric levels of some PFAAs. Indeed on Svalbard, precipitation is known to be greater during September – February, i.e. months with complete or partial darkness.[45]

4.4.2 Chemical Sources of PFCAs to Lomonosovfonna

Several laboratory-based studies have identified volatile neutral PFAS, such as FTOHs, FOSEs, FASAs, and FTAs to act as precursors and undergo a radical-mediated degradation to PFCAs.[10,17–20] These precursors are widespread in the Arctic atmosphere, with 8:2 FTOH being the dominant precursor.[12–16] According to the study by Ellis et al.,[10] the radical-mediated degradation of 8:2 FTOH should result in approximately equal molar quantities of PFOA and PFNA (0.95:1 molar ratio).[10] This may vary depending on the radical species present in the atmosphere and due to the presence of NO_x species. Nonetheless, the correlations between 45 pairs of PFCAs from TFA (C_2) – PFUnDA (C_{11}) were calculated (Table S13), since all these PFCAs were detected continuously in the ice core. All C_3 – C_6 PFCAs were significantly correlated ($r > 0.87$, $p < 0.001$) and sequential

pairs of C_7 – C_{11} PFCAs were also significantly correlated ($r > 0.69$, $p < 0.002$). TFA (C_2) was not significantly correlated with any other PFCA ($r < 0.52$, $p > 0.031$). These results suggest a distinct division between TFA (C_2), C_3 – C_6, and C_7 – C_{11} PFCA sources.

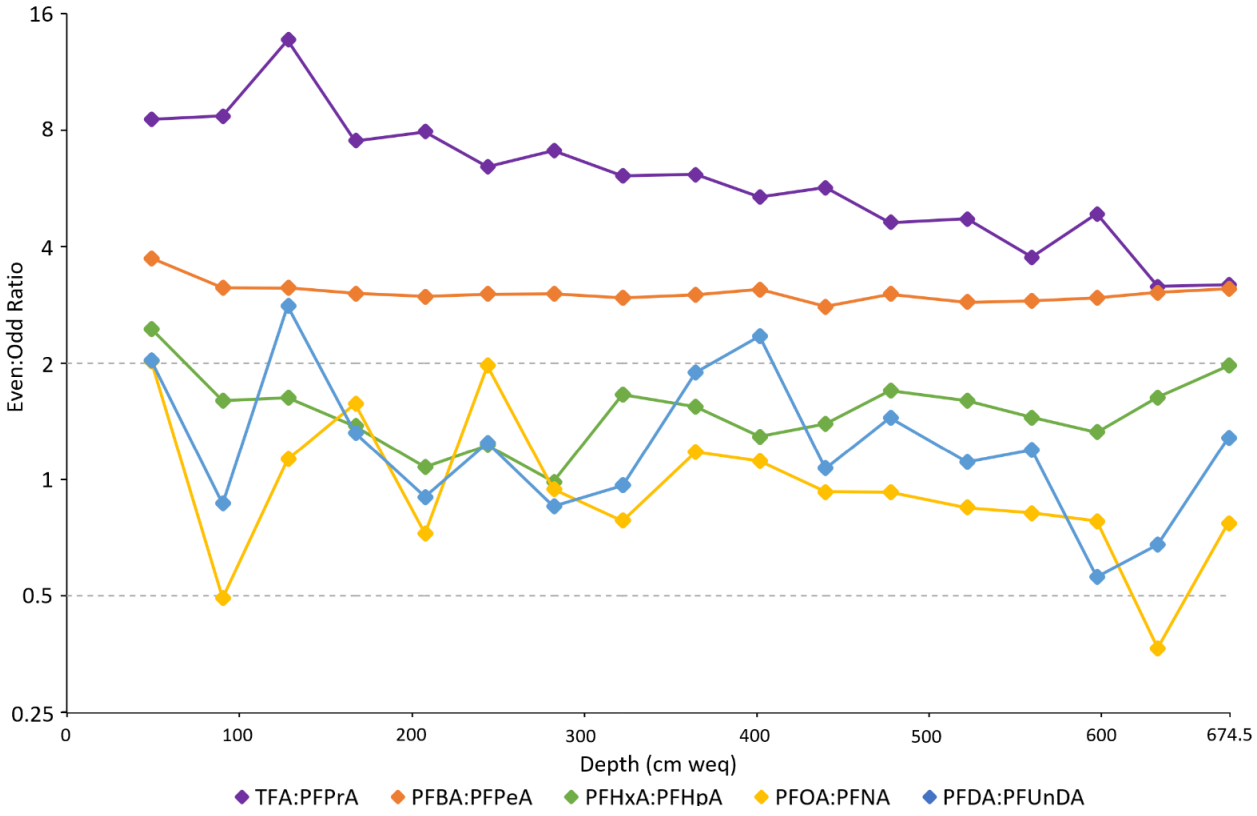


Figure 3. Even:Odd molar concentration ratios for C_2 – C_{11} PFCAs as a function of depth (cm weq) and year

As done previously for Arctic ice cores and snow pits, molar concentration ratios for even-odd PFCA homologues,[46] TFA:PFPrA, PFBA:PFPeA, PFHxA:PFHpA, PFOA:PFNA, and PFDA:PFUnDA, were calculated, as these would be expected to be roughly equal if the major precursor was 2:2 FTOH, 4:2 FTOH, 6:2 FTOH, 8:2 FTOH, and 10:2 FTOH, respectively (Figure 3). 82 – 94% of the molar concentration ratios of PFHxA:PFHpA, PFOA:PFNA, PFDA:PFUnDA were between 0.5 and 2 (i.e. within a factor of 2). Given that, of these pairs, only PFOA and PFNA

($r = 0.77$, $p < 0.001$), and PFDA and PFUnDA ($r = 0.89$, $p < 0.001$), were significantly correlated, this indicates that $C_8 – C_{11}$ PFCAs were mostly formed from the atmospheric degradation of 8:2 FTOH and 10:2 FTOH (or an equivalent fluorotelomer derived precursor e.g. 8:2 FTA and 10:2 FTA). For TFA:PFPrA and PFBA:PFPeA, their ratios were always >2.8, indicating an alternative major precursor source (or otherwise). In addition, the higher total molar quantity of PFNA compared to PFOA in the ice core (0.81:1) indicates a preference for the formation of PFNA over PFOA (Figures 1 and 2). This was also observed in the laboratory study of the degradation of 8:2 FTOH (0.94:1 molar ratio) by Ellis et al.[10] Despite the numerous PFAS compounds produced which could act as C_8 atmospheric precursors (e.g. FASAs/FOSEs), the slightly higher molar quantity of PFNA in the ice core over PFOA, indicates a stronger presence of a precursor(s) source that can degrade to both C_8 and C_9 PFCAs (i.e. 8:2 FTOH). This evidence, combined with the molar concentration ratios for PFOA:PFNA observed in this ice core, and other Arctic snow pits and ice cores, as well as widespread detection of 8:2 FTOH in the Arctic atmosphere, indicates that 8:2 FTOH continues to be a significant atmospheric source of PFOA and PFNA to the remote Arctic environment.

The PFCA homologue ratios for PFHxA:PFHpA, PFOA:PFNA, PFDA:PFUnDA at the Longyearbyen landfill (2.6, 3.8 and 4.2, respectively) and the Longyearbyen FFTS (3.3, 9.7 and <LOQ, respectively)[39] were in contrast to the results from the Lomonosovfonna ice core in this study (1.5, 0.81 and 0.93 respectively). This indicates that the input of PFAS to Lomonosovfonna from local sources in Longyearbyen is insignificant. This is likely due to the large distance between Longyearbyen and Lomonosovfonna (79 km), and the high elevation of Lomonosovfonna (1198 m.a.s.l.) above the atmospheric boundary layer. Pyramiden is closer to Lomonosovfonna (31 km) and could be a potential local source of PFAS to the ice core. However, the settlement has been

largely abandoned since 1998 (i.e. before the timespan of this ice core). Furthermore, Warner et al. found that PFAS in snow bunting (*Plectrophenax nivealis*) eggs had significantly lower levels in Pyramiden compared to Longyearbyen.[47] No local sources were identified and long-range sources such as FTOHs were thought to be a more important exposure for snow buntings in Pyramiden. Hence, Pyramiden does not provide a local source of PFAS to Lomonosovfonna, and the ice core in this study records an atmospheric record representative of a background location in the Arctic.

On Lomonosovfonna, the detection of 6:2 FTUCA (35% >MQL) and 8:2 FTUCA (6% >MQL) is further indicative of the FTOH degradation process.[10,48] During the radical-mediated degradation of 8:2 FTOH, it was found by Ellis et al. that 26% of the molar reaction product would be 8:2 fluorotelomer acid (8:2 FTCA).[10] The study reported that only the n:2 FTOH could yield the corresponding n:2 FTCA. Hence, the detection of FTUCAs in this ice core suggests that FTCAs have formed in the atmosphere. This is because any FTCAs formed will likely eliminate HF to form FTUCAs.[49,50] This elimination process could happen in the environment (e.g. during snowpack/firn processes) or during extraction/analysis (e.g. during the preparation of the extracts in methanol). Regardless, the detection of 6:2 FTUCA and 8:2 FTUCA suggests that 6:2 FTOH and 8:2 FTOH provide atmospheric sources of PFCAs and other PFAS degradation products to the remote Arctic.

FASAs and FOSEs are known to undergo radical-mediated degradation to PFCAs.[18,19] The four FASAs and FOSEs detected on Lomonosovfonna (MeFOSE, EtFOSE, MeFBSA, and EtFOSA) were also detected in surface snow from glaciers near Ny-Ålesund, Svalbard.[16] This suggests that these precursors can undergo long-range atmospheric transport to the Arctic and they can provide another precursor source for PFCAs, albeit possibly a minor one compared to FTOHs.

There was a significant correlation between all C_3 – C_6 PFCAs ($r > 0.87$, $p < 0.001$), but not TFA. This suggests a common chemical source or degradation pathway for C_3 – C_6 PFCAs. However, even-odd homologue ratios for C_3 – C_5 PFCAs do not suggest a fluorotelomer derived source (Figure 3). Furthermore, the large variations in the PFCA mass contributions of PFPrA (16%), PFBA (6%), PFPeA (2%), and PFHxA (1%) in the ice core, and the higher fluxes of these PFCAs compared to C_8 – C_{11} PFCAs, suggests a largely non-fluorotelomer derived source has contributed to their deposition (i.e. not FTOHs). The atmospheric deposition of PFPrA and PFBA are known to vary seasonally in the Arctic (Chapter 5).[29] This is because the photochemical conditions required for the radical-mediated degradation of C_3 and C_4 precursors were only found to exist during months with 24-hour daylight when solar radiation creates the atmospheric conditions for precursor degradation. Hence in this ice core, it is likely that PFPrA and PFBA, and by extension also PFPeA and PFHxA, have been formed during photochemical atmospheric conditions. A snowpit measured for PFAS on the Devon Ice Cap suggested that several non-fluorotelomer atmospheric sources for PFBA could for example include C_4 HFCs and HFEs, such as HFC-329 ($CF_3(CF_2)_3H$), HFE-7100 ($C_4F_9OCH_3$) and HFE-7200 ($C_4F_9OC_2H_5$).[46] These CFC replacement products, as well as other HFCs, HCFCs, HFEs and HFOs, provide an alternative atmospheric precursor source for short-chain PFCAs.[24–27,51] These four precursor groups are known to exist in the atmosphere and are known to photochemically degrade to PFCAs. Indeed, HFCs can provide a non-fluorotelomer precursor source for PFCAs of chain lengths greater than C_4. For example, HFC precursors could include HFC-52-13p ($CF_3(CF_2)_4CHF_2$, commercialized as AC-2000 or TH-6) for PFHxA (C_6) and HFC-569mccf ($CF_3(CF_2)_3CH_2CH_3$, commercialized as AC-4000 or TEH-4) for PFPeA (C_5).[52] Indeed, the troposphere lifetime of HFC-52-13p is 31 years, which is sufficient to be well distributed in the atmosphere globally.[53] Finally, the lack of

correlation between TFA and other PFCAs could be due to a different precursor source profile for TFA. Indeed, TFA is the potential degradation product of over 1 million chemicals.[54]

4.4.3 Chemical Sources of PFSAs to Lomonosovfonna

Observations of PFSAs were dominated by even chain length PFSAs over odd chain length PFSAs. For C_2 – C_{10} PFSAs, PFPeS was only found in one subsection and was the only odd chain length PFSA detected. In contrast, PFBS, PFHxS, and PFOS were detected in 24%, 65%, and 82% of subsections, respectively.

This study also quantified linear and branched isomers of PFHxS and PFOS. Inspecting the structural isomer profile is a useful tool in assigning sources of PFAS.[55] In addition to linear-PFHxS and linear-PFOS, several other structural isomers were targeted. A summary of the concentrations of linear and branched isomers of PFHxS and PFOS can be found in Tables S14 and S15. Targeted branched isomers of PFHxS were only detected in one section of the core (6% >MQL). In comparison, linear-PFHxS was detected in 65% of core sections, but the concentrations were close to the MQL. This will discriminate against the less abundant branched isomers of PFHxS, which, if present on Lomonosovfonna, would be below the MQL. PFHxS, produced by electrochemical fluorination (ECF), has been reported to consist of approximately 18% branched isomers.[56] In core sections that detected both linear and branched isomers of PFOS, 71 – 89% (average 81 %) were linear isomers. These results are similar to a standard PFOS product (76 – 79%) produced by ECF.[55] This suggests that changes to the PFOS isomer composition during transport to Lomonosovfonna are insignificant and therefore a direct particle-bound long-range atmospheric transport from Eurasian sources might explain the presence of PFOS on Lomonosovfonna. Two recent studies have found the percentage of PFOS in the atmosphere to be largely in the particle-bound phase at a background site in Europe (80%) and in oceanic air from

the Western Taiwan Strait (96%).[57,58] Alternatively the presence of branched PFOS isomers could suggest a branched precursor source, such as branched FOSA precursors.[59] In comparison to PFCAs, there is less evidence for precursors to act as an atmospheric source for PFSAs. Only one study has tenuously observed the formation of PFBS from *N*-methyl perfluorobutane sulfonamidoethanol (MeFBSE) in a simulated atmospheric laboratory study.[19] Hence in the atmosphere, the formation of PFSAs could proceed from the cleavage of S-N bonds in precursors such as FASAs and FOSEs, which are known to be present in the Arctic atmosphere.[12] In this ice core, PFOS was found to be significantly correlated with TFA ($r = 0.76$, $p < 0.001$). This could suggest that PFOS atmospheric formation and deposition is highly seasonal and dependent on the presence of hydroxyl radicals to enable the atmospheric degradation of its precursors, as is the case for TFA.[29] Further research is required to elucidate the significance of the particle-bound transport of PFSAs to the Arctic versus their atmospheric formation from precursors, or otherwise.

6:2 FTSA was detected in 41% of subsections. Like for PFCAs, photochemical precursors also exist for 6:2 FTSA. These include 6:2 fluorotelomer sulfonamide alkylamine, 6:2 fluorotelomer sulfonamide alkylbetaine, and 6:2 fluorotelomer sulfonamide. These compounds have been found in the environment and are known to photochemically degrade to 6:2 FTSA.[60–62] If some of these precursors, or others, would be sufficiently volatile to undergo long-range atmospheric transport to the Arctic, this could also explain the presence of 6:2 FTSA on Lomonosovfonna.

This study was unable to report TFMS concentrations. This is due to TFMS contamination introduced during the cutting and processing of the ice core in the cold lab (see *Quality Assurance and Quality Control*, pages S4 – S6). Nonetheless, Björnsdotter et al. (Chapter 5) recently reported the ubiquitous presence of TFMS in surface snow in the Arctic, including on Lomonosovfonna

and other high elevation remote glaciers.[29] However, this study was unable to assign a TFMS source. TFMS has not yet been targeted for a time series study in the Arctic, for example as part of atmospheric monitoring or an ice core. Such a study could help elucidate the source(s) of TFMS to the Arctic. Further work is required to assign the source(s) of TFMS in the Arctic.

4.4.4 Temporal Trends in PFAS Deposition

Temporal trends show an increase in TFA atmospheric deposition (Figure 4). This has also been observed in Germany and the Canadian Arctic.[30,31] This likely reflects recent amendments to the Montreal Protocol that will see the replacement of HFCs with HFOs.[63] High deposition fluxes and increasing temporal trends for TFA mean that limited knowledge about the safe levels of TFA in the environment needs addressing. C_3 – C_9 PFCAs and PFHxS show neither a significant increase or decrease, whereas PFDA and PFUnDA show a decreasing trend in atmospheric deposition. This possibly reflects decreasing emissions of 10:2 FTOH precursors during 2010 – 2018.[52] PFOS however showed an increasing trend, particularly after 2011. This possibly suggests increasing atmospheric levels of PFOS precursors in the Arctic, however this is at odds with estimated decreasing emissions of FOSA, FOSE and their associated compounds.[52]

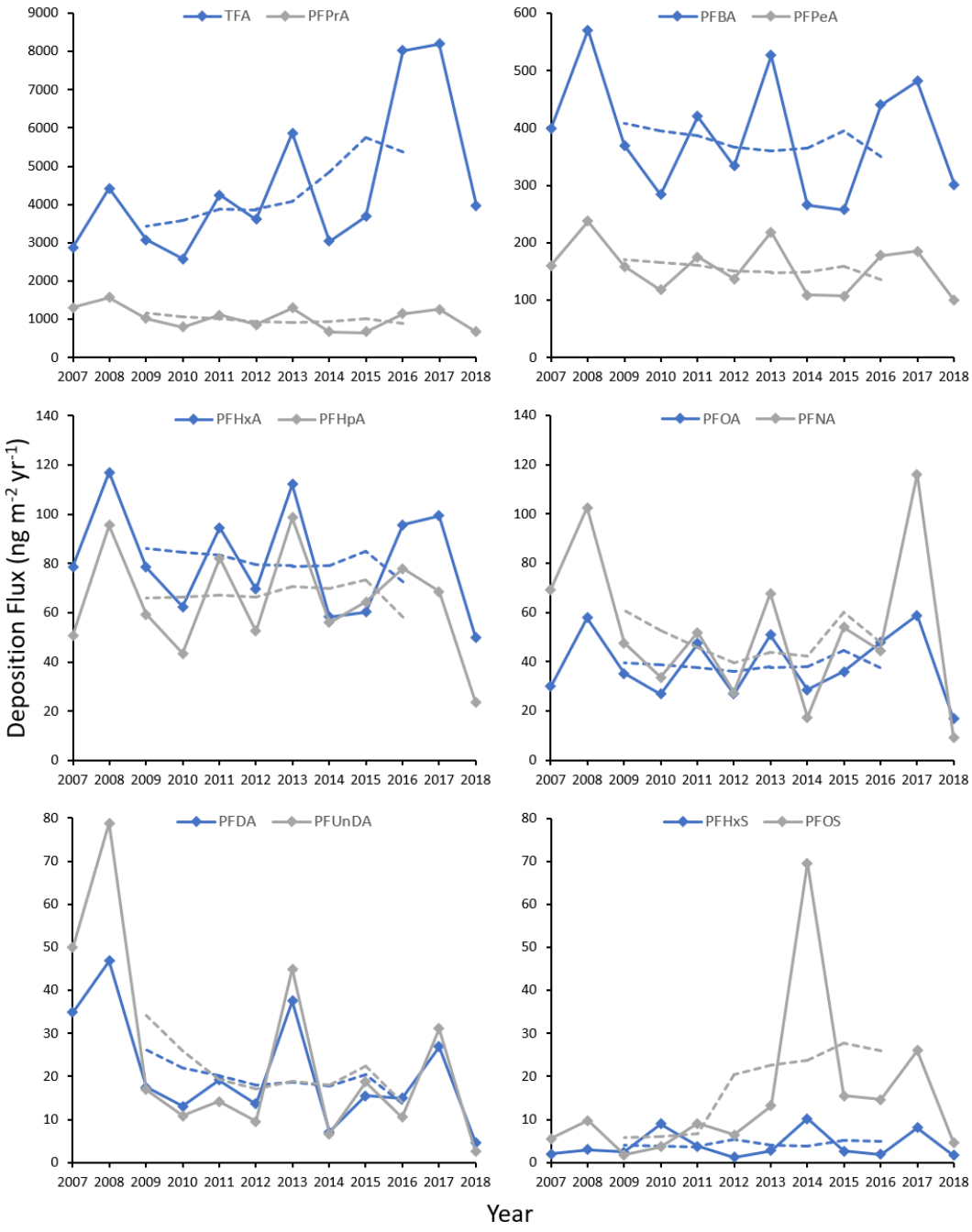


Figure 4. Records of the annual atmospheric deposition fluxes of C_2 – C_{11} PFCAs, PFHxS and PFOS. Solid line = annual deposition fluxes. Dashed line = 5-year moving average.

No correlations were found between deposition fluxes of C_6 – C_{10} PFCAs, PFOS and FOSA on Lomonosovfonna and the atmospheric levels observed at the Zeppelin Observatory in Ny-

Ålesund, Svalbard during the years 2007 – 2018 ($r < 0.17$, $p \geq 0.23$). This could be due to (i) differences in the measurement technique (Zeppelin only measures particle-bound PFAS, whereas photochemical degradation is likely gaseous),[10,18–20,64] (ii) differences in geographic location (Svalbard is known to have an east-west gradient in climate),[65] (iii) PFAS mobility in the firn/snowpack during summer melt disrupting the atmospheric record, (iv) the impact of local sources from Ny-Ålesund at the Zeppelin Observatory,[38] and (v) disparity in air concentrations compared to atmospheric deposition. Indeed, one of the advantages of ice cores, compared to atmospheric measurements is that it provides a record of what become deposited and can therefore enter the Arctic biosphere, compared to what is present in the air. The effects of melt percolation may also be significant in damaging the temporal trends in atmospheric deposition. To assist in overcoming this, a 5-year moving average was applied (see dashed lines in Figure 4). The mobility of PFAS during meltwater percolation is discussed further in section 4.4.7.

4.4.5 Marine environment as a source of PFAS

Several studies have identified marine aerosols as a potential mechanism for the long-range atmospheric transport of PFAS. For example, in a laboratory experiment, PFOA was found to be enriched in aerosols in the headspace above the parent water body.[66] In another study, several particle-bound PFAAs were found to significantly correlate with marine aerosols in the atmosphere at two sites in Norway.[9] Hence, marine aerosols could provide a mechanism for the transport of PFAS from the marine environment to Lomonosovfonna.

PFAS concentrations were investigated for correlations with Na^+ to investigate if marine aerosols were a source of PFAS to Lomonosovfonna (Table S16). Since Na^+ is expected to be entirely of a marine origin, Na^+ concentrations can be treated as a marine aerosol proxy. No PFAS were found to positively correlate with Na^+ ($r < 0.27$, $p > 0.063$). This indicates that marine aerosols

are not a significant source for PFAS in the Lomonosovfonna ice core. This is despite (i) the ability of PFAS to undergo long-range transport in the ocean, (ii) the variety of PFAS that have been measured in the Arctic basin,[8] and (iii) the proximity of Lomonosovfonna to several fjords (>20 km) and open sea (~120 km).

Several PFCAs and PFSAs have recently been found to significantly correlate with marine aerosols as part of long-term air monitoring at two sites in Norway.[9] However, this study only considers the PFAS captured by quartz fiber filters and therefore only records particle-bound PFAS. So whilst particle-bound atmospheric PFAS may be linked to marine aerosols, the radical-mediated atmospheric degradation of PFAS precursors is likely a gaseous process.[10,17–20] Therefore, PFCAs and PFSAs formed by this process are likely not to have been captured by this study, or other long-term air monitoring which measure PFAS using filters alone. Unfortunately, few studies have measured both particle-bound and gaseous PFAAs in atmospheric samples,[57,67] and therefore the relative importance of each process is unclear.

4.4.6 Air mass source regions

Air mass trajectory frequency plots have previously been used to assist in assigning source regions for organic contaminants in ice cores.[35] In this study, 4383 daily trajectories from 2007 – 2018, were used to understand relevant air mass movements corresponding to the time period recorded by the ice core. This included one plot for all complete annual layers in the core (2007 – 2018, Figure 5) and four further plots to investigate seasonal variations in air mass movements for these years (Figure S2).

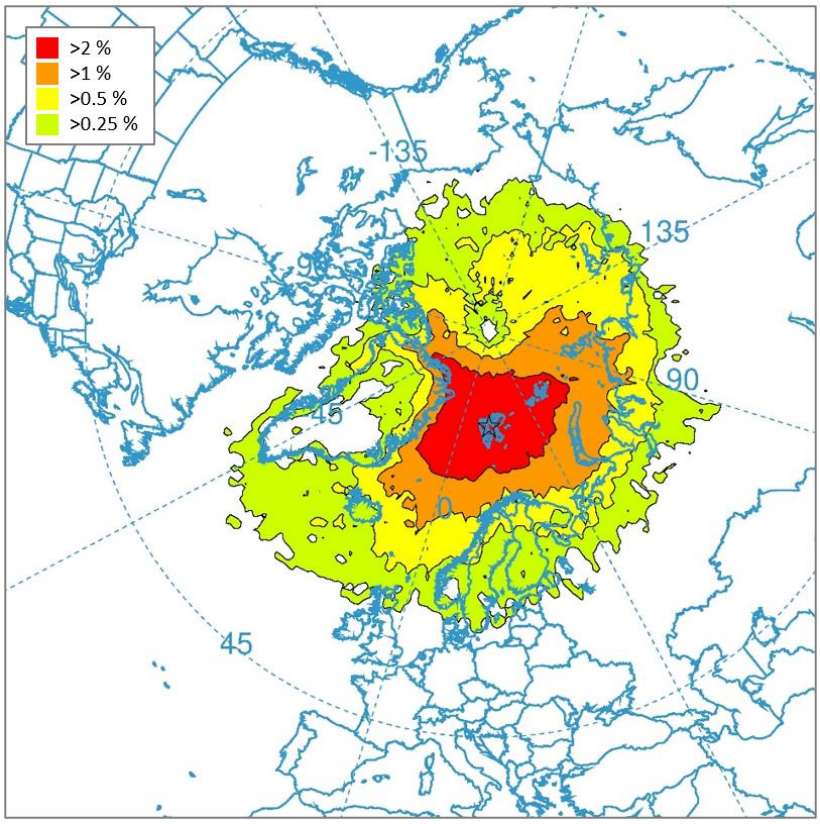


Figure 5. HYSPLIT air mass trajectory frequency plot for air masses ending at the Lomonosovfonna drilling site 2007 – 2018

The overall plot shows the trajectory frequency for 2007 – 2018 based on a 6-day backward air mass trajectory from Lomonosovfonna. 0.25% of trajectory endpoints passed over Arctic Canada, Greenland, Northern Europe, and Russia. Since Arctic Canada and Greenland are not highly populated or industrialized regions, this study suggests Eurasia as the main air mass source region to Lomonosovfonna. This would agree with previous contaminant records from Lomonosovfonna.[34,35] A pollen record from Lomonosovfonna also identified Fennoscandia as a source and not North America.[68]

Seasonal plots showed increased trajectory frequency over Eurasia during November, December, and January, as well as February, March, and April (i.e. months with complete or partial

darkness). During May, June, and July, trajectory densities over Eurasia were greatly reduced. Hence the long-range atmospheric transport of contaminants from Eurasian sources would likely be enhanced during winter months. This was also found to be the case during the seasonal air sampling of polycyclic aromatic hydrocarbons in Svalbard.[69] This is in contrast to $C_2 – C_4$ PFCAs which were found to have higher deposition fluxes from precursors degradations during months with 24-hour daylight (Chapter 5).[29]

Using HYSPLIT to assign geographical source regions has been shown to be effective for organic contaminants such as polychlorinated biphenyls (PCBs) in ice cores.[35] If PFAS on Lomonosovfonna have been transported by direct emissions or particle-bound processes like PCBs, then these trajectory frequency plots are also a helpful tool in assigning source regions. However, many of the PFAS observed in this ice core, such as PFCAs, are likely formed by the atmospheric degradation of precursors. PFAS precursors have long atmospheric lifetimes with respect to radical degradation (e.g. FTOHs – 20 days, HFC-134a – 14.1 years).[70,71] As a result, using HYSPLIT to assign geographical source regions is not possible. Since PFCAs have atmospheric lifetimes of several days with respect to wet and dry deposition (TFA – 9 days, PFOA – 12 days),[72,73] trajectory frequency plots instead represent regions where degradation products, such as PFCAs, could have been formed in the atmosphere rather than source regions of PFAS precursors.

4.4.7 Redistribution of PFAS during melt

Iizuka et al. have established a chemical melt proxy using Na^+ and Mg^{2+} ion concentrations for Svalbard ice cores.[74] This has been shown to be effective in recording historical melt for several Svalbard ice cores due to the preferential mobility of Mg^{2+} compared to Na^+ during meltwater

percolation in the snowpack/firn. This study uses the same chemical melt proxy by calculating $\log([Na^+]/[Mg^{2+}])$ values.

Since PFAS are likely ubiquitous in seasonal snow and post-industrial accumulation on glaciers in Svalbard, understanding the effects of meltwater percolation on the core could offer a route to understanding which PFAS are released preferentially during snowmelt and glacier runoff. This is important because runoff from glaciers could be a large seasonal source of PFAS to the fjord environment in Svalbard and the wider Arctic. PFCAs and PFSAs have high solubility and would be expected to be very mobile during events when meltwater percolates through the snowpack/firn.[6] Plassmann et al. investigated the influence of snowmelt on PFCAs and PFSAs in a snow chamber experiment and found that PFCAs and PFSAs of shorter chain lengths were preferentially eluted.[75] Field observations broadly found the same results that shorter chain length PFCAs were more mobile during melt of the seasonal snowpack.[38,76] To assess whether PFAS concentrations had been affected by percolating meltwater, their correlations with the melt proxy $\log([Na^+]/[Mg^{2+}])$ were investigated (Table S16). TFA ($r = -0.65$, $p < 0.05$) and PFOS ($r = -0.54$, $p < 0.05$) was found to have negative correlation with the melt proxy (i.e. TFA and PFOS concentrations were lower in subsections where Mg^{2+} concentrations had been depleted relative to Na^+ as a result of meltwater percolation). This suggests that TFA and PFOS are mobile during meltwater percolation through the snowpack/firn. Although other PFAS were not found to correlate with the melt proxy, it is still likely that other PFAS have been affected by meltwater percolation due to their high solubilities.[6] Hence, runoff from post-industrial accumulation on glaciers and seasonal snowmelt would be important in the seasonal input of TFA and PFOS, and possibly other PFAS, to the fjord environment in Svalbard and elsewhere in the Arctic.

Meltwater percolation of chemical species on Lomonosovfonna is well understood. In a previous ice core from Lomonosovfonna, one study found that meltwater was mostly refrozen within the annual layer,[77] whereas another study found that percolation may have extended up to 8 annual layers.[78] Regardless, these effects, combined with the short time period covered by the core (2006 – 2019) make it difficult to comment on the long-term trends in PFAS deposition fluxes in this ice core. Furthermore, this makes it challenging to assign geographical source regions for sections of the ice core which have higher individual PFAS fluxes. Meltwater percolation also damages the atmospheric signal from water stable isotopes and major ions. This can affect the accuracy of dating the ice core (and hence a ±2 year error has been assigned to the annual layer counting, Figure S2). Misassignment of annual layers could then affect the PFAS annual flux values reported in this study. Meltwater percolation in the snowpack/firn would also provide an alternative aqueous medium for degradations to occur. Indeed, the post-deposition degradation of PFAS precursors in the snowpack/firn, in addition to atmospheric degradations, could affect the PFAS observed in this study. The post-deposition transformation of other organic contaminants in the snowpack is already known,[79] and hence, could be possible for PFAS precursors. Several neutral PFAS are known to have positive and negative air-snow exchange fluxes, and therefore there can be post-deposition losses from the snowpack/firn back to the atmosphere.[16] The analysis of this ice core is unable to distinguish between particle-bound PFAS and non-particle-bound PFAS, and hence reports a sum value. However, given the collective evidence for precursor sources for C_2 – C_{11} PFCAs, and since this is known that their degradation is a gaseous process, it is likely that at least these degradation products exist mostly as non-particle-bound compounds in the ice core.

4.5 Conclusion

The presence of 26 of the 45 PFAS targeted were detected in a remote high elevation Arctic ice core suggests that PFAS contamination is chemically diverse and geographically widespread in the Arctic. The majority of PFAS frequently detected were PFCAs, and fluxes of PFCAs typically increased towards shorter chain lengths with TFA having the highest fluxes in the core. The distribution profile of PFAS detected suggests that FTOHs are likely the atmospheric precursor to C_8 – C_{11} PFCAs, whereas C_3 – C_6 PFCAs have an alternative source, such as HFCs and other CFC replacement compounds. In addition, the detection of FTUCAs confirmed the role of FTOHs as atmospheric precursors to PFCAs. It is unclear whether the presence of PFSAs, such as PFBS, PFHxS, and PFOS, on Lomonosovfonna could be explained by direct particle-bound transport or atmospheric degradation of precursors. Nonetheless, the structural isomer profile of PFOS on Lomonosovfonna indicated that it had been manufactured by ECF. No PFAS were found to positively correlate with the Na^+, a marine aerosol proxy, showing that marine aerosols are unimportant in the atmospheric transport of PFAS to the Arctic. HYSPLIT analysis revealed that any direct transport of contaminants would come from Eurasian sources. TFA and PFOS were found to be influenced by melt in the ice core, indicating the importance of glacier runoff as a seasonal source of PFAS input into Arctic fjords. In comparison with another Arctic ice core from the Devon Ice Cap (2007 – 2014), fluxes for C_2 and C_3 PFCAs were typically lower, but fluxes were similar or higher for C_4 – C_{13} PFCAs and PFOS on Lomonosovfonna.

Conflict of Interest

The authors declare no conflicts of interest.

CRediT Authorship Contribution Statement

William F. Hartz: Conceptualization, Methodology, Validation, Formal analysis, Investigation, Resources, Writing - Original Draft, Visualization, Project administration, Funding acquisition. **Maria K. Björnsdotter:** Conceptualization, Methodology, Validation, Formal analysis, Investigation, Resources, Writing - Review & Editing. **Leo W. Y. Yeung:** Conceptualization, Methodology, Validation, Formal analysis, Resources, Writing - Review & Editing, Supervision, Funding acquisition. **Andrew Hodson:** Resources, Writing - Review & Editing, Supervision, Project administration. **Elizabeth R. Thomas:** Formal analysis, Resources, Writing - Review & Editing, Supervision, Funding acquisition. **Jack D. Humby:** Methodology, Validation, Formal analysis, Investigation, Resources, Writing - Review & Editing. **Chris Day:** Methodology, Validation, Investigation, Resources, Writing - Review & Editing, Funding acquisition. **Ingrid Ericson Jogsten:** Resources, Writing - Review & Editing, Supervision, Funding acquisition. **Anna Kärrman:** Resources, Writing - Review & Editing, Supervision, Funding acquisition. **Roland Kallenborn:** Conceptualization, Resources, Writing - Review & Editing, Supervision, Project administration, Funding acquisition.

Acknowledgements

The authors gratefully acknowledge financial support from the Swedish Research Council Formas (2016-01284), the Swedish Environmental Protection Agency (2219-16-030 and 2219-17-012), the United Kingdom Research and Innovation Natural Environment Research Council and the Oxford Doctoral Training Partnership in Environmental Research (NE/L002612/1), the Burdett-

Coutts Trust, the Svalbard Science Forum Arctic Field Grant 2019 (RiS ID 11121), the Research Council of Norway (SvalPOP, 196218/S30), the Fram Centre Flagship program (PharmArctic, 534/75219) and the Knowledge Foundation (Enforce Research Project, 20160019). The authors would also like to thank the Logistics Department and colleagues at the University Centre in Svalbard for help organizing and assisting with fieldwork, and Veerle van Winden, Eirik Rolland Enger and Julien-Pooya Weihs for assistance in the field and laboratory.

Appendix A. Supplementary data

Full details of the drill site characteristics, chemicals and reagents, sample extraction, instrument analysis, quality control and quality assurance, HYSPLIT analysis, major ion analysis, and water stable isotope analysis can be found in the supporting information (pages S1 – S8). Lists of target analytes, abbreviations, CAS numbers, MRM transitions, internal and recovery standards used, LODs and MQLs, extraction efficiencies and the repeatability of the instrument method can also be found. Tables with PFAS fluxes and concentrations, as well as correlations, are also provided. Figures showing annual layer counting used in dating the ice core, and HYSPLIT seasonal trajectory frequency plots can also be found.

4.6 References

1. Wang, Z. *et al.* A New OECD Definition for Per- And Polyfluoroalkyl Substances. *Environ. Sci. Technol.* **55**, 15575–15578 (2021).
2. Frömel, T. & Knepper, T. P. Biodegradation of Fluorinated Alkyl Substances. in *Reviews of environmental contamination and toxicology* vol. 208 161–177 (2010).
3. Conder, J. M., Hoke, R. A., De Wolf, W., Russell, M. H. & Buck, R. C. Are PFCAs bioaccumulative? A critical review and comparison with regulatory criteria and persistent lipophilic compounds. *Environ. Sci. Technol.* **42**, 995–1003 (2008).
4. Jensen, A. A. & Leffers, H. Emerging endocrine disrupters: perfluoroalkylated substances. *Int. J. Androl.* **31**, 161–169 (2008).
5. Muir, D. *et al.* Levels and trends of poly- and perfluoroalkyl substances in the Arctic environment – An update. *Emerg. Contam.* **5**, 240–271 (2019).
6. Rayne, S. & Forest, K. Perfluoroalkyl sulfonic and carboxylic acids: A critical review of physicochemical properties, levels and patterns in waters and wastewaters, and treatment methods. *J. Environ. Sci. Heal. Part A* **44**, 1145–1199 (2009).
7. Benskin, J. P. *et al.* Perfluoroalkyl Acids in the Atlantic and Canadian Arctic Oceans. *Environ. Sci. Technol.* **46**, 5815–5823 (2012).
8. Yeung, L. W. *et al.* Vertical Profiles, Sources, and Transport of PFASs in the Arctic Ocean. *Environ. Sci. Technol.* **51**, 6735–6744 (2017).
9. Sha, B. *et al.* Sea Spray Aerosol (SSA) as a Source of Perfluoroalkyl Acids (PFAAs) to the Atmosphere: Field Evidence from Long-Term Air Monitoring. *Environ. Sci. Technol.* **56**, 228–238 (2022).
10. Ellis, D. A. *et al.* Degradation of fluorotelomer alcohols: a likely atmospheric source of perfluorinated carboxylic acids. *Environ. Sci. Technol.* **38**, 3316–21 (2004).
11. Young, C. J. *et al.* Perfluorinated Acids in Arctic Snow: New Evidence for Atmospheric Formation. *Environ. Sci. Technol.* **41**, 3455–3461 (2007).
12. Cai, M. *et al.* Polyfluorinated compounds in the atmosphere along a cruise pathway from the Japan Sea to the Arctic Ocean. *Chemosphere* **87**, 989–997 (2012).
13. Dreyer, A., Weinberg, I., Temme, C. & Ebinghaus, R. Polyfluorinated Compounds in the Atmosphere of the Atlantic and Southern Oceans: Evidence for a Global Distribution. *Environ. Sci. Technol.* **43**, 6507–6514 (2009).
14. Shoeib, M., Harner, T. & Vlahos, P. Perfluorinated chemicals in the arctic atmosphere. *Environ. Sci. Technol.* **40**, 7577–83 (2006).
15. Stock, N. L., Furdui, V. I., Muir, D. C. G. & Mabury, S. A. Perfluoroalkyl Contaminants in the Canadian Arctic: Evidence of Atmospheric Transport and Local Contamination. *Environ. Sci. Technol.* **41**, 3529–3536 (2007).
16. Xie, Z. *et al.* Neutral Poly-/perfluoroalkyl Substances in Air and Snow from the Arctic. *Sci. Rep.* **5**, 8912 (2015).
17. Sulbaek Andersen, M. P. *et al.* Atmospheric chemistry of 4:2 Fluorotelomer alcohol (n-C4F9CH2CH2OH): Products and mechanism of Cl atom initiated oxidation in the presence of NO x. *J. Phys. Chem. A* **109**, 1849–1856 (2005).
18. Martin, J. W., Ellis, D. A., Mabury, S. A., Hurley, M. D. & Wallington, T. J. Atmospheric chemistry of perfluoroalkanesulfonamides: kinetic and product studies of the OH radical and Cl atom initiated oxidation of N-ethyl perfluorobutanesulfonamide. *Environ. Sci. Technol.* **40**, 864–72 (2006).
19. D'eon, J. C., Hurley, M. D., Wallington, T. J. & Mabury, S. A. Atmospheric chemistry of N-methyl perfluorobutane sulfonamidoethanol, C4F9SO2N(CH3)CH2CH2OH: kinetics and mechanism of reaction with OH. *Environ. Sci. Technol.* **40**, 1862–8 (2006).
20. Butt, C. M., Young, C. J., Mabury, S. A., Hurley, M. D. & Wallington, T. J. Atmospheric Chemistry of 4:2 Fluorotelomer Acrylate [C4F9CH2CH2OC(O)CH═CH2]: Kinetics, Mechanisms, and Products of Chlorine-Atom- and OH-Radical-Initiated Oxidation. *J. Phys. Chem. A* **113**, 3155–3161 (2009).
21. Wang, X., Chen, M., Gong, P. & Wang, C. Perfluorinated alkyl substances in snow as an atmospheric tracer for tracking the interactions between westerly winds and the Indian Monsoon over western China. *Environ. Int.* **124**, 294–301 (2019).
22. Taniyasu, S. *et al.* Does wet precipitation represent local and regional atmospheric transportation by perfluorinated alkyl substances? *Environ. Int.* **55**, 25–32 (2013).

23. Pike, K. A., Edmiston, P. L., Morrison, J. J. & Faust, J. A. Correlation Analysis of Perfluoroalkyl Substances in Regional U.S. Precipitation Events. *Water Res.* **190**, 116685 (2021).
24. Young, C. J., Hurley, M. D., Wallington, T. J. & Mabury, S. A. Atmospheric chemistry of CF3CF2H and CF3CF2CF2CF2H: Kinetics and products of gas-phase reactions with Cl atoms and OH radicals, infrared spectra, and formation of perfluorocarboxylic acids. *Chem. Phys. Lett.* **473**, 251–256 (2009).
25. Wallington, T. J. *et al.* The Environmental Impact of CFC Replacements-HFCs and HCFCs. *Environ. Sci. Technol.* **28**, (1994).
26. Oyaro, N., Sellevåg, S. R. & Nielsen, C. J. Atmospheric chemistry of hydrofluoroethers: Reaction of a series of hydrofluoroethers with OH radicals and Cl atoms, atmospheric lifetimes, and global warming potentials. *J. Phys. Chem. A* **109**, 337–346 (2005).
27. Young, C. J., Hurley, M. D., Wallington, T. J. & Mabury, S. A. Atmospheric chemistry of perfluorobutenes (CF3CF=CFCF3 and CF3CF2CF=CF2): Kinetics and mechanisms of reactions with OH radicals and chlorine atoms, IR spectra, global warming potentials, and oxidation to perfluorocarboxylic acids. *Atmos. Environ.* **43**, 3717–3724 (2009).
28. Velders, G. J. M., Andersen, S. O., Daniel, J. S., Fahey, D. W. & McFarland, M. The importance of the Montreal Protocol in protecting climate. *Proc. Natl. Acad. Sci. U. S. A.* **104**, 4814–4819 (2007).
29. Björnsdotter, M. K. *et al.* Levels and Seasonal Trends of C1-C4 Perfluoroalkyl Acids and the Discovery of Trifluoromethane Sulfonic Acid in Surface Snow in the Arctic. *Environ. Sci. Technol.* **55**, 15853–15861 (2021).
30. Pickard, H. M. *et al.* Ice Core Record of Persistent Short-Chain Fluorinated Alkyl Acids: Evidence of the Impact From Global Environmental Regulations. *Geophys. Res. Lett.* **47**, (2020).
31. Freeling, F. *et al.* Levels and Temporal Trends of Trifluoroacetate (TFA) in Archived Plants: Evidence for Increasing Emissions of Gaseous TFA Precursors over the Last Decades. *Environ. Sci. Technol. Lett.* **9**, 400–405 (2022).
32. Pickard, H. M. *et al.* Continuous non-marine inputs of per- and polyfluoroalkyl substances to the High Arctic: a multi-decadal temporal record. *Atmos. Chem. Phys.* **18**, 5045–5058 (2018).
33. Isaksson, E. *et al.* Ice cores from Svalbard—useful archives of past climate and pollution history. *Phys. Chem. Earth, Parts A/B/C* **28**, 1217–1228 (2003).
34. Osmont, D. *et al.* An 800-year high-resolution black carbon ice core record from Lomonosovfonna, Svalbard. *Atmos. Chem. Phys.* **18**, 12777–12795 (2018).
35. Garmash, O. *et al.* Deposition history of polychlorinated biphenyls to the lomonosovfonna glacier, Svalbard: A 209 congener analysis. *Environ. Sci. Technol.* **47**, 12064–12072 (2013).
36. Barbaro, E. *et al.* Measurement report: Spatial variations in ionic chemistry and water-stable isotopes in the snowpack on glaciers across Svalbard during the 2015-2016 snow accumulation season. *Atmos. Chem. Phys.* **21**, 3163–3180 (2021).
37. Kwok, K. Y. *et al.* Transport of Perfluoroalkyl substances (PFAS) from an arctic glacier to downstream locations: Implications for sources. *Sci. Total Environ.* **447**, 46–55 (2013).
38. Skaar, J. S., Ræder, E. M., Lyche, J. L., Ahrens, L. & Kallenborn, R. Elucidation of contamination sources for poly- and perfluoroalkyl substances (PFASs) on Svalbard (Norwegian Arctic). *Environ. Sci. Pollut. Res.* **26**, 7356–7363 (2019).
39. Ali, A. M. *et al.* The fate of poly- And perfluoroalkyl substances in a marine food web influenced by land-based sources in the Norwegian Arctic. *Environ. Sci. Process. Impacts* **23**, 588–604 (2021).
40. *ISO 25101:2009 - Water quality — Determination of perfluorooctanesulfonate (PFOS) and perfluorooctanoate (PFOA) — Method for unfiltered samples using solid phase extraction and liquid chromatography/mass spectrometry*. https://www.iso.org/standard/42742.html (2009).
41. Burgay, F. *et al.* First discrete iron(II) records from Dome C (Antarctica) and the Holtedahlfonna glacier (Svalbard). *Chemosphere* **267**, 129335 (2021).
42. Karasiński, G. *et al.* Lidar Observations of Volcanic Dust over Polish Polar Station at Hornsund after Eruptions of Eyjafjallajökull and Grímsvötn. *Acta Geophys.* **62**, 316–339 (2014).
43. Kwok, K. Y. *et al.* Transport of Perfluoroalkyl substances (PFAS) from an arctic glacier to downstream locations: Implications for sources. *Sci. Total Environ.* **447**, 46–55 (2013).
44. Yde, J. C., Riger-Kusk, M., Christiansen, H. H., Knudsen, N. T. & Humlum, O. Hydrochemical characteristics of bulk meltwater from an entire ablation season, Longyearbreen, Svalbard. *J. Glaciol.* **54**, 259–272 (2008).
45. Wickström, S., Jonassen, M. O., Cassano, J. J. & Vihma, T. Present Temperature, Precipitation, and Rain-on-Snow Climate in Svalbard. *J. Geophys. Res. Atmos.* **125**, e2019JD032155 (2020).
46. MacInnis, J. J. *et al.* Emerging investigator series: a 14-year depositional ice record of perfluoroalkyl

substances in the High Arctic. *Environ. Sci. Process. Impacts* **19**, 22–30 (2017).
47. Warner, N. A. *et al.* Snow buntings (Plectrophenax nivealis) as bio-indicators for exposure differences to legacy and emerging persistent organic pollutants from the Arctic terrestrial environment on Svalbard. *Sci. Total Environ.* **667**, 638–647 (2019).
48. Styler, S. A., Myers, A. L. & Donaldson, D. J. Heterogeneous photooxidation of fluorotelomer alcohols: A new source of aerosol-phase perfluorinated carboxylic acids. *Environ. Sci. Technol.* **47**, 6358–6367 (2013).
49. Dinglasan, M. J. A., Ye, Y., Edwards, E. A. & Mabury, S. A. Fluorotelomer alcohol biodegradation yields poly- and perfluorinated acids. *Environ. Sci. Technol.* **38**, 2857–2864 (2004).
50. Loewen, M., Halldorson, T., Wang, F. & Tomy, G. Fluorotelomer carboxylic acids and PFOS in rainwater from an urban center in Canada. *Environ. Sci. Technol.* **39**, 2944–2951 (2005).
51. Montzka, S. A. *et al.* Recent Trends in Global Emissions of Hydrochlorofluorocarbons and Hydrofluorocarbons: Reflecting on the 2007 Adjustments to the Montreal Protocol. *Proc. Natl. Acad. Sci. U.S.A* **106**, (2009).
52. Wang, Z., Cousins, I. T., Scheringer, M., Buck, R. C. & Hungerbühler, K. Global emission inventories for C4-C14 perfluoroalkyl carboxylic acid (PFCA) homologues from 1951 to 2030, part II: The remaining pieces of the puzzle. *Environ. Int.* **69**, 166–176 (2014).
53. Chen, L., Tokuhashi, K., Kutsuna, S. & Sekiya, A. Rate constants for the gas-phase reaction of CF3CF2CF2CF2CF2CHF2 with OH radicals at 250–430 K. *Int. J. Chem. Kinet.* **36**, 26–33 (2004).
54. Solomon, K. R. *et al.* Sources, fates, toxicity, and risks of trifluoroacetic acid and its salts: Relevance to substances regulated under the Montreal and Kyoto Protocols. *J. Toxicol. Environ. Heal. Part B Crit. Rev.* **19**, 289–304 (2016).
55. Kärrman, A., Langlois, I., Bavel, B. van, Lindström, G. & Oehme, M. Identification and pattern of perfluorooctane sulfonate (PFOS) isomers in human serum and plasma. *Environ. Int.* **33**, 782–788 (2007).
56. Benskin, J. P., De Silva, A. O. & Martin, J. W. Isomer profiling of perfluorinated substances as a tool for source tracking: a review of early findings and future applications. *Rev. Environ. Contam. Toxicol.* **208**, 111–160 (2010).
57. Paragot, N. *et al.* Multi-year atmospheric concentrations of per- and polyfluoroalkyl substances (PFASs) at a background site in central Europe. *Environ. Pollut.* **265**, 114851 (2020).
58. Yamazaki, E., Taniyasu, S., Wang, X. & Yamashita, N. Per- and polyfluoroalkyl substances in surface water, gas and particle in open ocean and coastal environment. *Chemosphere* **272**, 129869 (2021).
59. Liu, P. *et al.* Theoretical studies of the conformations and 19F NMR spectra of linear and a branched perfluorooctanesulfonamide (PFOSAmide). *Chemosphere* **69**, 1213–1220 (2007).
60. Moe, M. K. *et al.* The structure of the fire fighting foam surfactant Forafac®1157 and its biological and photolytic transformation products. *Chemosphere* **89**, 869–875 (2012).
61. D'Agostino, L. A. & Mabury, S. A. Aerobic biodegradation of 2 fluorotelomer sulfonamide–based aqueous film–forming foam components produces perfluoroalkyl carboxylates. *Environ. Toxicol. Chem.* **36**, 2012–2021 (2017).
62. D'Agostino, L. A. & Mabury, S. A. Certain Perfluoroalkyl and Polyfluoroalkyl Substances Associated with Aqueous Film Forming Foam Are Widespread in Canadian Surface Waters. *Environ. Sci. Technol.* **51**, 13603–13613 (2017).
63. Polonara, F., Kuijpers, L. J. M. & Peixoto, R. A. Potential impacts of the Montreal Protocol Kigali Amendment to the choice of refrigerant alternatives. *Int. J. Heat Technol.* **35**, S1–S8 (2017).
64. Hurley, M. D. *et al.* Atmospheric Chemistry of 4:2 Fluorotelomer Alcohol (CF3(CF2)3CH2CH2OH): Products and Mechanism of Cl Atom Initiated Oxidation. *J. Phys. Chem. A* **108**, 5635–5642 (2004).
65. Beaudon, E. *et al.* Lomonosovfonna and Holtedahlfonna ice cores reveal east–west disparities of the Spitsbergen environment since AD 1700. *J. Glaciol.* **59**, 1069–1083 (2013).
66. McMurdo, C. J. *et al.* Aerosol enrichment of the surfactant PFO and mediation of the water--air transport of gaseous PFOA. *Environ. Sci. Technol.* **42**, 3969–74 (2008).
67. Wong, F. *et al.* Assessing temporal trends and source regions of per- and polyfluoroalkyl substances (PFASs) in air under the Arctic Monitoring and Assessment Programme (AMAP). *Atmos. Environ.* **172**, 65–73 (2018).
68. Hicks, S. & Isaksson, E. Assessing source areas of pollutants from studies of fly ash, charcoal, and pollen from Svalbard snow and ice. *J. Geophys. Res. Atmos.* **111**, (2006).
69. Drotikova, T., Dekhtyareva, A., Kallenborn, R. & Albinet, A. Polycyclic aromatic hydrocarbons (PAHs) and their nitrated and oxygenated derivatives in the Arctic boundary layer: seasonal trends and local anthropogenic influence. *Atmos. Chem. Phys* **21**, (2021).
70. Ellis, D. A. *et al.* Atmospheric lifetime of fluorotelomer alcohols. *Environ. Sci. Technol.* **37**, 3816–20 (2003).

71. Wild, O., Ratfigan, O. V, Jones, R. L., Pyle, J. A. & Cox, R. A. Two-Dimensional Modelling of Some CFC Replacement Compounds. *J. Atmos. Chem.* **25**, 167 (1996).
72. Kotamarthi, V. R. *et al.* Trifluoroacetic acid from degradation of HCFCs and HFCs: A three-dimensional modeling study. *J. Geophys. Res. Atmos.* **103**, 5747–5758 (1998).
73. Wallington, T. J. *et al.* Formation of C7F15COOH (PFOA) and other perfluorocarboxylic acids during the atmospheric oxidation of 8:2 fluorotelomer alcohol. *Environ. Sci. Technol.* **40**, 924–30 (2006).
74. Iizuka, Y., Igarashi, M., Kamiyama, K., Motoyama, H. & Watanabe, O. Ratios of Mg2+/Na+ in snowpack and an ice core at Austfonna ice cap, Svalbard, as an indicator of seasonal melting. *J. Glaciol.* **48**, 452–460 (2002).
75. Plassmann, M. M. *et al.* Laboratory Studies on the Fate of Perfluoroalkyl Carboxylates and Sulfonates during Snowmelt. *Environ. Sci. Technol* **45**, 6872–6878 (2011).
76. Codling, G. *et al.* The fate of per- and polyfluoroalkyl substances within a melting snowpack of a boreal forest. *Environ. Pollut.* **191**, 190–198 (2014).
77. Pohjola, V. A. *et al.* Effect of periodic melting on geochemical and isotopic signals in an ice core from Lomonosovfonna, Svalbard. *J. Geophys. Res.* **107**, 4036 (2002).
78. Moore, J. C., Grinsted, A., Kekonen, T. & Pohjola, V. Separation of melting and environmental signals in an ice core with seasonal melt. *Geophys. Res. Lett.* **32**, 1–4 (2005).
79. Matykiewiczová, N., Klánová, J. & Klán, P. Photochemical degradation of PCBs in snow. *Environ. Sci. Technol.* **41**, 8308–8314 (2007).

4.7 Supporting Information

Drill site characteristics 114

Chemicals and Reagents 114

Sample Extraction 115

Instrument Analysis 115

Quality Assurance and Quality Control 117

HYSPLIT analysis 119

Ion Chromatography for quantification of major ion concentrations 120

Isotope ratio mass spectrometry for quantification of water stable isotope ratios 121

References 121

Table S1. List of target analytes, abbreviations, and CAS numbers 122

Table S2. MRM transitions and, internal and recovery standards used for quantification. 123

Table S3. Instrument limits of quantification, method limits of quantification, extraction efficiencies and repeatability of the instrument method 124

Table S4. The extraction efficiency for those compounds with available equivalent mass-labelled internal and recovery standards 125

Table S5. Further extraction efficiencies for the nine neutral compounds 125

Table S6. MRM transitions, instrument limits of quantification (LOQ), and method limits of quantification (MQL) for branched isomers of PFHxS and PFOS. 125

Table S7. Fluxes of C_2 – C_{13} PFCAs 126

Table S8. Fluxes of PFHxS, PFOS, FSBA, FOSA 127

Table S9. Concentrations of C_2 – C_{14}, C_{16} and C_{18} PFCAs 128

Table S10. Concentrations of C_2 – C_{10} and C_{12} PFSAs 129

Table S11. Concentrations of nine neutral PFAS: FBSA, MeFBSA, FHxSA, MeFHxSA, FOSA, MeFOSA, EtFOSA, MeFOSE, and EtFOSE 130

Table S12. Concentrations of 4:2 FTSA, 6:2 FTSA, 8:2 FTSA, 6:2 FTUCA, 8:2 FTUCA, PFECHS, 6:2 Cl-PFESA, 8:2 Cl-PFESA, HFPO-DA and ADONA 131

Table S13. Correlations of C_2 – C_{13} PFCAs, PFOS, FBSA and FOSA 132

Table S14. Percentage of linear isomers and concentrations of linear and branched isomers of PFOS 133

Table S15. Percentage of linear isomers and concentrations of linear and branched isomers of PFHxS 134

Table S16. Correlations of C_2 – C_{13} PFCAs, PFOS, FBSA and FOSA with Na^+ and the melt proxy $\log([Na^+]/[Mg^{2+}])$ 135

Figure S1. Ice core dating with annual layer counting 136

Figure S2. HYSPLIT seasonal trajectory frequency plots for 2007 - 2018 138

TOC Art (Graphical Abstract) 139

Drill Site Characteristics

Lomonosovfonna is one of the highest elevation glacier plateaus on Svalbard (Figure 1). Located in central Spitsbergen, the drilling site was 31 km from Pyramiden (population <10) and 79 km from Longyearbyen (population approximately 2,400). The drilling site (1198 ma.s.l.) is a cupola and has been previously drilled in 2009.[1] A study investigating sources of major ions in snow pits from 22 sites on seven Svalbard glaciers concluded that sites above 600 – 700 m.a.s.l. would be less impacted by local emissions, and it identified Lomonosovfonna as an optimal site to investigate long-range pollution deposition on Svalbard.[2] Several studies have already used the 2009 Lomonosovfonna ice core to investigate the long-range atmospheric processes of contaminants such as black carbon and polychlorinated biphenyls.[3,4]

At the drilling site, the firn temperature at 10 m depth is 0 °C all year round, and by the end of the ablation season, the upper 10 m of firn/snowpack is isothermal at 0 °C.[5] It is well known that summer melt contributes to the partial redistribution of chemical species in Lomonosovfonna ice cores. This is also apparent from the melt features present within Lomonosovfonna ice cores, formed from the refreezing of percolating meltwater through the snowpack/firn.[1]

Chemicals and Reagents

Standards of native perfluoroalkyl carboxylic acids (PFCAs; C_4-C_{12}), perfluoroalkyl sulfonic acids (PFSAs; C_3-C_{10} and $C_{12,}$ including branched isomers), and mass-labelled standards of PFCAs (C_4-C_{12}), PFSAs (C_4, C_6, C_8) were from Wellington laboratories (Guelph, ON, Canada). Perfluoropropanoic acid was from Sigma-Aldrich, (Oakville, ON, Canada). Trifluoromethane sulfonic acid (TFMS) was from Sigma-Aldrich, (Stockholm, Sweden), and potassium salt of perfluoroethane sulfonate was obtained from Kanto Chemical Co., Inc., (Portland, OR, USA). The mass-labeled standard of TFA ($^{13}C_2$-TFA) was purchased from Toronto Research Chemicals Inc,

(Toronto, ON, Canada). The purity of all standards was above 97%. Ammonium acetate (≥99.0%) was purchased from Sigma-Aldrich, (Stockholm, Sweden). Glacial acetic acid (EMPARTA®, ≥99.7%) was purchased from Merck, (Darmstadt, Germany). The ammonia solution (puriss. p.a.) was purchased from Sigma-Aldrich, (Stockholm, Sweden). HPLC grade methanol (≥99.8%) and LC-MS grade methanol (≥99.9%) were from Fischer Scientific, (Ottawa, ON, Canada) and Merck, (Darmstadt, Germany). Weak anion exchange solid-phase extraction (WAX-SPE) cartridges were obtained from Waters Corporation, (Milford, MA, USA).

Sample Extraction

On average, 2160 mL of sample was extracted by weak anion exchange solid-phase extraction (Oasis® WAX, Waters Corporation, Milford, USA) following the ISO25101 method with some modifications. Prior to extraction, the pH of the samples was adjusted to pH 4 by addition of several drops of acetic acid. The cartridges were preconditioned with 12 mL 0.1% ammonium hydroxide in methanol followed by 12 mL methanol and 4 mL Milli-Q water. The samples were then loaded at approximately 1 drop per second onto the cartridges. After loading the samples, the cartridges were washed by passage of 4 mL of Milli-Q water followed by 8 mL ammonium acetate buffer solution (pH 4) and then dried under vacuum for 30 min before elution of target analytes. The neutral fraction was eluted by adding 12 mL methanol. The anionic fraction was then eluted by adding 12 mL 0.1% ammonium hydroxide in methanol. The eluates were then evaporated to approximately 0.5 mL at 60 °C and 400 mbar, transferred to an LC vial, and then further evaporated to 100 µL under a gentle stream of nitrogen.

Instrument Analysis

For quantification of $C_1 - C_3$ PFAAs, 40 µL of the anionic fraction was transferred to new LC vials and aliquots of 2 µL were injected into the supercritical fluid chromatography (SFC) tandem mass

spectrometry (MS/MS) system; details of the instrument setup are given below. For quantification of all other PFAS, in addition to PFBA, 40 µL of the anionic fraction was transferred to new LC vials and aliquots of 10 µL were injected into the ultra-performance liquid chromatography (UPLC) MS/MS system after addition of 60 µL of 2 mM aqueous ammonium acetate. For quantification of neutral PFASs, aliquots of 10 µL of the neutral fraction were injected into the UPLC-MS/MS system. Mass-labeled internal standards and recovery standards (1 ng) were added to the samples prior to extraction and prior to injection, respectively, to monitor the recovery of the method.

Separation and quantification of C_1 – C_3 PFAAs were performed using SFC-MS/MS (Acquity Ultra-performance Convergence Chromatograph and Xevo TQ-S micro, Waters Corporation, Milford, MA, USA) operated in negative electrospray ionization mode. An SFC Torus DIOL column (3.0 mm i.d., 150 mm length, 1.7 µm particle size) (Waters Corporation, Milford, MA, USA) maintained at 50 °C was used to achieve chromatographic separation. The mobile phase consisted of CO_2 (A) and 0.1% ammonium hydroxide in methanol (B). The gradient of the mobile phase started with an initial B concentration of 15%, which was then increased to 35% over 5 min. This was held for 1 min before returning to initial conditions over 1 min. The flow rate was 1.2 mL/min and the active back pressure regulator was set at 2000 psi throughout the chromatographic separation.

Separation and quantification of all other PFAS were performed using ultra-performance liquid chromatography (UPLC) MS/MS (Acquity Ultra-performance Liquid Chromatograph and Xevo TQ-S, Waters Corporation, Milford, MA, USA) operated in negative electrospray ionization mode. A UPLC BEH C18 column (2.1 mm i.d., 100 mm length, 1.7 µm particle size) (Waters Corporation, Milford, MA, USA) maintained at 50 °C was used to achieve chromatographic

separation. The mobile phase for UPLC-MS/MS analysis consisted of 2 mM NH4Ac in MeOH:Milli-Q (3:7) (A) and 2 mM NH4Ac in MeOH (B) at a flow rate of 0.3 mL/min. The gradient of the mobile phase started with an initial B concentration of 1% for 1 min. This was then increased to 100% over 12 min and held for 1 min and finally re-conditioned for 3 min.

The source parameters (for both instrumental setups) were set as following: capillary voltage, 0.7 kV; source temperature, 150 °C; desolvation temperature, 400 °C; cone gas flow, 150 L/h; desolvation gas flow, 800 L/h; collision gas flow, 0.2 mL/min; nebulizer, 6.5 bar. At least two transitions were monitored for each target analyte except for TFA, PFPrA, PFBA, PFPeA, MeFOSA, and EtFOSA where only one transition was monitored. MRM transitions for all target analytes are provided in Table S2 and S6.

Quality Assurance and Quality Control

Linear regression analysis showed good linearity for each analyte (R^2> 0.99) in the range from 2.0 to 100 ng/mL for UPLC and SFC. Instrumental limits of quantification (LOQs) were set as the lowest calibration point with a signal-to-noise ratio of at least ten. For UPLC the repeatability of the instrumental method was evaluated based on repeated injections (n = 8 for UPLC, n = 9 for SFC) of a standard with a concentration of 10 ng/mL, except for those PFAS measured by UPLC, whereby the standard had a concentration of 4 ng/mL. The relative standard deviation of repeated injections for UPLC and SFC was in the range 2.4 – 16 % for C_2 to C_{11} PFCAs and C_2 to C_{10} PFSAs

Isotope dilution was used for quantification. For those target analytes that did not have corresponding mass-labelled standards, the homologue closest in retention time was used for quantification (Table S2). Extraction efficiencies of all analytes were assessed based on the peak area of native standards spiked to test samples (n = 2) compared to that of the native standards in

solvent after subtraction of the background concentrations in the samples (Table S3). Test samples consisted of 50 mL of melted surface snow from Lomonosovfonna spiked with 1000 pg of native standard. The extraction efficiencies for C_2 to C_{11} PFCAs and C_2 to C_{10} PFSAs were in the range 45 – 123%. For those analytes with available corresponding mass-labeled internal and recovery standards (PFHxS, PFOS and C_{4-11} PFCAs), their extraction efficiency was also assessed by comparing the peak area of the spiked internal standard and recovery standard across all samples (n = 27). Their extraction efficiencies were in the range 72 – 98% (Table S4). The relative standard deviation was in the range 9 – 14%. For TFA, the extraction efficiency was assessed by comparing the peak area of a mass-labeled standard with an injection standard. This gave a recovery of 47% with a standard deviation of 15%. For the 9 neutral analytes, the extraction efficiencies were also assessed by comparing the peak areas of their respective internal and surrogate recovery standards, across all samples (n = 27). Their extraction efficiencies were in the range 17 – 77% (Table S5). The relative standard deviation was in the range 9 – 28%. The method limits of quantification (MQLs) were calculated as the average concentration in repeated blank extractions (n = 3) plus three times the standard deviation. For those analytes that were not observed in blank extractions, the instrument LOQ was used as the MQL. Detailed information about the precision of the instrument method repeatability, extraction efficiencies, LOQ, and MQL are provided in Tables S3, S4 and S5.

Prior to drilling, the core barrel was precleaned with soapy water, rinsed with tap water, Milli-Q water and finally methanol. During drilling, ice core sections were handled with nitrile gloves and personnel wore polypropylene non-participating coveralls. Core sections were sealed in low-density polyethylene lay flat tubing for transport and storage. The saw used to cut the core was precleaned with soapy water, rinsed with tap water, Milli-Q water, and finally methanol.

During core cutting and processing strict decontamination, removing 1.0 – 2.3 cm from the outside of the core, ensured that potential contamination during drilling, transport, and storage was removed. In the cold lab, a cold lab blank was used to assess contamination during cutting the core. The cold lab blank consisted of Milli-Q water that had been frozen. This was then cut and processed identically to the ice core sections. In comparison to a liquid Milli-Q water blank that was processed in parallel, no compounds were detected at increased levels in the cold lab blank, except for TFMS. TFMS levels in the cold lab blank were >80 times higher compared to the liquid Milli-Q water blank processed in parallel. Hence it was concluded that the ice core cutting and processing introduced TFMS contamination to the ice core samples. TFMS concentrations and fluxes are not reported.

HYSPLIT backward air mass trajectory analysis

The Hybrid Single-Particle Lagrangian Integrated Trajectory (HYSPLIT) model (Version 5.1.0, National Oceanic and Atmospheric Administration, Washington, DC) was used to assess air mass source regions.[6] The National Center for Environmental Prediction's Global Data Assimilation System (GDAS) model was used for the meteorological input data. 4383 daily 6-day backward air mass trajectories were calculated for the period of whole years recorded in the core (2007 – 2018), which ended at the drilling site on Lomonosovfonna (78°49.454'N, 17°26.193'E, 1198 m.a.s.l.). The atmospheric lifetime of PFAAs is assumed to be short and their removal from the atmosphere dominated by wet and dry deposition. A 6-day backward air mass trajectory was used, which is the atmospheric half-life of TFA with respect to wet and dry deposition.[7] These trajectories were plotted together on a frequency plot, whereby trajectory frequency is given as a percentage. This percentage was calculated based on the number of trajectory intersections in each 1-degree grid cell divided by the total number of trajectories.

Ion Chromatography for Quantification of Major Ion Concentrations

To prepare each sample for analysis, the 5 cm subsample for major ions was melted in a sealed centrifuge tube, in a fridge, to create a measurable water sample. Cation (Na^+, Mg^{2+}) and anion (Cl^-) concentrations were measured using Dionex ICS-4000 Integrion anion and cation systems. A Dionex AS-AP autosampler was used to supply sample to each instrument. Calibration was achieved using a range of calibration standards. All calibration standards were prepared from purchased Sigma Aldrich (1000 ppm) standards by a series of gravimetric dilutions.

The anion system used a Dionex Ionpac AG17-C (2 μm, 2 x 50 mm) guard column and AS17-C (2 x 250 mm) analytical column. Samples were loaded to a 250 μL sample loop. A 1 – 40 mM potassium hydroxide multistep eluent gradient was used for effective separation of the analytes. The eluent was produced using a Dionex eluent generator cartridge (EGC 500 KOH) and was pumped through the columns at a flow rate of 0.29 mL min^{-1} at a pressure of 2300 psi for a 20 min chromatogram. The eluent ions were removed from the column effluent using an anion electrolytically regenerated suppressor (Dionex AERS 500), before conductivity detection of the eluate.

The cation instrument used a Dionex Ionpac CG16-4μm (2 x 50 mm) guard column and CS16 (4 μm, 2 x 250 mm) analytical column. Samples were loaded into a 250 μL sample loop. A 32 – 42 mM methane sulfonic acid (MSA) multistep eluent gradient was used for effective separation of the analytes. The eluent was produced using a Dionex eluent generator cartridge (EGC 500 KOH) and was pumped through the columns at a flow rate of 0.20 mL min^{-1} at a pressure of 3300 psi for a 25 min chromatogram. The eluent ions were removed from the column effluent using a cation electrolytically regenerated suppressor (Dionex CERS 500), before conductivity detection of the effluent.

Isotope Ratio Mass Spectrometry for Quantification of Water Stable Isotope Ratios

All oxygen isotope measurements were performed on a Thermo Delta V Advantage isotope mass spectrometer fitted with a GasBench II at the Department of Earth Sciences, University of Oxford. To prepare each sample for analysis, the 5 cm subsample for isotope analysis was melted in a sealed centrifuge tube, to create a measurable water sample. A 0.5 mL aliquot was transferred to a 12 mL Exetainer container for $\delta^{18}O$ and δD analyses, using the method described in Nelson (2000).[8] Iso-Analytical Limited standards IA-RO63 and IA-RO65 were used for two-point linear normalization, with IA-RO63 $\delta^{18}O$ = -0.4 ± 0.1 (1σ), IA-RO63 δD = 11 ± 1.3‰ (1σ); and IA-RO65 $\delta^{18}O$ = -33.57 ± 0.08‰ (1σ), IA-RO65 δD = -269 ± 1.3‰ (1σ). Accuracy and external precision were checked with repeat measurements of Iso-Analytical standard IA-RO64, with our two-point normalized results IA-RO64 $\delta^{18}O$ = -12.39 ± 0.04‰ (1σ, n=15), IA-RO64 δD = -98.7 ± 0.8‰ (1σ, n=15) within error of Iso-Analytical Limited laboratory results IA-RO64 $\delta^{18}O$ = -12.3 ± 0.1‰ (1σ), IA-RO64 δD = -98 ± 1.1‰ (1σ). The $^{18}O/^{16}O$ and $^{2}H/^{1}H$ isotope ratio scales are defined in terms of V-SMOW and SLAP, such that the $^{18}O/^{16}O$ and $^{2}H/^{1}H$ isotopic composition of SLAP relative to V-SMOW is -55.5‰ for $\delta^{18}O$ and -428‰ for $\delta^{2}H$.

References

1. Wendl, I. A., Eichler, A., Isaksson, E., Martma, T. & Schwikowski, M. 800-year ice-core record of nitrogen deposition in Svalbard linked to ocean productivity and biogenic emissions. *Atmos. Chem. Phys* **15**, 7287–7300 (2015).
2. Barbaro, E. *et al.* Measurement report: Spatial variations in ionic chemistry and water-stable isotopes in the snowpack on glaciers across Svalbard during the 2015-2016 snow accumulation season. *Atmos. Chem. Phys.* **21**, 3163–3180 (2021).
3. Garmash, O. *et al.* Deposition history of polychlorinated biphenyls to the lomonosovfonna glacier, Svalbard: A 209 congener analysis. *Environ. Sci. Technol.* **47**, 12064–12072 (2013).
4. Osmont, D. *et al.* An 800-year high-resolution black carbon ice core record from Lomonosovfonna, Svalbard. *Atmos. Chem. Phys.* **18**, 12777–12795 (2018).
5. Marchenko, S., Pohjola, V., Pettersson, R., Van Pelt, W. & Reijmer, C. Thermal conductivity of firn at Lomonosovfonna, Svalbard, derived from subsurface temperature measurements. *Cryosph.* **13**, 1843–1859 (2019).
6. Stein, A. F. *et al.* NOAA's HYSPLIT Atmospheric Transport and Dispersion Modeling System. *Bull. Am. Meteorol. Soc.* **96**, 2059–2077 (2015).
7. Kotamarthi, V. R. *et al.* Trifluoroacetic acid from degradation of HCFCs and HFCs: A three-dimensional modeling study. *J. Geophys. Res. Atmos.* **103**, 5747–5758 (1998).
8. Nelson, S. T. A simple, practical methodology for routine VSMOW/SLAP normalization of water samples analyzed by continuous flow methods. *Rapid Commun. Mass Spectrom.* **14**, 1044–1046 (2000).

Table S1. List of target analytes, abbreviations, and CAS numbers

Abbreviation	Target analyte	CAS
TFA	Trifluoroacetic acid	76-05-1
PFPrA	Perfluoropropanoic acid	422-64-0
PFBA	Perfluorobutanoic acid	375-22-4
PFPeA	Perfluoropentanoic acid	2706-90-3
PFHxA	Perfluorohexanoic acid	307-24-4
PFHpA	Perfluoroheptanoic acid	375-85-9
PFOA	Perfluorooctanoic acid	335-67-1
PFNA	Perfluorononanoic acid	375-95-1
PFDA	Perfluorodecanoic acid	335-76-2
PFUnDA	Perfluoroundecanoic acid	2058-94-8
PFDoDA	Perfluorododecanoic acid	307-55-1
PFTrDA	Perfluorotridecanoic acid	72629-94-8
PFTeDA	Perfluorotetradecanoic acid	376-06-7
PFHxDA	Perfluorohexadecanoic acid	67905-19-5
PFOcDA	Perfluorooctadecanoic acid	16517-11-6
TFMS	Trifluoromethane sulfonic acid	1493-13-6
PFEtS	Perfluoroethane sulfonic acid	354-88-1
PFPrS	Perfluoropropane sulfonic acid	423-41-6
PFBS	Perfluorobutane sulfonic acid	375-73-5
PFPeS	Perfluoropentane sulfonic acid	2706-91-4
PFHxS	Perfluorohexane sulfonic acid	355-46-4
PFHpS	Perfluoroheptane sulfonic acid	375-92-8
PFOS	Perfluorooctane sulfonic acid	1763-23-1
PFNS	Perfluorononane sulfonic acid	68259-12-1
PFDS	Perfluorodecane sulfonic acid	335-77-3
PFDoDS	Perfluorododecane sulfonic acid	79780-39-5
4:2 FTSA	4:2 Fluorotelomer sulfonic acid	757124-72-4
6:2 FTSA	6:2 Fluorotelomer sulfonic acid	27619-97-2
8:2 FTSA	8:2 Fluorotelomer sulfonic acid	39108-34-4
6:2 FTUCA	6:2 Fluorotelomer unsaturated carboxylic acid	70887-88-6
8:2 FTUCA	8:2 Fluorotelomer unsaturated carboxylic acid	70887-84-2
PFECHS	Perfluoroethylcyclohexane sulfonic acid	72441-89-5
6:2 Cl-PFESA	6:2 Chlorinated polyfluorinated ether sulfonate	756426-58-1
8:2 Cl-PFESA	8:2 Chlorinated polyfluorinated ether sulfonate	763051-92-9
HFPO-DA	Hexafluoropropylene oxide dimer acid	13252-13-6
ADONA	3H-perfluoro-3-[(3-methoxy-propoxy)propanoic acid]	919005-14-4
FBSA	Perfluorobutane sulfonamide	30334-69-1
MeFBSA	Methyl perfluorobutane sulfonamide	68298-12-4
FHxSA	Perfluorohexane sulfonamide	41997-13-1
MeFHxSA	Methyl perfluorohexane sulfonamide	68259-15-4
FOSA	Perfluorooctane sulfonamide	754-91-6
MeFOSA	N-Methyl perfluorooctane sulfonamide	31506-32-8
EtFOSA	N-Ethyl perfluorooctane sulfonamide	4151-50-2
MeFOSE	N-Methyl perfluorooctane sulfonamidoethanol	24448-09-7
EtFOSE	N-Ethyl perfluorooctane sulfonamidoethanol	1691-99-2

Table S2. MRM transitions and internal standards used for quantification.

Abbreviation	1st MRM transition	2nd MRM transition	Internal standard	Recovery Standard
TFA	112.90 > 68.96	-	^{13}C-M2TFA	
PFPrA	162.97 > 118.90	-	^{13}C-M4PFBA	
PFBA	212.97 > 169.00	-	^{13}C-M4PFBA	^{13}C-M3PFBA
PFPeA	262.97 > 219.00	-	^{13}C-M3PFPeA	^{13}C-M5PFPeA
PFHxA	312.97 > 269.00	312.97 > 118.95	^{13}C-M2PFHxA	^{13}C-M5PFHxA
PFHpA	362.97 > 319.00	362.97 > 168.97	^{13}C-M4PFHpA	^{13}C-M8PFOA
PFOA	412.97 > 369.00	412.97 > 168.97	^{13}C-M4PFOA	^{13}C-M8PFOA
PFNA	462.99 > 419.00	462.99 > 219.00	^{13}C-M5PFNA	^{13}C-M9PFNA
PFDA	512.97 > 469.00	512.97 > 219.00	^{13}C-M2PFDA	^{13}C-M6PFDA
PFUnDA	562.97 > 268.99	562.97 > 519.00	^{13}C-M2PFUnDA	^{13}C-M7PFUnDA
PFDoDA	612.97 > 569.00	612.97 > 168.96	^{13}C-M2PFDoDA	
PFTrDA	662.90 > 619.00	662.90 > 168.96	^{13}C-M2PFDoDA	
PFTeDA	712.90 > 669.00	712.90 > 168.97	^{13}C-M2PFTeDA	
PFHxDA	812.90 > 769.00	812.90 > 168.96	^{13}C-M2PFHxDA	
PFOcDA	912.90 > 869.00	912.90 > 168.96	^{13}C-M2PFHxDA	
TFMS	149.12 > 79.91	149.12 > 98.95	^{13}C-M3PFBS	
PFEtS	198.80 > 79.80	198.80 > 98.90	^{13}C-M3PFBS	
PFPrS	248.90 > 79.90	248.90 > 98.90	^{13}C-M3PFBS	
PFBS	298.90 > 79.96	298.90 > 98.90	^{13}C-M3PFBS	
PFPeS	348.90 > 79.96	348.90 > 98.96	^{18}O-M2PFHxS	
PFHxS	398.90 > 79.96	398.90 > 98.90	^{18}O-M2PFHxS	^{13}C-M3PFHxS
PFHpS	448.97 > 79.96	448.97 > 98.90	^{13}C-M4PFOS	
PFOS	498.97 > 79.96	498.97 > 98.96	^{13}C-M4PFOS	^{13}C-M8PFOS
PFNS	548.90 > 79.96	548.90 > 98.96	^{13}C-M4PFOS	
PFDS	598.97 > 79.96	598.97 > 98.90	^{13}C-M4PFOS	
PFDoDS	698.90 > 79.96	698.90 > 98.90	^{13}C-M4PFOS	
4:2 FTSA	327.00 > 307.00	329.00 > 81.00	^{13}C-M2-6:2 FTSA	
6:2 FTSA	427.00 > 407.00	427.00 > 81.00	^{13}C-M2-6:2 FTSA	
8:2 FTSA	527.00 > 507.00	527.00 > 80.00	^{13}C-M2-8:2 FTSA	
6:2 FTUCA	356.90 > 292.91	356.9 > 242.95	^{13}C-M2-6:2 FTUCA	
8:2 FTUCA	456.90 > 392.94	456.90 > 342.88	^{13}C-M2-8:2 FTUCA	
PFECHS	460.84 > 380.942	460.84 > 98.882	^{13}C-M4PFOA	
6:2 Cl-PFESA	530.904 > 350.98	530.904 > 98.95	^{13}C-M4PFOS	
8:2 Cl-PFESA	630.904 > 450.98	630.904 > 98.95	^{13}C-M4PFOS	
HFPO-DA	284.90 > 168.70	284.9 > 184.80	^{13}C-M3HFPO-DA	
ADONA	376.97 > 250.83	376.97 > 84.69	^{13}C-M3HFPO-DA	
FBSA	297.90 > 77.92	297.90 > 118.94	^{13}C-M8FOSA	
MeFBSA	311.97 > 218.95	311.97 > 111.93	^{13}C-M8FOSA	
FHxSA	397.9 > 77.92	397.90 > 168.94	^{13}C-M8FOSA	
MeFHxSA	411.97 > 168.93	411.97 > 318.96	^{13}C-M8FOSA	
FOSA	497.90 > 78.00	497.90 > 168.90	^{13}C-M8FOSA	
Me-FOSA	512.00 > 169.00	-	^{13}C-d3-N-MeFOSA	
EtFOSA	526.00 > 169.00	-	^{13}C-d5-N-EtFOSA	
MeFOSE	616.00 > 59.00	556.03 > 121.99	^{13}C-d7-N-MeFOSE	
EtFOSE	630.00 > 59.00	570.096 > 135.983	^{13}C-d9-N-EtFOSE	

Table S3. Instrument limits of quantification (LOQ) (pg L^{-1}), method limits of quantification (MQL) (pg L^{-1}). The range in extraction efficiency (%) based on spiked blank samples and spiked test samples (n = 2). Repeatability (%) of the instrument method based on repeated standard injections (n = 8 for UPLC, n = 9 for SFC).

Analyte	LOQ (pg L^{-1})	MQL (pg L^{-1})	Extraction efficiency (%)	Separation method	Instrument method repeatability (%)
TFA	9.3	582	101 – 110	SFC	16
PFPrA	9.3	227	55 – 70	SFC	14
PFBA	9.3	60.0	65 – 93	UPLC	3.4
PFPeA	2.3	21.6	73 – 91	UPLC	3.2
PFHxA	2.3	13.3	78 – 88	UPLC	4.7
PFHpA	2.3	6.5	89 – 94	UPLC	2.5
PFOA	2.3	10.6	92 – 94	UPLC	2.8
PFNA	2.3	2.3	113 – 123	UPLC	2.7
PFDA	2.3	10.3	95 - 119	UPLC	3.8
PFUnDA	2.3	2.3	64 – 85	UPLC	4.6
PFDoDA	2.3	2.3	37 – 63	UPLC	3.5
PFTrDA	2.3	2.3	29 – 55	UPLC	5.6
PFTeDA	2.3	2.3	22 – 31	UPLC	8.3
PFHxDA	2.3	2.3	17 – 18	UPLC	12
PFOcDA	2.3	2.3	31 – 49	UPLC	30
TFMS	9.3	181	72 – 98	SFC	17
PFEtS	9.3	9.3	78 – 104	SFC	13
PFPrS	9.3	9.3	90 – 102	SFC	14
PFBS	2.3	20.4	100 – 101	UPLC	3.5
PFPeS	2.3	2.3	101 – 103	UPLC	2.6
PFHxS	2.3	4.4	101 – 110	UPLC	3.3
PFHpS	9.3	9.3	98 – 108	UPLC	2.4
PFOS	2.3	6.6	91 – 109	UPLC	3.6
PFNS	9.3	9.3	65 – 91	UPLC	2.9
PFDS	2.3	2.3	45 – 63	UPLC	4.1
PFDoDS	2.3	2.3	24 – 28	UPLC	4.0
4:2 FTSA	2.3	2.3	123 – 126	UPLC	3.8
6:2 FTSA	2.3	4.5	145 – 157	UPLC	2.2
8:2 FTSA	2.3	2.3	222 – 252	UPLC	5.7
6:2 FTUCA	2.3	2.3	25 – 39	UPLC	3.2
8:2 FTUCA	2.3	2.3	31 – 45	UPLC	2.4
PFECHS	2.3	2.3	98 – 107	UPLC	3.2
6:2 Cl-PFESA	2.3	2.3	73 – 101	UPLC	1.8
8:2 Cl-PFESA	2.3	2.3	37 – 62	UPLC	4.3
HFPO-DA	2.3	2.3	63 – 73	UPLC	2.6
ADONA	2.3	2.3	82 – 85	UPLC	3.5
FBSA	2.3	2.3	47 – 49	UPLC	5.2
MeFBSA	9.3	10.6	36 – 50	UPLC	5.5
FHxSA	2.3	2.3	39 – 52	UPLC	1.5
MeFHxSA	9.3	9.3	30 – 52	UPLC	1.9
FOSA	2.3	2.9	27 – 53	UPLC	1.4
MeFOSA	23.1	23.1	13 – 22	UPLC	4.9
EtFOSA	23.1	23.1	12 – 18	UPLC	1.2
MeFOSE	2.3	2.3	19 – 21	UPLC	2.3
EtFOSE	2.3	2.3	15 – 22	UPLC	1.2

Table S4. The extraction efficiency for those compounds with available equivalent mass-labelled internal and recovery standards, expressed as the average extraction efficiency ± standard deviation of spiked internal standards (n = 27)

Analyte	Internal standard	Recovery standard	Extraction efficiency (%)
PFBA	^{13}C-M4PFBA	^{13}C-M3PFBA	80 ± 9
PFPeA	^{13}C-M3PFPeA	^{13}C-M5PFPeA	80 ± 9
PFHxA	^{13}C-M2PFHxA	^{13}C-M5PFHxA	81 ± 9
PFHpA	^{13}C-M4PFHpA	^{13}C-M8PFOA	72 ± 10
PFOA	^{13}C-M4PFOA	^{13}C-M8PFOA	87 ± 9
PFNA	^{13}C-M5PFNA	^{13}C-M9PFNA	88 ± 10
PFDA	^{13}C-M2PFDA	^{13}C-M6PFDA	87 ± 11
PFUnDA	^{13}C-M2PFUnDA	^{13}C-M7PFUnDA	82 ± 14
PFHxS	^{18}O-M2PFHxS	^{13}C-M3PFHxS	98 ± 13
PFOS	^{13}C-M4PFOS	^{13}C-M8PFOS	94 ± 12

Table S5. The extraction efficiency for the nine neutral compounds, expressed as the average extraction efficiency ± standard deviation of spiked internal standards (n = 27)

Analyte	Internal standard	Recovery standard	Extraction efficiency (%)
FOSA	^{13}C-M8FOSA[a]	^{13}C-M8PFOS	77 ± 28
MeFOSA	^{13}C-d3-N-MeFOSA	^{13}C-M8PFOS	22 ± 11
EtFOSA	^{13}C-d5-N-EtFOSA	^{13}C-M8PFOS	17 ± 9
MeFOSE	^{13}C-d7-N-MeFOSE	^{13}C-M8PFOS	40 ± 20
EtFOSE	^{13}C-d9-N-EtFOSE	^{13}C-M8PFOS	32 ± 15

[a] ^{13}C-M8FOSA is also the internal standard for FBSA, MeFBSA, FHxSA and MeFHxSA

Table S6. MRM transitions, instrument limits of quantification (LOQ) (pg L^{-1}), and method limits of quantification (MQL) (pg L^{-1}) for branched isomers of PFHxS and PFOS.

Abbreviation	1st MRM transition	2nd MRM transition	LOQ (pg L^{-1})	MQL (pg L^{-1})
2/3/4-PFHxS	398.9 > 79.96	398.9 > 98.96	2.3	2.3
1-PFHxS	398.9 > 319.00	398.9 > 98.96	2.3	2.3
3/4/5-PFOS	498.97 > 79.96	498.97 > 98.96	2.3	2.3
6/2-PFOS	498.97 > 169.03	498.97 > 79.96	2.3	2.3
1-PFOS	498.97 > 419.00	498.97 > 169.03	2.3	2.3

Table S7. Fluxes (ng m^{-2} yr^{-1}) of C_2 – C_{13} PFCAs with detection frequencies >50% above the MQL. In the case of a concentration <MQL, half the MQL was substituted for the flux calculation. Note that the years 2006 and 2019 are only partly recorded by the ice core (see figure S1)

Year	TFA	PFPrA	PFBA	PFPeA	PFHxA	PFHpA	PFOA	PFNA	PFDA	PFUnDA	PFDoDA	PFTrDA
2019	2600	440	200	200	33	15	11	6.1	3.0	1.6	0.93	0.63
2018	4000	670	300	300	50	24	17	9.4	4.6	2.5	1.4	1.0
2017	8200	1300	480	480	99	69	59	120	27	31	5.4	5.9
2016	8000	1100	440	440	96	78	48	45	15	10	1.3	1.5
2015	3700	680	260	260	60	64	36	54	15	19	3.7	2.4
2014	3000	680	270	270	58	56	29	17	7.1	6.7	5.9	5.1
2013	5900	1300	530	530	110	99	51	68	38	45	11	8.5
2012	3600	860	330	330	70	52	27	28	14	9.5	1.4	1.2
2011	4300	1100	420	420	95	82	47	52	19	14	5.9	3.0
2010	2600	800	280	280	62	43	27	34	13	11	3.5	1.7
2009	3100	1000	370	370	79	59	35	48	18	17	5.3	2.2
2008	4400	1600	570	570	120	95	58	100	47	79	16	8.7
2007	2900	1300	400	400	79	51	30	69	35	50	9.1	4.2
2006	290	130	41	16	8.1	4.7	2.7	3.9	1.7	1.4	0.44	0.25

Table S8. Fluxes (ng m^{-2} yr^{-1}) of PFHxS, PFOS, FBSA and FOSA with detection frequencies >50% above the MQL. In the case of a concentration <MQL, half the MQL was substituted for the flux calculation. Note that the years 2006 and 2019 are only partly recorded by the ice core (see figure S1)

Year	PFHxS	PFOS	FBSA	FOSA
2019	1.1	3.0	0.46	0.24
2018	1.7	4.6	0.70	0.37
2017	8.1	26	2.6	4.2
2016	1.8	15	4.0	1.2
2015	2.7	15	1.4	1.5
2014	10	70	1.6	1.8
2013	2.8	13	4.1	4.6
2012	1.2	6.4	1.4	0.91
2011	3.8	9.1	3.2	1.8
2010	8.9	3.6	0.74	1.7
2009	2.4	1.7	1.3	1.7
2008	3.0	9.8	1.5	2.3
2007	2.0	5.6	0.64	2.0
2006	0.15	0.22	0.078	0.10

Table S9. Concentrations of C_2 – C_{14} and C_{16} PFCAs (pg L^{-1}). All subsections were <MQL for PFOcDA (C_{18})

Depth (cm weq)	TFA	PFPrA	PFBA	PFPeA	PFHxA	PFHpA	PFOA	PFNA	PFDA	PFUnDA	PFDoDA	PFTrDA	PFTeDA	PFHxDA
48.9	15500	2610	1170	388	195	92.2	65.8	36.4	18.0	9.72	5.54	3.79	<MQL	<MQL
90.5	13100	2170	809	318	173	126	112	254	55.8	70.8	11.9	12.9	4.53	<MQL
128.2	16500	1740	661	261	140	100	76.6	76.3	24.3	9.51	<MQL	2.62	<MQL	<MQL
170.2	7040	1350	526	214	115	97.3	50.6	36.1	14.0	11.6	<MQL	<MQL	<MQL	<MQL
207.8	10800	1970	748	311	175	189	106	164	46.7	57.0	10.2	6.33	<MQL	<MQL
245.5	8080	1810	711	291	156	148	76.7	43.7	17.2	15.2	15.7	13.6	14.4	15.0
282.4	7340	1490	549	224	123	145	64.3	76.4	40.5	52.2	14.5	10.1	<MQL	<MQL
322.3	9420	2220	952	399	197	138	81.4	117	66.7	76.0	15.7	14.3	<MQL	<MQL
364.6	7100	1660	643	264	134	101	50.0	47.6	23.2	13.5	<MQL	<MQL	<MQL	<MQL
401.6	6830	1830	672	268	148	133	77.3	77.6	29.0	13.5	6.63	3.40	<MQL	<MQL
440.0	5000	1270	496	219	115	96.0	54.8	66.2	24.1	24.8	9.43	4.85	<MQL	<MQL
477.5	4930	1540	543	222	121	82.8	51.4	62.2	23.7	18.0	5.92	3.18	<MQL	<MQL
522.0	6040	1840	667	287	140	102	64.0	85.0	34.4	34.0	10.6	4.11	<MQL	<MQL
559.7	5640	2160	779	332	167	134	74.0	101	32.5	29.9	9.52	4.22	<MQL	<MQL
597.3	6190	1830	758	318	155	136	85.8	123	55.0	108	23.6	15.1	6.85	<MQL
632.7	6980	3180	935	379	184	131	80.0	245	131	213	34.1	14.7	<MQL	<MQL
674.5	4240	1910	605	240	120	70.4	39.8	58.0	24.7	21.2	6.56	3.71	<MQL	6.17

Table S10. Concentrations of C_4 – C_6, C_8 PFSAs (pg L^{-1}). All subsections were <MQL for PFEtS (C_2), PFPrS (C_3), PFHpS (C_7), PFNS (C_9), PFDS (C_{10}) and PFDoS (C_{12})

Depth (cm weq)	PFBS	PFPeS	PFHxS	PFOS
48.9	26.3	<MQL	6.56	17.9
90.5	26.3	<MQL	17.9	54.6
128.2	<MQL	<MQL	<MQL	20.2
170.2	22.9	<MQL	<MQL	17.4
207.8	<MQL	<MQL	6.24	34.2
245.5	<MQL	3.15	28.3	195
282.4	<MQL	<MQL	5.92	23.7
322.3	<MQL	<MQL	<MQL	14.2
364.6	<MQL	<MQL	<MQL	12.6
401.6	28.4	<MQL	5.79	15.9
440.0	<MQL	<MQL	4.62	9.61
477.5	<MQL	<MQL	21.8	8.57
522.0	<MQL	<MQL	6.16	<MQL
559.7	<MQL	<MQL	<MQL	<MQL
597.3	<MQL	<MQL	4.47	15.4
632.7	<MQL	<MQL	6.23	22.2
674.5	<MQL	<MQL	<MQL	<MQL

Table S11. Concentrations of neutral PFAS FBSA, MeFBSA, FHxSA, MeFHxSA, FOSA, MeFOSA, EtFOSA, MeFOSE and EtFOSE (pg L^{-1}). All subsections were <MQL for MeFHxSA and MeFOSA.

Depth (cm weq)	FBSA	MeFBSA	FHxSA	FOSA	EtFOSA	MeFOSE	EtFOSE
48.9	2.72	20.8	<MQL	<MQL	<MQL	<MQL	<MQL
90.5	3.87	<MQL	4.36	9.56	<MQL	<MQL	<MQL
128.2	7.59	<MQL	<MQL	<MQL	<MQL	<MQL	<MQL
170.2	4.06	<MQL	<MQL	<MQL	<MQL	<MQL	<MQL
207.8	3.92	<MQL	<MQL	4.42	<MQL	<MQL	<MQL
245.5	3.93	<MQL	<MQL	4.56	<MQL	12.2	22.4
282.4	8.15	25.7	<MQL	7.48	<MQL	<MQL	<MQL
322.3	3.52	<MQL	<MQL	5.68	<MQL	<MQL	<MQL
364.6	2.46	13.0	<MQL	<MQL	<MQL	<MQL	<MQL
401.6	5.79	13.9	<MQL	<MQL	<MQL	7.35	11.3
440.0	3.16	16.4	<MQL	3.34	<MQL	<MQL	<MQL
477.5	<MQL	<MQL	<MQL	3.36	59.4	65.8	97.8
522.0	2.56	<MQL	<MQL	3.29	<MQL	<MQL	4.02
559.7	2.45	<MQL	<MQL	3.40	<MQL	4.72	5.85
597.3	2.47	<MQL	<MQL	<MQL	<MQL	<MQL	<MQL
632.7	<MQL	<MQL	<MQL	7.54	<MQL	<MQL	2.53
674.5	<MQL	<MQL	<MQL	<MQL	<MQL	<MQL	<MQL

Table S12. Concentrations of 4:2 FTSA, 6:2 FTSA, 8:2 FTSA, 6:2 FTUCA, 8:2 FTUCA, PFECHS, 6:2 Cl-PFESA, 8:2 Cl-PFESA, HFPO-DA and ADONA (pg L^{-1}). All subsections were <MQL for 4:2 FTSA, 8:2 FTSA, PFECHS, 6:2 Cl-PFESA, 8:2 Cl-PFESA, HFPO-DA and ADONA.

Depth (cm weq)	6:2 FTSA	6:2 FTUCA	8:2 FTUCA
48.9	6.66	71.2	<MQL
90.5	6.22	87.6	194
128.2	4.69	52.2	<MQL
170.2	<MQL	<MQL	<MQL
207.8	<MQL	<MQL	<MQL
245.5	14.1	28.9	<MQL
282.4	6.01	<MQL	<MQL
322.3	<MQL	45.7	<MQL
364.6	<MQL	<MQL	<MQL
401.6	<MQL	51.6	<MQL
440.0	<MQL	<MQL	<MQL
477.5	<MQL	<MQL	<MQL
522.0	5.66	<MQL	<MQL
559.7	<MQL	<MQL	<MQL
597.3	<MQL	<MQL	<MQL
632.7	6.61	<MQL	<MQL
674.5	<MQL	<MQL	<MQL

Table S13. Spearman correlation coefficients (r) and statistical significance (p) for $C_2 – C_{13}$ PFCAs, PFOS, FBSA and FOSA. Strong correlations (>0.70) and statistically significant p-values are in bold ($p < 0.001$).

	TFA	PFPrA	PFBA	PFPeA	PFHxA	PFHpA	PFOA	PFNA	PFDA	PFUnDA	PFDoDA	PFTrDA	PFHxS	PFOS	FBSA
PFPrA	r = 0.27														
	p = 0.300														
PFBA	r = 0.46	**r = 0.91**													
	p = 0.061	**p < 0.001**													
PFPeA	r = 0.39	**r = 0.91**	**r = 0.99**												
	p = 0.119	**p < 0.001**	**p < 0.001**												
PFHxA	r = 0.52	**r = 0.87**	**r = 0.97**	**r = 0.97**											
	p = 0.031	**p < 0.001**	**p < 0.001**	**p < 0.001**											
PFHpA	r = 0.34	r = 0.20	r = 0.40	r = 0.43	r = 0.51										
	p = 0.178	p = 0.434	p = 0.107	p = 0.084	p = 0.035										
PFOA	r = 0.50	r = 0.55	**r = 0.72**	r = 0.68	**r = 0.77**	r = 0.69									
	p = 0.039	p = 0.021	p = 0.001	p = 0.002	**p < 0.001**	p = 0.002									
PFNA	r = 0.08	r = 0.53	r = 0.51	r = 0.53	r = 0.54	r = 0.52	**r = 0.77**								
	p = 0.765	p = 0.029	p = 0.037	p = 0.028	p = 0.025	p = 0.033	**p < 0.001**								
PFDA	r = 0.06	r = 0.57	r = 0.51	r = 0.54	r = 0.53	r = 0.49	r = 0.67	**r = 0.94**							
	p = 0.823	p = 0.017	p = 0.036	p = 0.025	p = 0.029	p = 0.046	p = 0.003	**p < 0.001**							
PFUnDA	r = -0.14	r = 0.44	r = 0.39	r = 0.45	r = 0.42	r = 0.51	r = 0.56	**r = 0.83**	**r = 0.89**						
	p = 0.580	p = 0.076	p = 0.117	p = 0.068	p = 0.092	p = 0.035	p = 0.018	**p < 0.001**	**p < 0.001**						
PFDoDA	r = -0.01	r = 0.41	r = 0.47	r = 0.52	r = 0.51	r = 0.69	r = 0.64	r = 0.65	**r = 0.71**	**r = 0.85**					
	p = 0.970	p = 0.106	p = 0.054	p = 0.034	p = 0.037	p = 0.002	p = 0.006	p = 0.004	p = 0.002	**p < 0.001**					
PFTrDA	r = 0.11	r = 0.47	r = 0.56	r = 0.59	r = 0.59	r = 0.64	**r = 0.70**	r = 0.65	r = 0.70	**r = 0.84**	**r = 0.96**				
	p = 0.684	p = 0.059	p = 0.020	p = 0.012	p = 0.013	p = 0.006	p = 0.002	p = 0.005	p = 0.002	**p < 0.001**	**p < 0.001**				
PFHxS	r = 0.17	r = 0.16	r = 0.21	r = 0.17	r = 0.30	r = 0.16	r = 0.33	r = 0.11	r = 0.02	r = 0.15	r = 0.35	r = 0.33			
	p = 0.507	p = 0.532	p = 0.415	p = 0.507	p = 0.237	p = 0.548	p = 0.200	p = 0.663	p = 0.954	p = 0.555	p = 0.165	p = 0.198			
PFOS	**r = 0.76**	r = 0.11	r = 0.29	r = 0.20	r = 0.37	r = 0.50	r = 0.58	r = 0.16	r = 0.11	r = 0.07	r = 0.31	r = 0.36	r = 0.36		
	p < 0.001	p = 0.673	p = 0.259	p = 0.438	p = 0.143	p = 0.043	p = 0.014	p = 0.540	p = 0.673	p = 0.779	p = 0.233	p = 0.160	p = 0.044		
FBSA	r = 0.6	r = -0.35	r = -0.14	r = -0.21	r = -0.06	r = 0.40	r = 0.27	r = -0.08	r = -0.11	r = -0.27	r = -0.06	r = -0.06	r = -0.06	r = 0.61	
	p = 0.010	p = 0.173	p = 0.592	p = 0.416	p = 0.829	p = 0.111	p = 0.299	p = 0.750	p = 0.666	p = 0.303	p = 0.814	p = 0.833	p = 0.943	p = 0.010	
FOSA	r = 0.18	r = 0.31	r = 0.32	r = 0.35	r = 0.43	r = 0.52	r = 0.49	r = 0.57	r = 0.56	r = 0.67	r = 0.69	r = 0.66	r = 0.66	r = 0.43	r = 0.04
	p = 0.482	p = 0.222	p = 0.214	p = 0.168	p = 0.084	p = 0.032	p = 0.047	p = 0.018	p = 0.018	p = 0.004	p = 0.002	p = 0.004	p = 0.058	p = 0.089	p = 0.884

Table S14. Percentage of linear isomers and concentrations (pg L^{-1}) of linear and branched isomers of PFOS. 1-PFOS was <MQL for all subsections.

Depth (cm weq)	3/4/5-PFOS	6/2-PFOS	Linear-PFOS	Linear-PFOS (%)
48.9	3.31	4.03	17.9	71
90.5	6.98	<MQL	54.6	89
128.2	<MQL	<MQL	20.2	n/a
170.2	<MQL	<MQL	17.4	n/a
207.8	5.56	6.65	34.2	74
245.5	16.7	15.2	194.8	86
282.4	<MQL	3.52	23.7	87
322.3	2.58	<MQL	14.2	85
364.6	<MQL	<MQL	12.6	n/a
401.6	2.84	2.79	15.9	74
440.0	<MQL	<MQL	9.6	n/a
477.5	<MQL	<MQL	8.6	n/a
522.0	<MQL	<MQL	<MQL	n/a
559.7	<MQL	3.17	<MQL	n/a
597.3	<MQL	2.89	15.4	84
632.7	4.36	<MQL	22.2	84
674.5	<MQL	<MQL	<MQL	n/a

n/a: not applicable

Table S15. Percentage of linear isomers and concentrations (pg L^{-1}) of linear and branched isomers of PFHxS. 1-PFHxS was <MQL for all subsections.

Depth (cm weq)	2/3/4-PFHxS	Linear-PFHxS	Linear-PFHxS (%)
48.9	<MQL	6.56	n/a
90.5	<MQL	17.9	n/a
128.2	<MQL	<MQL	n/a
170.2	<MQL	<MQL	n/a
207.8	<MQL	6.24	n/a
245.5	2.96	28.3	91
282.4	<MQL	5.92	n/a
322.3	<MQL	<MQL	n/a
364.6	<MQL	<MQL	n/a
401.6	<MQL	5.79	n/a
440.0	<MQL	4.62	n/a
477.5	<MQL	21.8	n/a
522.0	<MQL	6.16	n/a
559.7	<MQL	<MQL	n/a
597.3	<MQL	4.47	n/a
632.7	<MQL	6.23	n/a
674.5	<MQL	<MQL	n/a

n/a: not applicable

Table S16. Spearman correlation coefficients (r) and statistical significance (p) for C_2 – C_{13} PFCAs, PFOS, FBSA and FOSA with Na^+ and the melt proxy $\log([Na^+]/[Mg^{2+}])$. Moderate positive correlations ($r > 0.50$) and statistically significant p-values are in bold ($p < 0.05$). For $\log([Na^+]/[Mg^{2+}])$, moderate negative correlations ($r < -0.50$) are also in bold.

	Na^+	$\log([Na^+]/[Mg^{2+}])$
TFA	r = 0.25	**r = -0.65**
	p = 0.333	**p = 0.005**
PFPrA	r = -0.19	r = -0.10
	p = 0.474	p = 0.701
PFBA	r = -0.12	r = -0.14
	p = 0.653	p = 0.593
PFPeA	r = -0.16	r = -0.09
	p = 0.548	p = 0.743
PFHxA	r = -0.05	r = -0.14
	p = 0.844	p = 0.586
PFHpA	r = -0.34	r = -0.08
	p = 0.188	p = 0.758
PFOA	r = -0.05	r = -0.07
	p = 0.859	p = 0.786
PFNA	r = -0.25	r = 0.21
	p = 0.323	p = 0.422
PFDA	r = -0.39	r = 0.12
	p = 0.119	p = 0.653
PFUnDA	r = -0.46	r = 0.22
	p = 0.063	p = 0.406
PFDoDA	r = -0.55	r = 0.08
	p = 0.021	p = 0.764
PFTrDA	r = -0.43	r = -0.03
	p = 0.082	p = 0.903
PFHxS	r = 0.07	r = -0.08
	p = 0.778	p = 0.771
PFOS	r = -0.01	**r = -0.54**
	p = 0.963	**p = 0.024**
FBSA	r = 0.27	r = -0.49
	p = 0.299	**p = 0.048**
FOSA	r = -0.33	r = -0.19
	p = 0.192	p = 0.458

Figure S1a. Annual layer counting showed the ice core dating 2006 – 2019. $\delta^{18}O$ (‰, blue points) data had a 3-point moving average applied (blue line) to show the seasonal cycles. $nssSO_4^{2-}$ (ueq/L, yellow points) had a 3-point moving average also applied (orange line). The peak in $nssSO_4^{2-}$ at 404.5 cm weq assigned to be the 2011 Grímsvötn volcanic eruption in Iceland.

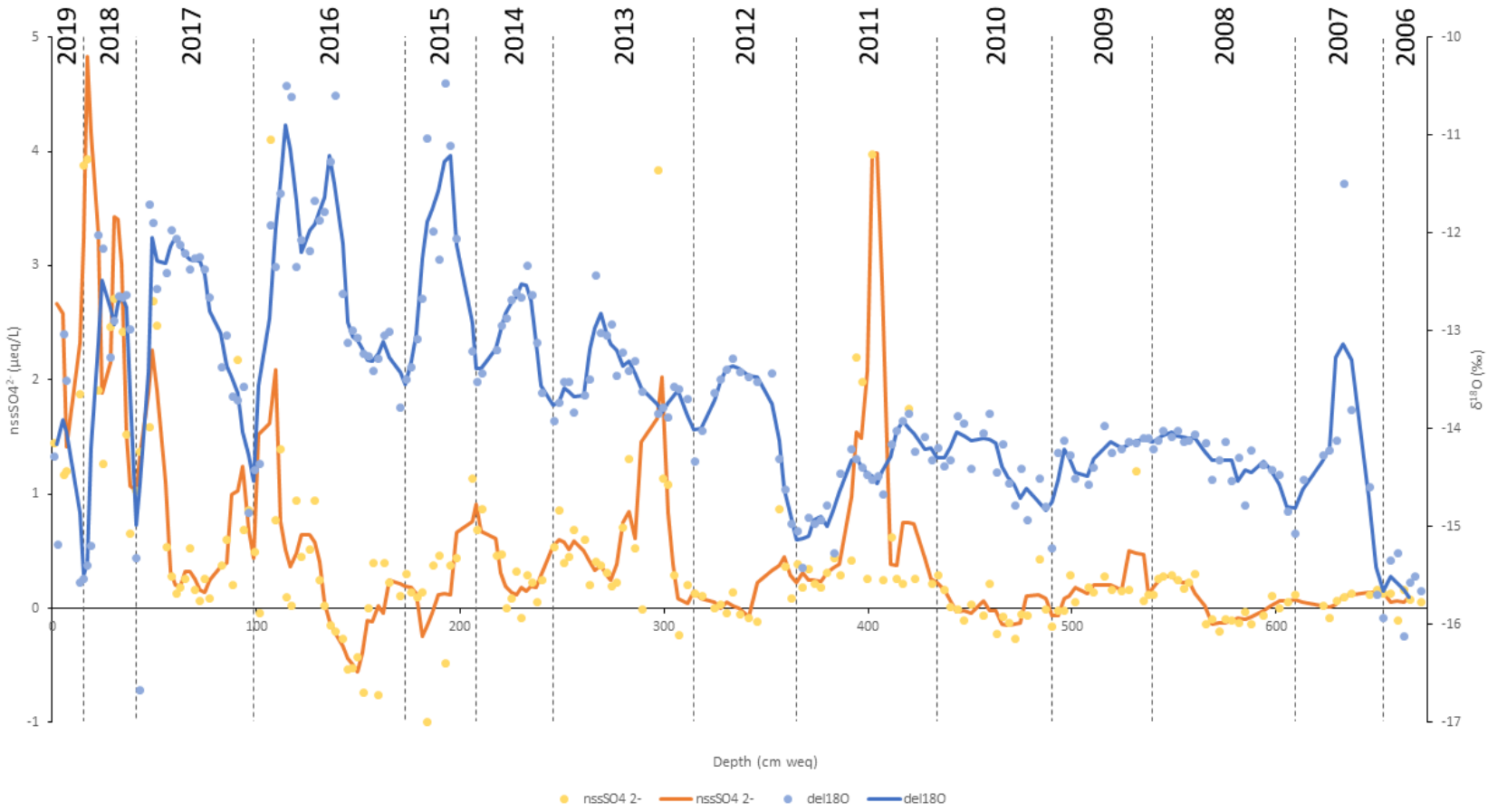


Figure S1b. Annual layer counting was assisted by seasonal variations in $[Na^+]/[Cl^-]$ (grey points). A 3-point moving average was also applied (grey line).

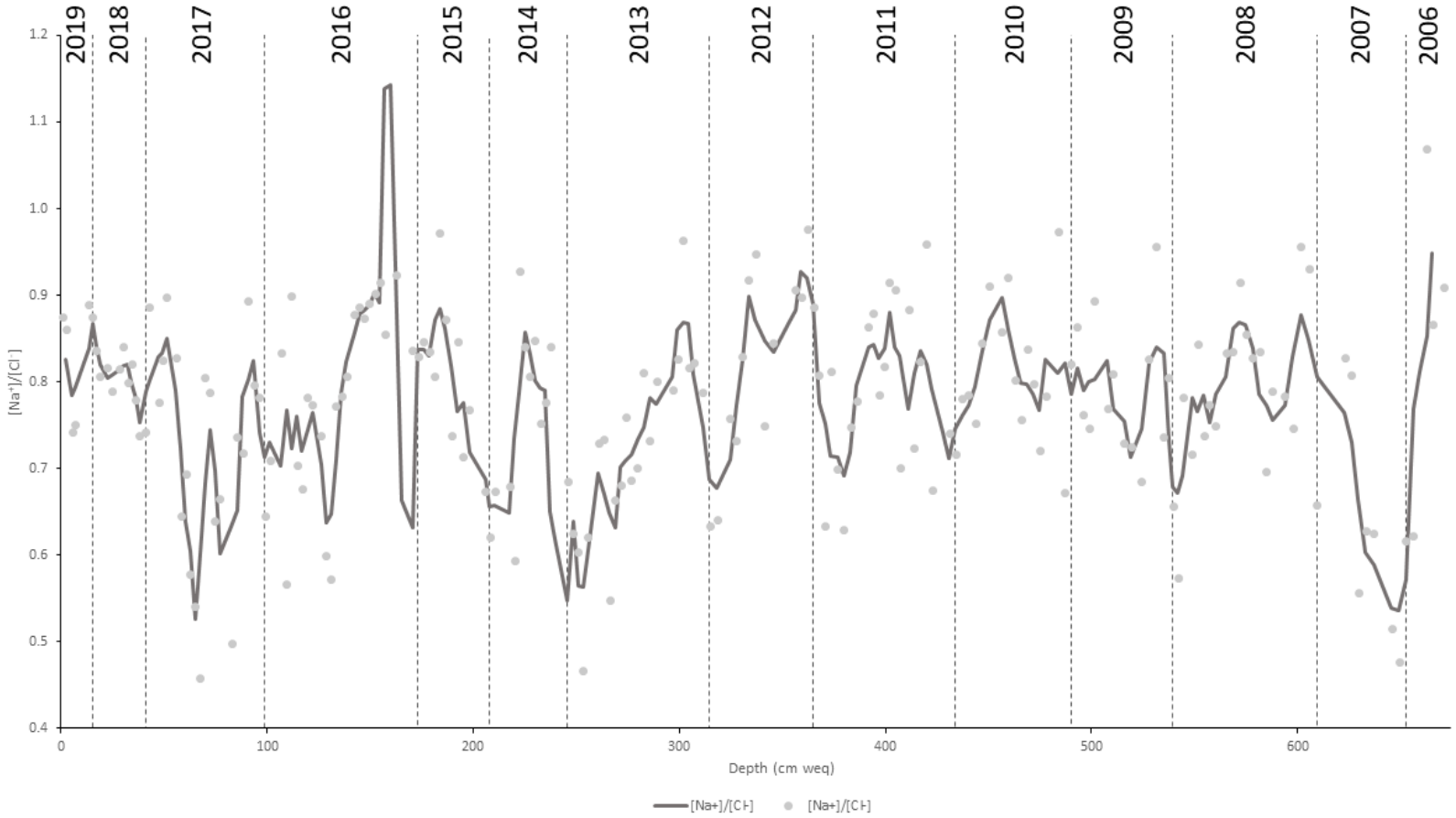
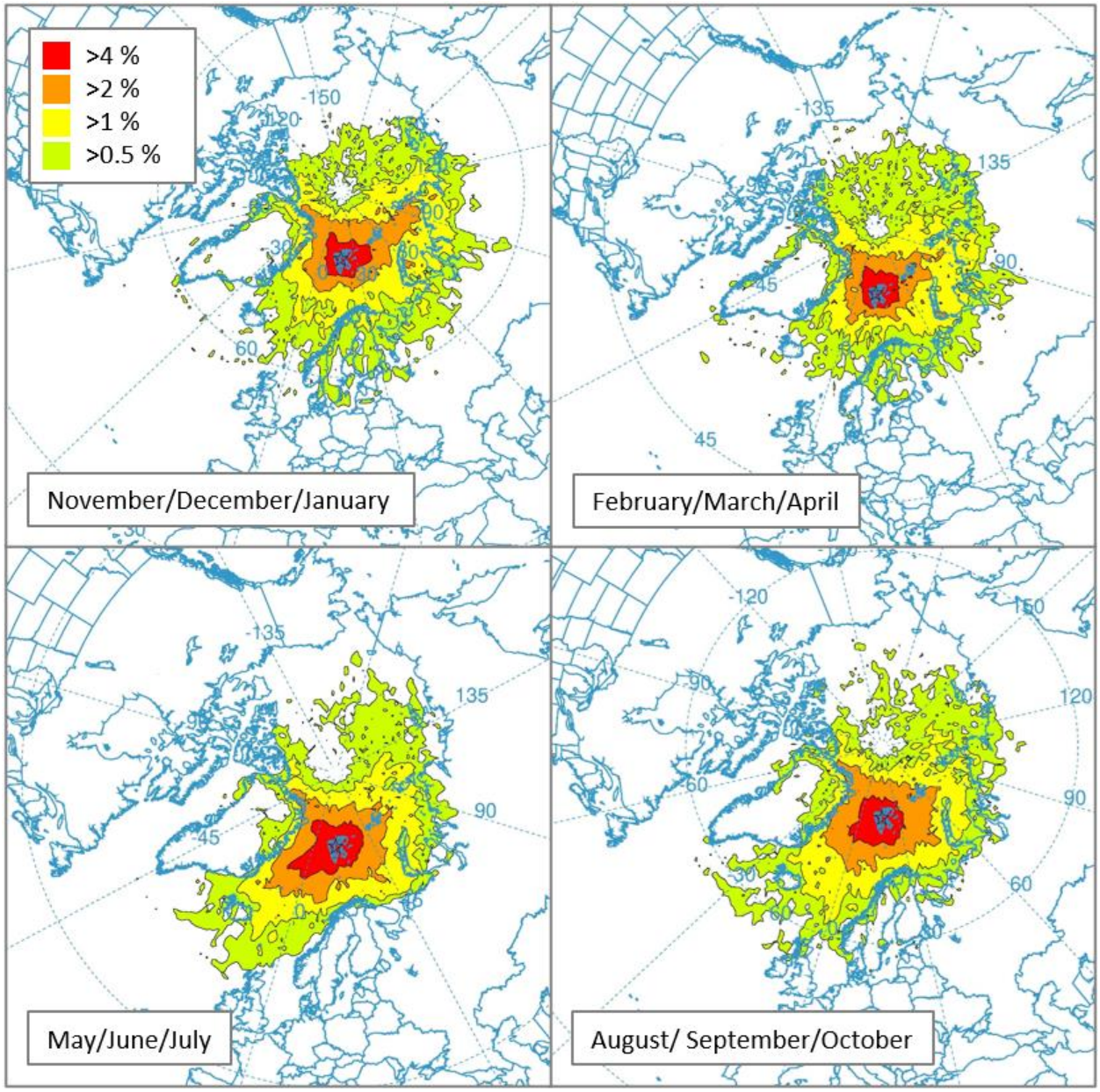
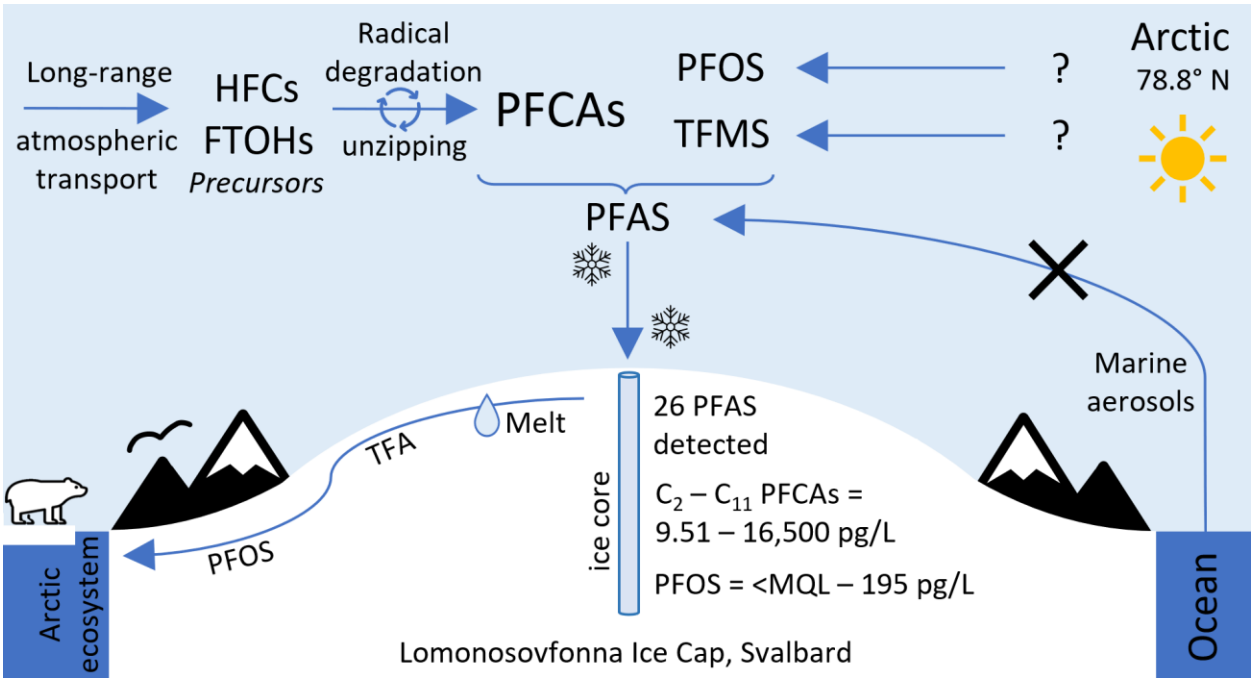


Figure S2. HYSPLIT seasonal trajectory frequency plots for 2007 – 2018.



TOC Art (Graphical Abstract)



Chapter 5

Levels and seasonal trends of C_1 – C_4 perfluoroalkyl acids and the discovery of trifluoromethane sulfonic acid in surface snow in the Arctic

Maria K. Björnsdotter,[a]* William F. Hartz,[b,c,] Roland Kallenborn,[d,e] Ingrid Ericson Jogsten[a] Jack D. Humby,[f] Anna Kärrman,[a] Leo W. Y. Yeung,[a]

Published in Environmental Science & Technology, 55, no. 23 (2021): 15853-15861

5.1 Abstract 143
5.2 Introduction 144
5.3 Materials and Methods 147
5.3.1 Chemicals and Reagents 147
5.3.2 Sample Collection 147
5.3.3 Sample Preparation and Analysis 151
5.3.4 Statistical Analysis 153
5.3.5 Quality Assurance and Quality Control 153
5.3.6 Air Mass Trajectories and Solar Radiation 154
5.4 Results and Discussion 155
5.4.1 C_1 – C_4 PFAAs in Surface Snow 155
5.4.2 Seasonal Variation of TFA, PFPrA, and PFBA in Surface snow 157
5.4.3 Discovery of TFMS at Foxfonna Ice Cap 159
5.5 References 162
5.6 Supporting Information 165

This chapter was conceptualised by William F. Hartz, who also undertook the fieldwork, sample preparation, data interpretation and atmospheric modelling as well as writing first drafts of parts of the introduction, methods and discussion, and assisting with ion chromatography analysis. Other major contributions include PFAS sample extraction, analysis, data processing and writing by Maria K. Björnsdotter and ion chromatography analysis by Jack Humby. All co-authors have assisted in editing of the manuscript.

[a]Man-Technology-Environment Research Centre (MTM), Örebro University, SE-701 82 Örebro, Sweden

[b]Department of Earth Sciences, University of Oxford, South Parks Road, Oxford, OX1 3AN, United Kingdom

[c]Department of Arctic Geology, University Centre in Svalbard (UNIS), NO-9171, Longyearbyen, Svalbard, Norway

[d]Faculty of Chemistry, Biotechnology and Food Sciences (KBM), Norwegian University of Life Sciences (NMBU), NO-1432 Ås, Norway

[e]Department of Arctic Technology, University Centre in Svalbard (UNIS), NO-9171, Longyearbyen, Svalbard, Norway

[f]Ice Dynamics and Paleoclimate, British Antarctic Survey, High Cross, Cambridge, CB3 0ET, United Kingdom

5.1 Abstract

$C_1 – C_4$ perfluoroalkyl acids (PFAAs) are highly persistent chemicals that have been found in the environment. To date, much uncertainty still exists about their sources and fate. The importance of the atmospheric degradation of volatile precursors to $C_1 – C_4$ PFAAs were investigated by studying the distribution and seasonal variation in remote Arctic locations. $C_1 – C_4$ PFAAs were measured in surface snow on the island of Spitsbergen in the Norwegian Arctic during January – August 2019. Trifluoroacetic acid (TFA), perfluoropropanoic acid (PFPrA), perfluorobutanoic acid (PFBA), and trifluoromethane sulfonic acid (TFMS) were detected in most samples, including samples collected at locations presumably receiving PFAA input solely from long range processes. The flux of TFA, PFPrA, PFBA, and TFMS per precipitation event was in the range 22 – 1 800 ng/m^2, 0.79 – 16 ng/m^2, 0.19 – 170 ng/m^2, and 1.5 – 57 ng/m^2, respectively. A positive correlation between the flux of TFA, PFPrA and PFBA with downward short-wave solar radiation was observed. No correlation was observed between the flux of TFMS and solar radiation. These findings suggest that atmospheric transport of volatile precursors and their subsequent degradation plays a major role in the global distribution of $C_2 – C_4$ perfluoroalkyl carboxylic acids and their consequential deposition in Arctic environments. The discovery of TFMS in surface snow at these remote Arctic locations suggests that TFMS is globally distributed. However, the transport mechanism to the Arctic environment remains unknown.

Synopsis

Atmospheric oxidation of volatile precursors is a major source of $C_2 – C_4$ perfluoroalkyl carboxylic acids in Arctic environments.

Keywords: perfluoroalkyl substances, ultra-short chain perfluoroalkyl acids, trifluoroacetic acid, solar radiation, atmospheric oxidation, atmospheric deposition, precursors, Arctic.

5.2 Introduction

Perfluoroalkyl acids (PFAAs) are highly persistent, man-made chemicals that are ubiquitous in the environment. $C_1 – C_4$ PFAAs are perfluoroalkyl carboxylic acids (PFCAs) and perfluoroalkyl sulfonic acids (PFSAs) with alkyl chain length of one to four carbon atoms. These include trifluoroacetic acid (TFA), perfluoropropanoic acid (PFPrA), perfluorobutanoic acid (PFBA), trifluoromethane sulfonic acid (TFMS), perfluoroethane sulfonic acid (PFEtS), perfluoropropane sulfonic acid (PFPrS) and perfluorobutane sulfonic acid (PFBS). The acidic functional group in combination with the small molecular structure result in highly polar compounds. High concentrations in biological matrices have not been reported, but due to the persistence to degradation, precautionary measures should be taken.[1] TFA can accumulate in aquatic environments[2] and contamination of drinking water has been shown.[3]

TFA is a transformation product of hydrofluorocarbons (HFCs) and hydrochlorofluorocarbons (HCFCs)[4] which were introduced as replacements of the ozone depleting chlorofluorocarbons used as cooling agents, after the introduction of the Montreal protocol in 1989. TFA has been studied since the early 1990s and has been frequently reported in the environment since then. TFA seems to be ubiquitous in surface snow even at very remote sites[5, 6] and the environmental concentrations are increasing.[7] It has been frequently reported in the scientific literature that the environmental levels of TFA from the breakdown of HFCs, HCFCs, and from hydrofluoro olefins (HFOs), which are recently introduced replacements due to the lower global warming potential, do not pose a threat to humans or the environment.[8-11] TFA is a substance of multiple sources that are still uncertain, and it is a potential degradation product of more than one million chemicals.[10] Continued attention is needed considering the long environmental lifetime.

Among the $C_1 – C_4$ PFCAs, PFPrA and PFBA have not been studied as thoroughly as TFA, yet they have also been reported in surface snow and surface water.[12-15] TFA, PFPrA, and PFBA were recently reported in ice caps in remote locations[16] showing that they are globally distributed, including across polar regions. The formation of $C_1 – C_4$ PFAAs from the atmospheric degradation of volatile precursors is today considered as a pathway to remote locations. Such precursors include fluorotelomer alcohols, perfluoroalkane sulfonamides, and perfluoroalkane sulfonamidoethanols, of which organofluorine compounds with C_4 to C_{14} chain lengths have been frequently detected in the Arctic.[17-21] In addition, thermolysis of fluoropolymers used in consumer products result in direct- and indirect formation of PFCAs.[22] While direct formation mainly lead to elevated concentrations locally, the indirect formation can result in global distribution because of the long-range atmospheric transport of volatile intermediates. Another transport mechanism to remote locations is via marine aerosols, which involves the transfer of PFAAs into the atmosphere from the ocean via sea spray formation as a result of strong wind and breaking waves.[23]

The formation of TFA, PFPrA, and PFBA from the degradation of precursors has been demonstrated under laboratory conditions.[24-26] These degradations were initiated by the light dependent formation of hydroxyl radicals. Through a hydroxyl radical mediated unzipping cycle, longer chain $>C_4$ precursor compounds can contribute to the atmospheric formation $C_1 – C_4$ PFAAs.[24] Modelling studies found Arctic atmospheric PFOA concentrations, as a result of 8:2 fluorotelomer alcohol atmospheric degradation, to be 15 – 20 times higher during July compared to January.[27] This was attributed to the large seasonal variations in radiation causing a seasonal variation in the atmospheric hydroxyl radical concentration. Other potential atmospheric precursor sources are HFCs and HCFCs. These have been detected globally, including in the Arctic.[28] PFAAs have a short atmospheric half-life of several days with respect to wet deposition and are

effectively scavenged by wet deposition.[29, 30] Hence during snowfall, it would be expected that almost all atmospheric PFAAs become deposited, regardless of the type of source. Sampling fresh snowfall can therefore offer a route to understanding atmospheric PFAA processes.

One study has investigated the formation of PFBS from the degradation of N-methyl perfluorobutane sulfonamidoethanol,[25] but data about the formation of $C_1 – C_4$ PFSAs from volatile precursors is still scarce and little is known about their global distribution. A few studies have reported $C_1 – C_4$ PFSAs in wastewater[31] and, in surface water and groundwater which were connected to suspected point sources such as landfills, military training sites and waste management facilities.[15, 32] A recent study reported TFMS in surface water and groundwater far away from primary environmental emission points.[33] The potential sources and the environmental fate of these substances are not yet well understood. However, with respect to their high polarity and high persistence, contamination in the aqueous environment could be expected.

Local sources of PFAAs in the Arctic have also been identified. On Spitsbergen in the Norwegian Arctic, PFBA and PFBS has been linked with local sources in the settlement of Longyearbyen such as a firefighting training site (FFTS) and a landfill.[34, 35] PFBS was found in one snow sample (and at several trophic levels in local biota). In another study PFBA was detected in snow in Longyearbyen.[36] Otherwise there has been no further study into the sources and processes of $C_1 – C_4$ PFAAs in snow in the Arctic.

The aim of the present study was to assess the seasonal deposition, sources, and geographical distribution of $C_1 – C_4$ PFAAs in the Arctic. For this purpose, seven PFAAs, namely TFA, PFPrA, PFBA, TFMS, PFEtS, PFPrS, and PFBS, were measured in surface snow samples collected at several locations on the island of Spitsbergen in the Norwegian Arctic, including around the settlement of Longyearbyen. The correlation between the observed flux and solar

radiation was examined to elucidate the relevance of the atmospheric degradation of volatile precursors as a pathway to remote locations.

5.3 Materials and Methods

5.3.1 Chemicals and Reagents

Native standards of PFBA, PFPrS and PFBS and mass-labelled standards of PFBA and PFBS were purchased from Wellington Laboratories (Guelph, ON, Canada). TFA was purchased from Sigma-Aldrich, (Munich, Germany). PFPrA was from Sigma-Aldrich, (Oakville, ON, Canada). TFMS was from Sigma-Aldrich, (Stockholm, Sweden), and potassium salt of PFEtS was obtained from Kanto Chemical Co., Inc., (Portland, OR, USA). Mass-labelled standard of TFA ($^{13}C_2$-TFA) was purchased from Toronto Research Chemicals Inc, (Toronto, ON, Canada). Mass-labelled standards for PFPrA, TFMS, PFEtS and PFPrS were not available commercially. The purity of all standards was above 97%. Ammonium acetate (≥99.0%) was purchased from Sigma-Aldrich, (Stockholm, Sweden). Glacial acetic acid (EMPROVE® EXPERT, Ph. Eur., JP, USP) was purchased from Merck, (Darmstadt, Germany). Analytical reagent grade ammonia solution, HPLC grade methanol (≥99.8%) and LC-MS grade methanol (≥99.9%) were from Fischer Scientific, (Ottawa, ON, Canada).

5.3.2 Sample Collection

Seven sampling locations were chosen for surface snow sampling. Three sites were sampled several times from January 2019 to August 2019. These three sampling sites were chosen to represent a range of potential locally contaminated and background sites, whilst being easily accessible all year round to allow for seasonal sampling. These three sites were in settlement of Longyearbyen (n = 8, 78°13.288'N 15°39.041'E, 13 m.a.s.l.), up the hill from the Kjell Henriksen

Observatory (KHO; *n* = 9, 78°08.807'N 16°02.781'E, 532 m.a.s.l.), and on the summit of Foxfonna ice cap (*n* = 10, 78°07.736'N 16°10.791'E, 800 m.a.s.l.). The sampling locations are shown in Figure 1.

The site in Longyearbyen was located in a fenced off area of tundra outside the University Centre in Svalbard (UNIS) which, whilst being in the center of town, was a location where the surface snow remained undisturbed by traffic or pedestrians. This site was 360 m from the fjords coastline. It was chosen to investigate local sources and the possible associated seasonal variations in these. The site at KHO was located 150 m away, uphill, of the Kjell Henriksen Observatory. This site was chosen due to its proximity to the Foxfonna sampling site (4.7 km away), allowing for direct comparison between the sites, and to understand possible PFAA contamination from the active coal mine in Longyearbyen (1.3 km from the KHO sampling site). The Foxfonna sampling site was chosen to represent a potential remote location due to its high altitude (800 m.a.s.l.) and position upwind from Longyearbyen (16 km) with respect to the easterly prevailing winds. Sampling at the site in Longyearbyen was conducted 8 times from January 2019 to May 2019 (samples UNIS01 – UNIS08). Sampling at KHO was conducted 9 times from January 2019 to June 2019 (KHO01 – KHO09). Sampling at the Foxfonna site was conducted 10 times from January 2019 to August 2019 (samples Fox01 – Fox10). Sampling at these three sites was conducted as soon as possible after a chosen precipitation event (typically <1 day – 7 days for Foxfonna sampling site, average 3.7 days), such that each snow sample represents a single precipitation event whereby post depositional processes have been minimized.

Four high elevation sites on glaciers around Spitsbergen were chosen for snow sampling as these most likely represented background reference locations presumably receiving PFAA input solely from atmospheric long-range processes (Figure 2). Sampling was conducted at these sites

February to April 2019 at Drønbreen (*n* = 1, 78°06.185'N 16°39.182'E, 707 m.a.s.l.), Lomonosovfonna (*n* = 2, 78°49.454'N 17°26.253'E, 1198 m.a.s.l.), Grønfjordbreen (*n* = 1, 77°53.222'N 14°13.745'E, 574 m.a.s.l.) and Nordmannsfonna (*n* = 1, 78°15.894'N 18°23.717'E, 498 m.a.s.l.).

When collecting the surface snow samples, the site was approached by ski or snowmobile, with the final approach to the sampling site undertaken from downwind on foot. Nitrile gloves were worn during snow sampling. PFAAs have been shown to be effectively scavenged from the atmosphere by wet deposition and most of the PFAA removal is expected to occur at the beginning of a rainfall.[30] A similar process during a snow precipitation event is likely and the initial snowfall would presumably have higher PFAA concentrations. However, due to windy conditions in Svalbard, it was assumed that the snow was well mixed by both snow blowing in the atmosphere and surface snow drifting before it became deposited and hence the PFAA concentrations within the fresh snowfall were homogeneous. A precleaned aluminum shovel was used to collect the upper 0 – 5 cm of the fresh surface snow into a precleaned high-density polyethylene barrel. The sampling area for the 32 surface snow samples was between 0.8 – 3.9 m^2 (average 1.8 m^2). The barrel was then sealed and transported back to UNIS, where it was melted at 5 °C, bottled into precleaned polypropylene containers and stored in the fridge 2 – 4 °C. The samples were then transported cold to Örebro University, Sweden and stored at 8 °C until further processing.

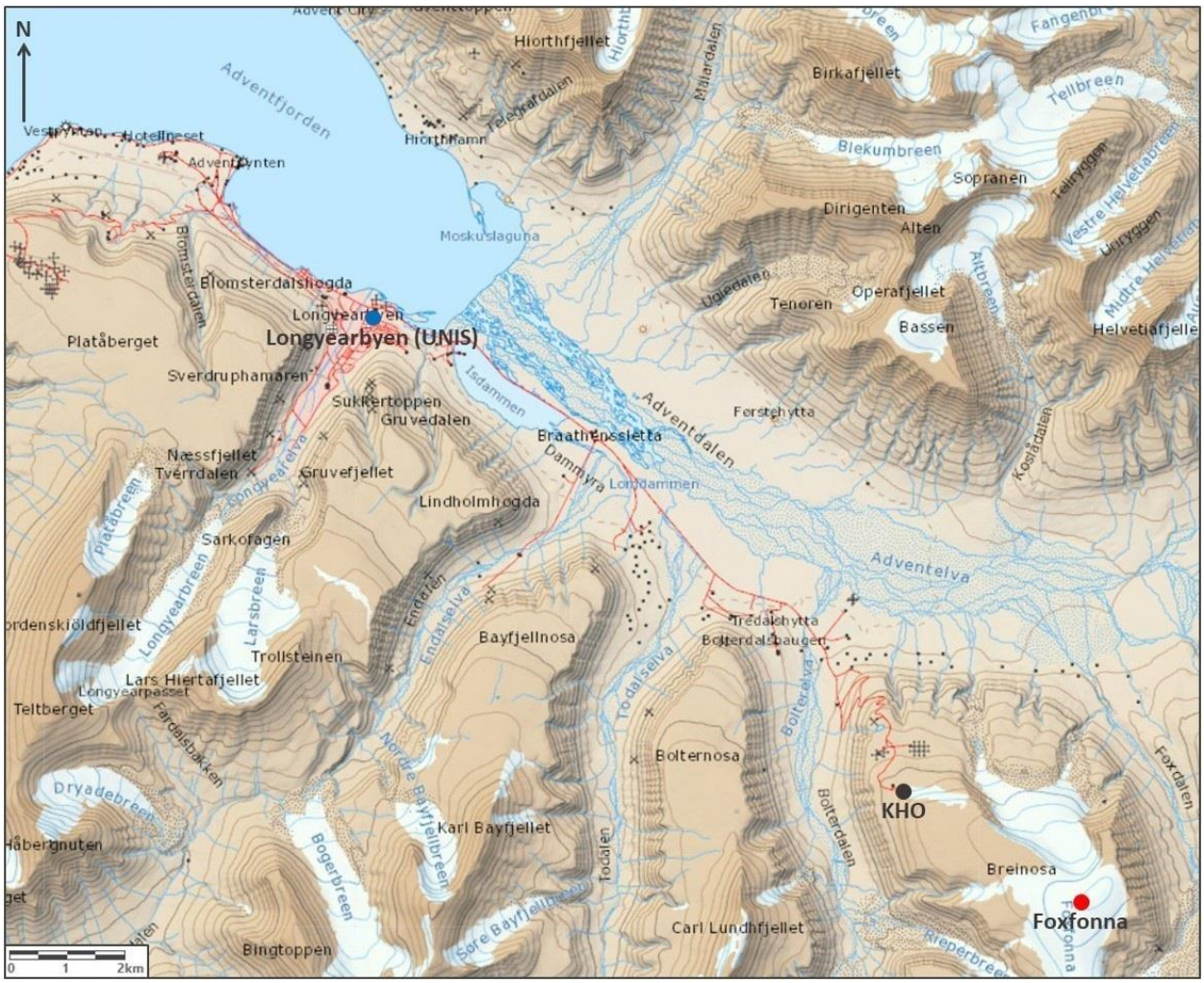


Figure 1. Sampling locations in Longyearbyen (*n* = 8), Kjell Henriksen Observatory (KHO, *n* = 9) and Foxfonna (*n* = 10). The map was reproduced from TopoSvalbard, Norwegian Polar Institute.



Figure 2. The reference snow sampling locations on Spitsbergen glaciers: Lomonosovfonna (*n* = 2), Nordmannsfonna (*n* = 1), Drønbreen (*n* = 1) and Grønfjordbreen (*n* = 1). The map was reproduced from TopoSvalbard, Norwegian Polar Institute.

5.3.3 Sample Preparation and Analysis

All samples were ultrasonicated for 10 min to desorb target analytes possibly sorbed to the inner surface of the containers. The inner surface of the containers was rinsed with methanol once the sample was taken out for filtration and the methanol was combined with the sample. Surface snow samples were filtered with glass microfiber filters (Whatman, Grade GF/B, 1.2 µm) prior to

extraction. The filters were extracted three times with methanol by ultrasonication for 30 min followed by centrifugation at 8000 rpm for 5 min. The filter extract was combined with the water sample. The pH of the samples was adjusted to 4 by addition of acetic acid prior to extraction.

Approximately 2200 mL sample was extracted by weak anion exchange solid-phase extraction (Oasis® WAX, Waters Corporation, Milford, USA) following the ISO25101 method with some modifications. The cartridges were preconditioned with 4 mL 0.1% ammonium hydroxide in methanol followed by 4 mL methanol and 4 mL Milli-Q water. The samples were then loaded at approximately 1 drop/s onto the cartridges. After loading the samples, the cartridges were washed by passage of 4 mL Milli-Q water followed by 4 mL ammonium acetate buffer solution (pH 4) and then dried under vacuum for 30 min before elution of target analytes. The neutral fraction was eluted by adding 4 mL methanol. The anionic fraction was then eluted by adding 4 mL 0.1% ammonium hydroxide in methanol. In the present study, only the anionic fraction was analyzed. The eluate was evaporated to approximately 0.5 mL at 60 °C and 400 mbar, transferred to an LC vial and then further evaporated to 100 µL under a gentle stream of nitrogen. Mass-labelled internal standards (1 ng) were added to the samples prior to filtration to monitor the recovery of the method. Aliquots of 2 µL were injected into the supercritical fluid chromatography (SFC) tandem mass spectrometry system (MS/MS) for quantification of $C_1 – C_4$ PFAAs.

Separation and quantification were performed using SFC-MS/MS (Acquity Ultra Performance Convergence Chromatograph and Xevo TQ-S micro, Waters Corporation, Milford, MA, USA) operated in negative electrospray ionization mode. An SFC Torus DIOL column (3.0 mm i.d., 150 mm length, 1.7 µm particle size from Waters Corporation, Milford, MA, USA) maintained at 50 °C was used to achieve chromatographic separation. The mobile phase consisted of CO_2 (A) and 0.1% ammonium hydroxide in methanol (B). The gradient of the mobile phase

started with an initial B concentration of 15%, which was then increased to 35% over 5 min. This was held for 1 min before returning to initial conditions over 1 min. The flow rate was 1.2 mL/min and the active back pressure regulator was set at 2000 psi throughout the chromatographic separation. The source parameters were set as following: capillary voltage, 0.7 kV; source temperature, 150 °C; desolvation temperature, 400 °C; cone gas flow, 150 L/h; desolvation gas flow, 800 L/h; collision gas flow, 0.2 mL/min; nebulizer, 6.5 bar. Two transitions were monitored for TFMS, PFEtS, PFPrS, and PFBS, respectively. Only one transition was monitored for TFA, PFPrA, and PFBA. MRM transitions for all target analytes are provided in Table S1.

5.3.4 Statistical Analysis

Spearman rank correlations between the PFAA flux in surface snow and solar radiation, as well as between the TFMS flux and the flux of sodium ions were calculated using Microsoft Excel version 2105.

5.3.5 Quality Assurance and Quality Control

Linear regression analysis showed good linearity for each analyte (R^2> 0.99) in the range from 2 to 100 ng/mL. Instrumental limits of quantification (LOQ) were set as the lowest calibration point with a signal-to-noise ratio of at least ten. The repeatability of the analytical method was evaluated based on repeated injections (n = 10) of a standard with a concentration of 4 ng/mL. The relative standard deviation of repeated injections was in the range 0.33% to 4.1%. Isotope dilution was used for quantification. For those target analytes that did not have corresponding mass-labelled standards, the homologue closest in retention time was used for quantification (Table S1). Extraction efficiencies were assessed based on the peak area of native standards spiked to test samples (n = 3) after subtraction of the background concentrations in the samples. For TFA, the extraction efficiency was assessed based on the peak area of a mass-labelled standard spiked to

test samples (n = 3). The extraction efficiency was in the range 58 – 126%. The repeatability of the extraction method was evaluated based on the relative standard deviation of spiked test samples (n = 3) at a concentration of 1 ng per 250 mL sample. The relative standard deviation of spiked test samples was in the range 2.2 – 15%. The method limits of quantification (MQLs) were calculated as the average concentration in repeated blank extractions (n=5) plus three times the standard deviation. For those analytes that were not observed in blank extractions, the instrument LOQ was used as the MDL. A field blank was included to ensure that no contamination occurred during sampling. The field blank comprised of purified water in a sample container that was brought to the field and opened during the time of the sampling. The container was resealed and transported to the laboratory where it was treated in the same way as the samples. None of the target analytes were observed in the field blank (TFA <0.009 ng/L; PFPrA <0.009 ng/L; PFBA <0.058 ng/L; TFMS <0.009 ng/L; PFEtS <0.05 ng/L; PFPrS <0.009 ng/L; PFBS <0.01 ng/L). Detailed information about the precision of the analytical method, extraction efficiencies and repeatability, and LOQ and MQL are provided in Table S2.

5.3.6 Air Mass Trajectories and Solar Radiation

At the Foxfonna sampling site, the Hybrid Single-Particle Lagrangian Integrated Trajectory (HYSPLIT) model was used to assess whether downward short-wave radiation may be linked to precursor degradation, and hence the flux of C_1 – C_4 PFAAs. The National Center for Environmental Prediction's Global Data Assimilation System (GDAS) model was used for the meteorological input data. A single backwards 6-day air mass trajectory was calculated for each of the 10 snow sampling rounds, which ended at the Foxfonna sampling site (at 800 m.a.s.l.). The trajectory was timed to end at the onset of the precipitation event that was subsequently sampled. The onset of the precipitation event was established by inspecting meteorological data from the

Adventdalen weather station (11.4 km from the Foxfonna sampling site (data was retrieved from the Norwegian Meteorological Institute). An integrated radiation value was then calculated from each trajectory by summing the downward short-wave radiation associated with each hourly point on the trajectory. This served as a record of the downward short-wave radiation each air mass parcel had been subject to that was associated with each snow sample (in kWh/m^2). The atmospheric lifetime of $C_1 – C_4$ PFAAs are assumed to be short and the removal dominated by wet- and dry-deposition, similar as to other strong acids such as nitric acid.[29] A 6-day backwards air mass trajectory was used, which is the global average half-life of nitric acid with respect to wet and dry deposition.

5.4 Results and Discussion

5.4.1 $C_1 – C_4$ PFAAs in Surface Snow

Detailed information about the PFAA concentrations measured in surface snow is provided in Tables S3-S6 and the deposition fluxes of PFAAs per precipitation event is provided in Tables S7 – S10. TFA, PFPrA and TFMS were detected in all surface snow samples, including those collected at the reference locations. The flux was in the range 22 – 1 800 ng/m^2, 0.79 – 16 ng/m^2, and 1.5 – 57 ng/m^2 for TFA, PFPrA, and TFMS, respectively. PFBA was detected in 97% of the surface snow samples, and in all samples collected at reference locations, at fluxes in the range 0.19 – 170 ng/m^2. PFPrS was not detected in any of the samples. Neither PFEtS nor PFBS were detected in samples collected at the remote sites. PFEtS was not detected at the Foxfonna sampling site but was detected in 22% of the samples collected at KHO and in all samples collected in Longyearbyen (UNIS) at fluxes in the range 0.52 – 55 ng/m^2. PFBS was not detected at locations outside of the Longyearbyen settlement (Foxfonna and KHO) but was detected in 63% of the samples collected in Longyearbyen in the concentration range 0.17 – 26 ng/m^2. The detection of

PFEtS and PFBS in surface snow samples in Longyearbyen is likely due to local sources. PFBS has previously been reported in runoff from a FFTS and in landfill leachate in Longyearbyen[34, 35] and PFEtS has been linked to similar sources.[15, 32] The median flux of PFBA was 8 times higher in Longyearbyen (UNIS) (34 ng/m^2) compared to Foxfonna (4.1 ng/m^2). This indicates local sources of PFBA exist within the settlement.

TFA, PFPrA, PFBA and TFMS were all detected at Foxfonna sampling site and at the four high elevation reference sites (Drønbreen, Lomonosovfonna, Grønfjordbreen, and Nordmannsfonna) which are thought to represent input solely from long-range processes. The observed flux was highest for TFA ranging from 22 ng/m^2 to 1 800 ng/m^2 at Foxfonna sampling site. PFPrA, PFBA, and TFMS, were detected at Foxfonna sampling site at fluxes ranging 0.79 – 16 ng/m^2 (PFPrA), <0.99 – 20 ng/m^2 (PFBA), and 2.2 – 11 ng/m^2 (TFMS). The concentrations of TFA (5.6 – 270 ng/L), PFPrA (0.21 – 1.5 ng/L), and PFBA (0.10 – 10 ng/L) in surface snow is in the same range as previously reported in precipitation in urban areas[13, 31, 37-44] and similar concentrations of TFA has previously been reported in precipitation in remote locations.[6] A significant correlation was observed between the flux of TFA and PFPrA ($r=0.93$, $p<0.01$), TFA and PFBA ($r=0.85$, $p<0.01$), and PFPrA and PFBA ($r=0.81$, $p<0.01$) in samples collected at Foxfonna sampling site (Table S11). These findings suggest that TFA, PFPrA, and PFBA share similar atmospheric sources and fate in remote Arctic environments.

It has been suggested that marine aerosols play an important role in the global distribution of TFA.[45] No significant correlation was observed between TFA, PFPrA, and PFBA with sodium (Table S11). Previous work with remote snow samples have also observed this lack of correlation for C_2 – C_4 PFCAs.[46] The lack of correlations observed in the present study supports the

observation by Pickard *et al.* (2018) that marine aerosol inputs are unimportant to the long-range transport of C_2 – C_4 PFCAs to remote Arctic environments.

5.4.2 Seasonal Variation of TFA, PFPrA, and PFBA in Surface snow

To investigate seasonal variations in long range processes, data from the Foxfonna ice cap was used since this offered the longest time series. As the fluxes of TFA, PFPrA and PFBA from the snow samples at the reference sites were of a similar range as the fluxes in the snow samples from Foxfonna, equivalent long-range processes are dominating the explanation for the presence of these compounds in the snow samples from Foxfonna. This evidence, combined with Foxfonna's high elevation site up wind of Longyearbyen with respect to the prevailing winds, means this site offers the best potential for a remote site of the three main sampling locations.

The observed median fluxes of TFA, PFPrA, and PFBA in surface snow on Foxfonna were higher, by 36, 6 and 2 times for TFA, PFPrA and PFBA respectively, during precipitation event sampling in April – August 2019 (rounds 6 – 10, samples Fox06 – Fox10) compared to sampling in January – March 2019 (rounds 1 – 5, samples Fox01 – Fox05). This sampling was done during the polar summer period with 24-hour daylight in April – August (Fox06 – Fox10) and compared with samples collected during the polar night with complete 24-hour, or partial (0 – 10 hours daylight), darkness in January – March (Fox01 – Fox05). These results are in line with previous modelled results which found that the atmospheric concentrations of PFOA, having formed *via* hydroxyl radical mediated degradation of 8:2 FTOH, would be 15 – 20 times higher in the Arctic in July compared to January.[27] This was attributed to seasonal variations in atmospheric hydroxyl radical concentrations. The amplitude of the seasonal variations for the different PFAAs observed might be linked to different sources.

To inspect this relationship further, HYSPLIT modeling was used to simulate the relationship between atmospheric hydroxyl radical concentrations and the flux of precursor degradation products (in this instance TFA, PFPrA and PFBA in surface snow). Since hydroxyl radicals are produced by incoming solar radiation into the atmosphere,[47] the downward short-wave radiation was used to access the seasonal variations in hydroxyl radicals in the Arctic atmosphere. A backwards air mass trajectory of six days from the time of sampling was used to represent the air mass that brought the precipitation event that was consequently sampled in the surface snow at Foxfonna (Figure S1). A backwards air mass trajectory of length six days was used since it was expected that that atmospheric half-life of TFA with respect to wet/dry deposition would be similar to that of nitric acid.[29] Therefore, the majority of TFA observed in the surface snow would be expected to come from precursor degradations that occurred during the 6-day transport of this air mass parcel that carried the precipitation event to Foxfonna.

Integrated values for the downward short-wave solar radiation along the 144 hour (6-day) backwards trajectory were found to be on average 39 times higher for samples Fox06 – Fox10 (19.1 – 42.8 kWh/m^2) compared to samples Fox01 – Fox05 (0 – 2.5 kWh/m^2). This is a result of the rapid shift from polar night to midnight sun at high latitudes during winter to summer. A positive correlation was found between the integrated downward short-wave solar radiation and the flux of TFA ($r = 0.89$, $p < 0.01$), PFPrA ($r = 0.72$, $p < 0.05$), and PFBA ($r = 0.81$, $p < 0.01$) (Figure 3, Table S11). These findings suggest that the atmospheric transport of volatile precursors and the hydroxyl radical driven atmospheric oxidation of these plays a major role in the formation and subsequent deposition of $C_2 – C_4$ PFCAs to the Arctic environment. The higher flux of PFAAs observed during summer compared to winter could also be influenced by factors such as temperature, humidity, and seasonal variations in emission rates. In addition, it is possible that

solar radiation is correlated with air masses originating from source regions in Eurasia and that this could contribute to the correlations observed between solar radiation and increased flux of PFAAs. However, samples Fox07 and Fox09 all have backwards air mass trajectories originating over the Arctic Ocean away from source regions and still have high TFA fluxes (Figure S1). This suggests that solar radiation is a more important factor than air mass source region.

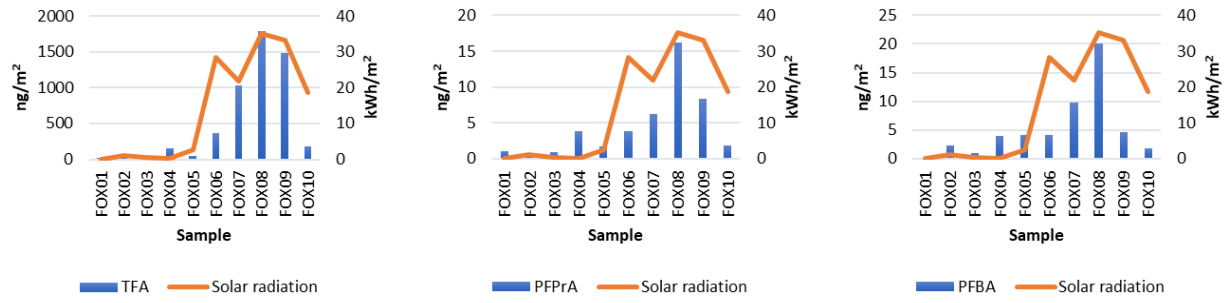


Figure 3. Flux (ng/m^2) of TFA, PFPrA, and PFBA in surface snow samples collected at the Foxfonna ice cap from January 2019 (Fox01) to August 2019 (Fox10) and short-wave solar radiation (kWh/m^2) along the backwards trajectory.

5.4.3 Discovery of TFMS at Foxfonna Ice Cap

TFMS was detected in all surface snow samples, including those collected at the reference locations, at fluxes in the range 1.5 – 57 ng/m^2. The detection of TFMS in surface snow at remote locations in the Arctic indicate that this compound may be globally distributed. To the best of our knowledge, this is the first study to report concentrations of TFMS not only in surface snow, but also at remote locations. No seasonal variation was observed, and the concentrations were not related to solar radiation or notably higher at any sampling location. There are limited data available on the formation of C_1 – C_4 PFSAs from volatile precursors. Formation of PFBS from the degradation of N-methyl perfluorobutane sulfonamidoethanol[25] has been illustrated. However, the findings in the present study suggest that atmospheric sources other than atmospheric

degradation of precursor compounds are involved in the long-range atmospheric transport of C_1 – C_4 PFSAs to remote locations. To examine the influence of long-range oceanic transport on TFMS deposition at Foxfonna sampling site, the flux of TFMS in surface snow samples from Foxfonna ice cap was compared to the flux of sodium ions, which is a tracer for marine aerosols. No correlation was observed between sodium ions and TFMS (Table S11).

The PFAA flux in the current study is based on measured PFAA concentrations in a relatively low amount of snow events. Some studies have estimated that TFA is removed by dry deposition at a rate approximately 20% of the wet deposition rate and hence wet deposition is the dominating process for the removal of PFAAs from the atmosphere.[29, 48] The sampling was conducted as soon as possible after a certain precipitation event, in some cases sampling was not possible until up to 7 days at Foxfonna. Transformation of precursor compounds in surface snow resulting in the formation of PFCAs has previously been suggested to explain higher concentrations of PFCAs in aged snow compared to fresh snow.[30] This is likely to occur in presence of solar radiation and has not been accounted for in the present work. The current solar radiation assessment (using HYSPLIT) only accounts for the degradations that are occurring in the atmosphere rather than in the deposited snow. Other post depositional effects are also not accounted for such as re-volatilization of PFAAs back into the atmosphere.[21]

C_1 – C_4 PFAAs were frequently detected in snow samples, even in those collected at remote, high-altitude sites. The results suggest that hydroxyl radical driven atmospheric oxidation plays a major role in the global distribution of C_2 – C_4 PFCAs and the consequential deposition in Arctic environments. The discovery of TFMS in surface snow at remote locations indicates that TFMS could be globally distributed. However, the transport mechanism to the Arctic environment is still unknown. Despite the absence of correlation between C_1 – C_4 PFSAs and solar radiation,

the formation from degradation of volatile precursors cannot be ruled out, even if this source might be of minor importance. Atmospheric transport of TFMS to the Arctic could also be a particle-bound process. Further research is needed to investigate the formation of TFMS by atmospheric degradation of volatile precursors as well as the transport mechanism to remote locations.

Supporting Information

List of target analytes, abbreviations, MRM transitions and internal standard used for quantification, limits of detection, recoveries and repeatability, and Spearman rank correlations.

Conflict of Interest

The authors declare no conflicts of interest.

Acknowledgements

The authors gratefully acknowledge financial support from the Swedish Research Council Formas (2016-01284), the Swedish Environmental Protection Agency (2219-16-030 and 2219-17-012), the British National Environmental Research Council and the Oxford Doctoral Training Partnership in Environmental Research (NE/L002612/1), the Burdett-Coutts Trust, the Svalbard Science Forum Arctic Field Grant 2019 (RiS ID 11121), the Research Council of Norway (SvalPOP, 196218/S30), the Fram Centre Flagship program (PharmArctic, 534/75219) and the Knowledge Foundation (Enforce Research Project, 20160019). The authors would also like to thank the Logistics Department and colleagues at the University Centre in Svalbard for help organizing and assisting with fieldwork.

5.5 References

1. Cousins, I. T.; Ng, C. A.; Wang, Z.; Scheringer, M., Why is high persistence alone a major cause of concern? *Environmental Science: Processes & Impacts* **2019,** *21*, 781-792.
2. Wujcik, C. E.; Cahill, T. M.; Seiber, J. N., Determination of trifluoroacetic acid in 1996-1997 precipitation and surface waters in California and Nevada. *Environ. Sci. Technol.* **1999,** *33*, (10), 1747-1751.
3. Scheurer, M.; Nödler, K.; Freeling, F.; Janda, J.; Happel, O.; Riegel, M.; Müller, U.; Rüdiger Storck, F.; Fleig, M.; Lange, F. T.; Brunsch, A.; Brauch, H. J., Small, mobile, persistent: Trifluoroacetate in the water cycle - Overlooked sources, pathways and consequences for drinking water supply. *Water Res.* **2017,** *126*, 460-471.
4. Wallington, T. J.; Schneider, W. F.; Worsnop, D. R.; Nielsen, O. J.; Sehested, J.; Debruyn, W. J.; Shorter, J. A., The environmental impact of CFC replacements - HFCs and HCFCs. *Environ. Sci. Technol.* **1994,** *28*, (7), 320-326.
5. Scott, B. F.; Mactavish, D.; Spencer, C.; Strachan, W. M. J.; Muir, D. C. G., Haloacetic acids in canadian lake waters and precipitation. *environ. Sci. Technol.* **2000,** *30*, (20), 4266-4272.
6. Von Sydow, L. M.; Grimvall, A. B.; Borén, H. B.; Laniewski, K.; Nielsen, A. T., Natural background levels of trifluoroacetate in rain and snow. *Environ. Sci. Technol.* **2000,** *34*, (15), 3115-3118.
7. Zhai, Z.; Wu, J.; Hu, X.; Li, L.; Guo, J.; Zhang, B.; Hu, J.; Zhang, J., A 17-fold increase of trifluoroacetic acid in landscape waters of Beijing, China during the last decade. *Chemosphere* **2015,** *129*, 110–117.
8. Boutonnet, J. C.; Bingham, P.; Calamari, D.; de Rooij, C.; Franklin, J.; Kawano, T.; Libre, J. M.; McCul-loch, A.; Malinverno, G.; Odom, J. M.; Rusch, G. M.; Smythe, K.; Sobolev, I.; Thompson, R.; Tiedje, J. M., Environmental risk assessment of trifluoroacetic acid. *Hum. Ecol. Risk Assess.* **1999,** *5*, (1), 59-124.
9. Hurley, M. D.; Wallington, T. J.; Javadi, M. S.; Nielsen, O. J., Atmospheric chemistry of CF3CF=CH2: Products and mechanisms of Cl atom and OH radical initiated oxidation. *Chem. Phys. Lett.* **2008,** *450*, 263-267.
10. Solomon, K. R.; Velders, G. J. M.; Wilson, S. R.; Madronich, S.; Longstreth, J.; Aucamp, P. J.; Bornman, J. F., Sources, fates, toxicity, and risks of trifluoroacetic acid and its salts: Relevance to substances regulated under the Montreal and Kyoto Protocols. *J. Toxicol. Environ. Health, Part B* **2016,** *19*, (7), 289-304.
11. Neale, R. E.; Barnes, P. W.; Robson, T. M.; Neale, P. J.; Williamson, C. E.; Zepp, R. G.; Wilson, S. R.; Madronich, S.; Andrady, A. L.; Heikkilä, A. M.; Bernhard, G. H.; Bais, A. F.; Aucamp, P. J.; Banaszak, A. T.; Bornman, J. F.; Bruckman, L. S.; Byrne, S. N.; Foereid, B.; Häder, D. P.; Hollestein, L. M.; Hou, W. C.; Hylander, S.; Jansen, M. A. K.; Klekociuk, A. R.; Liley, J. B.; Longstreth, J.; Lucas, R. M.; Martinez-Abaigar, J.; McNeill, K.; Olsen, C. M.; Pandey, K. K.; Rhodes, L. E.; Robinson, S. A.; Rose, K. C.; Schikowski, T.; Solomon, K. R.; Sulzberger, B.; Ukpebor, J. E.; Wang, Q. W.; Wängberg, S. Å.; White, C. C.; Yazar, S.; Young, A. R.; Young, P. J.; Zhu, L.; Zhu, M., Environmental effects of stratospheric ozone depletion, UV radiation, and interactions with climate change: UNEP Environmental Effects Assessment Panel, Update 2020. *Photochem. Photobiol. Sci.* **2021,** *20*, 1-67.
12. Scott, B. F.; Moody, C. A.; Spencer, C.; Small, J. M.; Muir, D. C. G.; Mabury, S. A., Analysis of perfluorocarboxylic acids/anions in surface waters and precipitation using GC-MS and analysis of PFOA from large-volume samples. *Environ. Sci. Technol.* **2006,** *40*, (20), 6405-6410.
13. Taniyasu, S.; Kannan, K.; Yeung, L. W. Y.; Kwok, K. Y.; Lam, P. K. S.; Yamashita, N., Analysis of trifluoroacetic acid and other short-chain perfluorinated acids (C2-C4) in precipitation by liquid chromatography-tandem mass spectrometry: Comparison to patterns of long-chain perfluorinated acids (C5-C8). *Anal. Chim. Acta* **2008,** *619*, 221-230.
14. Yeung, L. W. Y.; Stadey, C.; Mabury, S. A., Simultaneous analysis of perfluoroalkyl and polyfluoroalkyl substances including ultrashort-chain C2 and C3 compounds in rain and river water samples by ultra performance convergence chromatography. *J. Chromatogr. A* **2017,** *1522*, 78-85.
15. Björnsdotter, M. K.; Yeung, L. W. Y.; Kärrman, A.; Ericson Jogsten, I., Ultra-Short-Chain Perfluoroalkyl Acids Including Trifluoromethane Sulfonic Acid in Water Connected to Known and Suspected Point Sources in Sweden. *Environ. Sci. Technol.* **2019,** *53*, 11093-11101.
16. Pickard, H. M.; Criscitiello, A. S.; Persaud, D., Spencer, C.; Muir, D. C. G.; Lehnherr, I.; Sharp, M.; De Silva, A. O.; Young, C. J., Ice Core Record of Persistent Short-Chain Fluorinated Alkyl Acids: Evidence of the Impact From Global Environmental Regulations. *Geophys. Res. Lett.* **2020,** *47*, 1-11.
17. Shoeib, M.; Harner, T.; Vlahos, P., Perfluorinated Chemicals in the Arctic Atmosphere. *Environ. Sci. Technol.* **2006,** *40*, 7577-7583.
18. Stock, N. L.; Furdui, V. I.; Muir, D. C. G.; Mabury, S. A., Perfluoroalkyl Contaminants in the Canadian Arctic: Evidence of Atmospheric Transport and Local Contamination. *Environ. Sci. Technol.* **2007,** *41*, 3529-3536.
19. Dreyer, A.; Weinberg, I.; Temme, C.; Ebinghaus, R., Polyfluorinated Compounds in the Atmosphere of the Atlantic and Southern Oceans: Evidence for a

Global Distribution. *Environ. Sci. Technol.* **2009,** *43*, 6507-6514.
20. Cai, M.; Xie, Z.; Möller, A.; Yin, Z.; Huang, P.; Cai, M.; Yang, H.; Sturm, R.; He, J.; Ebinghaus, R., Polyfluorinated compounds in the atmosphere along a cruise pathway from the Japan Sea to the Arctic Ocean. *Chemosphere* **2012,** *87*, 989-997.
21. Xie, Z.; Wang, Z.; Mi, W.; Möller, A.; Wolschke, H.; Ebinghaus, R., Neutral Poly-/perfluoroalkyl Substances in Air and Snow from the Arctic. *Sci. Rep.* **2015,** *5*, 8912.
22. Ellis, D. A.; Mabury, S. A.; Martin, J. W.; Muir, D. C. G., Thermolysis of fluoropolymers as a potential source of halogenated organic acids in the environment. *Nature* **2001,** *412*, 321-324.
23. Johansson, J. H.; Salter, M. E.; Acosta Navarro, J. C.; Leck, C.; Nilsson, E. D.; Cousins, I. T., Global transport of perfluoroalkyl acids via sea spray aerosol. *Environ. Sci.: Processes Impacts* **2019,** *21*, 635-649.
24. Ellis, D. A.; Martin, J. W.; De Silva, A. O.; Mabury, S. A.; Hurley, M. D.; Sulbaek Andersen, M. P.; Wallington, T. J., Degradation of fluorotelomer alcohols: a likely atmospheric source of perfluorinated carboxylic acids. *Environ. Sci. Technol.* **2004,** *38*, 3316-3321.
25. D'eon, J.; Hurley, M. D.; Wallington, T. J.; Mabury, S. A., Atmospheric chemistry of N-methyl perfluorobutane sulfonamidoethanol, C4F9SO2N(CH3)CH2CH2OH: kinetics and mechanism of reaction with OH. *Environ. Sci. Technol.* **2006,** *40*, 1862-1868.
26. Martin, J. W.; Ellis, D. A.; Mabury, S. A., Atmospheric Chemistry of Perfluoroalkanesulfonamides: Kinetic and Product Studies of the OH Radical and Cl Atom Initiated Oxidation of N-Ethyl Perfluorobutanesulfonamide. *Environ. Sci. Technol.* **2006,** *40*, (3), 864-872.
27. Wallington, T. J.; Hurley, M. D.; Xia, J.; Wuebbles, D. J.; Sillman, S.; Ito, A.; Penner, E.; Ellis, D. A.; Martin, J.; Mabury, S. A.; Nielsen, O. J.; Sulbaek Andersen, M. P., Formation of C7F15COOH (PFOA) and Other Perfluorocarboxylic Acids during the Atmospheric Oxidation of 8:2 Fluorotelomer Alcohol. *Environ. Sci. Technol.* **2006,** *40*, 924-930.
28. Montzka, S. A.; McFarland, M.; Andersen, S. O.; Miller, B. R.; Fahey, D. W.; Hall, B. D.; Hu, L.; Siso, C.; Elkins, J. W., Recent Trends in Global Emissions of Hydrochlorofluorocarbons and Hydrofluorocarbons: Reflecting on the 2007 Adjustments to the Montreal Protocol. *J. Phys. Chem. A* **2015,** *119*, 4439-4449.
29. Kotamarthi, V. R.; Rodriguez, J. M.; Ko, M. K. W.; Tromp, T. K.; Sze, N. D., Trifluoroacetic Acid from Degradation of HCFCs and HFCs: A Three-Dimensional Modeling Study. *J. Geophys. Res. Atmos.* **1998,** *103*, 5747-5758.
30. Taniyasu, S.; Yamashita, N.; Moon, H. B.; Kwok, K. Y.; Lam, P. K. S.; Horii, Y.; Petrick, G.; Kannan, K., Does wet precipitation represent local and regional atmospheric transportation by perfluorinated alkyl substances? *Environ. Int.* **2013,** *55*, 25-32.
31. Zhang, W.; Zhang, Y.; Taniyasu, S.; Yeung, L. W. Y.; Lam, P. K. S.; Wang, J.; Li, X.; Yamashita, N.; Dai, J., Distribution and fate of perfluoroalkyl substances in municipal wastewater treatment plants in economically developed areas of China. *Environ. Pollut.* **2013,** *176*, 10-17.
32. Barzen-Hanson, K. A.; Field, J. A., Discovery and implications of C2 and C3 perfluoroalkyl sulfonates in aqueous film-forming foams and groundwater. *Environ. Sci. Technol. Lett.* **2015,** *2*, (4), 95-99.
33. Schulze, S.; Zahn, D.; Montes, R.; Rodil, R.; Quintana, J. B.; Knepper, T. P.; Reemtsma, T.; Berger, U., Occurence of emerging persistent and mobile organic contaminants in European water samples. *Water Res.* **2019,** *153*, 80-90.
34. Skaar, J. S.; Raeder, E. M.; Lyche, J. L.; Ahrens, L.; Kallenborn, K., Elucidation of contamination sources for poly- and perfluoroalkyl substances (PFASs) on Svalbard (Norwegian Arctic). *Environ. Sci. Pollut. Res.* **2019,** *26*, 7356-7363.
35. Ali, A. M.; Langberg, H. A.; Hale, S. E.; Kallenborn, K.; Hartz, W. F.; Mortensen, Å. K.; Ciesielski, T. M.; McDonough, C. A.; M., J. B.; Breedveld, G. D., The fate of poly- and perfluoroalkyl substances in a marine food web influenced by land-based sources in the Norwegian Arctic. *Environ. Sci.: Processes Impacts* **2021,** *23*, 588-604.
36. Kwok, K. Y.; Yamazaki, E.; Yamashita, N.; Taniyasu, S.; Murphy, M. B.; Horii, Y.; Petrick, G.; Kallenborn, K.; Kannan, K.; Murano, K.; Lam, P. K. S., Transport of Perfluoroalkyl substances (PFAS) from an arctic glacier to downstream locations: Implications for sources. *Sci. Total. Environ.* **2013,** *447*, 46-55.
37. Wujcik, C. E.; Cahill, T. M.; Seiber, J. N., Extraction and Analysis of Trifluoroacetic Acid in Environmental Waters. *Anal. Chem.* **1998,** *70*, 4074-4080.
38. Jordan, A.; Frank, H., Trifluoroacetate in the environment. Evidence for sources other than HFC/HCFCs. *Environ. Sci. Technol.* **1999,** *33*, (4), 522-527.
39. Berg, M.; Müller, S. R.; Mühlemann, J.; Wiedmer, A.; Schwarzenbach, R. P., Concentrations and mass fluxes of chloroacetic acids and trifluoroacetic acid in rain and natural waters in Switzerland. *Environ. Sci. Technol.* **2000,** *34*, (13), 2675-2683.

40. Römpp, A.; Klemm, O.; Fricke, W.; Frank, H., Haloacetates in fog and rain. *environ. Sci. Technol.* **2001,** *35*, (7), 1294-1298.
41. Scott, B. F.; Spencer, C.; Martin, J. W.; Barra, R.; Bootsma, H. A.; Jones, K. C.; Johnston, A. E.; Muir, D. C. G., Comparison of haloacetic acids in the environment of the northern and southern hemispheres. *environ. Sci. Technol.* **2005,** *39*, 8664-8670.
42. Scott, B. F.; Spencer, C.; Mabury, S. A.; Muir, D. C. G., Poly and perfluorinated carboxylates in North American precipitation. *Environ. Sci. Technol.* **2006,** *40*, (23), 7167-7174.
43. Kwok, K. Y.; Taniyasu, S.; Yeung, L. W. Y.; Murphy, M. B.; Lam, P. K. S.; Horii, Y.; Kannan, K.; Petrick, G.; Sinha, R. K.; Yamashita, N., Flux of perfluorinated chemicals through wet deposition in Japan, the United States, and several other countries. *Environ. Sci. Technol.* **2010,** *44*, (18), 7043-7049.
44. Wang, Q.; Wang, X.; Ding, X., Rainwater trifluoroacetic acid (TFA) in Guangzhou, South China: Levels, wet deposition fluxes and source implication. *Sci. Total. Environ.* **2014,** *468-469*, 272–279.
45. EFCTC (European Fluorocarbons Technical Committee) *Transport of naturally occurring trifluoroacetic acid (TFA) by sea salt aerosol*; 2020.
46. Pickard, H. M.; Criscitiello, A. S.; Spencer, C.; Sharp, M.; Muir, D. C. G.; De Silva, A. O.; Young, C. J., Continuous non-marine inputs of per- and polyfluoroalkyl substances to the High Arctic: a multi-decadal temporal record. *Atmos. Chem. Phys.* **2018,** *18*, 5045-5058.
47. Rohrer, F.; Berresheim, H., Strong correlation between levels of tropospheric hydroxyl radicals and solar ultraviolet radiation. *Nature* **2006,** *442*, 184-187.
48. Kazil, J.; McKeen, S.; Kim, S. W.; Ahmadov, R.; Grell, G. A.; Talukdar, R. K.; Ravishankara, A. R., Deposition and rainwater concentrations of trifluoroacetic acid in the United States from the use of HFO-1234yf. *J. Geophys. Res. Atmos.* **2014,** *119*, 14059-14079.

5.6 Supporting Information

Table S1. List of target analytes, MRM transitions and internal standards used for quantification. 166
Table S2. Limits of quantification, extraction efficiency and repeatability, and instrument precision. 166
Table S3. Concentrations of C_1 – C_4 PFAAs (ng/L) and Sodium (Na^+) ions (ppb) in surface snow collected on the summit of Foxfonna ice cap (FOX), and the short-wave solar radiation (kWh/m^2), during January to August 2019. 167
Table S4. Concentrations of C_1 – C_4 PFAAs (ng/L) in surface snow collected up the hill from the Kjell Henriksen Observatory (KHO) during January to June 2019. 167
Table S5. Concentrations of C_1 – C_4 PFAAs (ng/L) in surface snow collected in Longyearbyen, outside the University Centre in Svalbard (UNIS) during January to May 2019. 168
Table S6. Concentrations of C_1 – C_4 PFAAs (ng/L) in surface snow collected at four high elevation sites on glaciers around Svalbard Spitsbergen during February to April 2019. 168
Table S7. Flux of C_1 – C_4 PFAAs (ng/m^2) and Sodium (Na^+) ions (µg/m^2) in surface snow collected on the summit of Foxfonna ice cap (FOX), and the short-wave solar radiation (kWh/m^2), during January to August 2019. 169
Table S8. Flux of C_1 – C_4 PFAAs (ng/m^2) in surface snow collected up the hill from the Kjell Henriksen Observatory (KHO) during January to June 2019. 169
Table S9. Flux of C_1 – C_4 PFAAs (ng/m^2) in surface snow collected in Longyearbyen, outside the University Centre in Svalbard (UNIS) during January to May 2019. 170
Table S10. Flux of C_1 – C_4 PFAAs (ng/m^2) in surface snow collected at four high elevation sites on glaciers around Svalbard Spitsbergen during February to April 2019. 170
Table S11. Spearman rank correlations. 170

Ion Chromatography for quantification of Na^+ concentrations 171

Figure S1. HYSPLIT backwards air mass trajectories for Fox01 – Fox10 and the hourly downward solar radiation along the trajectory (W/m^2). 172

Table S1. List of target analytes, IUPAC names, CAS numbers, abbreviations, MRM transitions and internal standards used for quantification.

Target analyte	CAS	Abbreviation	1st MRM transition	2nd MRM transition	Internal standard
Trifluoroacetic acid	76-05-1	TFA	112.90 > 68.96	-	^{13}C-M2TFA
Perfluoropropanoic acid	422-64-0	PFPrA	162.97 > 118.90	-	^{13}C-M4PFBA
Perfluorobutanoic acid	375-22-4	PFBA	212.97 > 169.00	-	^{13}C-M4PFBA
Trifluoromethane sulfonic acid	1493-13-6	TFMS	149.12 > 79.91	149.12 > 98.95	^{13}C-M3PFBS
Perfluoroethane sulfonic acid	354-88-1	PFEtS	198.80 > 79.80	198.80 > 98.90	^{13}C-M3PFBS
Perfluoropropane sulfonic acid	423-41-6	PFPrS	248.9 > 79.90	248.9 > 98.90	^{13}C-M3PFBS
Perfluorobutane sulfonic acid	375-73-5	PFBS	298.90 > 79.96	298.90 > 98.90	^{13}C-M3PFBS

Table S2. Instrument limits of quantification (LOQ) (ng/L), method limits of quantification (MQL) (ng/L). Extraction efficiency (%) and repeatability (%) based on spiked blank samples and spiked test samples (*n*=3). Repeatability (%) of the analytical method based on repeated standard injections (*n*=10).

	LOQ (ng/L)	MQL (ng/L)	Extraction efficiency (%)	Extraction method repeatability (%)	Analytical method repeatability (%)
TFA	0.009	0.009	121 ± 5	2.7	4.1
PFPrA	0.009	0.009	67 ± 8	11	2.4
PFBA	0.009	0.058	71 ± 6	14	3.0
TFMS	0.009	0.009	80 ± 16	15	2.8
PFEtS	0.009	0.045	81 ± 9	2.2	0.33
PFPrS	0.009	0.009	83 ± 8	6.0	2.4
PFBS	0.002	0.013	80 ± 12	3.3	1.7

Table S3. Concentrations of $C_1 – C_4$ PFAAs (ng/L) and sodium (Na^+) ions (ppb) in surface snow collected on the summit of the Foxfonna ice cap (Fox), and the downward short-wave solar radiation (kWh/m^2), during January to August 2019.

	TFA	**PFPrA**	**PFBA**	**TFMS**	**PFEtS**	**PFPrS**	**PFBS**	**Na^+ (ppb)**	**Solar radiation (kWh/m^2)**
Fox01	7.4	0.31	<0.06	1.3	<0.05	<0.009	<0.01	660	0.0
Fox02	13	0.36	1.1	5.1	<0.05	<0.009	<0.01	600	1.3
Fox03	7.3	0.29	0.33	0.92	<0.05	<0.009	<0.01	480	0.0
Fox04	16	0.41	0.43	1.0	<0.05	<0.009	<0.01	700	0.37
Fox05	11	0.41	0.98	0.53	<0.05	<0.009	<0.01	190	2.5
Fox06	54	0.57	0.61	0.63	<0.05	<0.009	<0.01	17	27
Fox07	170	1.0	1.6	0.36	<0.05	<0.009	<0.01	240	33
Fox08	170	1.5	1.9	0.29	<0.05	<0.009	<0.01	430	43
Fox09	270	1.5	0.84	1.7	<0.05	<0.009	<0.01	650	41
Fox10	49	0.51	0.49	1.3	<0.05	<0.009	<0.01	460	19

Table S4. Concentrations of $C_1 – C_4$ PFAAs (ng/L) in surface snow collected up the hill from the Kjell Henriksen Observatory (KHO) during January to June 2019.

	TFA	**PFPrA**	**PFBA**	**TFMS**	**PFEtS**	**PFPrS**	**PFBS**
KHO01	5.6	0.21	0.57	1.0	0.10	<0.009	<0.01
KHO02	16	0.54	1.1	1.3	0.11	<0.009	<0.01
KHO03	7.7	0.32	0.10	3.0	<0.05	<0.009	<0.01
KHO04	12	0.29	0.35	1.9	<0.05	<0.009	<0.01
KHO05	17	0.46	0.34	0.97	<0.05	<0.009	<0.01
KHO06	80	0.55	0.62	0.50	<0.05	<0.009	<0.01
KHO07	100	1.0	0.56	0.15	<0.05	<0.009	<0.01
KHO08	93	0.96	0.90	0.22	<0.05	<0.009	<0.01
KHO09	73	0.89	1.0	0.22	<0.05	<0.009	<0.01

Table S5. Concentrations of $C_1 – C_4$ PFAAs (ng/L) in surface snow collected in Longyearbyen, outside the University Centre in Svalbard (UNIS) during January to May 2019.

	TFA	**PFPrA**	**PFBA**	**TFMS**	**PFEtS**	**PFPrS**	**PFBS**
UNIS01	18	0.66	3.4	2.6	0.24	<0.009	2.4
UNIS02	24	0.74	3.6	2.4	0.71	<0.009	0.1
UNIS03	16	0.46	10	2.1	0.35	<0.009	<0.01
UNIS04	70	0.86	2.8	1.3	0.22	<0.009	<0.01
UNIS05	27	1.2	2.7	1.2	0.29	<0.009	<0.01
UNIS06	110	0.75	2.0	1.0	0.24	<0.009	0.03
UNIS07	190	1.1	6.2	0.65	0.26	<0.009	0.07
UNIS08	50	0.72	8.8	2.9	2.8	<0.009	0.09

Table S6. Concentrations of $C_1 – C_4$ PFAAs (ng/L) in surface snow collected at four high elevation sites on glaciers around Spitsbergen during February to April 2019.

	TFA	**PFPrA**	**PFBA**	**TFMS**	**PFEtS**	**PFPrS**	**PFBS**
Lomonosovfonna01	18	0.34	0.37	0.37	<0.05	<0.009	<0.01
Lomonosovfonna02	30	0.53	0.57	0.89	<0.05	<0.009	<0.01
Drønbreen	13	0.40	0.58	1.1	<0.05	<0.009	<0.01
Grønfjordbreen	90	1.1	0.82	1.5	<0.05	<0.009	<0.01
Nordmannsfonna	62	0.75	0.63	1.5	<0.05	<0.009	<0.01

Table S7. Flux of $C_1 – C_4$ PFAAs (ng/m^2) and Sodium (Na^+) ions ($\mu g/m^2$) in surface snow collected on the summit of the Foxfonna ice cap (Fox), and the downward short-wave solar radiation (kWh/m^2), during January to August 2019.

	TFA	**PFPrA**	**PFBA**	**TFMS**	**PFEtS**	**PFPrS**	**PFBS**	**Na^+ ($\mu g/m^2$)**	**Solar radiation (kWh/m^2)**
Fox01	23	0.99	<0.19	4.0	<0.14	<0.03	<0.04	2100	0.0
Fox02	28	0.79	2.4	11	<0.10	<0.02	<0.03	1300	1.1
Fox03	22	0.87	0.99	2.8	<0.14	<0.03	<0.04	1400	0.41
Fox04	150	3.9	4.0	9.7	<0.42	<0.09	<0.12	6600	0.18
Fox05	46	1.7	4.2	2.3	<0.19	<0.04	<0.05	800	2.6
Fox06	360	3.8	4.1	4.2	<0.30	<0.06	<0.09	120	28
Fox07	1000	6.2	9.8	2.2	<0.28	<0.06	<0.08	1500	22
Fox08	1800	16	20	3.1	<0.48	<0.10	<0.14	4600	35
Fox09	1500	8.3	4.6	9.4	<0.25	<0.05	<0.07	3600	33
Fox10	180	1.8	1.8	4.9	<0.16	<0.03	<0.05	1700	19

Table S8. Flux of $C_1 – C_4$ PFAAs (ng/m^2) in surface snow collected up the hill from the Kjell Henriksen Observatory (KHO) during January to June 2019.

	TFA	**PFPrA**	**PFBA**	**TFMS**	**PFEtS**	**PFPrS**	**PFBS**
KHO01	82	3.0	8.3	15	1.5	<0.13	<0.19
KHO02	72	2.5	4.8	6.1	0.52	<0.04	<0.06
KHO03	41	1.7	0.51	16	<0.24	<0.05	<0.07
KHO04	123	2.9	3.5	19	<0.45	<0.09	<0.13
KHO05	89	2.4	1.8	5.1	<0.24	<0.05	<0.07
KHO06	690	4.7	5.3	4.3	<0.39	<0.08	<0.11
KHO07	1000	11	5.7	1.5	<0.46	<0.09	<0.13
KHO08	640	6.6	6.1	1.5	<0.31	<0.06	<0.09
KHO09	560	6.8	7.9	1.6	<0.34	<0.07	<0.10

Table S9. Flux of $C_1 – C_4$ PFAAs (ng/m^2) in surface snow collected in Longyearbyen, outside the University Centre in Svalbard (UNIS) during January to May 2019.

	TFA	PFPrA	PFBA	TFMS	PFEtS	PFPrS	PFBS
UNIS01	190	7.1	36	28	2.6	<0.10	26
UNIS02	220	6.7	32	22	6.4	<0.08	0.93
UNIS03	120	3.3	75	15	2.5	<0.07	<0.09
UNIS04	480	5.9	19	9.0	1.5	<0.06	<0.09
UNIS05	140	6.2	14	6.3	1.5	<0.05	<0.07
UNIS06	720	4.8	13	6.4	1.5	<0.06	0.17
UNIS07	1800	10	59	6.2	2.5	<0.09	0.65
UNIS08	980	14	170	57	55	<0.18	1.7

Table S10. Flux of $C_1 – C_4$ PFAAs (ng/m^2) in surface snow collected at four high elevation sites on glaciers around Spitsbergen during February to April 2019.

	TFA	PFPrA	PFBA	TFMS	PFEtS	PFPrS	PFBS
Lomonosovfonna01	160	3.0	3.3	3.3	<0.40	<0.08	<0.11
Lomonosovfonna02	330	5.9	6.3	9.9	<0.50	<0.10	<0.14
Drønbreen	66	2.0	3.0	5.8	<0.23	<0.05	<0.07
Grønfjordbreen	710	8.9	6.5	12	<0.35	<0.07	<0.10
Nordmannsfonna	210	2.6	2.1	5.1	<0.15	<0.03	<0.04

Table S11. Spearman rank correlations (r) between the flux of TFA, PFPrA, PFBA and TFMS (ng/m^2); Na^+ ($\mu g/m^2$) and solar radiation (kWh/m^2).

	TFA		PFPrA		PFBA		TFMS	
	r	**p**	**r**	**p**	**r**	**p**	**r**	**p**
PFPrA	**0.93**	**<0.01**						
PFBA	**0.85**	**<0.01**	**0.81**	**<0.01**				
TFMS	-0.03	0.93	-0.12	0.75	-0.27	0.45		
Solar radiation	**0.89**	**<0.01**	**0.72**	**<0.05**	**0.81**	**<0.01**	-0.14	0.70
Na^+	0.33	0.35	0.55	0.10	0.14	0.70	0.26	0.47

Ion Chromatography for quantification of Na^+ concentrations

Na^+ concentrations were measured using a Dionex ICS-4000 Integrion system. A Dionex AS-AP autosampler was used to supply sample to the instrument. Calibration of IC data was achieved using a range of calibration standards. All calibration standards were prepared from purchased Sigma Aldrich (1000 ppm) standards by a series of gravimetric dilutions.

The columns used were a Dionex Ionpac CG16-4μm (2 x 50 mm) guard column and CS16 (4 μm, 2 x 250 mm) analytical column. Samples were loaded to a 250 μL sample loop. A 32 – 42 mM methane sulfonic acid (MSA) multistep eluent gradient was used for effective separation of the analytes. The eluent was produced using a Dionex eluent generator cartridge (EGC 500 KOH) and was pumped through the columns at a flow rate of 0.20 mL min^{-1} at a pressure of 3300 psi for a 25 min chromatogram. The eluent ions were removed from the column effluent using a cation electrolytically regenerated suppressor (Dionex CERS 500), before conductivity detection of the effluent.

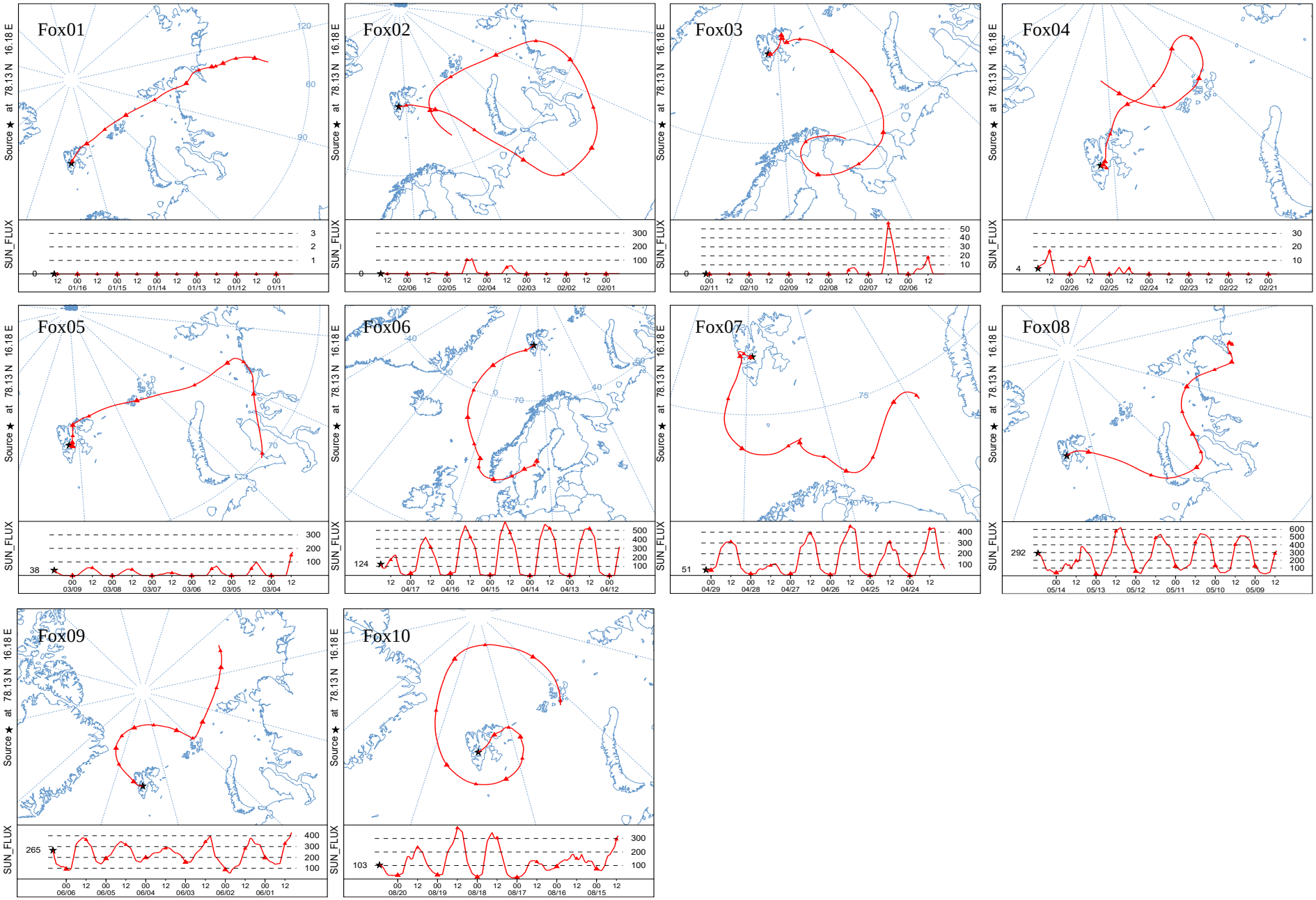


Figure S1. HYSPLIT backwards air mass trajectories for Fox01 – Fox10 and the hourly downward solar radiation along the trajectory (W/m^2) from Chapter 5.

Chapter 6

Levels and Seasonal Variations of Per- and Polyfluoroalkyl Substances (PFAS) in Surface Snow in the Arctic

William F. Hartz,[a,b] Maria K. Björnsdotter,[c,d] Leo W. Y. Yeung,[d] Jack D. Humby,[e] Ingrid Ericson Jogsten,[d] Anna Kärrman,[d] Roland Kallenborn,[f,g]

Drafted for submission to Environmental Science and Technology

6.1 Abstract 175
6.2 Introduction 176
6.3 Materials and Methods 179
6.3.1 Target Analysis 179
6.3.2 Sample Collection 179
6.3.3 Sample Extraction and PFAS analysis 182
6.3.4 Data Treatment 183
6.4 Results and Discussion 184
6.4.1 Concentrations and fluxes of PFAS in Surface Snow 184
6.4.2 Comparison of surface snow with the Lomonosovfonna 2019 ice core 187
6.4.3 Seasonal variations of PFAS in Surface Snow in Longyearbyen 191
6.4.4 Seasonal variations of PFAS in Surface Snow on Foxfonna 192
6.5 References 200
6.6 Supporting Information 202

This chapter was conceptualised by William F. Hartz, who also undertook the fieldwork, sample preparation, data interpretation and writing as well as assisting with ion chromatography. Other major contributions include PFAS sample extraction, analysis, and data processing by Maria K. Björnsdotter and ion chromatography analysis by Jack Humby. Maria K. Björnsdotter and Jack Humby wrote part of the methods in the Supporting Information. A few co-authors have assisted in editing of the manuscript. Chapter 6 was prepared separately to Chapter 5 due to differences in the PFAS analytical technique used in each study.

[a]Department of Earth Sciences, University of Oxford, South Parks Road, Oxford, OX1 3AN, United Kingdom

[b]Department of Arctic Geology, University Centre in Svalbard (UNIS), NO-9171, Longyearbyen, Svalbard, Norway

[c]Institute of Environmental Assessment and Water Research (IDAEA-CSIC), C/Jordi Girona, 18-26, 08034 Barcelona, Catalonia, Spain

[d]Man-Technology-Environment Research Centre (MTM), Örebro University, SE-701 82 Örebro, Sweden

[e]Ice Dynamics and Paleoclimate, British Antarctic Survey, High Cross, Cambridge, CB3 0ET, United Kingdom

[f]Faculty of Chemistry, Biotechnology and Food Sciences (KBM), Norwegian University of Life Sciences (NMBU), NO-1432 Ås, Norway

[g]Department of Arctic Technology, University Centre in Svalbard (UNIS), NO-9171, Longyearbyen, Svalbard, Norway

6.1 Abstract

Per- and polyfluoroalkyl substances (PFAS) are a group of persistent anthropogenic organofluorine contaminants, some of which are known to be toxic and bioaccumulative. Perfluoroalkyl carboxylic acids (PFCAs) and perfluoroalkyl sulfonic acids (PFSAs) can form from the atmospheric degradation of precursors such as fluorotelomer alcohols (FTOHs) as well as hydrochlorofluorocarbons (HFCs) and other ozone-depleting chlorofluorocarbon (CFC) replacement compounds. Since PFCAs and PFSAs will readily be removed from the atmosphere during wet deposition, snow and ice cores can be used to understand PFAS atmospheric processes in the Arctic. A total of 45 PFAS were measured in this chapter and in Chapter 5 combined, of which 37 were detected, in surface snow on the island of Spitsbergen in the Norwegian Arctic during January – August 2019 (i.e. 24-hour darkness to 24-hour daylight). PFAS contamination was found to be widespread, including at remote high elevation sites. Surface snow in Longyearbyen was influenced by local sources of C_4 – C_{11} PFCAs, PFHxS and PFOS, whose concentrations were 2.3 – 22 times higher compared to at remote sites. Surface snow from Foxfonna was found to receive PFAS input predominantly from long-range atmospheric processes. At this location, the median deposition fluxes of C_2 – C_{11} PFCAs, PFHxS, PFOS and HFPO-DA (GenX) were found to be 2.0 – 38 times higher during 24-hour daylight. These PFAS were found to positively correlate with solar radiation. This suggests seasonal light in the Arctic is important in the atmospheric degradation of PFAS precursors, and their subsequent deposition in the remote Arctic environment. In contrast, marine aerosols were not found to be significant for PFAS atmospheric transport. For some PFCAs, FTOHs were thought to contribute to their seasonal deposition, whereas the long-range atmospheric process which led to HFPO-DA (GenX) deposition in the remote Arctic was unclear.

6.2 Introduction

Per- and polyfluoroalkyl substances (PFAS) are a diverse group of organofluorine contaminants, used in a variety of industrial and consumer applications.[1] Their high mobility and environmental persistence, as well as their ability to undergo transformation in the environment, has led them to being detected ubiquitously in the environment.[2] This includes, for example, Arctic biota and abiota.[3] However, many PFAS are known to be toxic and bioaccumulative.[4,5]

A large focus of research has been on perfluoroalkyl acids (PFAAs), including perfluoroalkyl carboxylic acids (PFCAs) and perfluoroalkyl sulfonic acids (PFSAs). Several long-range distribution mechanisms and their interactions explain the presence of PFAAs and other PFAS in the Arctic. These include ocean currents,[6,7] marine aerosols,[8] local sources,[9] and the long-range atmospheric transport of volatile neutral PFAS (so called precursors) followed by their atmospheric degradation and subsequent deposition.[10,11]

Measuring precipitation provides a route to understanding the atmospheric processes of PFAS.[12,13] Several studies have used remote snowpits and ice cores to provide a record of the overall atmospheric processes over several years,[14] whereas measuring just surface snow can provide information about the atmospheric conditions for the precipitation event sampled.[15] Only one study has used surface snow to investigate seasonal variations in PFAA deposition. Björnsdotter et al. (Chapter 5) found that the deposition of C_2 – C_4 PFCAs would be highly seasonal in the Arctic.[16] This study and others have linked trifluoroacetic acid (TFA) deposition with solar radiation.[17,18] This is expected since solar radiation is able to initiate the atmospheric formation of radicals (e.g. hydroxyl radicals), which are known to degrade TFA precursors, including hydrofluorocarbons (HFCs),[19] hydrochlorofluorocarbons (HCFCs),[20] hydrofluoroethers (HFEs),[21] and hydrofluoroolefins (HFOs)[22]. These were introduced in the 1990s as replacement

products after the Montreal protocol banned ozone-depleting chlorofluorocarbons (CFCs).[23] The atmospheric levels for many HFCs, and related compounds, are increasing,[24] as is TFA depositon.[25]

Other precursors, such as fluorotelomer alcohols (FTOHs), N-alkylated perfluoroalkane sulfonamides (FASAs), perfluoroalkane sulfonamido ethanols (FOSEs), and fluorotelomer acrylates (FTAs) are known to exist in the Arctic atmosphere,[26–30] and they are also able to undergo radical mediated degradation to PFAAs.[10,31–34] The degradation of an n:2 FTOH will produce approximately equal molar quantities of the corresponding C_n and C_{n+1} PFCAs (see Chapter 1, Section 1.3.2).[10] Using this approach, FTOHs have been found to be a major source of PFCA deposition in the remote Arctic (for example, Chapter 4).[11,15,35] Nonetheless, local sources can also contribute to PFAS deposition in surface snow.[36]

In Svalbard (Norwegian Arctic), significant local sources in Longyearbyen and Ny-Ålesund, from landfill and firefighting training sites (FFTS) have been found.[3,9,36] Ali et al. found high levels of PFAS runoff from the FFTS in Longyearbyen (Σ_{14}PFAS = 57.4 ± 4.0 ng L^{-1}), where aqueous film forming foams (AFFF) are regularly in use for firefighting training purposes. PFOS (35%) had the largest mass contribution in runoff followed by: PFHxS (22%), PFHxA (18%), PFOA (11%), PFHpA (6%) and 6:2 FTSA (3%). In landfill leachate in Longyearbyen (Σ_{14}PFAS = 643 ± 84 ng L^{-1}), PFOS also had the highest mass contribution (48%) followed by C_6 – C_{11} PFCAs (43%) including PFOA (20%).

Nonetheless, results from Chapter 5 suggested that the source of C_2 – C_4 PFCAs in surface snow from Foxfonna (800 m.a.s.l., 16 km from Longyearbyen upwind of prevailing winds) was predominantly from long-range atmospheric processes, despite the location's proximately to Longyearbyen settlement. The present study uses the same sample set previously analyzed in

Chapter 5 (for C_1 – C_4 PFAAs using supercritical fluid chromatography, SFC), to measure 38 further PFAS (using ultra performance liquid chromatography, UPLC) in surface snow in Svalbard (Norwegian Arctic). This was with the aim to investigate (i) the levels and seasonal variations of PFAS deposition in the Arctic (ii) the extent of PFAS contamination in surface snow from local sources in Longyearbyen and (iii) the atmospheric processes of PFAS in the remote Arctic.

6.3 Materials and Methods

6.3.1 Target Analysis

In total, 45 different PFAS were targeted as follows. PFAAs targeted were C_2 – C_{14}, C_{16}, and C_{18} PFCAs, and C_1 – C_{10} and C_{12} PFSAs. Fluorotelomers targeted were 4:2 FTSA, 6:2 FTSA, 8:2 FTSA, 6:2 FTUCA and 8:2 FTUCA. Further anionic target analytes included 6:2 Cl-PFESA, 8:2 Cl-PFESA, HFPO-DA (GenX), and ADONA. 9 neutral compounds were also targeted: FBSA, MeFBSA, FHxSA, MeFHxSA, FOSA, MeFOSA, EtFOSA, MeFOSE and EtFOSE. C_2 – C_4 PFCAs and C_1 – C_4 PFSAs were measured by SFC tandem mass spectrometry (MS/MS) system and concentrations were previously reported in Chapter 5. The other 38 anionic and neutral analytes were measured by UPLC MS/MS and are reported in the present study. A full list of names, abbreviations and instrument methods are described in Table S1.

6.3.2 Sample Collection

This study uses the same sample set previously used in Chapter 5 to report concentrations of C_1 – C_4 PFAAs. A summary of the sampling procedure is described herein. In total seven locations were chosen for surface snow sampling. Three of the sites offered a range of potential locally contaminated and background locations (Figure 1A) which were sampled several times during 2019 (n = 8 – 10). These three sites were in Longyearbyen (78°13.288'N 15°39.041'E, 13 m.a.s.l.), up the hill from the Kjell Henriksen Observatory (KHO; 78°08.807'N 16°02.781'E, 532 m.a.s.l.), and on the summit of Foxfonna ice cap (78°07.736'N 16°10.791'E, 800 m.a.s.l.)

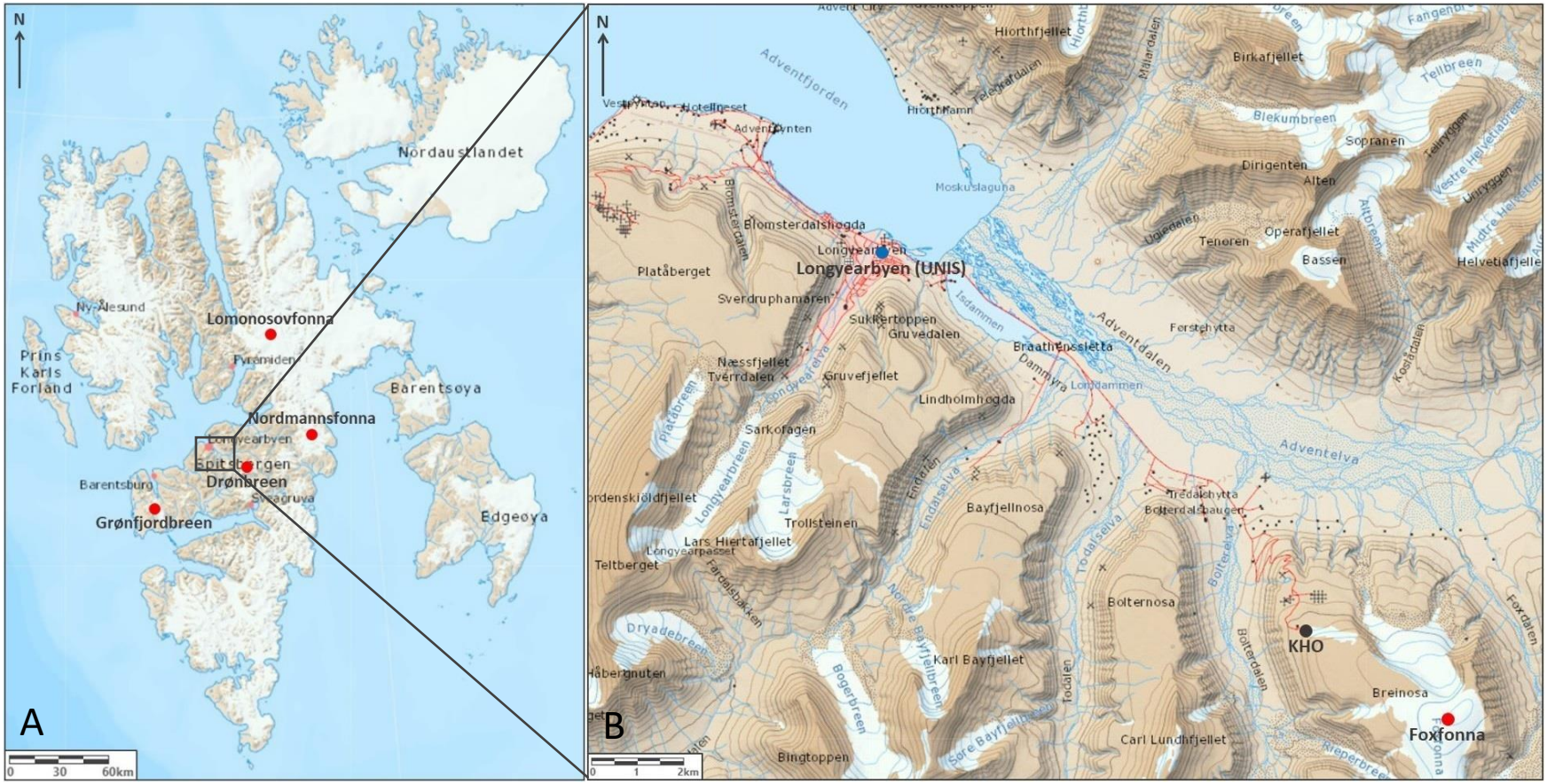


Figure 1. A) The reference snow sampling locations on Spitsbergen glaciers: Lomonosovfonna (n = 2), Nordmannsfonna (n = 1), Drønbreen (n = 1) and Grønfjordbreen (n = 1). The map was reproduced from Björnsdotter et al.[16] and TopoSvalbard, Norwegian Polar Institute. B) Sampling locations in Longyearbyen (n = 8), near the Kjell Henriksen Observatory (KHO, n = 9) and on Foxfonna (n = 10).

The site on the summit of the Foxfonna ice cap was chosen as a potentially remote location owing to its high altitude (800 m.a.s.l.) and position eastwards upwind from the Longyearbyen settlement (16 km away). Close to Foxfonna, (4.7 km away) sampling was also conducted 150 m uphill from the Kjell Henriksen Observatory (KHO). This site was also located 1.3 km away from an active coal mine. Sampling was also undertaken in the settlement of Longyearbyen (approximately 2,400 inhabitants), outside the University Centre in Svalbard (UNIS). This was situated in approximately in the center of the town, 360 m from the fjord in a fenced off area such that the snow was not directly disturbed by pedestrians or traffic. Sampling at Foxfonna was undertaken from January – August 2019 (samples Fox01 – Fox10, n = 10). Sampling at KHO was undertaken from January – June 2019 (samples KHO01 – KHO09, n = 9). Sampling at UNIS was undertaken January – May 2019 (samples UNIS01 – UNIS08, n = 8). This represents the time of year when the seasonal light is changing from 24-hour darkness in winter to 24-hour daylight summer. 24-hour daylight began on 19th April 2019 and continued for the rest of the sampling period.

Each snow sample represents a single precipitation event whereby post-depositional effects have been minimized. This was achieved by sampling as soon as possible after a chosen precipitation event. This was typically <1 – 7 days (average 3.7 days) at the Foxfonna sampling site. Surface snow samples (n = 5) from four high elevation remote sites on glaciers were also collected (Figure 1B). These reference locations were selected as they would presumably receive PFAS input from long-range atmospheric processes only. Sampling was conducted during February – April 2019 on Drønbreen (n = 1, 78°06.185'N 16°39.182'E, 707 m.a.s.l.), Lomonosovfonna (n = 2, 78°49.454'N 17°26.253'E, 1198 m.a.s.l.), Grønfjordbreen (n = 1,

77°53.222'N 14°13.745'E, 574 m.a.s.l.) and Nordmannsfonna (*n* = 1, 78°15.894'N 18°23.717'E, 498 m.a.s.l.).

The upper 0 – 5 cm of the surface snow was collected into a precleaned high-density polyethylene barrel using a precleaned aluminum shovel. Due to windy conditions on Svalbard, it was assumed that the snow was well mixed by snow blowing in the atmosphere and surface snow drifting before final deposition,[37] and hence PFAS distribution in the surface snow after precipitation was homogeneous. The area sampled was 0.8 – 3.9 m^2 (average 1.8 m^2) for the 32 surface snow samples. The barrel was sealed and transported back to UNIS, where the snow was then melted at 5 °C, bottled into precleaned polypropylene containers. Subsamples from the barrel were also taken for major ion analysis.

6.3.3 Sample Extraction and PFAS analysis

All samples were extracted according to the methods described in detail in Chapter 5. In summary, samples were extracted by weak anion exchange solid-phase extraction (Oasis® WAX, Waters Corporation, Milford, USA) following the ISO25101 method with some modifications. After extraction, two fractions containing target analytes were eluted from the cartridge. The first fraction containing neutral target analytes was eluted by adding 4 mL methanol. The second fraction containing anionic target analytes was eluted by adding 4 mL 0.1% ammonium hydroxide in methanol. The anionic fraction has already been analyzed by supercritical fluid chromatography (SFC) tandem mass spectrometry system (MS/MS) for quantification of C_1 – C_4 PFAAs. Their concentrations and instrument methods are reported by in Chapter 5. Quantification of the remaining 38 anionic and neutral PFAS by UPLC-MS/MS, as well as full details of the chemicals and reagents, quality control and quality assurance, MQLs (method quantification limits), Hybrid

Single-Particle Lagrangian Integrated Trajectory model (HYSPLIT) analysis and major ion analysis can be found in the supporting information.

6.3.4 Data Treatment

Concentrations of PFAS are reported in pg L^{-1}. To remove the effects of variations in snow fluxes for each precipitation event, PFAS concentrations were multiplied by the snow flux of each precipitation event (in kg m^{-2}) to yield PFAS fluxes (in pg m^{-2} per precipitation event). Spearman rank correlation coefficients (r) were used to investigate correlations. Tests for statistical significance were performed using a two-tailed Student's t-test (p).

6.4 Results and Discussion

6.4.1 Concentrations and fluxes of PFAS in Surface Snow

In this study, C_5 – C_8 PFCAs, PFHxS, PFOS, 6:2 FTSA and FHxSA were detected in all surface snow samples, in addition to TFA, PFPrA and TFMS, as reported previously in Chapter 5.[16] HFPO-DA (GenX), PFBA, PFNA, PFDA, PFUnDA, PFDoDA PFTrDA, PFTDA, 6:2 FTUCA, MeFBSA, FBSA and FOSA were also detected in >50% of surface snow samples. PFHxDA, PFOcDA, PFEtS, PFBS, PFHpS, 8:2 FTSA, 8:2 FTUCA, PFECHS, ADONA, MeFOSA, EtFOSA, MeFOSE and EtFOSE were detected in <50% of surface snow samples, whereas MeFHxSA, PFPrS, PFNS, PFDS, PFDoDS, 4:2 FTSA, 6:2 Cl-PFESA and 8:2 Cl-PFESA were not detected in any samples. The widespread detection (80 – 100%), including at the reference locations, of C_2 – C_9 PFCAs, PFUnDA, PFTrDA, HFPO-DA (GenX), TFMS, PFHxS, PFOS, 6:2 FTSA, FBSA, FHxSA and FOSA, suggests that long-range atmospheric processes are an effective source for the deposition of PFAS in the remote Arctic. This result broadly agrees with two remote Arctic ice cores, from Lomonosovfonna, Svalbard and the Devon Ice Cap, Canada, which found widespread detection of C_2 – C_{11} PFCAs, PFOS and FOSA reported in Chapter 4 and by Pickard et al.[14,38] Further information on detection, concentrations, and fluxes can be found in Tables S7 – S12.

The widespread detection of C_2 – C_{11} PFCAs in these remote Arctic ice cores was previously considered to be from the transformation products derived from the radical mediated atmospheric degradation of FTOHs as well as HFCs, and related compounds (Chapter 4).[14,38] It is highly likely that these precursors are also a major source of the PFCAs detected in snow this study. The widespread detection of HFPO-DA (GenX) and 6:2 FTSA in surface snow, including at the reference sites, suggests that long-range atmospheric processes can contribute to their deposition in the Arctic. Their physicochemical properties do not intuitively promote their direct

long-range atmospheric transport. 6:2 fluorotelomer sulfonamide alkylamine, 6:2 fluorotelomer sulfonamide alkylbetaine, and 6:2 fluorotelomer sulfonamide were previously suggested as possible atmospheric precursors to 6:2 FTSA (Chapter 4). It is unclear what atmospheric mechanism could contribute to the remote deposition of HFPO-DA in the Arctic.

At the reference sites, there was frequent detection of FBSA (80%), FHxSA (100%) and FOSA (80%), MeFOSA (20%) and MeFOSE (60%). Their presence could be explained by their direct long-range transport from source regions. FBSA, FHxSA and FOSA could also be the degradation products of FASAs[32] and FOSEs. This transformation is known to be possible during the biodegradation of FASAs and FOSEs.[39,40] Regardless, the detection of FASAs and FOSEs at the reference sites is in agreement with the detection of these compounds in snow on glaciers near Ny-Ålesund and an ice core from Lomonosovfonna, Svalbard.[30] This confirms that these known PFAA precursors exist in the Arctic atmosphere.[32,33]

6:2 FTCA was previously identified as an atmospheric degradation product of 6:2 FTOH in a Svalbard ice core (Chapter 4). FTCA will eliminate HF to form 6:2 FTUCA in the environment (e.g. during snowpack/firn processes) or during extraction/analysis (e.g. during the preparation of the extracts in MeOH).[41,42] Hence, the detection of 6:2 FTUCA is evidence for the atmospheric oxidation of the terminal alcohol of 6:2 FTOH. This study detected 6:2 FTUCA with highest frequencies at the reference sites (100%, elevations 498 – 1198 m.a.s.l.), then Foxfonna (80%, 800 m.a.s.l.), KHO, (78%, 532 m.a.s.l.) then at UNIS (38%, 13 m.a.s.l.). The lesser detection frequency at lower elevation sites could be due to its higher rates of post-deposition degradation. 6:2 FTCA has a -CH_2- moiety that will be vulnerable to further degradation, for example, as part of post-depositional processes. This could also explain its low detection frequency in the Lomonosovfonna

ice core (35%), where there will be significant post-deposition processes for example firnification and melt water percolation.

Like TFMS,[16] PFHxS and PFOS were also detected at all snow samples. This study also quantified branched isomers of PFHxS and PFOS (Table S15 and S16). Inspecting the structural isomer profile is a useful tool in assigning sources of PFAS.[43] Linear-PFHxS was detected in all snow samples and was the only isomer detected in 97% of all surface snow samples. This agrees with the findings from the Lomonosovfonna ice core where linear-PFHxS was the dominant isomer of PFHxS detected. PFHxS produced by electrochemical fluorination (ECF) is known to produce 18% branched PFHxS isomers.[44] Given that the linear-PFHxS concentrations were often close to the MQL, it would be therefore likely that any branched PFHxS would be below the MQL. In contrast, branched isomers of PFOS were observed in every sample as well as linear-PFOS. The percentage of linear isomers of PFOS at Foxfonna, KHO and UNIS was 82 ± 4%, 79 ± 3%, and 83 ± 3%, respectively. These results match the Lomonosovfonna ice core (81 ± 6%, Chapter 4), but were slightly higher than runoff from the FFTS (69 ± 1%), landfill leachate (73 ± 1%), and river in Longyearbyen (74 ± 1%).[3] Regardless, all these locations likely indicate an ECF manufactoring process.[43,44] Therefore, if PFOS deposition at remote locations can be explained by precursor degradations then PFOS precursors have likely been manufactured by ECF, assuming that PFOS precursors have been produced from ECF manufactured perfluorooctane sulfonyl fluoride (POSF).

The reference surface snow sample collected on the Grønfjordbreen glacier had the largest contribution of branched PFOS isomers (68% linear-PFOS). This result was not in line with the percentage of linear-PFOS found at other reference locations, which ranged from 80 – 82%. Hence, it was thought that this sample might have been influenced by local sources from the settlement of

Barentsburg (9 km away).[9] Furthermore, this sample from Grønfjordbreen has the highest levels of several PFAS when compared to the other reference sites. In addition, it was also the only surface snow sample to detect MeFOSA and the only surface snow sample to detect PFHpS outside of Longyearbyen. It was concluded that this sample was not in line with the other reference locations, and it is discluded from the reference locations in further discussions. Herein, only the samples from Lomonosovfonna (n = 2), Nordmannsfonna (n = 1), Drønbreen (n = 1) were used to understand the typical levels of PFAS a reference location.

6.4.2 Comparison of surface snow with the Lomonosovfonna 2019 ice core

An ice core from Lomonosovfonna, Svalbard (spanning 2006 – 2019) has been analyzed for the same 45 PFAS as in this study (Chapter 4). The concentrations of $C_2 – C_{11}$ PFCAs, TFMS, PFHxS, PFOS and HFPO-DA (GenX) in the Lomonosovfonna ice core were compared with the concentrations of these same PFAS in surface snow reported in this study and in Chapter 5 (Figure 2). Since the Lomonosovfonna ice core has likely only received PFAS input from long range atmospheric sources, this approach gives an insight into whether the site at UNIS in settlement of Longyearbyen, and Foxfonna may have received PFAS contamination predominantly from long-range atmospheric processes, local sources in Longyearbyen or indeed a mixed signal. KHO was discluded from this comparison since it may have been influenced by, as yet unconfirmed, local sources relating to a nearby coal mine.[3] By comparing the levels of different PFAS at these four locations, this can be used to understand whether each site represents a local or background signal. Chapter 5 found that surface snow at UNIS (Longyearbyen) was influenced by local sources of PFBA and PFBS, whereas Foxfonna represented a suitable location for understanding the long-range atmospheric processes of TFA, PFPrA, PFBA, and TFMS.

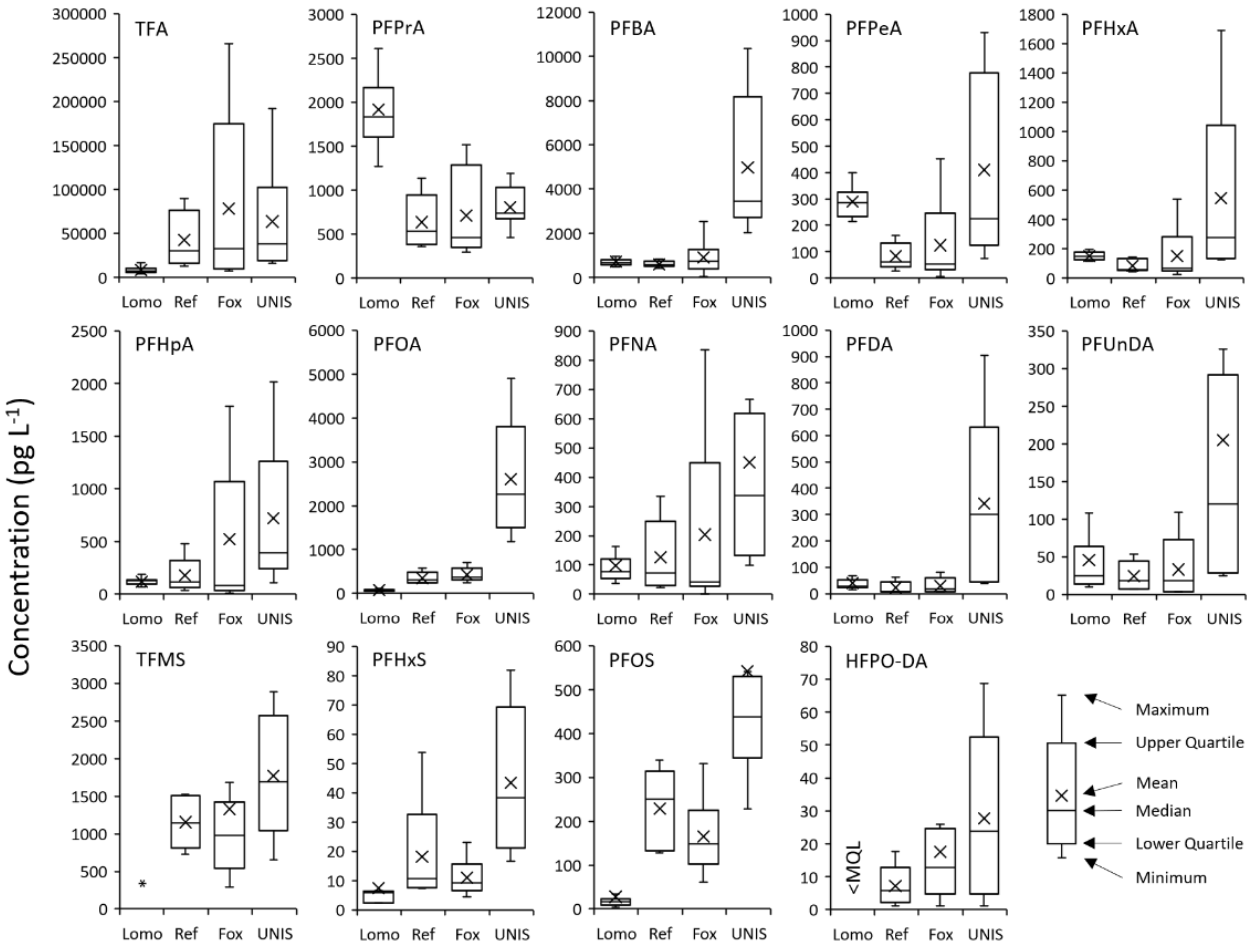


Figure 2. Boxplot to show the concentrations (pg L^{-1}) of C_2 – C_{11} PFCAs, TFMS, PFHxS, PFOS and HFPO-DA (GenX) in an ice core from Lomonosovfonna (Lomo) spanning 2006 – 2019 (*n* = 17, Chapter 4) and surface snow from reference sites (Ref), Foxfonna (Fox) and Longyearbyen (UNIS). Concentrations of TFMS and C_2 – C_4 PFCAs in the surface snow have previously been reported in Chapter 5. *Not able to be reported in the Lomonosovfonna ice core.

The median concentrations of C_5 – C_{11} PFCAs, PFHxS and PFOS were 2.3 - 22 times higher, when comparing snow at UNIS with the reference sites (Table 1). This indicates that surface snow in Longyearbyen has been influenced by local sources. This reflects existing knowledge about PFAS sources in Longyearbyen.[3,9,36] In contrast, median concentrations of C_5 – C_{11} PFCAs were similar on Foxfonna when compared to the reference sites (0.8 – 1.4 times higher,

Table 1). Concentrations of PFHxS and PFOS were 1.0 and 0.8 times higher on Foxfonna compared to the reference sites. This suggests that Foxfonna receives input of these PFAS predominantly from long-range atmospheric processes, as was found previously for C_1 – C_4 PFAAs.[16] This would be expected since the sampling site is located above the atmospheric boundary layer and is 16 km upwind from Longyearbyen with respect to the prevailing wind direction. To support this observation further, TFA (C_2) made up 92% and 95% of the mass of C_2 – C_{11} PFCAs at the reference sites and on Foxfonna respectively, whereas other PFCAs individually contributed <2.5%. In contrast, TFA made up 81% of C_2 – C_{11} PFCAs in surface snow in Longyearbyen, with other PFCAs individually contributing up to 7.3%. These differences and similarities in PFCA distribution suggest that similar atmospheric processes are contributing to PFCA deposition at the reference sites and Foxfonna, whereas different sources exist for the surface snow in Longyearbyen.

Variations in the range of concentrations between different snow sampling sites of C_2 – C_7, C_9 and C_{11} PFCAs, PFHxS and PFOS could be due to slight variations in the time of year in which sampling was conducted (Ref = February – April, Fox = January – August, UNIS = January – May). Large seasonal variation in C_2 – C_4 deposition in the Arctic is known.[16] Lower TFA concentrations (and other PFAS such as PFOA and PFOS) in the Lomonosovfonna ice core could be due to losses from runoff or percolation too deeper layers in the ice core. Indeed, TFA and PFOS are known to be mobile during melt water percolation (Chapter 4). Alternatively, variations between the PFAS concentrations in the ice core and the surface snow (e.g. lower TFA and higher PFPrA concentrations) could also be in part due to variations in the past atmospheric levels of precursors during 2006 – 2019 (i.e. the timespan of the ice core), in contrast to atmospheric levels in 2019 alone, when the surface snow sampling in this study conducted.

HFPO-DA (GenX) was detected at most surface snow sampling locations (75 – 90%) but was not detected in the Lomonosovfonna ice core (Chapter 4). It was however detected in surface snow at the same location on Lomonosovfonna (3.26 and 5.72 pg L^{-1}). This could indicate that post-depositional processes degrade HFPO-DA, or effective dilution from low HFPO-DA concentration snow during mid-winter brings concentrations in the ice core below the MQL. It is difficult to understand whether Foxfonna represents a remote location for studying HFPO-DA deposition, since little is known about its atmospheric sources or local sources in Longyearbyen.

The situation for PFOA was also unclear as median concentrations were low in the ice core (74.0 pg L^{-1}), but higher in the reference sites (283 pg L^{-1}) and on Foxfonna (379 pg L^{-1}). Furthermore, two surface snow samples collected during April 2019 from Lomonosovfonna had PFOA concentrations of 305 and 243 pg L^{-1}, which were also higher than the concentrations in the ice core drilled at the same site (39.8 – 112 pg L^{-1}). 82% of the PFOA:PFNA ratios were between 0.5 and 2 indicating a FTOH precursor source for the ice core. However, for the reference sites (including surface snow from Lomonosovfonna) and on Foxfonna, just 20% and 33% of the ratios fell between 0.5 and 2, resepectievly (for those samples >MQL). The specific reasons for the differences in these concentrations and PFOA:PFNA ratios are unclear, but it points to a possible division in the processes that exist for ice cores and surface snow for PFOA (see Seasonal variations of PFAS in Surface Snow on Foxfonna). Indeed, an ice core provides a record of the overall atmospheric process over several years, whereas surface snow samples provide only information about the atmospheric conditions associated with the individual precipitation event sampled. Regardless, for all PFAS in Figure 2, concentrations in the Lomonosovfonna ice core were, in the most case, similar or lower than those in surface snow from the reference sites. This

suggests that this ice core was drilled at a location receiving PFAS input overwhelmingly from long-range atmospheric processes.

6.4.3 Seasonal variations of PFAS in Surface Snow in Longyearbyen

As discussed previously, surface snow at UNIS in Longyearbyen has likely been influenced by local sources of $C_4 – C_{11}$ PFCAs, PFHxS and PFOS. This confirms existing knowledge that human activities contribute to the PFAS input in the Arctic.[3] Investigating the fluxes of PFAS in surface snow sampled January – May 2019 outside UNIS in Longyearbyen offered the opportunity to inspect for seasonal variations in PFAS in surface snow as a result of seasonal variations of human activities in the settlement, see Figure 3 (a) and (b).

Several PFAS were found to have higher deposition fluxes in surface snow after UNIS06, sampled on 23rd April 2019. The highest fluxes for most PFCAs and PFSAs were observed in the samples UNIS07 (6th May 2019) and UNIS08 (21st May 2019). These higher fluxes could be due to several reasons such as: (i) increased PFAS usage during May (and possibly also during summer) (ii) snow melt in Longyearbyen in May uncovered local sources that have otherwise been frozen over with snow and ice during winter/spring (ii) increased degradation in the atmosphere/snow surface from local sources of precursors after 24-hour daylight started on 19th April 2019.

6.4.4 Seasonal variations of PFAS in Surface Snow on Foxfonna

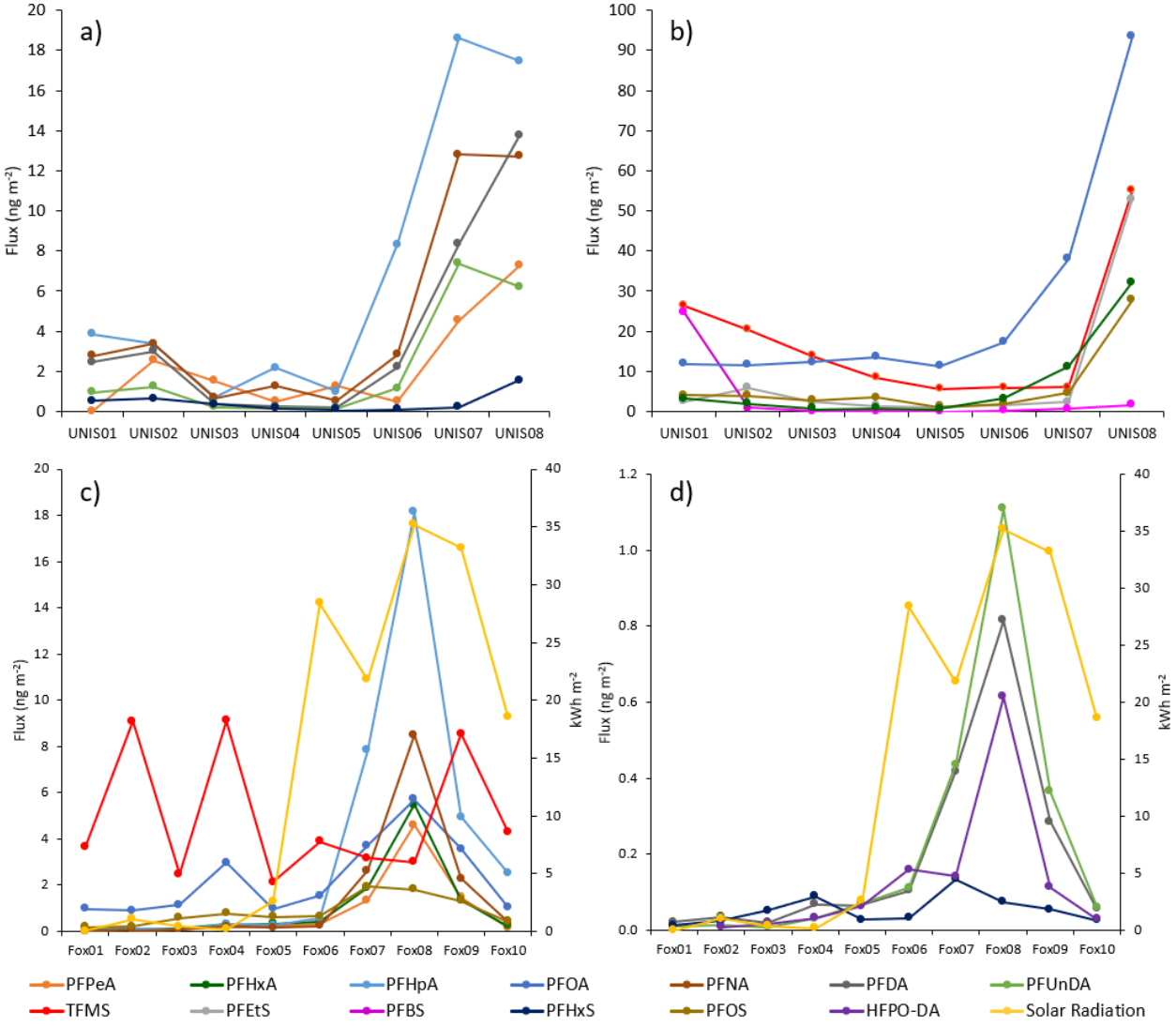


Figure 3. (a) and (b): Deposition fluxes per precipitation event (ng m^{-2}) of TFMS, PFEtS, PFBS, PFOS and C_4 – C_{11} PFCAs in surface snow outside UNIS in Longyearbyen during January – May 2019. (c) and (d): Deposition fluxes per precipitation event (ng m^{-2}) of PFHxS, PFOS, HFPO-DA and C_5 – C_{11} PFCAs in surface snow on Foxfonna during January to August 2019, plotted alongside the solar radiation (kWh m^{-2})

As discussed previously, Foxfonna represented a location receiving input predominantly from long range atmospheric processes of TFMS, PFHxS, PFOS, C_2 – C_7 and C_9 – C_{11} PFCAs, and possibly also PFOA and HFPO-DA (GenX). Foxfonna also had the longest sampling time series (January – August 2019) of the sites in this study. This offered the best opportunity to understand the seasonal variations in PFAS deposition in the remote Arctic.

Table 1. Results from investigations into PFAS atmospheric processes for surface snow This includes: (i) the median times higher concentrations at UNIS compared to then reference sites (Ref), (ii) the median times higher concentrations at Foxfonnna compared to then reference sites (Ref), (iii) times higher median fluxes of PFAS during months with 24-hour daylight at Foxfonna (Fox06 – Fox10 compared to Fox01 – Fox05), (iv) correlations of PFAS from Foxfonna with solar radiation calculated using backward air mass trajectories, (v) correlations of PFAS from Foxfonna with Na^+ (a marine aerosol proxy), (vi) the percentage of PFAS that was deposited in three samples during late April – May (Fox07 - Fox09) across all 10 samples from Foxfonna and (vii) the percentage of consecutive even:odd molar ratios that were between 0.5 and 2, indicating a possible FTOH source to Foxfonna. Statistically significant spearman correlations (r) are in bold ($p < 0.05$). Correlations for C_2 - C_4 PFAAs were previously reported in Chapter 5.

	Times higher at UNIS vs Ref	**Times higher at Foxfonna vs Ref**	**Times higher median fluxes during 24-hour daylight**	**Correlation with Solar Radiation**	**Correlation with Na^+**	**Percentage of the total flux in samples Fox07 – Fox09 (%)**	**Even:Odd molar ratios between 0.5 and 2 (%)**
TFA	1.6	1.3	36	**r = 0.89, p < 0.01**	r = 0.33, p = 0.35	85%	0%
PFPrA	1.6	1.0	6.3	**r = 0.72, p < 0.05**	r = 0.55, p = 0.10	70%	
PFBA	6.0	1.3	2.0	**r = 0.81, p < 0.01**	r = 0.14, p = 0.70	70%	0%
PFPeA	3.8	0.9	14	**r = 0.88, p < 0.01**	r = 0.31, p = 0.38	87%	
PFHxA	4.8	1.2	10	**r = 0.85, p < 0.01**	r = 0.30, p = 0.40	85%	50%
PFHpA	3.8	0.8	38	**r = 0.87, p < 0.01**	r = 0.41, p = 0.24	89%	
PFOA	8.0	1.3	3.7	r = 0.61, p = 0.06	r = 0.59, p = 0.07	58%	33%
PFNA	6.3	0.8	29	**r = 0.85, p < 0.01**	r = 0.38, p = 0.28	92%	
PFDA	22	1.3	8.1	**r = 0.81, p < 0.01**	r = 0.45, p = 0.19	80%	86%
PFUnDA	9.4	1.4	25	**r = 0.89, p < 0.01**	r = 0.28, p = 0.43	85%	
TFMS	1.7	1.0	1.1	r = -0.14, p = 0.70	r = 0.26, p = 0.47	30%	n/a
PFHxS	4.2	1.0	2.0	r = 0.41, p = 0.24	r = 0.54, p = 0.11	50%	n/a
PFOS	2.3	0.8	2.3	**r = 0.67, p < 0.05**	r = 0.47, p = 0.38	59%	n/a
HFPO-DA (GenX)	5.3	2.8	7.8	**r = 0.85, p < 0.01**	r = 0.14, p = 0.70	73%	n/a

A previous study by Björnsdotter et al. into the seasonal deposition of C_2 – C_4 PFAAs on Foxfonna also found the location the be representative of a remote Arctic location (Chapter 5). The median fluxes of TFA, PFPrA and PFBA were found to be higher during 24-hour daylight and that they were well correlated with solar radiation (Table 1). Solar radiation varied between 0 – 2.6 kWh m^{-2} for Fox01 – Fox05 (January – March) during complete or partial darkness, and between 19 − 35 kWh m^{-2} for Fox06 – Fox10 during 24-hour daylight (April – August).

Similar seasonal variations for C_2 – C_4 PFCAs was also observed for several other PFAS on Foxfonna in this study (Figure 3 c) and d) and Chapter 5, Figure 3). Several of these PFAS were found to correlate with solar radiation (Table 1), using the same solar radiation values calculated in Chapter 5 (when concentrations of a PFAS was <MQL, they were substituted with MQL/2 before being recalculated as a flux value for the correlation). C_5 – C_{11} PFCAs (discluding PFOA) were found to significantly correlate with solar radiation ($0.81 \leq r \leq 0.89$, $p < 0.01$) and their median fluxes were 8 – 38 times higher (Fox06 – Fox10 compared to Fox01 – Fox05) during 24-hour daylight (in comparison the median solar radiation was 69 times higher). This was also found to be the case for PFOS ($r = 0.67$, $p < 0.05$) and HFPO-DA (GenX) ($r = 0.85$, $p < 0.01$), whose median fluxes were 2 and 8 times higher during 24-hour daylight. This suggests that solar radiation was important for the initiation of radical based chemistry (e.g. OH radicals) for the atmospheric formation of PFCAs, PFOS and HFPO-DA in the Arctic. The fluxes of C_5 – C_{11} PFCAs and PFOS were found to be highest in samples Fox07 – Fox09, however these samples had backwards air mass trajectories which originated away from populated/industrialized regions (Figure S1). Therefore, it was concluded that direct transport from Eurasian sources was unimportant to the deposition of PFAS on Foxfonna. These three samples, collected during late April – May 2019, represented 58 – 92% of the total fluxes of PFCAs and, 59% and 73% for PFOS and HFPO-DA,

respectively, for all samples from Foxfonna (similarly, these samples made up 69% of the solar radiation of all 10 precipitation events from Foxfonna). During establishment of the polar night during September – December, this would not be expected to be a significant time for radical driven precursor degradations. As a result, this period during late spring/early summer likely represents an important time for PFAS degradation and deposition in the Arctic.

The deposition of TFA in the Arctic is known to be highly dependent on atmospheric precursor degradations. Hence, the correlation of PFOS with TFA in the Lomonosovfonna ice core (Chapter 4), and in this study with solar radiation, indicates that the deposition of PFOS in the Arctic is likely dependent on the atmospheric radical mediated degradation of PFOS precursors. There is limited evidence for the formation of PFSAs from volatile precursors, although one study has observed the formation of PFBS from N-methyl perfluorobutane sulfonamidoethanol. Whilst several atmospheric precursors have been identified for PFCAs, it is unclear what the atmospheric precursor could be for HFPO-DA.

To understand whether FTOHs could be a possible source of PFCAs to Foxfonna, even:odd molar ratios were calculated for C_2 – C_{11} PFCAs (Table 1), as was done for the Lomonosovfonna ice core previously (Chapter 4). Furthermore, these calculations were expected to contribute to a better understanding of the sources of PFOA. Surface snow samples, where the PFCA in question was <MQL were not used in the calculation. The ratios of TFA:PFPrA and PFBA:PFPeA were all >3.6, indicating a non-fluorotelomer source. This is in agreement with the Lomonosovfonna ice core record (where their ratios were >2.8). For PFHxA:PFHpA, 50% of the ratios were between 0.5 and 2 (i.e. within a factor of two). This indicates that 6:2 FTOH could be a possible precursor source to PFHxA and PFHpA. More significant was the ratio for PFDA:PFUnDA where 86% was between 0.5 and 2. This indicates that 10:2 FTOH was a likely source of PFDA and PFUnDA at

Foxfonna. This is in agreement with the findings on Lomonosovfonna (where 82% was between 0.5 and 2). Ratios for PFOA:PFNA were only between 33% between 0.5 and 2 indicating that 8:2 FTOH was possibly not the dominant precursor. This is in contrast to what was observed on Lomonosovfonna (82%). Nonetheless those values between 0.5 and 2 at Foxfonna all occurred during consecutive sampling in late April – June 2019 (samples Fox07 – Fox09). It could be possible that during this time, when solar radiation was high, degradation from 8:2 FTOH became the dominant source of PFOA to Foxfonna. However, outside of this period (when ratios ranged 2.9 – 16.5) an alternative source/atmospheric process was dominant. It cannot be ruled out that this could be from a long-range atmospheric process since the PFOA:PFNA molar ratios in surface snow were also high at reference sites (2.5 – 15), including on Lomonosovfonna. Nonetheless the PFOA and PFNA deposited by these three precipitation events (Fox07 – Fox09), represented 58% and 92% of the total flux of PFOA and PFNA (Table 1), respectively, across all 10 samples collected from Foxfonna. This suggests that this period was a significant time for 8:2 FTOH degradation and that this precursor was possibly still the largest contributor to PFOA and PFNA deposition on Foxfonna.

PFAS were also investigated for correlations with Na^+ (Table 1). No $C_5 – C_{11}$ PFCA were found to have significant positive correlation with Na^+ ($r < 0.59$, $p > 0.07$), despite Foxfonna's coastal location (15 km to the fjord). The same was also observed for HFPO-DA ($r = 0.14$, $p = 0.70$), PFHxS ($r = 0.54$, $p = 0.11$) and PFOS ($r = 0.47$, $p = 0.38$). These results are in agreement with the findings discussed in Chapter 5 where Na^+ was also not found to correlate with TFA, PFPrA, PFBA, and TFMS in surface snow on Foxfonna. This was also the case for remote Arctic ice core records from Lomonosovfonna, Svalbard (Chapter 4) and the Devon Ice Cap in Arctic Canada.[38] Hence, marine aerosols do not likely provide an atmospheric pathway for the movement

of PFAS to the Arctic or within the Arctic. This is an important as observation since the Arctic Ocean contains a variety of PFAS,[7] and it is therefore likely that this is not able to be significantly redistributed to the terrestrial Arctic environment (e.g. ice caps) via marine aerosols.

Here we have made a comparison with major ions and solar radiation based on fluxes, but when comparing the surface snow samples with the Lomonosovfonna ice core, it has only been possible to compare PFAS deposition based on their concentrations (Figure 2). This is not an ideal comparison since variations in snow flux per precipitation event/per year can change the deposition concentrations independent of the source(s). Since it is not possible to distinguish between individual deposition events in the ice core, PFAS fluxes on Lomonosovfonna can only be reported as mass per unit area per year. In contrast, PFAS fluxes in surface snow can only be reported as PFAS mass per unit area per precipitation event. There are also questions about how representative a single snow sample is owing to variations in atmospheric conditions. Differences between surface snow on Lomonosovfonna and the ice core drilled at the same location suggest that an ice core reflects an overview of the atmospheric processes, whereas surface snow samples, only represent the atmospheric conditions with respect to the precipitation event sampled. This study has sampled a large area per precipitation event (0.8 – 3.9 m^2, average 1.8 m^2), however variations on a potentially heterogenous snow surface could contribute to the variations in PFAS fluxes. This study has endeavored to sample snow as soon as possible after the targeted precipitation event. This is important since re-emission from surface snow back to the atmosphere is known to occur for volatile neutral PFAS.[30] Furthermore, transformations of PFAAs post-deposition is known to be possible in surface snow and this could contribute to changes in PFAS fluxes after the precipitation event.[12] This study has been able to collect samples as soon as possible after the precipitation event, whereas some PFAS in the Lomonosovfonna ice core has been subject to >10

years of post-deposition effects, such as meltwater percolation (Chapter 4). Like the study on Lomonosovfonna, this study has also been unable to distinguish between particle bound and non-particle bound PFAS in the surface snow. Particle-bound transport may be important to the deposition of some PFAS. However, since it is known that the formation of PFAAs from the degradation of precursors is likely a gaseous process, it is likely many PFAAs exist as non-particle bound.

In conclusion, 37 of the 45 PFAS targeted were detected in surface snow. This showed that PFAS contamination was widespread in the Arctic, including at remote high elevation sites. Surface snow sampled at UNIS in Longyearbyen was influenced by local sources for C_4 – C_{11} PFCAs as well as PFHxS and PFOS. In contrast, Foxfonna most likely received PFAS deposition predominantly from long-range processes. Many PFCAs showed large seasonal variations in their deposition fluxes at Foxfonna, which was found to be linked to solar radiation. This was suggested to be as a result of solar radiation forming radicals (e.g. hydroxyl radicals) which initiated degradation of PFAS precursors. No PFAS were found to correlate with Na^+ ions at Foxfonna, indicating that marine aerosols were insignificant in the deposition of PFAS in the remote Arctic. Finally, despite the Lomonosovfonna ice core being influenced by post-depositional processes, it was found to provide a good indication of the dominant atmospheric processes of PFAS in the remote Arctic (Chapter 4).

Supporting Information

Full details of the chemicals and reagents, sample extraction, instrument analysis, quality control and quality assurance, HYSPLIT modelling, and major ion analysis can be found in the supporting information. Lists of target analytes, abbreviations, CAS numbers, MRM transitions, internal and recovery standards used, LODs and MQLs, extraction efficiencies, and the repeatability of the instrument method can also be found. Tables with PFAS concentrations and fluxes can also be found as well as a figure showing the backward air mass trajectories from Foxfonna calculated using HYSPLIT.

Conflict of Interest

The authors declare no conflicts of interest.

Acknowledgements

The authors gratefully acknowledge financial support from the Swedish Research Council Formas (2016-01284), the Swedish Environmental Protection Agency (2219-16-030 and 2219-17-012), the British National Environmental Research Council and the Oxford Doctoral Training Partnership in Environmental Research (NE/L002612/1), the Burdett-Coutts Trust, the Svalbard Science Forum Arctic Field Grant 2019 (RiS ID 11121), the Research Council of Norway (SvalPOP, 196218/S30), the Fram Centre Flagship program (PharmArctic, 534/75219) and the Knowledge Foundation (Enforce Research Project, 20160019). The authors would also like to thank the Logistics Department and colleagues at the University Centre in Svalbard for help organizing with the fieldwork, and Veerle van Winden, Eirik Rolland Enger and Eivind Stensrud for assistance in the field.

6.5 References

1. Wang, Z. *et al.* A New OECD Definition for Per- And Polyfluoroalkyl Substances. *Environ. Sci. Technol.* **55**, 15575–15578 (2021).
2. Giesy, J. P. & Kannan, K. Global Distribution of Perfluorooctane Sulfonate in Wildlife. *Environ. Sci. Technol.* **35**, 1339–1342 (2001).
3. Ali, A. M. *et al.* The fate of poly- And perfluoroalkyl substances in a marine food web influenced by land-based sources in the Norwegian Arctic. *Environ. Sci. Process. Impacts* **23**, 588–604 (2021).
4. Conder, J. M., Hoke, R. A., De Wolf, W., Russell, M. H. & Buck, R. C. Are PFCAs bioaccumulative? A critical review and comparison with regulatory criteria and persistent lipophilic compounds. *Environ. Sci. Technol.* **42**, 995–1003 (2008).
5. Jensen, A. A. & Leffers, H. Emerging endocrine disrupters: perfluoroalkylated substances. *Int. J. Androl.* **31**, 161–169 (2008).
6. Benskin, J. P. *et al.* Perfluoroalkyl acids in the atlantic and Canadian arctic oceans. *Environ. Sci. Technol.* **46**, 5815–5823 (2012).
7. Yeung, L. W. *et al.* Vertical Profiles, Sources, and Transport of PFASs in the Arctic Ocean. *Environ. Sci. Technol.* **51**, 6735–6744 (2017).
8. Sha, B. *et al.* Sea Spray Aerosol (SSA) as a Source of Perfluoroalkyl Acids (PFAAs) to the Atmosphere: Field Evidence from Long-Term Air Monitoring. *Environ. Sci. Technol.* **56**, 228–238 (2022).
9. Skaar, J. S., Ræder, E. M., Lyche, J. L., Ahrens, L. & Kallenborn, R. Elucidation of contamination sources for poly- and perfluoroalkyl substances (PFASs) on Svalbard (Norwegian Arctic). *Environ. Sci. Pollut. Res.* **26**, 7356–7363 (2019).
10. Ellis, D. A. *et al.* Degradation of fluorotelomer alcohols: a likely atmospheric source of perfluorinated carboxylic acids. *Environ. Sci. Technol.* **38**, 3316–21 (2004).
11. Young, C. J. *et al.* Perfluorinated Acids in Arctic Snow: New Evidence for Atmospheric Formation. *Environ. Sci. Technol.* **41**, 3455–3461 (2007).
12. Taniyasu, S. *et al.* Does wet precipitation represent local and regional atmospheric transportation by perfluorinated alkyl substances? *Environ. Int.* **55**, 25–32 (2013).
13. Pike, K. A., Edmiston, P. L., Morrison, J. J. & Faust, J. A. Correlation Analysis of Perfluoroalkyl Substances in Regional U.S. Precipitation Events. *Water Res.* **190**, 116685 (2021).
14. Pickard, H. M. *et al.* Ice Core Record of Persistent Short-Chain Fluorinated Alkyl Acids: Evidence of the Impact From Global Environmental Regulations. *Geophys. Res. Lett.* **47**, (2020).
15. Wang, X., Chen, M., Gong, P. & Wang, C. Perfluorinated alkyl substances in snow as an atmospheric tracer for tracking the interactions between westerly winds and the Indian Monsoon over western China. *Environ. Int.* **124**, 294–301 (2019).
16. Björnsdotter, M. K. *et al.* Levels and Seasonal Trends of C1-C4 Perfluoroalkyl Acids and the Discovery of Trifluoromethane Sulfonic Acid in Surface Snow in the Arctic. *Environ. Sci. Technol.* **55**, 15853–15861 (2021).
17. Freeling, F. *et al.* Trifluoroacetate in Precipitation: Deriving a Benchmark Data Set. *Environ. Sci. Technol* **54**, 11210–11219 (2020).
18. Björnsdotter, M. K., Yeung, L. W. Y., Kärrman, A. & Jogsten, I. E. Mass Balance of Perfluoroalkyl Acids, Including Trifluoroacetic Acid, in a Freshwater Lake. *Environ. Sci. Technol.* **56**, 251–259 (2022).
19. Young, C. J., Hurley, M. D., Wallington, T. J. & Mabury, S. A. Atmospheric chemistry of CF3CF2H and CF3CF2CF2CF2H: Kinetics and products of gas-phase reactions with Cl atoms and OH radicals, infrared spectra, and formation of perfluorocarboxylic acids. *Chem. Phys. Lett.* **473**, 251–256 (2009).
20. Wallington, T. J. *et al.* The Environmental Impact of CFC Replacements-HFCs and HCFCs. *Environ. Sci. Technol.* **28**, (1994).
21. Oyaro, N., Sellevåg, S. R. & Nielsen, C. J. Atmospheric chemistry of hydrofluoroethers: Reaction of a series of hydrofluoroethers with OH radicals and Cl atoms, atmospheric lifetimes, and global warming potentials. *J. Phys. Chem. A* **109**, 337–346 (2005).
22. Young, C. J., Hurley, M. D., Wallington, T. J. & Mabury, S. A. Atmospheric chemistry of perfluorobutenes (CF3CF=CFCF3 and CF3CF2CF=CF2): Kinetics and mechanisms of reactions with OH radicals and chlorine atoms, IR spectra, global warming potentials, and oxidation to perfluorocarboxylic acids. *Atmos. Environ.* **43**, 3717–3724 (2009).
23. Velders, G. J. M., Andersen, S. O., Daniel, J. S., Fahey, D. W. & McFarland, M. The importance of the Montreal Protocol in protecting climate. *Proc. Natl. Acad. Sci. U. S. A.* **104**, 4814–4819 (2007).

24. Platt, S. M. *et al.* Atmospheric composition in the European Arctic and 30 years of the Zeppelin Observatory, Ny-Ålesund. *Atmos. Chem. Phys* **22**, 3321–3369 (2022).
25. Freeling, F. *et al.* Levels and Temporal Trends of Trifluoroacetate (TFA) in Archived Plants: Evidence for Increasing Emissions of Gaseous TFA Precursors over the Last Decades. *Environ. Sci. Technol. Lett.* **9**, 400–405 (2022).
26. Cai, M. *et al.* Polyfluorinated compounds in the atmosphere along a cruise pathway from the Japan Sea to the Arctic Ocean. *Chemosphere* **87**, 989–997 (2012).
27. Dreyer, A., Weinberg, I., Temme, C. & Ebinghaus, R. Polyfluorinated Compounds in the Atmosphere of the Atlantic and Southern Oceans: Evidence for a Global Distribution. *Environ. Sci. Technol.* **43**, 6507–6514 (2009).
28. Shoeib, M., Harner, T. & Vlahos, P. Perfluorinated chemicals in the arctic atmosphere. *Environ. Sci. Technol.* **40**, 7577–83 (2006).
29. Stock, N. L., Furdui, V. I., Muir, D. C. G. & Mabury, S. A. Perfluoroalkyl Contaminants in the Canadian Arctic: Evidence of Atmospheric Transport and Local Contamination. *Environ. Sci. Technol.* **41**, 3529–3536 (2007).
30. Xie, Z. *et al.* Neutral Poly-/perfluoroalkyl Substances in Air and Snow from the Arctic. *Sci. Rep.* **5**, 8912 (2015).
31. Sulbaek Andersen, M. P. *et al.* Atmospheric chemistry of 4:2 Fluorotelomer alcohol (n-C4F9CH2CH2OH): Products and mechanism of Cl atom initiated oxidation in the presence of NO x. *J. Phys. Chem. A* **109**, 1849–1856 (2005).
32. Martin, J. W., Ellis, D. A., Mabury, S. A., Hurley, M. D. & Wallington, T. J. Atmospheric chemistry of perfluoroalkanesulfonamides: kinetic and product studies of the OH radical and Cl atom initiated oxidation of N-ethyl perfluorobutanesulfonamide. *Environ. Sci. Technol.* **40**, 864–72 (2006).
33. D'eon, J. C., Hurley, M. D., Wallington, T. J. & Mabury, S. A. Atmospheric chemistry of N-methyl perfluorobutane sulfonamidoethanol, C4F9SO2N(CH3)CH2CH2OH: kinetics and mechanism of reaction with OH. *Environ. Sci. Technol.* **40**, 1862–8 (2006).
34. Butt, C. M., Young, C. J., Mabury, S. A., Hurley, M. D. & Wallington, T. J. Atmospheric Chemistry of 4:2 Fluorotelomer Acrylate [C4F9CH2CH2OC(O)CH═CH2]: Kinetics, Mechanisms, and Products of Chlorine-Atom- and OH-Radical-Initiated Oxidation. *J. Phys. Chem. A* **113**, 3155–3161 (2009).
35. MacInnis, J. J. *et al.* Emerging investigator series: a 14-year depositional ice record of perfluoroalkyl substances in the High Arctic. *Environ. Sci. Process. Impacts* **19**, 22–30 (2017).
36. Kwok, K. Y. *et al.* Transport of Perfluoroalkyl substances (PFAS) from an arctic glacier to downstream locations: Implications for sources. *Sci. Total Environ.* **447**, 46–55 (2013).
37. Sauter, T. *et al.* Snowdrift modelling for the Vestfonna ice cap, north-eastern Svalbard. *Cryosph.* **7**, 1287–1301 (2013).
38. Pickard, H. M. *et al.* Continuous non-marine inputs of per- and polyfluoroalkyl substances to the High Arctic: a multi-decadal temporal record. *Atmos. Chem. Phys.* **18**, 5045–5058 (2018).
39. Zhang, W. *et al.* Biotransformation of perfluoroalkyl acid precursors from various environmental systems: advances and perspectives. *Environ. Pollut.* **272**, (2021).
40. Benskin, J. P. *et al.* Biodegradation of N-ethyl perfluorooctane sulfonamido ethanol (EtFOSE) and EtFOSE-based phosphate diester (SAmPAP diester) in marine sediments. *Environ. Sci. Technol.* **47**, 1381–1389 (2013).
41. Dinglasan, M. J. A., Ye, Y., Edwards, E. A. & Mabury, S. A. Fluorotelomer alcohol biodegradation yields poly- and perfluorinated acids. *Environ. Sci. Technol.* **38**, 2857–2864 (2004).
42. Loewen, M., Halldorson, T., Wang, F. & Tomy, G. Fluorotelomer carboxylic acids and PFOS in rainwater from an urban center in Canada. *Environ. Sci. Technol.* **39**, 2944–2951 (2005).
43. Kärrman, A., Langlois, I., Bavel, B. van, Lindström, G. & Oehme, M. Identification and pattern of perfluorooctane sulfonate (PFOS) isomers in human serum and plasma. *Environ. Int.* **33**, 782–788 (2007).
44. Benskin, J. P., De Silva, A. O. & Martin, J. W. Isomer profiling of perfluorinated substances as a tool for source tracking: a review of early findings and future applications. *Rev. Environ. Contam. Toxicol.* **208**, 111–160 (2010).

6.6 Supporting Information

Chemicals and Reagents	203
Instrument Analysis	203
Quality Assurance and Quality Control	204
HYSPLIT Modelling	206
Ion Chromatography for Quantification of Major Ion Concentrations	207
Table S1. List of target analytes, abbreviations, and CAS numbers	209
Table S2. MRM transitions and, internal and recovery standards used for quantification.	210
Table S3. Instrument limits of quantification, method limits of quantification, extraction efficiencies and repeatability of the instrument method	211
Table S4. The extraction efficiency for those compounds with available equivalent mass-labelled internal and recovery standards	212
Table S5. Further extraction efficiencies for the nine neutral compounds	212
Table S6. MRM transitions, instrument limits of quantification (LOQ), and method limits of quantification (MQL) for branched isomers of PFHxS and PFOS.	212
Table S7. Concentrations (pg L^{-1}) of PFAS at the reference sites	213
Table S8. Concentrations (pg L^{-1}) of PFAS at Foxfonna	214
Table S9. Concentrations (pg L^{-1}) of PFAS at KHO	215
Table S10 Concentrations (pg L^{-1}) of PFAS at UNIS, Longyearbyen	216
Table S11. Fluxes (pg m^{-2}) of PFAS at the reference sites	217
Table S12. Fluxes (pg m^{-2}) of PFAS at Foxfonna	218
Table S13. Fluxes (pg m^{-2}) of PFAS at KHO	219
Table S14. Fluxes (pg m^{-2}) of PFAS at UNIS, Longyearbyen	220
Table S15. Percentage of linear isomers, and concentrations of linear and branched isomers of PFOS	221
Table S16. Percentage of linear isomers, and concentrations of linear and branched isomers of PFHxS	222
Figure S1. HYSPLIT backwards air mass trajectories for Fox01 – Fox10	223

Chemicals and Reagents

Standards of native perfluoroalkyl carboxylic acids (PFCAs; C_4-C_{12}), perfluoroalkyl sulfonic acids (PFSAs; C_3-C_{10} and C_{12} including branched standards) and mass-labelled standards of PFCAs (C_4-C_{12}), PFSAs (C_4, C_6, C_8) were from Wellington laboratories (Guelph, ON, Canada). Perfluoropropanoic acid was from Sigma-Aldrich, (Oakville, ON, Canada). Trifluoromethane sulfonic acid (TFMS) was from Sigma-Aldrich, (Stockholm, Sweden), and potassium salt of perfluoroethane sulfonate was obtained from Kanto Chemical Co., Inc., (Portland, OR, USA). Mass-labelled standard of TFA ($^{13}C_2$-TFA) was purchased from Toronto Research Chemicals Inc, (Toronto, ON, Canada). The purity of all standards was above 97%. Glass microfiber filters (Whatman) and ammonium acetate (≥99.0%) was purchased from Sigma-Aldrich, (Stockholm, Sweden). Glacial acetic acid (EMPROVE® EXPERT, Ph. Eur., JP, USP) was purchased from Merck, (Darmstadt, Germany). Analytical reagent grade ammonia solution, HPLC grade methanol (≥99.8%) and LC-MS grade methanol (≥99.9%) were from Fischer Scientific, (Ottawa, ON, Canada). Weak anion exchange solid-phase extraction (WAX-SPE) cartridges were obtained from Waters Corporation, (Milford, MA, USA).

Instrument Analysis

Both neutral and anionic elutes were evaporated to approximately 0.5 mL at 60 °C and 400 mbar, transferred to an LC vial and then further evaporated to 100 µL under a gentle stream of nitrogen. For quantification of the anionic PFAS, 40 µL of the anionic fraction was transferred to new LC vials and of 10 µL were injected into the ultra-performance liquid chromatography (UPLC) MS/MS system after addition of 60 µL of 2 mM aqueous ammonium acetate. For quantification of neutral PFAS, aliquots of 10 µL of the neutral fraction were injected into the UPLC-MS/MS

system. Mass-labelled internal standards and recovery standards (1 ng) were added to the samples prior to filtration and prior to injection, respectively, to monitor the recovery of the method.

Separation and quantification of the neutral PFAS and the remaining anionic PFAS was performed using ultra performance liquid chromatography (UPLC) MS/MS (Acquity Ultra Performance Liquid Chromatograph and Xevo TQ-S, Waters Corporation, Milford, MA, USA) operated in negative electrospray ionization mode. A UPLC BEH C18 column (2.1 mm i.d., 100 mm length, 1.7 µm particle size) (Waters Corporation, Milford, MA, USA) maintained at 50 °C was used to achieve chromatographic separation. The mobile phase for UPLC-MS/MS analysis consisted of 2 mM NH4Ac in MeOH:Milli-Q (3:7) (A) and 2 mM NH4Ac in MeOH (B) at a flow rate of 0.3 mL/min. The gradient of the mobile phase started with an initial B concentration of 1% for 1 min. This was then increased to 100% over 12 min, held for 1 min, and finally re-conditioned for 3 min. The source parameters were set as following: capillary voltage, 0.7 kV; source temperature, 150 °C; desolvation temperature, 400 °C; cone gas flow, 150 L/h; desolvation gas flow, 800 L/h; collision gas flow, 0.2 mL/min; nebulizer, 6.5 bar. At least two MRM transitions were monitored for each target analyte except MeFOSA and EtFOSA where only one transition was monitored. MRM transitions for all target analytes are provided in Table S2.

Quality Assurance and Quality Control

Linear regression analysis showed good linearity for each analyte ($R^2 > 0.99$) in the range from 2.0 to 100 ng/mL for UPLC and SFC. Instrumental limits of quantification (LOQs) were set as the lowest calibration point with a signal-to-noise ratio of at least ten. For UPLC the repeatability of the instrumental method was evaluated based on repeated injections (n = 8) of a standard with a concentration of 4 ng/mL (or 10 ng/mL for neutral target analytes), the relative standard deviation of repeated injections was in the range 1.0 – 3.7 % for C_5 to C_{11} PFCAs and C_5 – C_{10} PFSAs.

Isotope dilution was used for quantification. For those target analytes that did not have corresponding mass-labelled standards, the homologue closest in retention time was used for quantification (Table S2). Extraction efficiencies of all analytes were assessed based on the peak area of native standards spiked to test samples (n = 3) compared to that of the native standards in solvent after subtraction of the background concentrations in the samples (Table S3). Test samples consisted of 250 mL of melted surface snow from one sample from Foxfonna, spiked with 1000 pg of native standard. The extraction efficiencies for C_5 to C_{11} PFCAs, PFHxS and PFOS were in the range 33 – 69%. The repeatability of the extraction method was evaluated based on the relative standard deviation of spiked test samples (n = 3) at a concentration of 1 ng per 250 mL sample. The relative standard deviation of spiked test samples was in the range 8.7 – 21% for C_5 to C_{11} PFCAs, PFHxS and PFOS. For those analytes with available corresponding mass-labeled internal and recovery standards (C_5 – C_{11} PFCAs, PFHxS and PFOS), their extraction efficiency was also assessed by comparing the peak area of the spiked internal standard and recovery standard across all samples (n = 36). Their extraction efficiencies were in the range 58 – 86% (Table S4), and the relative standard deviation was in the range 10 – 14%. For the 9 neutral analytes, the extraction efficiencies were also assessed by comparing the peak areas of their respective internal and surrogate recovery standards, across all samples (n = 36). Their extraction efficiencies were in the range 3.1 – 42% (Table S5), and the relative standard deviation was in the range 2.0 – 28%. The method limits of quantification (MQLs) were calculated as the average concentration in repeated blank extractions (n = 5) plus three times the standard deviation. For those analytes that were not observed in blank extractions, the instrument LOQ was used as the MQL. Detailed information about the precision of the analytical method, internal and recovery standards, extraction efficiencies and repeatability, and LOQs and MQLs, are provided in Tables S3 – S5.

Prior to sample collection a high-density polyethylene barrel and aluminum shovel were precleaned with soapy water, followed by rising several times with tap water, Milli-Q water rinse five times and then methanol rinse three times. Transport to each sampling site was done by ski or snowmobile. The final approach to the sampling site was done on foot from downwind. Nitrile gloves were worn during snow sampling. The upper 0 – 5 cm of the surface snow was collected into the barrel, which was then sealed and transported back to the University Centre in Svalbard (UNIS), where it was melted in the fridge at 5 °C and bottled into precleaned polypropylene containers. Polypropylene containers were precleaned with soapy water, followed by rinsing several times with tap water, Milli-Q water rinse five times, and then a rinse with acetone followed by methanol. It was then rinsed three times with the melted snow sample from the barrel, prior to filling the container. Subsamples from the barrel were also taken for major ion analysis. The bottled and melted snow samples for PFAS analysis were then stored in the fridge at 2 – 4 °C until they were transported cold to Örebro University, Sweden where they were stored at 8 °C until extraction.

A field blank was included to ensure that no contamination occurred during surface snow sampling. The field blank comprised of Milli-Q water in a sample container that was brought to the field and kept opened for the duration of sampling. The container was then resealed and transported to the laboratory where it was treated in the same way as the samples. None of the target analytes in the field blank were detected >MQL.

HYSPLIT Modelling

To investigate the air mass source region and the solar radiation linked to each precipitation event that was sampled on Foxfonna, this study used the same backward airmass calculations reported in Björnsdotter et al. In summary, a 6 day backward airmass trajectory was calculated for each of

the 10 sampling rounds using the Hybrid Single-Particle Lagrangian Integrated Trajectory (HYSPLIT). This was timed to end at the onset of the precipitation event that was sampled. The solar radiation each precipitation event had been subject to was calculated by summing the downward short-wave radiation (W/m^2) for each hourly point on the trajectory. This yielded a solar radiation value (in kWh/m^2) for each surface snow sample from Foxfonna.

Ion Chromatography for Quantification of Major Ion Concentrations

A 50 mL subsample for major ion analysis was collected from the melted snow sample and stored in a fridge. Cation and anion concentrations were measured using Dionex ICS-4000 Integrion anion and cation systems. A Dionex AS-AP autosampler was used to supply sample to each instrument. Calibration was achieved using a range of calibration standards. All calibration standards were prepared from purchased (1000 ppm) Sigma Aldrich (U.K.) standards by a series of gravimetric dilutions.

The cation instrument used a Dionex Ionpac CG16-4μm (2 x 50 mm) guard column and CS16 (4 μm, 2 x 250 mm) analytical column. Samples were loaded into a 250 μL sample loop. A 32 – 42 mM methane sulfonic acid (MSA) multistep eluent gradient was used for effective separation of the analytes. The eluent was produced using a Dionex eluent generator cartridge (EGC 500 KOH) and was pumped through the columns at a flow rate of 0.20 mL min^{-1} at a pressure of 3300 psi for a 25 min chromatogram. The eluent ions were removed from the column effluent using a cation electrolytically regenerated suppressor (Dionex CERS 500), before conductivity detection of the effluent.

The anion system used a Dionex Ionpac AG17-C (2 μm, 2 x 50 mm) guard column and AS17-C (2 x 250 mm) analytical column. Samples were loaded to a 250 μL sample loop. A 1 – 40 mM potassium hydroxide multistep eluent gradient was used for effective separation of the

analytes. The eluent was produced using a Dionex eluent generator cartridge (EGC 500 KOH) and was pumped through the columns at a flow rate of 0.29 mL min^{-1} at a pressure of 2300 psi for a 20 min chromatogram. The eluent ions were removed from the column effluent using an anion electrolytically regenerated suppressor (Dionex AERS 500), before conductivity detection of the eluate.

Table S1. List of target analytes, abbreviations, and CAS numbers

Abbreviation	Target analyte	CAS
TFA	Trifluoroacetic acid	76-05-1
PFPrA	Perfluoropropanoic acid	422-64-0
PFBA	Perfluorobutanoic acid	375-22-4
PFPeA	Perfluoropentanoic acid	2706-90-3
PFHxA	Perfluorohexanoic acid	307-24-4
PFHpA	Perfluoroheptanoic acid	375-85-9
PFOA	Perfluorooctanoic acid	335-67-1
PFNA	Perfluorononanoic acid	375-95-1
PFDA	Perfluorodecanoic acid	335-76-2
PFUnDA	Perfluoroundecanoic acid	2058-94-8
PFDoDA	Perfluorododecanoic acid	307-55-1
PFTrDA	Perfluorotridecanoic acid	72629-94-8
PFTeDA	Perfluorotetradecanoic acid	376-06-7
PFHxDA	Perfluorohexadecanoic acid	67905-19-5
PFOcDA	Perfluorooctadecanoic acid	16517-11-6
TFMS	Trifluoromethane sulfonic acid	1493-13-6
PFEtS	Perfluoroethane sulfonic acid	354-88-1
PFPrS	Perfluoropropane sulfonic acid	423-41-6
PFBS	Perfluorobutane sulfonic acid	375-73-5
PFPeS	Perfluoropentane sulfonic acid	2706-91-4
PFHxS	Perfluorohexane sulfonic acid	355-46-4
PFHpS	Perfluoroheptane sulfonic acid	375-92-8
PFOS	Perfluorooctane sulfonic acid	1763-23-1
PFNS	Perfluorononane sulfonic acid	68259-12-1
PFDS	Perfluorodecane sulfonic acid	335-77-3
PFDoDS	Perfluorododecane sulfonic acid	79780-39-5
4:2 FTSA	4:2 Fluorotelomer sulfonic acid	757124-72-4
6:2 FTSA	6:2 Fluorotelomer sulfonic acid	27619-97-2
8:2 FTSA	8:2 Fluorotelomer sulfonic acid	39108-34-4
6:2 FTUCA	6:2 Fluorotelomer unsaturated carboxylic acid	70887-88-6
8:2 FTUCA	8:2 Fluorotelomer unsaturated carboxylic acid	70887-84-2
PFECHS	Perfluoroethylcyclohexane sulfonic acid	72441-89-5
6:2 Cl-PFESA	6:2 Chlorinated polyfluorinated ether sulfonate	756426-58-1
8:2 Cl-PFESA	8:2 Chlorinated polyfluorinated ether sulfonate	763051-92-9
HFPO-DA	Hexafluoropropylene oxide dimer acid	13252-13-6
ADONA	3H-perfluoro-3-[(3-methoxy-propoxy)propanoic acid]	919005-14-4
FBSA	Perfluorobutane sulfonamide	30334-69-1
MeFBSA	Methyl perfluorobutane sulfonamide	68298-12-4
FHxSA	Perfluorohexane sulfonamide	41997-13-1
MeFHxSA	Methyl perfluorohexane sulfonamide	68259-15-4
FOSA	Perfluorooctane sulfonamide	754-91-6
MeFOSA	N-Methyl perfluorooctane sulfonamide	31506-32-8
EtFOSA	N-Ethyl perfluorooctane sulfonamide	4151-50-2
MeFOSE	N-Methyl perfluorooctane sulfonamidoethanol	24448-09-7
EtFOSE	N-Ethyl perfluorooctane sulfonamidoethanol	1691-99-2

Table S2. MRM transitions and internal standards used for quantification.

Abbreviation	1st MRM transition	2nd MRM transition	Internal standard	Recovery Standard
TFA	112.90 > 68.96	-	^{13}C-M2TFA	
PFPrA	162.97 > 118.90	-	^{13}C-M4PFBA	
PFBA	212.97 > 169.00	-	^{13}C-M4PFBA	^{13}C-M3PFBA
PFPeA	262.97 > 219.00	-	^{13}C-M3PFPeA	^{13}C-M5PFPeA
PFHxA	312.97 > 269.00	312.97 > 118.95	^{13}C-M2PFHxA	^{13}C-M5PFHxA
PFHpA	362.97 > 319.00	362.97 > 168.97	^{13}C-M4PFHpA	^{13}C-M8PFOA
PFOA	412.97 > 369.00	412.97 > 168.97	^{13}C-M4PFOA	^{13}C-M8PFOA
PFNA	462.99 > 419.00	462.99 > 219.00	^{13}C-M5PFNA	^{13}C-M9PFNA
PFDA	512.97 > 469.00	512.97 > 219.00	^{13}C-M2PFDA	^{13}C-M6PFDA
PFUnDA	562.97 > 268.99	562.97 > 519.00	^{13}C-M2PFUnDA	^{13}C-M7PFUnDA
PFDoDA	612.97 > 569.00	612.97 > 168.96	^{13}C-M2PFDoDA	
PFTrDA	662.90 > 619.00	662.90 > 168.96	^{13}C-M2PFDoDA	
PFTeDA	712.90 > 669.00	712.90 > 168.97	^{13}C-M2PFTeDA	
PFHxDA	812.90 > 769.00	812.90 > 168.96	^{13}C-M2PFHxDA	
PFOcDA	912.90 > 869.00	912.90 > 168.96	^{13}C-M2PFHxDA	
TFMS	149.12 > 79.91	149.12 > 98.95	^{13}C-M3PFBS	
PFEtS	198.80 > 79.80	198.80 > 98.90	^{13}C-M3PFBS	
PFPrS	248.90 > 79.90	248.90 > 98.90	^{13}C-M3PFBS	
PFBS	298.90 > 79.96	298.90 > 98.90	^{13}C-M3PFBS	
PFPeS	348.90 > 79.96	348.90 > 98.96	^{18}O-M2PFHxS	
		398.90 > 98.90		
PFHxS	398.90 > 79.96	398.90 > 119.01	^{18}O-M2PFHxS	^{13}C-M3PFHxS
		398.90 > 319.00		
PFHpS	448.97 > 79.96	448.97 > 98.90	^{13}C-M4PFOS	
		498.97 > 98.96		
PFOS	498.97 > 79.96	498.97 > 169.03	^{13}C-M4PFOS	^{13}C-M8PFOS
		498.97 > 419.00		
PFNS	548.90 > 79.96	548.90 > 98.96	^{13}C-M4PFOS	
PFDS	598.97 > 79.96	598.97 > 98.90	^{13}C-M4PFOS	
PFDoDS	698.90 > 79.96	698.90 > 98.90	^{13}C-M4PFOS	
4:2 FTSA	327.00 > 307.00	329.00 > 81.00	^{13}C-M2-6:2 FTSA	
6:2 FTSA	427.00 > 407.00	427.00 > 81.00	^{13}C-M2-6:2 FTSA	
8:2 FTSA	527.00 > 507.00	527.00 > 80.00	^{13}C-M2-8:2 FTSA	
6:2 FTUCA	356.90 > 292.91	356.9 > 242.95	^{13}C-M2-6:2 FTUCA	
8:2 FTUCA	456.90 > 392.94	456.90 > 342.88	^{13}C-M2-8:2 FTUCA	
PFECHS	460.84 > 380.942	460.84 > 98.882	^{13}C-M4PFOA	
6:2 Cl-PFESA	530.904 > 350.98	530.904 > 98.95	^{13}C-M4PFOS	
8:2 Cl-PFESA	630.904 > 450.98	630.904 > 98.95	^{13}C-M4PFOS	
HFPO-DA	284.90 > 168.70	284.9 > 184.80	^{13}C-M3HFPO-DA	
ADONA	376.97 > 250.83	376.97 > 84.69	^{13}C-M3HFPO-DA	
FBSA	297.90 > 77.92	297.90 > 118.94	^{13}C-M8FOSA	
MeFBSA	311.97 > 218.95	311.97 > 111.93	^{13}C-M8FOSA	
FHxSA	397.9 > 77.92	397.90 > 168.94	^{13}C-M8FOSA	
MeFHxSA	411.97 > 168.93	411.97 > 318.96	^{13}C-M8FOSA	
FOSA	497.90 > 78.00	497.90 > 168.90	^{13}C-M8FOSA	
Me-FOSA	512.00 > 169.00		^{13}C-d3-N-MeFOSA	
EtFOSA	526.00 > 169.00		^{13}C-d5-N-EtFOSA	
MeFOSE	616.00 > 59.00	556.03 > 121.99	^{13}C-d7-N-MeFOSE	
EtFOSE	630.00 > 59.00	570.096 > 135.983	^{13}C-d9-N-EtFOSE	

Table S3. Instrument limits of quantification (LOQ) (pg L^{-1}) and method limits of quantification (MQL) (pg L^{-1}). Extraction efficiencies (%) and repeatability (%) is based spiked test samples (*n* = 3). Repeatability (%) of the instrument method was based on repeated standard injections (*n* = 8)

Analyte	LOQ (pg/L)	MQL (pg/L)	Extraction efficiency (%)	Extraction method repeatability (%)	Instrument method repeatability (%)
TFA[a]	9.1	9.1	121 ± 5	2.7	4.1
PFPrA[a]	9.1	9.1	67 ± 8	11	2.4
PFBA[a]	9.1	58.2	71 ± 6	14	3.0
PFPeA	2.3	5.9	69 ± 15	4.3	1.2
PFHxA	2.3	5.2	65 ± 10	4.9	1.2
PFHpA	2.3	4.3	63 ± 14	8.9	2.0
PFOA	2.3	65.2	57 ± 21	15	1.0
PFNA	2.3	4.1	46 ± 14	27	1.4
PFDA	2.3	15.5	40 ± 8.7	26	2.5
PFUnDA	2.3	6.9	33 ± 11	27	3.7
PFDoDA	2.3	2.6	28 ± 14	49	1.9
PFTrDA	2.3	1.7	31 ± 18	44	3.7
PFTeDA	2.3	2.3	46 ± 29	49	4.7
PFHxDA	2.3	7.9	53 ± 23	50	3.7
PFOcDA	2.3	3.1	85 ± 88	110	25
TFMS[a]	9.1	9.1	80 ± 16	15	2.8
PFEtS[a]	9.1	45	81 ± 9	2.2	0.33
PFPrS[a]	9.1	9.1	83 ± 8	6.0	2.4
PFBS[a]	2.3	12.9	80 ± 12	3.3	1.7
PFPeS	2.3	2.3	69 ± 10	9.2	1.6
PFHxS	2.3	2.7	58 ± 11	17	1.2
PFHpS	9.1	9.1	48 ± 11	21	2.7
PFOS	2.3	7.9	42 ± 9.1	15	2.1
PFNS	9.1	9.1	30 ± 5.8	18	2.8
PFDS	2.3	2.3	24 ± 10	39	1.5
PFDoDS	2.3	2.3	27 ± 16	38	2.1
4:2 FTSA	2.3	2.3	160 ± 42	13	3.1
6:2 FTSA	2.3	8.4	180 ± 89	50	5.0
8:2 FTSA	2.3	2.3	78 ± 14	29	5.0
6:2 FTUCA	2.3	2.3	10 ± 4.0	42	1.8
8:2 FTUCA	2.3	2.3	2.1 ± 1.2	60	2.3
PFECHS	2.3	2.3	49 ± 11	21	1.4
6:2 Cl-PFESA	2.3	2.3	37 ± 8.6	28	1.6
8:2 Cl-PFESA	2.3	2.3	26 ± 12	46	1.6
HFPO-DA	2.3	2.3	50 ± 10	11	2.5
ADONA	2.3	2.3	53 ± 7.2	13	1.5
FBSA	2.3	2.3	38 ± 20	40	6.8
MeFBSA	9.1	9.1	12 ± 8.6	73	12
FHxSA	2.3	2.3	29 ± 13	44	8.6
MeFHxSA	9.1	9.1	4.9 ± 4.5	91	7.7
FOSA	2.3	3.6	23 ± 7.8	31	7.9
MeFOSA	22.7	22.7	6.6 ± 6.0	91	12
EtFOSA	22.7	22.7	6.4 ± 5.1	69	13
MeFOSE	2.3	16.7	13 ± 2.6	35	12
EtFOSE	2.3	11.9	14 ± 4.0	40	12

[a]Previously reported in Chapter 5

Table S4. The extraction efficiency for those compounds with available equivalent mass-labelled internal and recovery standards, expressed as the average extraction efficiency ± standard deviation of spiked internal standards (n = 36)

Analyte	Internal standard	Recovery standard	Extraction efficiency (%)
PFBA	^{13}C-M4PFBA	^{13}C-M3PFBA	69 ± 12
PFPeA	^{13}C-M3PFPeA	^{13}C-M5PFPeA	70 ± 11
PFHxA	^{13}C-M2PFHxA	^{13}C-M5PFHxA	72 ± 12
PFHpA	^{13}C-M4PFHpA	^{13}C-M8PFOA	70 ± 13
PFOA	^{13}C-M4PFOA	^{13}C-M8PFOA	71 ± 11
PFNA	^{13}C-M5PFNA	^{13}C-M9PFNA	65 ± 12
PFDA	^{13}C-M2PFDA	^{13}C-M6PFDA	58 ± 13
PFUnDA	^{13}C-M2PFUnDA	^{13}C-M7PFUnDA	54 ± 14
PFHxS	^{18}O-M2PFHxS	^{13}C-M3PFHxS	86 ± 10
PFOS	^{13}C-M4PFOS	^{13}C-M8PFOS	65 ± 11

Table S5. The extraction efficiency for the nine neutral compounds, expressed as the average extraction efficiency ± standard deviation of spiked internal standards (n = 36)

Analyte	Internal standard	Recovery standard	Extraction efficiency (%)
FOSA	^{13}C-M8FOSA[a]	^{13}C-M8PFOS	42 ± 28
MeFOSA	^{13}C-d3-N-MeFOSA	^{13}C-M8PFOS	4.3 ± 2.6
EtFOSA	^{13}C-d5-N-EtFOSA	^{13}C-M8PFOS	3.1 ± 2.0
MeFOSE	^{13}C-d7-N-MeFOSE	^{13}C-M8PFOS	27 ± 19
EtFOSE	^{13}C-d9-N-EtFOSE	^{13}C-M8PFOS	16 ± 12

[a] ^{13}C-M8FOSA is also the internal standard for FBSA, MeFBSA, FHxSA and MeFHxSA

Table S6. MRM transitions, instrument limits of quantification (LOQ) (pg L^{-1}), and method limits of quantification (MQL) (pg L^{-1}) for branched isomers of PFHxS and PFOS.

Abbreviation	1st MRM transition	2nd MRM transition	LOQ (pg L^{-1})	MQL (pg L^{-1})
2/3/4-PFHxS	398.9 > 79.96	398.9 > 98.96	2.3	2.3
1-PFHxS	398.9 > 319.00	398.9 > 98.96	2.3	2.3
3/4/5-PFOS	498.97 > 79.96	498.97 > 98.96	2.3	2.3
6/2-PFOS	498.97 > 169.03	498.97 > 79.96	2.3	2.3
1-PFOS	498.97 > 419.00	498.97 > 169.03	2.3	2.3

Table S7. Concentrations (pg L^{-1}) of PFAS at the reference sites from February – April 2019

	Drønbreen	Lomonosovfonna01	Lomonosovfonna02	Grønfjordbreen	Nordmannsfonna
FBSA	5.58	3.59	<MQL	10	8.15
MeFBSA	11	52.1	31.6	<MQL	18.3
FHxSA	27.5	18.5	9.43	26.7	33.1
MeFHxSA	<MQL	<MQL	<MQL	<MQL	<MQL
FOSA	4.52	4.44	<MQL	5.38	4.96
MeFOSA	<MQL	<MQL	<MQL	24.9	<MQL
EtFOSA	<MQL	<MQL	<MQL	<MQL	<MQL
MeFOSE	18.9	<MQL	17.1	<MQL	20.4
EtFOSE	<MQL	<MQL	<MQL	<MQL	<MQL
PFPeA	61.5	27.7	57.3	104	162
PFHxA	55.5	45.5	59.6	143	124
PFHpA	89.9	34.9	115	165	477
PFOA	260	305	243	581	370
PFNA	35.3	22.1	71.7	334	166
PFDA	<MQL	<MQL	<MQL	63.4	26.3
PFUnDA	7.54	6.94	18.0	53.2	35.7
PFDoDA	4.13	3.26	<MQL	13.4	8.65
PFTrDA	3.11	<MQL	3.07	19.6	8.28
PFTDA	<MQL	2.83	2.28	3.96	3.28
PFHxDA	<MQL	<MQL	<MQL	<MQL	<MQL
PFOcDA	<MQL	<MQL	<MQL	<MQL	<MQL
PFPeS	<MQL	<MQL	<MQL	<MQL	<MQL
PFHxS	11.5	7.7	7.39	53.7	10.6
PFHpS	<MQL	<MQL	<MQL	13.3	<MQL
PFOS	287	128	251	339	136
PFNS	<MQL	<MQL	<MQL	<MQL	<MQL
PFDS	<MQL	<MQL	<MQL	<MQL	<MQL
PFDoDS	<MQL	<MQL	<MQL	<MQL	<MQL
4:2 FTSA	<MQL	<MQL	<MQL	<MQL	<MQL
6:2 FTSA	19.9	13.3	13.5	15.8	16.9
8:2 FTSA	<MQL	<MQL	<MQL	<MQL	<MQL
6:2 FTUCA	66.8	22.8	76.9	38.9	40
8:2 FTUCA	31.7	<MQL	54.1	<MQL	<MQL
PFECHS	<MQL	<MQL	<MQL	22.6	<MQL
6:2 Cl-PFESA	<MQL	<MQL	<MQL	<MQL	<MQL
8:2 Cl-PFESA	<MQL	<MQL	<MQL	<MQL	<MQL
HFPO-DA	<MQL	3.26	5.72	17.8	7.74
ADONA	<MQL	<MQL	<MQL	<MQL	<MQL

Table S8. Concentrations (pg L^{-1}) of PFAS at Foxfonna from January – August 2019

	Fox01	**Fox02**	**Fox03**	**Fox04**	**Fox05**	**Fox06**	**Fox07**	**Fox08**	**Fox09**	**Fox10**
FBSA	2.63	<MQL	<MQL	2.52	6.4	183	99.9	192	76.3	57.6
MeFBSA	<MQL	<MQL	<MQL	<MQL	13.3	51.3	31.8	<MQL	43.0	19.4
FHxSA	16.5	21.2	12.8	5.65	6.05	9.02	29.5	13.5	19.3	41.3
MeFHxSA	<MQL	<MQL	<MQL	<MQL	<MQL	<MQL	<MQL	<MQL	<MQL	<MQL
FOSA	14.6	12.4	<MQL	20.6	4.6	4.01	5.4	15.3	46.2	13.2
MeFOSA	<MQL	<MQL	<MQL	<MQL	<MQL	<MQL	<MQL	<MQL	<MQL	<MQL
EtFOSA	<MQL	128	<MQL	<MQL	<MQL	<MQL	<MQL	<MQL	<MQL	<MQL
MeFOSE	<MQL	103	<MQL	<MQL	21.8	16.9	24.3	<MQL	<MQL	<MQL
EtFOSE	13.4	247	<MQL	17.7	13.0	<MQL	<MQL	<MQL	<MQL	<MQL
PFPeA	6.04	45.0	35.2	22.9	55.7	54.1	231	453	290	49.9
PFHxA	23.6	58.1	50.6	35.3	80.0	67.5	326	540	265	69.6
PFHpA	9.63	72.3	31.3	33.5	64.8	88.9	1350	1790	974	787
PFOA	336	494	422	334	241	248	640	563	704	327
PFNA	<MQL	41.8	28.7	23	40.9	38.4	449	836	449	128
PFDA	<MQL	19.7	<MQL	<MQL	16.7	16.9	72.0	80.3	56.5	17.8
PFUnDA	<MQL	8.01	<MQL	<MQL	17.7	18.2	75.0	109	72.1	19.3
PFDoDA	3.15	<MQL	2.63	<MQL	<MQL	6.47	16	14.4	<MQL	<MQL
PFTrDA	<MQL	1.95	1.96	1.85	5.17	9.36	19.1	12.7	10.1	2.85
PFTDA	<MQL	<MQL	<MQL	<MQL	<MQL	2.8	5.64	5.24	2.28	<MQL
PFHxDA	<MQL	<MQL	<MQL	<MQL	<MQL	<MQL	<MQL	<MQL	<MQL	<MQL
PFOcDA	<MQL	<MQL	<MQL	<MQL	<MQL	<MQL	<MQL	<MQL	<MQL	<MQL
PFPeS	<MQL	<MQL	<MQL	<MQL	<MQL	<MQL	<MQL	<MQL	<MQL	<MQL
PFHxS	4.47	14.4	19.1	10.2	7.01	5.26	23.1	7.42	10.8	8.39
PFHpS	<MQL	<MQL	<MQL	<MQL	<MQL	<MQL	<MQL	<MQL	<MQL	<MQL
PFOS	61.9	113	214	88.7	159	107	331	177	258	137
PFNS	<MQL	<MQL	<MQL	<MQL	<MQL	<MQL	<MQL	<MQL	<MQL	<MQL
PFDS	<MQL	<MQL	<MQL	<MQL	<MQL	<MQL	<MQL	<MQL	<MQL	<MQL
PFDoDS	<MQL	<MQL	<MQL	<MQL	<MQL	<MQL	<MQL	<MQL	<MQL	<MQL
4:2 FTSA	<MQL	<MQL	<MQL	<MQL	<MQL	<MQL	<MQL	<MQL	<MQL	<MQL
6:2 FTSA	11.2	13.9	13.5	13.1	15.4	15	40.8	24.1	28.3	17.3
8:2 FTSA	<MQL	<MQL	<MQL	<MQL	<MQL	<MQL	<MQL	2.66	<MQL	<MQL
6:2 FTUCA	6.44	17.8	37.8	64.4	13.8	47.3	<MQL	31.4	<MQL	51.6
8:2 FTUCA	<MQL	<MQL	<MQL	<MQL	<MQL	<MQL	<MQL	<MQL	<MQL	<MQL
PFECHS	<MQL	<MQL	<MQL	<MQL	<MQL	<MQL	<MQL	<MQL	<MQL	<MQL
6:2 Cl-PFESA	<MQL	<MQL	<MQL	<MQL	<MQL	<MQL	<MQL	<MQL	<MQL	<MQL
8:2 Cl-PFESA	<MQL	<MQL	<MQL	<MQL	<MQL	<MQL	<MQL	<MQL	<MQL	<MQL
HFPO-DA	<MQL	5.04	6.72	3.75	16.2	25.9	24.4	60.5	22.4	9.23
ADONA	<MQL	<MQL	<MQL	<MQL	<MQL	<MQL	3.19	<MQL	<MQL	<MQL

Table S9. Concentrations (pg L^{-1}) of PFAS at KHO from January – June 2019

	KHO01	KHO02	KHO03	KHO04	KHO05	KHO06	KHO07	KHO08	KHO09
FBSA	3.91	4.71	<MQL	3.06	2.74	134	26.9	52.2	25.3
MeFBSA	10.0	18.5	<MQL	<MQL	<MQL	<MQL	<MQL	<MQL	<MQL
FHxSA	24.7	40.1	12.9	6.47	3.89	10.7	13.6	10.3	9.27
MeFHxSA	<MQL	<MQL	<MQL	<MQL	<MQL	<MQL	<MQL	<MQL	<MQL
FOSA	43.7	11.4	4.25	<MQL	3.71	3.94	10.8	6.01	8.00
MeFOSA	<MQL	<MQL	<MQL	<MQL	<MQL	<MQL	<MQL	<MQL	<MQL
EtFOSA	28.8	<MQL	<MQL	<MQL	<MQL	<MQL	<MQL	<MQL	<MQL
MeFOSE	53.5	<MQL	<MQL	<MQL	<MQL	<MQL	22.3	<MQL	27.1
EtFOSE	178	<MQL	<MQL	<MQL	<MQL	12.3	16.2	<MQL	14.8
PFPeA	45.7	57.9	20.9	13.0	38.5	31.6	169	141	233
PFHxA	45.8	36.5	32.6	34.1	30.5	39.4	90.8	224	234
PFHpA	75.3	119	99.6	19.9	91.3	32.5	706	1080	902
PFOA	1330	533	114	487	325	323	444	509	514
PFNA	42.4	114	35.1	18.8	42.8	13.4	173	176	364
PFDA	18.2	<MQL	<MQL	<MQL	<MQL	<MQL	30.4	48.1	46.5
PFUnDA	8.13	10.4	12.3	<MQL	7.91	<MQL	26.4	36.7	58.4
PFDoDA	4.04	2.82	3.58	2.75	<MQL	<MQL	5.83	13.4	11.0
PFTrDA	2.8	2.68	5.09	<MQL	2.43	2.19	5.5	16.7	16.1
PFTDA	<MQL	2.42	<MQL	<MQL	<MQL	<MQL	3.23	5.66	5.12
PFHxDA	<MQL	<MQL	<MQL	<MQL	<MQL	<MQL	<MQL	<MQL	<MQL
PFOcDA	<MQL	<MQL	<MQL	<MQL	<MQL	<MQL	<MQL	<MQL	<MQL
PFPeS	<MQL	3.96	<MQL	<MQL	<MQL	<MQL	<MQL	<MQL	<MQL
PFHxS	16.1	43.2	6.9	13.8	9.9	6.65	7.26	8.78	7.52
PFHpS	<MQL	<MQL	<MQL	<MQL	<MQL	<MQL	<MQL	<MQL	<MQL
PFOS	172	312	64.2	142	60.9	71.6	55.8	95.4	79.5
PFNS	<MQL	<MQL	<MQL	<MQL	<MQL	<MQL	<MQL	<MQL	<MQL
PFDS	<MQL	<MQL	<MQL	<MQL	<MQL	<MQL	<MQL	<MQL	<MQL
PFDoDS	<MQL	<MQL	<MQL	<MQL	<MQL	<MQL	<MQL	<MQL	<MQL
4:2 FTSA	<MQL	<MQL	<MQL	<MQL	<MQL	<MQL	<MQL	<MQL	<MQL
6:2 FTSA	10.8	14.4	9.38	12.5	12.1	11.5	13.8	16.1	15.8
8:2 FTSA	<MQL	<MQL	<MQL	<MQL	<MQL	<MQL	<MQL	<MQL	<MQL
6:2 FTUCA	<MQL	8.75	<MQL	6.87	19.2	8.14	2.70	38.6	5.51
8:2 FTUCA	<MQL	<MQL	<MQL	<MQL	<MQL	<MQL	3.32	<MQL	17.7
PFECHS	<MQL	10.7	<MQL	<MQL	<MQL	<MQL	<MQL	<MQL	<MQL
6:2 Cl-PFESA	<MQL	<MQL	<MQL	<MQL	<MQL	<MQL	<MQL	<MQL	<MQL
8:2 Cl-PFESA	<MQL	<MQL	<MQL	<MQL	<MQL	<MQL	<MQL	<MQL	<MQL
HFPO-DA	<MQL	14.0	<MQL	7.14	3.89	7.44	22.5	19.7	25.5
ADONA	<MQL	<MQL	<MQL	<MQL	<MQL	<MQL	<MQL	<MQL	4.05

Table S10. Concentrations (pg L^{-1}) of PFAS at UNIS, Longyearbyen from January – May 2019

	UNIS01	UNIS02	UNIS03	UNIS04	UNIS05	UNIS06	UNIS07	UNIS08
FBSA	1350	116	22.2	38.7	30.5	1120	714	381
MeFBSA	92.9	73.8	74.2	18.2	29.3	21.6	46.1	48.2
FHxSA	125	83.9	40.4	16.7	14.3	132	117	184
MeFHxSA	<MQL	<MQL	<MQL	<MQL	<MQL	<MQL	<MQL	<MQL
FOSA	31.5	14.2	16.4	8.16	11.9	17.8	156	23.3
MeFOSA	<MQL	<MQL	<MQL	<MQL	<MQL	<MQL	<MQL	<MQL
EtFOSA	<MQL	<MQL	<MQL	<MQL	<MQL	<MQL	<MQL	<MQL
MeFOSE	<MQL	<MQL	<MQL	26.2	35.9	<MQL	<MQL	68.2
EtFOSE	<MQL	<MQL	501	131	132	58.8	431	<MQL
PFPeA	253	183	75.1	196	105	749	787	932
PFHxA	319	229	123	130	138	523	1210	1690
PFHpA	384	401	106	338	211	1370	2020	917
PFOA	1180	1390	1850	2120	2400	2860	4120	4900
PFNA	274	402	100	196	111	470	1390	667
PFDA	244	359	55.8	37.2	39.4	366	904	720
PFUnDA	93.6	147	32.6	27.0	24.4	190	799	325
PFDoDA	48.4	81.5	16.3	<MQL	<MQL	124	1320	417
PFTrDA	24.5	50.3	7.25	5.86	3.26	62.2	567	206
PFTDA	20.8	23.8	8.67	9.19	6.17	51.6	1580	380
PFHxDA	12.5	8.75	<MQL	13.0	9.18	24.4	771	272
PFOcDA	11.0	<MQL	<MQL	28.4	<MQL	<MQL	280	142
PFPeS	<MQL	<MQL	9.28	<MQL	<MQL	<MQL	<MQL	<MQL
PFHxS	52.2	74.7	52.7	24.5	20.3	16.5	23.7	81.9
PFHpS	<MQL	13.8	<MQL	23.1	<MQL	<MQL	<MQL	20.5
PFOS	405	463	411	541	228	324	497	1460
PFNS	<MQL	<MQL	<MQL	<MQL	<MQL	<MQL	<MQL	<MQL
PFDS	<MQL	<MQL	<MQL	<MQL	<MQL	<MQL	<MQL	<MQL
PFDoDS	<MQL	<MQL	<MQL	<MQL	<MQL	<MQL	<MQL	<MQL
4:2 FTSA	<MQL	<MQL	<MQL	<MQL	<MQL	<MQL	<MQL	<MQL
6:2 FTSA	20.4	17.5	28.6	26.2	25.2	40.2	117	149
8:2 FTSA	<MQL	<MQL	<MQL	<MQL	11.6	<MQL	<MQL	21.8
6:2 FTUCA	<MQL	<MQL	133	45.9	83.8	<MQL	<MQL	<MQL
8:2 FTUCA	<MQL	<MQL	<MQL	16.2	55.9	<MQL	<MQL	<MQL
PFECHS	15.3	25.6	5.26	6.43	2.92	<MQL	8.39	<MQL
6:2 Cl-PFESA	<MQL	<MQL	<MQL	<MQL	<MQL	<MQL	<MQL	<MQL
8:2 Cl-PFESA	<MQL	<MQL	<MQL	<MQL	<MQL	<MQL	<MQL	<MQL
HFPO-DA	16.0	26.9	22.8	24.6	<MQL	68.7	60.9	<MQL
ADONA	<MQL	<MQL	<MQL	<MQL	<MQL	<MQL	<MQL	<MQL

Table S11. Fluxes (pg m^{-2}) of PFAS at the reference sites from February – April 2019

	Drønbreen	**Lomonosovfonna01**	**Lomonosovfonna02**	**Grønfjordbreen**	**Nordmannsfonna**
FBSA	26	30	<MQL	74	26
MeFBSA	51	430	330	<MQL	57
FHxSA	130	150	99	200	100
MeFHxSA	<MQL	<MQL	<MQL	<MQL	<MQL
FOSA	21	37	<MQL	40	16
MeFOSA	<MQL	<MQL	<MQL	180	<MQL
EtFOSA	<MQL	<MQL	<MQL	<MQL	<MQL
MeFOSE	88	<MQL	180	<MQL	64
EtFOSE	<MQL	<MQL	<MQL	<MQL	<MQL
PFPeA	290	230	600	760	510
PFHxA	260	380	630	1100	390
PFHpA	420	290	1200	1200	1500
PFOA	1200	2500	2500	4300	1200
PFNA	160	180	750	2500	520
PFDA	<MQL	<MQL	<MQL	470	82
PFUnDA	35	58	190	390	110
PFDoDA	19	27	<MQL	98	27
PFTrDA	15	<MQL	32	140	26
PFTDA	<MQL	24	24	29	10
PFHxDA	<MQL	<MQL	<MQL	<MQL	<MQL
PFOcDA	<MQL	<MQL	<MQL	<MQL	<MQL
PFPeS	<MQL	<MQL	<MQL	<MQL	<MQL
PFHxS	54	64	77	390	33
PFHpS	<MQL	<MQL	<MQL	98	<MQL
PFOS	1300	1100	2600	2500	430
PFNS	<MQL	<MQL	<MQL	<MQL	<MQL
PFDS	<MQL	<MQL	<MQL	<MQL	<MQL
PFDoDS	<MQL	<MQL	<MQL	<MQL	<MQL
4:2 FTSA	<MQL	<MQL	<MQL	<MQL	<MQL
6:2 FTSA	93	110	140	120	53
8:2 FTSA	<MQL	<MQL	<MQL	<MQL	<MQL
6:2 FTUCA	310	190	810	290	130
8:2 FTUCA	150	<MQL	570	<MQL	<MQL
PFECHS	<MQL	<MQL	<MQL	170	<MQL
6:2 Cl-PFESA	<MQL	<MQL	<MQL	<MQL	<MQL
8:2 Cl-PFESA	<MQL	<MQL	<MQL	<MQL	<MQL
HFPO-DA	<MQL	27	60	130	24
ADONA	<MQL	<MQL	<MQL	<MQL	<MQL

Table S12. Fluxes (pg m^{-2}) of PFAS at Foxfonna from January – August 2019

	Fox01	**Fox02**	**Fox03**	**Fox04**	**Fox05**	**Fox06**	**Fox07**	**Fox08**	**Fox09**	**Fox10**
FBSA	7.6	<MQL	<MQL	22	26	1100	580	1900	390	180
MeFBSA	<MQL	<MQL	<MQL	<MQL	53	320	190	<MQL	220	62
FHxSA	48	38	35	50	24	56	170	140	98	130
MeFHxSA	<MQL	<MQL	<MQL	<MQL	<MQL	<MQL	<MQL	<MQL	<MQL	<MQL
FOSA	42	22	<MQL	180	18	25	31	160	230	42
MeFOSA	<MQL	<MQL	<MQL	<MQL	<MQL	<MQL	<MQL	<MQL	<MQL	<MQL
EtFOSA	<MQL	230	<MQL	<MQL	<MQL	<MQL	<MQL	<MQL	<MQL	<MQL
MeFOSE	<MQL	190	<MQL	<MQL	87	100	140	<MQL	<MQL	<MQL
EtFOSE	39	440	<MQL	160	52	<MQL	<MQL	<MQL	<MQL	<MQL
PFPeA	18	81	95	200	220	340	1300	4600	1500	160
PFHxA	69	100	140	310	320	420	1900	5500	1300	220
PFHpA	28	130	84	300	260	550	7800	18000	4900	2500
PFOA	980	890	1100	3000	960	1500	3700	5700	3600	1000
PFNA	<MQL	75	78	200	160	240	2600	8500	2300	410
PFDA	<MQL	35	<MQL	<MQL	67	100	420	820	290	57
PFUnDA	<MQL	14	<MQL	<MQL	71	110	440	1100	370	62
PFDoDA	9.2	<MQL	7.1	<MQL	<MQL	40	93	150	<MQL	<MQL
PFTrDA	<MQL	3.5	5.3	16	21	58	110	130	51	9.2
PFTDA	<MQL	<MQL	<MQL	<MQL	<MQL	17	33	53	12	<MQL
PFHxDA	<MQL	<MQL	<MQL	<MQL	<MQL	<MQL	<MQL	<MQL	<MQL	<MQL
PFOcDA	<MQL	<MQL	<MQL	<MQL	<MQL	<MQL	<MQL	<MQL	<MQL	<MQL
PFPeS	<MQL	<MQL	<MQL	<MQL	<MQL	<MQL	<MQL	<MQL	<MQL	<MQL
PFHxS	13	26	52	90	28	33	130	75	55	27
PFHpS	<MQL	<MQL	<MQL	<MQL	<MQL	<MQL	<MQL	<MQL	<MQL	<MQL
PFOS	180	200	580	780	640	660	1900	1800	1300	440
PFNS	<MQL	<MQL	<MQL	<MQL	<MQL	<MQL	<MQL	<MQL	<MQL	<MQL
PFDS	<MQL	<MQL	<MQL	<MQL	<MQL	<MQL	<MQL	<MQL	<MQL	<MQL
PFDoDS	<MQL	<MQL	<MQL	<MQL	<MQL	<MQL	<MQL	<MQL	<MQL	<MQL
4:2 FTSA	<MQL	<MQL	<MQL	<MQL	<MQL	<MQL	<MQL	<MQL	<MQL	<MQL
6:2 FTSA	32	25	36	120	62	93	240	250	140	55
8:2 FTSA	<MQL	<MQL	<MQL	<MQL	<MQL	<MQL	<MQL	27	<MQL	<MQL
6:2 FTUCA	19	32	100	570	55	290	<MQL	320	<MQL	170
8:2 FTUCA	<MQL	<MQL	<MQL	<MQL	<MQL	<MQL	<MQL	<MQL	<MQL	<MQL
PFECHS	<MQL	<MQL	<MQL	<MQL	<MQL	<MQL	<MQL	<MQL	<MQL	<MQL
6:2 Cl-PFESA	<MQL	<MQL	<MQL	<MQL	<MQL	<MQL	<MQL	<MQL	<MQL	<MQL
8:2 Cl-PFESA	<MQL	<MQL	<MQL	<MQL	<MQL	<MQL	<MQL	<MQL	<MQL	<MQL
HFPO-DA	<MQL	9.1	18	33	65	160	140	610	110	30
ADONA	<MQL	<MQL	<MQL	<MQL	<MQL	<MQL	19	<MQL	<MQL	<MQL

Table S13. Fluxes (pg m^{-2}) of PFAS at KHO from January – June 2019

	KHO01	KHO02	KHO03	KHO04	KHO05	KHO06	KHO07	KHO08	KHO09
FBSA	54	19	<MQL	29	13	1100	260	330	180
MeFBSA	140	76	<MQL	<MQL	<MQL	<MQL	<MQL	<MQL	<MQL
FHxSA	340	160	62	61	19	88	130	65	67
MeFHxSA	<MQL	<MQL	<MQL	<MQL	<MQL	<MQL	<MQL	<MQL	<MQL
FOSA	600	47	20	<MQL	18	32	100	38	58
MeFOSA	<MQL	<MQL	<MQL	<MQL	<MQL	<MQL	<MQL	<MQL	<MQL
EtFOSA	400	<MQL	<MQL	<MQL	<MQL	<MQL	<MQL	<MQL	<MQL
MeFOSE	740	<MQL	<MQL	<MQL	<MQL	<MQL	210	<MQL	200
EtFOSE	2500	<MQL	<MQL	<MQL	<MQL	100	160	<MQL	110
PFPeA	630	240	100	120	190	260	1600	890	1700
PFHxA	630	150	160	320	150	320	870	1400	1700
PFHpA	1000	490	480	190	440	270	6800	6900	6500
PFOA	18000	2200	550	4600	1600	2700	4300	3200	3700
PFNA	580	470	170	180	210	110	1700	1100	2600
PFDA	250	<MQL	<MQL	<MQL	<MQL	<MQL	290	310	340
PFUnDA	110	43	59	<MQL	38	<MQL	250	230	420
PFDoDA	56	12	17	26	<MQL	<MQL	56	85	80
PFTrDA	39	11	25	<MQL	12	18	53	110	120
PFTDA	<MQL	9.9	<MQL	<MQL	<MQL	<MQL	31	36	37
PFHxDA	<MQL	<MQL	<MQL	<MQL	<MQL	<MQL	<MQL	<MQL	<MQL
PFOcDA	<MQL	<MQL	<MQL	<MQL	<MQL	<MQL	<MQL	<MQL	<MQL
PFPeS	<MQL	16	<MQL	<MQL	<MQL	<MQL	<MQL	<MQL	<MQL
PFHxS	220	180	33	130	48	55	70	56	54
PFHpS	<MQL	<MQL	<MQL	<MQL	<MQL	<MQL	<MQL	<MQL	<MQL
PFOS	2400	1300	310	1300	300	590	540	610	570
PFNS	<MQL	<MQL	<MQL	<MQL	<MQL	<MQL	<MQL	<MQL	<MQL
PFDS	<MQL	<MQL	<MQL	<MQL	<MQL	<MQL	<MQL	<MQL	<MQL
PFDoDS	<MQL	<MQL	<MQL	<MQL	<MQL	<MQL	<MQL	<MQL	<MQL
4:2 FTSA	<MQL	<MQL	<MQL	<MQL	<MQL	<MQL	<MQL	<MQL	<MQL
6:2 FTSA	150	59	45	120	59	94	130	100	110
8:2 FTSA	<MQL	<MQL	<MQL	<MQL	<MQL	<MQL	<MQL	<MQL	<MQL
6:2 FTUCA	<MQL	36	<MQL	64	93	67	26	250	40
8:2 FTUCA	<MQL	<MQL	<MQL	<MQL	<MQL	<MQL	32	<MQL	130
PFECHS	<MQL	44	<MQL	<MQL	<MQL	<MQL	<MQL	<MQL	<MQL
6:2 Cl-PFESA	<MQL	<MQL	<MQL	<MQL	<MQL	<MQL	<MQL	<MQL	<MQL
8:2 Cl-PFESA	<MQL	<MQL	<MQL	<MQL	<MQL	<MQL	<MQL	<MQL	<MQL
HFPO-DA	<MQL	57	<MQL	67	19	61	220	130	180
ADONA	<MQL	<MQL	<MQL	<MQL	<MQL	<MQL	<MQL	<MQL	29

Table S14. Fluxes (pg m^{-2}) of PFAS at UNIS, Longyearbyen from January – May 2019

	UNIS01	UNIS02	UNIS03	UNIS04	UNIS05	UNIS06	UNIS07	UNIS08
FBSA	14000	970	150	250	140	6800	6600	7300
MeFBSA	930	620	490	120	140	130	430	920
FHxSA	1300	700	270	110	67	800	1100	3500
MeFHxSA	<MQL	<MQL	<MQL	<MQL	<MQL	<MQL	<MQL	<MQL
FOSA	320	120	110	52	56	110	1400	440
MeFOSA	<MQL	<MQL	<MQL	<MQL	<MQL	<MQL	<MQL	<MQL
EtFOSA	<MQL	<MQL	<MQL	<MQL	<MQL	<MQL	<MQL	<MQL
MeFOSE	<MQL	<MQL	<MQL	170	170	<MQL	<MQL	1300
EtFOSE	<MQL	<MQL	3300	840	620	360	4000	<MQL
PFPeA	2500	1500	500	1300	490	4500	7300	18000
PFHxA	3200	1900	820	830	650	3200	11000	32000
PFHpA	3900	3400	710	2200	990	8300	19000	17000
PFOA	12000	12000	12000	14000	11000	17000	38000	93000
PFNA	2800	3400	670	1300	520	2800	13000	13000
PFDA	2500	3000	370	240	180	2200	8300	14000
PFUnDA	940	1200	220	170	110	1100	7400	6200
PFDoDA	490	680	110	<MQL	<MQL	750	12000	8000
PFTrDA	250	420	48	38	15	380	5200	3900
PFTDA	210	200	58	59	29	310	15000	7300
PFHxDA	130	73	<MQL	84	43	150	7100	5200
PFOcDA	110	<MQL	<MQL	180	<MQL	<MQL	2600	2700
PFPeS	<MQL	<MQL	62	<MQL	<MQL	<MQL	<MQL	<MQL
PFHxS	520	630	350	160	95	100	220	1600
PFHpS	<MQL	120	<MQL	150	<MQL	<MQL	<MQL	390
PFOS	4100	3900	2700	3500	1100	2000	4600	28000
PFNS	<MQL	<MQL	<MQL	<MQL	<MQL	<MQL	<MQL	<MQL
PFDS	<MQL	<MQL	<MQL	<MQL	<MQL	<MQL	<MQL	<MQL
PFDoDS	<MQL	<MQL	<MQL	<MQL	<MQL	<MQL	<MQL	<MQL
4:2 FTSA	<MQL	<MQL	<MQL	<MQL	<MQL	<MQL	<MQL	<MQL
6:2 FTSA	200	150	190	170	120	240	1100	2800
8:2 FTSA	<MQL	<MQL	<MQL	<MQL	54	<MQL	<MQL	420
6:2 FTUCA	<MQL	<MQL	880	290	390	<MQL	<MQL	<MQL
8:2 FTUCA	<MQL	<MQL	<MQL	100	260	<MQL	<MQL	<MQL
PFECHS	150	210	35	41	14	<MQL	77	<MQL
6:2 Cl-PFESA	<MQL	<MQL	<MQL	<MQL	<MQL	<MQL	<MQL	<MQL
8:2 Cl-PFESA	<MQL	<MQL	<MQL	<MQL	<MQL	<MQL	<MQL	<MQL
HFPO-DA	160	230	150	160	<MQL	420	560	<MQL
ADONA	<MQL	<MQL	<MQL	<MQL	<MQL	<MQL	<MQL	<MQL

Table S15. Percentage of linear isomers and concentrations (pg L^{-1}) of linear and branched isomers of PFOS. 1-PFOS was <MQL for all subsections.

Depth (cm weq)	3/4/5-PFOS	6/2-PFOS	Linear-PFOS	Linear-PFOS (%)
Drønbreen	30.3	30.8	287	82%
Lomonosovfonna01	96.7	64.3	339	80%
Lomonosovfonna02	16.9	15.9	136	82%
Grønfjordbreen	16.1	16.5	128	68%
Nordmannsfonna	31.0	23.0	251	81%
Fox01	7.75	7.22	61.9	81%
Fox02	16.2	16.2	113	78%
Fox03	33.9	23.8	214	79%
Fox04	13.5	10.2	88.7	79%
Fox05	18.5	9.55	159	85%
Fox06	<MQL	11.0	107	91%
Fox07	47.1	38.6	331	79%
Fox08	18.4	17.4	177	83%
Fox09	27.1	26.5	258	83%
Fox10	19.3	13.9	137	81%
KHO01	19.6	16.3	172	83%
KHO02	52.0	42.6	312	77%
KHO03	9.91	11.9	64.2	75%
KHO04	17.6	15.3	142	81%
KHO05	11.5	8.17	60.9	76%
KHO06	8.58	4.86	71.6	84%
KHO07	9.49	6.97	55.8	77%
KHO08	14.1	16.5	95.4	76%
KHO09	9.66	10.9	79.5	79%
UNIS01	53.5	34.9	405	82%
UNIS02	61.1	61.5	463	79%
UNIS03	54.1	46.3	411	80%
UNIS04	49.2	42.8	541	85%
UNIS05	25.3	27.8	228	81%
UNIS06	26.2	26.3	324	86%
UNIS07	25.0	36.4	497	89%
UNIS08	144	173	1460	82%

Table S16. Percentage of linear isomers and concentrations (pg L^{-1}) of linear and branched isomers of PFHxS. 1-PFHxS was <MQL for all subsections.

Depth (cm weq)	2/3/4-PFHxS	Linear-PFHxS	Linear-PFHxS (%)
Drønbreen	<MQL	11.5	100%
Lomonosovfonna01	<MQL	53.7	100%
Lomonosovfonna02	<MQL	10.6	100%
Grønfjordbreen	<MQL	7.70	100%
Nordmannsfonna	<MQL	7.39	100%
Fox01	<MQL	4.47	100%
Fox02	<MQL	14.4	100%
Fox03	<MQL	19.1	100%
Fox04	<MQL	10.2	100%
Fox05	<MQL	7.01	100%
Fox06	<MQL	5.26	100%
Fox07	<MQL	23.1	100%
Fox08	<MQL	7.42	100%
Fox09	<MQL	10.8	100%
Fox10	<MQL	8.39	100%
KHO01	<MQL	16.1	100%
KHO02	<MQL	43.2	100%
KHO03	<MQL	6.90	100%
KHO04	3.99	13.8	78%
KHO05	<MQL	9.90	100%
KHO06	<MQL	6.65	100%
KHO07	<MQL	7.26	100%
KHO08	<MQL	8.78	100%
KHO09	<MQL	7.52	100%
UNIS01	<MQL	52.2	100%
UNIS02	<MQL	74.7	100%
UNIS03	<MQL	52.7	100%
UNIS04	<MQL	24.5	100%
UNIS05	<MQL	20.3	100%
UNIS06	<MQL	16.5	100%
UNIS07	<MQL	23.7	100%
UNIS08	<MQL	81.9	100%

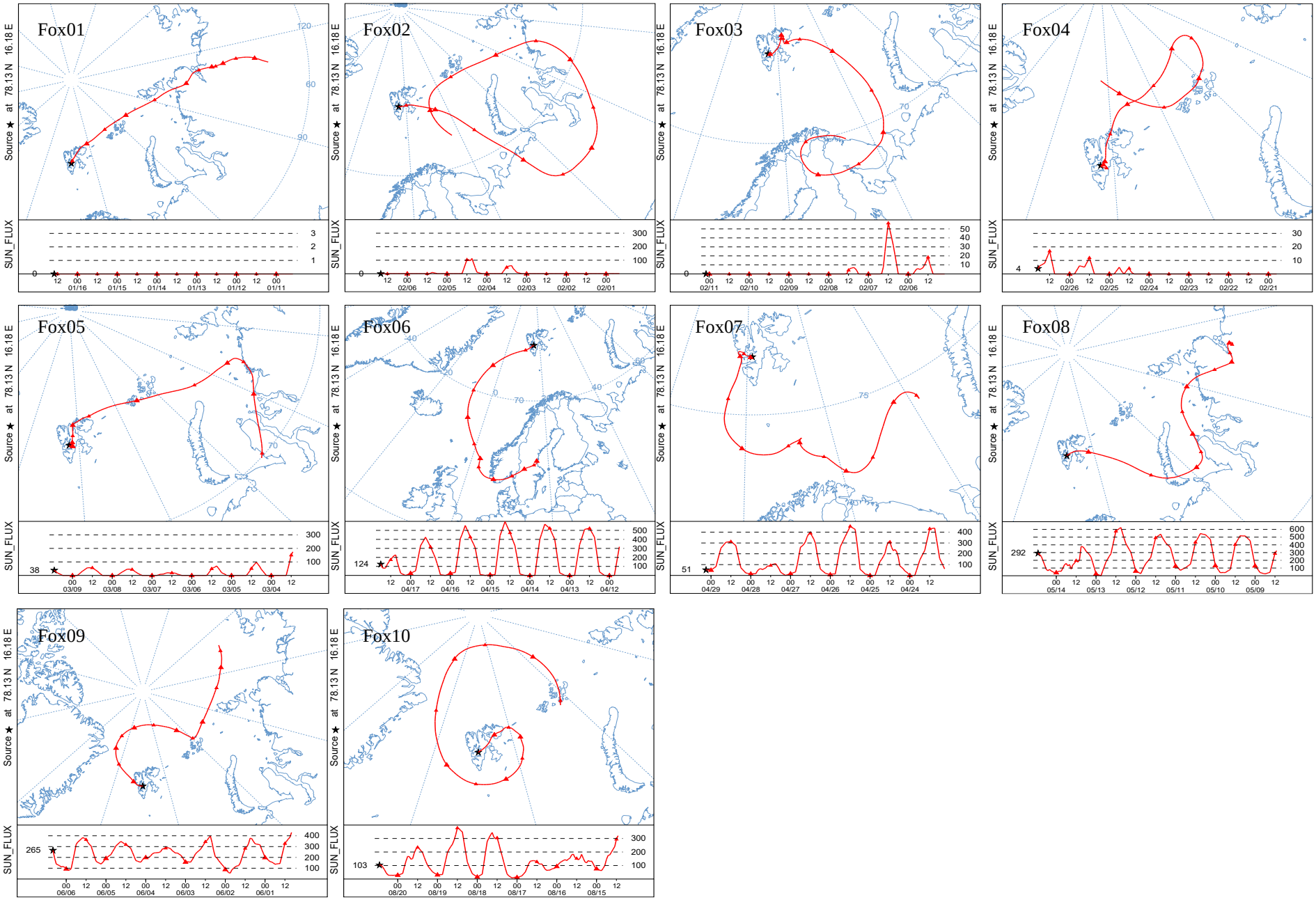


Figure S1. HYSPLIT backwards air mass trajectories for Fox01 – Fox10 and the hourly downward solar radiation along the trajectory (W/m^2) from Chapter 5.

Chapter 7

Arctic Springtime Atmospheric Degradation of Per- and Polyfluoroalkyl Substance (PFAS) Precursors driven by Bromine Radicals

William F. Hartz,[a,b]* Maria K. Björnsdotter,[c,d] Leo W. Y. Yeung,[d] Andrew Hodson,[b,e] Elizabeth R. Thomas,[f] Jack D. Humby,[f] Chris Day,[a] Ingrid Ericson Jogsten,[d] Anna Kärrman,[d] Roland Kallenborn[g,h]

Drafted for submission to Nature Communications

7.1 Abstract 227
7.2 Introduction 228
7.3 Results and Discussion 231
7.3.1 Evidence for bromine radical driven degradation of precursors in Snow from Foxfonna 231
7.3.2 Evidence for bromine radical driven degradation in the 2019 Lomonosovfonna Ice Core 233
7.3.3 Environmental Implications 235
7.4 Materials and Methods 237
7.4.1 Target Analytes 237
7.4.2 Ice Core Drilling and Analysis 237
7.4.3 Surface Snow Sampling 238
7.4.4 Data Treatment 238
7.5 References 240
7.6 Supporting Information 244

The study conceptualising. data interpretation, writing and of this study was done by William F Hartz. See chapters 4 – 6 for the contributions of co-authors. A few co-authors have assisted in editing of the manuscript.

[a]Department of Earth Sciences, University of Oxford, South Parks Road, Oxford, OX1 3AN, United Kingdom

[b]Department of Arctic Geology, University Centre in Svalbard (UNIS), NO-9171, Longyearbyen, Svalbard, Norway

[c]Institute of Environmental Assessment and Water Research (IDAEA-CSIC), C/Jordi Girona, 18-26, 08034 Barcelona, Catalonia, Spain

[d]Man-Technology-Environment Research Centre (MTM), Örebro University, SE-701 82 Örebro, Sweden

[e]Department of Environmental Sciences, Western Norway University of Applied Sciences, NO-6851, Sogndal, Norway

[f]Ice Dynamics and Paleoclimate, British Antarctic Survey, High Cross, Cambridge, CB3 0ET, United Kingdom

[g]Faculty of Chemistry, Biotechnology and Food Sciences (KBM), Norwegian University of Life Sciences (NMBU), NO-1432 Ås, Norway

[h]Department of Arctic Technology, University Centre in Svalbard (UNIS), NO-9171, Longyearbyen, Svalbard, Norway

7.1 Abstract

Per- and polyfluoroalkyl substances (PFAS) are persistent organofluorine contaminants. Many PFAS are toxic and bioaccumulative, with high levels in apex predators such as polar bears (*Ursus maritimus*). The formation and deposition of perfluoroalkyl acids (PFAAs) in the Arctic has previously been considered to come from the hydroxyl radical mediated atmospheric degradation of precursors. Results in this study from a glacier ice core and surface snow samples collected seasonally (January – August 2019), indicated that bromine (Br) radicals play a more significant role in the atmospheric formation and deposition of PFAAs in the Arctic. Br radicals released during sea ice formation in Arctic Springtime, are important to the input of mercury into the Arctic ecosystem through atmospheric mercury depletion events (AMDEs). This study suggests that an equivalent process - 'atmospheric PFAS precursor depletion events' (APPDEs) could also occur. This would enhance PFAS input into the Arctic biosphere more than previously considered.

7.2 Introduction

Per- and polyfluoroalkyl substances (PFAS) are persistent organic contaminants with high levels in Arctic apex predators.[1–3] However, some PFAS are also known to be toxic and bioaccumulative.[4,5] Several long-range mechanisms exist for their transport to, and distribution within, the remote Arctic environment. These include ocean currents[6,7] and marine aerosols.[8] However, the long-range atmospheric transport of volatile neutral PFAS (so called precursors) followed by their atmospheric degradation and subsequent deposition,[9,10] has also led to PFAS being detected ubiquitously in Arctic snow and ice cores (for example, Chapters 4 – 6).[10]

Several precursors have been identified as sources of perfluoroalkyl carboxylic acids (PFCAs) and perfluoroalkyl sulfonic acids (PFSAs). These include fluorotelomer alcohols (FTOHs),[9,11] *N*-alkylated perfluoroalkane sulfonamides (FASAs),[12] perfluoroalkane sulfonamido ethanols (FOSEs),[13] and fluorotelomer acrylates (FTAs).[14] Other precursors include hydrofluorocarbons (HFCs),[15] hydrochlorofluorocarbons (HCFCs),[16] hydrofluoroethers (HFEs),[17] and hydrofluoroolefins (HFOs),[18] which were introduced in the 1990s after the Montreal Protocol banned ozone depleting chlorofluorocarbons (CFCs).[19] All these precursors are also known to exist in the Arctic atmosphere.[20–25] However, studies into their degradation have focused on degradations initiated by hydroxyl (OH) radicals. In some of these studies, chlorine radicals were used as a substitute, indicating that degradation of these precursors can alternatively be initiated by halogen radicals.[9]

During polar sunrise in the northern hemisphere spring, first year sea ice and frost flowers are known to be a major source of bromine (Br) radicals to the Arctic troposphere.[26–29] Br radicals are released to the atmosphere in events known as ‘bromine explosions’. Br radicals play a key role in atmospheric mercury depletion events (AMDEs) of gaseous elemental mercury, and ozone

depletion events (ODEs), where BrO is formed by reaction of Br radicals with O_3.[30] AMDEs and ODEs were both found to be most significant on Svalbard (Norwegian Arctic) during April – June each year.[31–34] For example, in spring 2019, 9 AMDEs were reported in Ny-Ålesund, Svalbard, between 1st April and 4th June.[32] During AMDEs, mercury is readily deposited in snow in the Arctic.[35] AMDEs are known to play a significant role in the input of mercury into the Arctic food web.[36]

Br radicals are also important in the atmospheric formation and deposition of HNO_3 in the Arctic.[37–39] BrO can react with NO_2 to form $BrONO_2$. This can then be followed by hydrolysis to form HNO_3. In this process NO_x is overall converted to HNO_3, which can then be deposited in the Arctic snowpack.[38] In the Arctic atmosphere, emissions of Br radicals from sea ice likely means that the majority of the conversion NO_x to NO_3^-, involves BrO.[39] Similarly, BrO radicals can play a significant role in the oxidation of dimethyl sulfide (DMS) to methane sulfonic acid (MSA, CH_3SO_3H) and sulfur dioxide (SO_2) in the Arctic troposphere.[40]

The sources and processes of ions such as Br^-, NO_3^- and MSA in Svalbard snow and ice cores have been well studied.[27,38,41,42] On Lomonosovfonna, a site well established for ice core records,[43] it was found that Br^- deposition was enriched (relative to seawater) as a result of Br emission during first year sea ice formation.[42] This was due to the proximity of Lomonosovfonna to areas that are often covered by first year sea ice in eastern Svalbard. A Br enrichment factor for three snowpits on Lomonosovfonna had Br_{enr} values > 1 (where $Br_{enr} = Br^-/(0.0065 \cdot Na^+)$, and where 0.0065 is the mean seawater mass ratio for $Br^-:Na^+$).[42] This indicated an additional Br^- source besides marine aerosols. Also on Lomonosovfonna, MSA has been used as a sea ice proxy, since its precursor DMS is mostly emitted by phytoplankton at the sea ice edge.[41] Like ODEs and AMDEs, atmospheric MSA formation is known to peak on Svalbard during May and June each

year.[44,45]

This study provides the first evidence for the enhanced radical degradation of PFAS precursors by Br radicals in the Arctic atmosphere during springtime. This raises the possibility for atmospheric PFAS precursor depletion events (APPDEs) in the Arctic, as earlier reported for mercury (AMDEs) and ozone (ODEs). To investigate this, 10 surface snow samples (Fox01 – Fox10, collected seasonally (January – August 2019) from the Foxfonna Ice Cap, Svalbard (Chapters 5 and 6), and a 12.3 m ice core (spanning 2006 – 2019) from the Lomonosovfonna ice cap, Svalbard (Chapter 4), were used. PFAS levels were then compared with major ions to investigate potentially common atmospheric processes. These ions were K^+, Mg^{2+}, Ca^{2+}, MSA, Cl^-, Br^-, NO_3^-, SO_4^{2-} and nss-SO_4^{2-} (non-sea-salt SO_4^{2-}). Chapters 4 – 6 have already used the Na^+ ion to establish that marine aerosols were not the source of PFAS is the same surface snow and ice core.

7.3 Results and Discussion

7.3.1 Evidence for bromine radical driven degradation of precursors in Snow from Foxfonna

Sampling surface snow is an effective tool to understanding the atmospheric processes of PFAS (for example, in Chapters 5 and 6).[46,47] In this study, each surface snow sample represents a single precipitation event, since surface snow was collected as soon as possible after a targeted precipitation event (sampled January – August 2019). The levels of several PFAS were found to be significantly correlated with major ions in surface snow collected seasonally from Foxfonna (Table S2). These included C_2 – C_{11} PFCAs, HFPO-DA, PFHxS, and PFOS. These were only significant ($p < 0.01$) for Br^- and NO_3^-. For Br^- specifically, fluxes of PFPrA, PFBA, PFPeA, and PFDA ($0.64 \leq r \leq 0.78$, $p < 0.05$) were correlated. Fluxes of C_2 – C_{11} PFCAs and HFPO-DA, but excluding PFOA, were correlated with NO_3^- ($0.66 \leq r \leq 0.95$, $p < 0.05$). PFHxS ($r = 0.68$, $p < 0.05$) and PFOS ($r = 0.87$, $p < 0.01$) were also correlated with NO_3^-. Herein these observations are discussed further.

Br_{env} factors for surface snow on Foxfonna were >1 ($Br_{enr} = 4.0 \pm 6.4$) suggesting that deposition was enriched with an additional source of Br other than marine aerosols. In this study, the correlation of Br^- with PFPrA ($r = 0.78$, $p < 0.01$) as well as PFBA, PFPeA, PFDA, and PFOS ($0.64 \leq r \leq 0.68$, $p < 0.05$), therefore indicates the importance of Br radicals in the radical mediated atmospheric formation of both PFCAs and PFSAs in the Arctic. Halogen radicals are already known to be able to degrade PFAS precursors.[9]

NO_3^- formation in the Arctic atmosphere is known to be enhanced by Br radicals.[38] Hence the correlations of several PFAS (C_2 – C_7 and C_9 – C_{11} PFCAs, HFPO-DA, PFHxS and PFOS) with NO_3^-, is likely because both the atmospheric formation of PFAAs and NO_3^- is enhanced by the presence of Br radicals. Alternatively, it could be that the correlations between NO_3^- and

several of the PFAS observed here are as a result of the long-range transport of air masses from Eurasia with high levels of both PFAS and nitrogen chemical species (e.g. peroxyacyl nitrates or particle-bound NO_3^-). However, three surface snow samples (Fox07 – Fox09) had high levels of NO_3^- and several PFAS (C_2 – C_{11} PFCAs, PFOS and HFPO-DA), but had backwards airmass trajectories that originated over the Arctic Ocean and away from industrialised regions (Chapter 5, Figure S1). In summary, the correlation between the fluxes of several PFAS with NO_3^-, likely arises as a result of their common dependency on Br radicals to enhance their atmospheric formation in the Arctic.

In summary, seasonal surface snow samples, show that Br radicals play an important role in the atmospheric degradation of PFAS precursors. The peak PFAS deposition in 2019 occurred between 30th April – 10th June, when 58 – 92% of the total fluxes of C_2 – C_{11} PFCAs and, 59% and 73% for PFOS and HFPO-DA, respectively, were deposited (in samples Fox07 – Fox09). This was in agreement with the peak in AMDEs for mercury, ODEs for ozone, and MSA atmospheric formation on Svalbard.[31–34,44,45] Indeed in 2019, nine AMDEs were detected in Ny-Ålesund (129 km away) during approximately the same period (1st April – 4th June 2019) as peak PFAS deposition. This indicates the importance of this time of year for PFAS and mercury deposition on Svalbard and suggests that equivalent atmospheric PFAS precursor depletion events (APPDEs) could occur, as is known for mercury in the Arctic (AMDEs). Lastly, no major ion was correlated with TFMS ($r < 0.4$, $p > 0.19$). Hence, this study was unable to find a source explaining the presence of TFMS in Arctic surface snow. As yet, no study has identified the long-range atmospheric process that contributes to TFMS deposition in the remote Arctic (Chapter 5).

7.3.2 Evidence for bromine radical driven degradation in the 2019 Lomonosovfonna Ice Core

Unlike the surface snow samples, the Lomonosovfonna ice core has been subject to post-deposition effects such as meltwater percolation and firnification processes (Chapter 4) Nonetheless, the ice core offers a route to understanding the dominant processes of PFAS in the Arctic atmosphere and represents a record of over a decade of PFAS depositon. This is significant since it provides a way to confirm the importance of Br radicals in the overall deposition of PFAS in the remote Arctic as well as being able to assess the significance of Br enhanced precursor degradations on a longer time scale (2006 – 2019) than for the surface snow sampling (January – August 2019).

In the Lomonosovfonna ice core, Br_{enr} values ranged from 1.0 – 42 (Br_{enr} = 7.7 ± 6.4), indicating an enrichment of Br^- deposition from, in particular, first year sea ice formation and frost flowers. Nonetheless, Br^- was correlated with Na^+ in the ice core indicating a contribution from marine aerosols ($r = 0.53$, $p < 0.001$). However, Br^- was more significantly correlated with MSA ($r = 0.62$, $p < 0.001$) and SO_4^{2-} ($r = 0.59$, $p < 0.001$). This likely arises as a result of Br radicals' role in the oxidation of DMS to form MSA and SO_2 in the Arctic atmosphere. No ions were found to correlate with a chemical melt proxy ($\log([Na^+]/[Mg^{2+}])$. Nonetheless, $\log([Na^+]/[Mg^{2+}])$ values were often >1 in the lower half of the ice core, indicating that this half had been more influenced by melt, and the increased presence of melt features supported this (Figure S1).

In the ice core, TFA was found to positively correlate with Br^- ($r = 0.68$, $p < 0.01$), MSA ($r = 0.78$, $p < 0.01$) and SO_4^{2-} ($r = 0.56$, $p < 0.05$). FBSA was also found to correlate with Br^- ($r = 0.55$, $p < 0.05$), MSA ($r = 0.74$, $p < 0.01$) and SO_4^{2-} ($r = 0.59$, $p < 0.05$), and PFOS with MSA ($r = 0.62$, $p < 0.01$). The correlation of TFA and FBSA with Br^- suggests that their atmospheric processes are linked and that the degradation of TFA and FBSA precursors is promoted by Br

radicals in the Arctic atmosphere. This is supported further by the correlations of TFA, FBSA and PFOS, with DMS degradation products (MSA and SO_4^{2-}). Since it is known that atmospheric Br radical chemistry can make a large contribution to the degradation of DMS (which then forms SO_4^{2-}) in the Arctic,[40] this suggests their deposition is highly dependent on the atmospheric degradation precursors by Br radicals. This broadly supports the findings in surface snow, where the atmospheric formation of several PFCAs and PFOS were found to have been promoted by Br radicals. The correlations of TFA, PFOS and FBSA in this ice core suggest that Br radicals can play a significant role in the atmospheric formation of a variety of PFAS in the Arctic and have done for over a decade. All correlations for the ice core between major ions and PFAS are shown in Table S3.

TFA and PFOS were found to have been mobile during melt water percolation on Lomonosovfonna (Chapter 4). Hence, post-depositional affects may have influenced the records of major ions and PFAS in the core. For example, the negative and positive correlations of TFA, PFOS and FBSA with several metal ions, is possibly due to post-depositional effects as anions migrate and associate themselves with metal ions (e.g. Ca^{2+} and NO_3^- on Lomonosovfonna).[48]

Measurements of PFAS in frost flowers (i.e. a major source of Br radicals) in a sea ice chamber found very high levels of PFAS relative to the bulk sea water.[49] It was thought that frost flowers had become enriched with PFAS from the bulk sea water as a result of their chemical sorption to surfaces within the frost flower during freezing. Hence, it could be alternatively that frost flower aerosol explained the deposition of PFAS in the remote Arctic in this study, however no PFAS were found to correlate with Na^+, a marine aerosol proxy, in the surface snow or ice core (Chapters 4 – 6). Frost flower aerosol will only partly be depleted in Na^+, and therefore Na^+ could also serve as a tracer for frost flower aerosol.[50] Frost flower aerosol would be expected to be

completely depleted in SO_4^{2-}, but no PFAS were found to have a significant negative correlation with SO_4^{2-} in the surface snow or ice core. Nonetheless, frost flower formation could become enriched in volatile neutral PFAS (precursors) from the sea water, promoting their revolatilisation into the atmosphere, followed by their potential atmospheric degradation.

7.3.3 Environmental Implications

The indication that bromine radicals enhance the atmospheric formation of PFCAs and PFSAs in the Arctic atmosphere has significant implications for the Arctic ecosystems. Firstly, this is because, bromine radicals produced during springtime after polar sunrise, will significantly degrade PFAS precursors in the atmosphere in the immediate vicinity (i.e. above areas of newly forming sea ice). The short atmospheric lifetimes of PFAS will mean than they become rapidly deposited back into the sea ice and surface sea waters after formation. Like for the AMDEs known to exist for mercury in the Arctic, PFAS deposition in the study was found to peak during April - June, indicating the possibility for a parallel process for PFAS during Arctic springtime - atmospheric PFAS precursor depletion events (APPDEs). However, unlike mercury, PFCAs and PFSAs will not be sufficiently volatile to be remitted back into the atmosphere from the snow surface and they will then accumulate in the seasonal snowpack.

Like AMDEs for mercury, APPDEs for PFAS will also occur at the time when Arctic biota are in preparation for peak summer activity. Primary production at sea ice margins during Arctic springtime, is an important time for nutrient uptake into Arctic marine food webs. Efficient atmospheric formation and deposition of PFAS at the sea ice edge, will expose primary producers, such as sea ice algae, to high levels of PFAS input. Sea ice algae are known contribute to 74% of total primary production under landfast sea ice in the Arctic and up to 60% in the central Arctic

Ocean.[51,52] This puts the Arctic marine food web at increased exposure to PFAS than perhaps previously considered.

Hence PFAS deposition through APPDEs provide a potentially important pathway for PFAS input into the Arctic biosphere, just like AMDEs are known to do for mercury.[36] When combined with the bioaccumulative ability of many PFAS, and the extended Arctic marine food web, this additional factor can also contribute to explaining the high levels of some PFAS known to exist in Arctic apex predators such as polar bears and glaucus gulls.[2,3]

Secondly, bromine explosions in the Arctic are known to be carried long distances from sources.[53] Bromine explosions occur in Arctic Springtime, when the return of sunlight significantly increases the photolysis of Br_2 to produce Br radicals. This will enable enhanced atmospheric precursor degradations to continue throughout large parts of the Arctic atmosphere and promote the widespread distribution and deposition of PFAS in the Arctic. This is supported by the measurement of PFAS on several remote high elevation ice caps (form example, Chapters 4 – 6).[10] To the best of our knowledge, the role of other radicals in the degradation of PFAS precursors in the Arctic troposphere, beyond that of OH radicals, has not previously been considered. Many existing models rely only on OH radicals as an atmospheric oxidizing agent.[54,55] Hence, future studies must consider potentially significant additional bromine radical sources. Furthermore, measurements of surface waters in the North Atlantic and Arctic Ocean have shown that the Arctic is, through ocean currents, a net exporter of those PFAS whose deposition is controlled by atmospheric degradations.[56] The enhanced degradation of PFAS precursors in the Arctic troposphere by Br radicals could explain this observation, since sea ice is not be widely present outside of the Arctic (or Antarctic).

Finally, with climate change increasing the areas of first year sea ice in the Arctic Ocean,[57,58] this could lead to higher levels of Br radicals to the Arctic troposphere in the coming decades. With a greater oxidising capacity of the atmosphere, it would be expected that PFAS degradation and deposition in the Arctic increases, above and beyond the increased emissions of several PFAS precursors that have already accounted for.

7.4 Materials and Methods

7.4.1 Target Analytes

In total, 45 different PFAS analytes were targeted as follows. Perfluoroalkyl acids (PFAAs) targeted were C_2 – C_{14}, C_{16}, and C_{18} PFCAs, and C_1 – C_{10} and C_{12} PFSAs. Fluorotelomers targeted were 4:2 FTSA, 6:2 FTSA, 8:2 FTSA, 6:2 FTUCA and 8:2 FTUCA. Further anionic target analytes included 6:2 Cl-PFESA, 8:2 Cl-PFESA, HFPO-DA (GenX), and ADONA. Nine neutral compounds were also targeted: FBSA, MeFBSA, FHxSA, MeFHxSA, FOSA, MeFOSA, EtFOSA, MeFOSE and EtFOSE. A full list of names and abbreviations are described in Table S1.

7.4.2 Ice Core Drilling and Analysis

In April 2019, a 12.3 m ice core (2006 – 2019), diameter 14.0 cm, was drilled on Lomonosovfonna (78°49.454'N, 17°26.193'E, 1198 m.a.s.l.) in Svalbard (Norwegian Arctic). The core was analysed for 45 different PFAS as described above. The core was dated using a multi-proxy approach, including seasonal variations in the stable isotope ratio $\delta^{18}O$. The core was also analysed for major ions from 5 cm subsamples (n = 204). Full details of the core's analyses are described in Chapter 4. Using the same methods for major ion analysis, the present study also uses the concentrations of K^+, Mg^{2+}, Ca^{2+}, MSA, Cl^-, Br^-, NO_3^-, and SO_4^{2-} in the core to investigate PFAS sources and processes.

7.4.3 Surface Snow Sampling

Surface snow samples (n = 10) were collected from the Foxfonna Ice Cap, Svalbard (78°07.736'N 16°10.791'E, 800 m.a.s.l.) from January – August 2019 (0 – 5 cm). This represents the time of year when the seasonal light is changing from 24-hour darkness in winter to 24-hour daylight in summer. 24-hour daylight began on 19th April 2019 and continued for the rest of the sampling period. Since this location was found to predominantly receive PFAS input from long-range sources, it offered a good location to study the background atmospheric processes of PFAS in the Arctic. Each surface snow sample was analysed for the same 45 PFAS as in the ice core. In addition to the Na^+ concentrations previously reported by Björnsdotter et al, the same snow samples were also analysed for K^+, Mg^{2+}, Ca^{2+}, MSA, Cl^-, Br^-, NO_3^-, and SO_4^{2-} using the same ion chromatography methods. The limits of detection (LOD) for the ion chromatography analysis were < 2.9 ng/mL for every ion. The LOD was calculated as the average of repeated blank injections of Milli-Q water plus three times the standard deviation.[a1]With concentrations in μeq/L, nss-SO_4^{2-}, was calculated $[SO_4^{2-}] - 0.12\times[Na^+] = [nssSO_4^{2-}]$. Further details of the surface snow samples' analyses are discussed in Chapters 5 and 6.

7.4.4 Data Treatment

To remove the effects of variations in snow fluxes for each precipitation event for the surface snow samples, PFAS and major ion concentrations were multiplied by the snow flux of each precipitation event (in kg m^{-2}) to yield PFAS fluxes (in pg m^{-2} per precipitation event). Spearman

[a] Due to intrument downtime from delays in delivery of spare parts to the British Antartic Survey, results from procedual blanks cannot be provided at this stage. However, ions with known contamination/analytical issues have been omitted (NH_4^+, acetate, formate and oxalate). No issues thus far yet been observed for Br^- ions. The results from procedual blanks will be added to the manuscript prior to submission to the jounal.

rank correlation coefficients (r) were used to calculate correlations between PFAS and major ions, tests for statistical significance were performed using a two-tailed Student's t-test (p).

7.5 References

1. Wang, Z. *et al.* A New OECD Definition for Per- And Polyfluoroalkyl Substances. *Environ. Sci. Technol.* **55**, 15575–15578 (2021).
2. Smithwick, M. *et al.* Temporal trends of perfluoroalkyl contaminants in polar bears (Ursus maritimus) from two locations in the North American Arctic, 1972-2002. *Environ. Sci. Technol.* **40**, 1139–1143 (2006).
3. Verreault, J. *et al.* Perfluorinated Alkyl Substances in Plasma, Liver, Brain, and Eggs of Glaucous Gulls (Larus hyperboreus) from the Norwegian Arctic. *Environ. Sci. Technol.* **39**, 7439–7445 (2005).
4. Conder, J. M., Hoke, R. A., De Wolf, W., Russell, M. H. & Buck, R. C. Are PFCAs bioaccumulative? A critical review and comparison with regulatory criteria and persistent lipophilic compounds. *Environ. Sci. Technol.* **42**, 995–1003 (2008).
5. Jensen, A. A. & Leffers, H. Emerging endocrine disrupters: perfluoroalkylated substances. *Int. J. Androl.* **31**, 161–169 (2008).
6. Benskin, J. P. *et al.* Perfluoroalkyl acids in the atlantic and Canadian arctic oceans. *Environ. Sci. Technol.* **46**, 5815–5823 (2012).
7. Yeung, L. W. *et al.* Vertical Profiles, Sources, and Transport of PFASs in the Arctic Ocean. *Environ. Sci. Technol.* **51**, 6735–6744 (2017).
8. Sha, B. *et al.* Sea Spray Aerosol (SSA) as a Source of Perfluoroalkyl Acids (PFAAs) to the Atmosphere: Field Evidence from Long-Term Air Monitoring. *Environ. Sci. Technol.* **56**, 228–238 (2022).
9. Ellis, D. A. *et al.* Degradation of fluorotelomer alcohols: a likely atmospheric source of perfluorinated carboxylic acids. *Environ. Sci. Technol.* **38**, 3316–21 (2004).
10. Young, C. J. *et al.* Perfluorinated Acids in Arctic Snow: New Evidence for Atmospheric Formation. *Environ. Sci. Technol.* **41**, 3455–3461 (2007).
11. Sulbaek Andersen, M. P. *et al.* Atmospheric chemistry of 4:2 Fluorotelomer alcohol (n-C4F9CH2CH2OH): Products and mechanism of Cl atom initiated oxidation in the presence of NO x. *J. Phys. Chem. A* **109**, 1849–1856 (2005).
12. Martin, J. W., Ellis, D. A., Mabury, S. A., Hurley, M. D. & Wallington, T. J. Atmospheric chemistry of perfluoroalkanesulfonamides: kinetic and product studies of the OH radical and Cl atom initiated oxidation of N-ethyl perfluorobutanesulfonamide. *Environ. Sci. Technol.* **40**, 864–72 (2006).
13. D'eon, J. C., Hurley, M. D., Wallington, T. J. & Mabury, S. A. Atmospheric chemistry of N-methyl perfluorobutane sulfonamidoethanol, C4F9SO2N(CH3)CH2CH2OH: kinetics and mechanism of reaction with OH. *Environ. Sci. Technol.* **40**, 1862–8 (2006).
14. Butt, C. M., Young, C. J., Mabury, S. A., Hurley, M. D. & Wallington, T. J. Atmospheric Chemistry of 4:2 Fluorotelomer Acrylate [C4F9CH2CH2OC(O)CH═CH2]: Kinetics, Mechanisms, and Products of Chlorine-Atom- and OH-Radical-Initiated Oxidation. *J. Phys. Chem. A* **113**, 3155–3161 (2009).
15. Young, C. J., Hurley, M. D., Wallington, T. J. & Mabury, S. A. Atmospheric chemistry of CF3CF2H and CF3CF2CF2CF2H: Kinetics and products of gas-phase reactions with Cl atoms and OH radicals, infrared spectra, and formation of perfluorocarboxylic acids. *Chem. Phys. Lett.* **473**, 251–256 (2009).
16. Wallington, T. J. *et al.* The Environmental Impact of CFC Replacements-HFCs and HCFCs. *Environ. Sci. Technol.* **28**, (1994).
17. Oyaro, N., Sellevåg, S. R. & Nielsen, C. J. Atmospheric chemistry of hydrofluoroethers: Reaction of a series of hydrofluoroethers with OH radicals and Cl atoms, atmospheric lifetimes, and global warming potentials. *J. Phys. Chem. A* **109**, 337–346 (2005).
18. Young, C. J., Hurley, M. D., Wallington, T. J. & Mabury, S. A. Atmospheric chemistry of perfluorobutenes (CF3CF=CFCF3 and CF3CF2CF=CF2): Kinetics and mechanisms of reactions with OH radicals and chlorine atoms, IR spectra, global warming potentials, and oxidation to perfluorocarboxylic acids. *Atmos. Environ.* **43**, 3717–3724 (2009).
19. Velders, G. J. M., Andersen, S. O., Daniel, J. S., Fahey, D. W. & McFarland, M. The importance of the Montreal Protocol in protecting climate. *Proc. Natl. Acad. Sci. U. S. A.* **104**, 4814–4819 (2007).
20. Stock, N. L., Furdui, V. I., Muir, D. C. G. & Mabury, S. A. Perfluoroalkyl Contaminants in the Canadian Arctic: Evidence of Atmospheric Transport and Local Contamination. *Environ. Sci. Technol.* **41**, 3529–3536 (2007).
21. Cai, M. *et al.* Polyfluorinated compounds in the atmosphere along a cruise pathway from the Japan Sea to the Arctic Ocean. *Chemosphere* **87**, 989–997 (2012).
22. Dreyer, A., Weinberg, I., Temme, C. & Ebinghaus, R. Polyfluorinated Compounds in the Atmosphere of the

Atlantic and Southern Oceans: Evidence for a Global Distribution. *Environ. Sci. Technol.* **43**, 6507–6514 (2009).
23. Shoeib, M., Harner, T. & Vlahos, P. Perfluorinated chemicals in the arctic atmosphere. *Environ. Sci. Technol.* **40**, 7577–83 (2006).
24. Xie, Z. *et al.* Neutral Poly-/perfluoroalkyl Substances in Air and Snow from the Arctic. *Sci. Rep.* **5**, 8912 (2015).
25. Platt, S. M. *et al.* Atmospheric composition in the European Arctic and 30 years of the Zeppelin Observatory, Ny-Ålesund. *Atmos. Chem. Phys* **22**, 3321–3369 (2022).
26. Spolaor, A. *et al.* Seasonality of halogen deposition in polar snow and ice. *Atmos. Chem. Phys.* **14**, 9613–9622 (2014).
27. Spolaor, A. *et al.* Sea ice dynamics influence halogen deposition to Svalbard. *Cryosphere* **7**, 1645–1658 (2013).
28. Nghiem, S. V. *et al.* Field and satellite observations of the formation and distribution of Arctic atmospheric bromine above a rejuvenated sea ice cover. *J. Geophys. Res. Atmos.* **117**, (2012).
29. Bougoudis, I. *et al.* Long-term time series of Arctic tropospheric BrO derived from UV-VIS satellite remote sensing and its relation to first-year sea ice. *Atmos. Chem. Phys* **20**, 11869–11892 (2020).
30. Wang, S. *et al.* Direct detection of atmospheric atomic bromine leading to mercury and ozone depletion. *Proc. Natl. Acad. Sci. U. S. A.* **116**, 14479–14484 (2019).
31. Herrmann, M. *et al.* Ozone depletion events in the Arctic spring of 2019: A new modeling approach to bromine emissions. *Atmos. Chem. Physics. Prepr.* (2022).
32. Osterwalder, S. *et al.* Fate of Springtime Atmospheric Reactive Mercury: Concentrations and Deposition at Zeppelin, Svalbard. *ACS Earth Sp. Chem.* **5**, 3234–3246 (2021).
33. Sprovieri, F., Pirrone, N., Landis, M. S. & Stevens, R. K. Atmospheric mercury behavior at different altitudes at Ny Alesund during Spring 2003. *Atmos. Environ.* **39**, 7646–7656 (2005).
34. Lehrer, E., Wagenbach, D. & Platt, U. Aerosol chemical composition during tropospheric ozone depletion at Ny Ålesund/Svalbard. *Tellus B* **49**, 486–495 (1997).
35. Steffen, A. *et al.* A synthesis of atmospheric mercury depletion event chemistry in the atmosphere and snow. *Atmos. Chem. Phys.* **8**, 1445–1482 (2008).
36. Schroeder, W. H. *et al.* Arctic springtime depletion of mercury. *Nature* **394**, 331–332 (1998).
37. Custard, K. D. *et al.* The NOx dependence of bromine chemistry in the Arctic atmospheric boundary layer. *Atmos. Chem. Phys.* **15**, 10799–10809 (2015).
38. Björkman, M. P. *et al.* Nitrate postdeposition processes in Svalbard surface snow. *J. Geophys. Res. Atmos.* **119**, 12,953-12,976 (2014).
39. Morin, S. *et al.* Tracing the origin and fate of NOx in the arctic atmosphere using stable isotopes in nitrate. *Science (80-.).* **322**, 730–732 (2008).
40. Toumi, R. BrO as a sink for dimethylsulphide in the marine atmosphere. *Geophys. Res. Lett.* **21**, 117–120 (1994).
41. Isaksson, E., Kekonen, T., Moore, J. & Mulvaney, R. The methanesulfonic acid (MSA) record in a Svalbard ice core. *Ann. Glaciol.* **42**, 345–351 (2005).
42. Barbaro, E. *et al.* Measurement report: Spatial variations in ionic chemistry and water-stable isotopes in the snowpack on glaciers across Svalbard during the 2015-2016 snow accumulation season. *Atmos. Chem. Phys.* **21**, 3163–3180 (2021).
43. Isaksson, E. *et al.* Ice cores from Svalbard—useful archives of past climate and pollution history. *Phys. Chem. Earth, Parts A/B/C* **28**, 1217–1228 (2003).
44. Becagli, S. *et al.* Biogenic Aerosol in the Arctic from Eight Years of MSA Data from Ny Ålesund (Svalbard Islands) and Thule (Greenland). *Atmos. 2019, Vol. 10, Page 349* **10**, 349 (2019).
45. Jang, S. *et al.* Large seasonal and interannual variations of biogenic sulfur compounds in the Arctic atmosphere (Svalbard; 78.9g N, 11.9g E). *Atmos. Chem. Phys.* **21**, 9761–9777 (2021).
46. Taniyasu, S. *et al.* Does wet precipitation represent local and regional atmospheric transportation by perfluorinated alkyl substances? *Environ. Int.* **55**, 25–32 (2013).
47. Wang, X., Chen, M., Gong, P. & Wang, C. Perfluorinated alkyl substances in snow as an atmospheric tracer for tracking the interactions between westerly winds and the Indian Monsoon over western China. *Environ. Int.* **124**, 294–301 (2019).
48. Kekonen, T. *et al.* A 800 year record of nitrate from the Lomonosovfonna ice core, Svalbard. *Ann. Glaciol.* **35**, 261–265 (2002).
49. Garnett, J. *et al.* Investigating the Uptake and Fate of Poly- And Perfluoroalkylated Substances (PFAS) in Sea

Ice Using an Experimental Sea Ice Chamber. *Environ. Sci. Technol.* **55**, 9601–9608 (2021).
50. Rankin, A. M., Wolff, E. W. & Martin, S. Frost flowers: Implications for tropospheric chemistry and ice core interpretation. *J. Geophys. Res. Atmos.* **107**, AAC 4-1-AAC 4-15 (2002).
51. Fernández-Méndez, M. *et al.* Photosynthetic production in the central Arctic Ocean during the record sea-ice minimum in 2012. *Biogeosciences* **12**, 3525–3549 (2015).
52. Lee, S. H., Whitledge, T. E. & Kang, S. H. Spring time production of bottom ice algae in the landfast sea ice zone at Barrow, Alaska. *J. Exp. Mar. Bio. Ecol.* **367**, 204–212 (2008).
53. Zhao, X. *et al.* A case study of a transported bromine explosion event in the Canadian high arctic. *J. Geophys. Res. Atmos.* **121**, 457–477 (2016).
54. Thackray, C. P., Selin, N. E. & Young, C. J. A global atmospheric chemistry model for the fate and transport of PFCAs and their precursors. *Environ. Sci. Process. Impacts* **22**, 285–293 (2020).
55. Wallington, T. J. *et al.* Formation of C7F15COOH (PFOA) and other perfluorocarboxylic acids during the atmospheric oxidation of 8:2 fluorotelomer alcohol. *Environ. Sci. Technol.* **40**, 924–30 (2006).
56. Joerss, H. *et al.* Transport of Legacy Perfluoroalkyl Substances and the Replacement Compound HFPO-DA through the Atlantic Gateway to the Arctic Ocean - Is the Arctic a Sink or a Source? *Environ. Sci. Technol.* **54**, 9958–9967 (2020).
57. Stroeve, J. & Notz, D. Changing state of Arctic sea ice across all seasons. *Environ. Res. Lett.* **13**, 103001 (2018).
58. Shimizu, Y., Chen, L.-C. & Kim, D. W. Arctic sea ice thickness, volume, and multiyear ice coverage: losses and coupled variability (1958–2018). *Environ. Res. Lett.* **13**, 105005 (2018).

Acknowledgements

The authors gratefully acknowledge financial support from the Swedish Research Council Formas (2016-01284), the Swedish Environmental Protection Agency (2219-16-030 and 2219-17-012), the United Kingdom Research and Innovation Natural Environment Research Council and the Oxford Doctoral Training Partnership in Environmental Research (NE/L002612/1), the Burdett-Coutts Trust, the Svalbard Science Forum Arctic Field Grant 2019 (RiS ID 11121), the Research Council of Norway (SvalPOP, 196218/S30), the Fram Centre Flagship program (PharmArctic, 534/75219) and the Knowledge Foundation (Enforce Research Project, 20160019). The authors would also like to thank the Logistics Department and colleagues at the University Centre in Svalbard for help organizing and assisting with fieldwork, and Veerle van Winden, Eirik Rolland Enger and Julien-Pooya Weihs for assistance in the field and laboratory.

Competing interests

The authors declare no conflicts of interest.

7.6 Supporting Information

Table S1. List of target analytes, abbreviations, and CAS numbers 245

Table S2. Correlation coefficients for major ions with PFAS in surface snow from Foxfonna 246

Table S3. Correlation coefficients for major ions with PFAS in the Lomonosovfonna ice core 247

Figure S1. Chemical melt proxy and effective melt layer thickness as a function of depth 248

Table S1. List of target analytes, abbreviations, and CAS numbers

Abbreviation	Target analyte	CAS
TFA	Trifluoroacetic acid	76-05-1
PFPrA	Perfluoropropanoic acid	422-64-0
PFBA	Perfluorobutanoic acid	375-22-4
PFPeA	Perfluoropentanoic acid	2706-90-3
PFHxA	Perfluorohexanoic acid	307-24-4
PFHpA	Perfluoroheptanoic acid	375-85-9
PFOA	Perfluorooctanoic acid	335-67-1
PFNA	Perfluorononanoic acid	375-95-1
PFDA	Perfluorodecanoic acid	335-76-2
PFUnDA	Perfluoroundecanoic acid	2058-94-8
PFDoDA	Perfluorododecanoic acid	307-55-1
PFTrDA	Perfluorotridecanoic acid	72629-94-8
PFTeDA	Perfluorotetradecanoic acid	376-06-7
PFHxDA	Perfluorohexadecanoic acid	67905-19-5
PFOcDA	Perfluorooctadecanoic acid	16517-11-6
TFMS	Trifluoromethane sulfonic acid	1493-13-6
PFEtS	Perfluoroethane sulfonic acid	354-88-1
PFPrS	Perfluoropropane sulfonic acid	423-41-6
PFBS	Perfluorobutane sulfonic acid	375-73-5
PFPeS	Perfluoropentane sulfonic acid	2706-91-4
PFHxS	Perfluorohexane sulfonic acid	355-46-4
PFHpS	Perfluoroheptane sulfonic acid	375-92-8
PFOS	Perfluorooctane sulfonic acid	1763-23-1
PFNS	Perfluorononane sulfonic acid	68259-12-1
PFDS	Perfluorodecane sulfonic acid	335-77-3
PFDoDS	Perfluorododecane sulfonic acid	79780-39-5
4:2 FTSA	4:2 Fluorotelomer sulfonic acid	757124-72-4
6:2 FTSA	6:2 Fluorotelomer sulfonic acid	27619-97-2
8:2 FTSA	8:2 Fluorotelomer sulfonic acid	39108-34-4
6:2 FTUCA	6:2 Fluorotelomer unsaturated carboxylic acid	70887-88-6
8:2 FTUCA	8:2 Fluorotelomer unsaturated carboxylic acid	70887-84-2
PFECHS	Perfluoroethylcyclohexane sulfonic acid	72441-89-5
6:2 Cl-PFESA	6:2 Chlorinated polyfluorinated ether sulfonate	756426-58-1
8:2 Cl-PFESA	8:2 Chlorinated polyfluorinated ether sulfonate	763051-92-9
HFPO-DA	Hexafluoropropylene oxide dimer acid	13252-13-6
ADONA	3H-perfluoro-3-[(3-methoxy-propoxy)propanoic acid]	919005-14-4
FBSA	Perfluorobutane sulfonamide	30334-69-1
MeFBSA	Methyl perfluorobutane sulfonamide	68298-12-4
FHxSA	Perfluorohexane sulfonamide	41997-13-1
MeFHxSA	Methyl perfluorohexane sulfonamide	68259-15-4
FOSA	Perfluorooctane sulfonamide	754-91-6
MeFOSA	N-Methyl perfluorooctane sulfonamide	31506-32-8
EtFOSA	N-Ethyl perfluorooctane sulfonamide	4151-50-2
MeFOSE	N-Methyl perfluorooctane sulfonamidoethanol	24448-09-7
EtFOSE	N-Ethyl perfluorooctane sulfonamidoethanol	1691-99-2

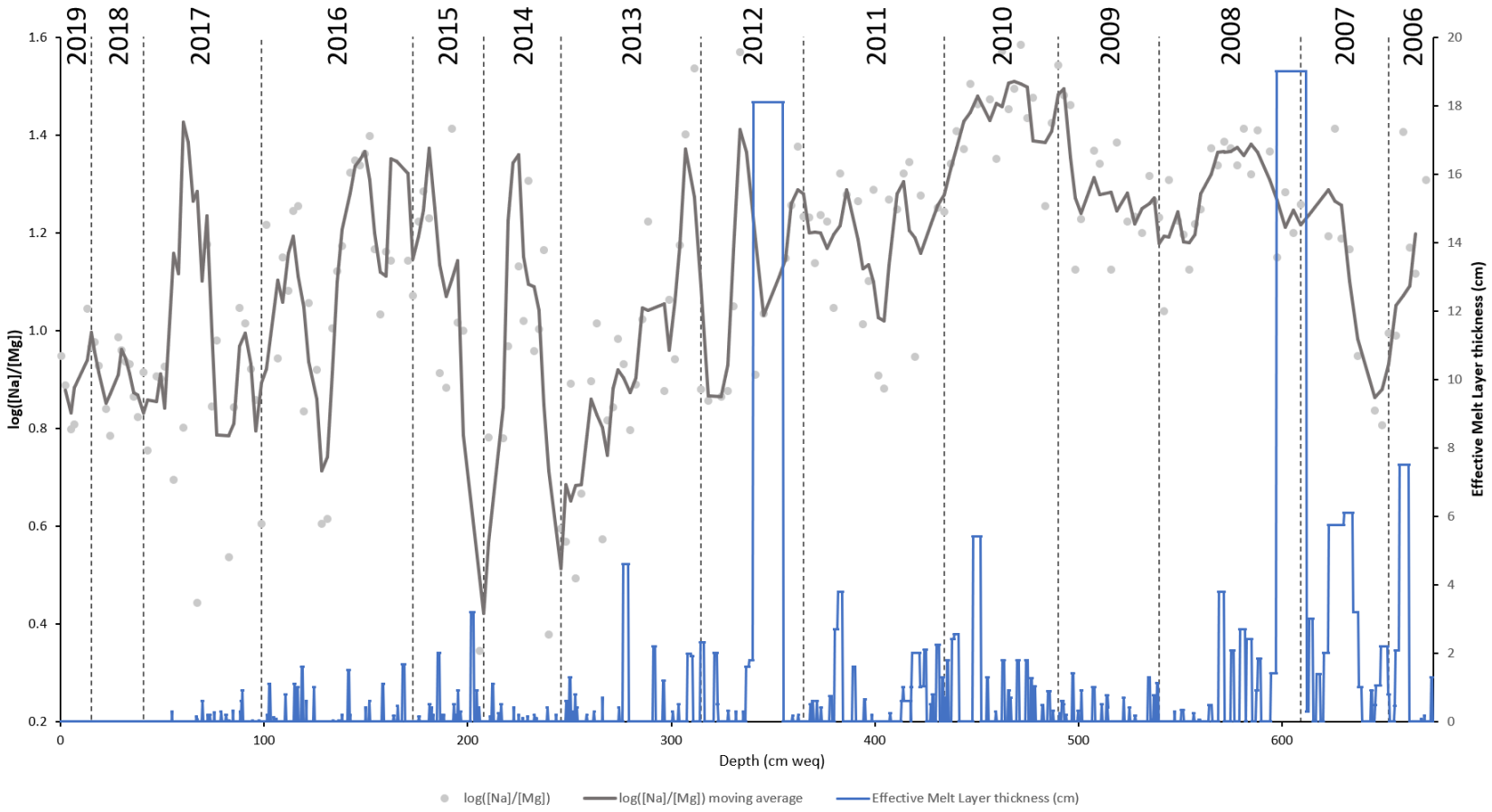
Table S2. Spearman correlation coefficients (r) and statistical significance (p) for correlations of $C_2 - C_{11}$ PFCAs, TFMS, PFHxS, PFOS and HFPO-DA with major ions in surface snow from Foxfonna. Strong correlations (>0.75) and statistically significant p-values are in bold ($p < 0.01$).

	TFMS	PFHxS	PFOS	HFPO-DA	TFA	PFPrA	PFBA	PFPeA	PFHxA	PFHpA	PFOA	PFNA	PFDA	PFUnDA
K^+	r = 0.36	r = 0.58	r = 0.49	r = 0.15	r = 0.41	r = 0.58	r = 0.47	r = 0.30	r = 0.31	r = 0.42	r = 0.60	r = 0.39	r = 0.47	r = 0.30
	p = 0.31	p = 0.08	p = 0.15	p = 0.68	p = 0.24	p = 0.08	p = 0.17	p = 0.40	p = 0.38	p = 0.23	p = 0.07	p = 0.26	p = 0.17	p = 0.40
Mg^{2+}	r = 0.32	r = 0.53	r = 0.49	r = 0.20	r = 0.48	r = 0.62	r = 0.50	r = 0.37	r = 0.36	r = 0.47	r = 0.62	r = 0.44	r = 0.50	r = 0.36
	p = 0.37	p = 0.12	p = 0.15	p = 0.58	p = 0.16	p = 0.05	p = 0.14	p = 0.29	p = 0.31	p = 0.17	p = 0.05	p = 0.20	p = 0.14	p = 0.31
Ca^{2+}	r = 0.28	r = 0.54	r = 0.56	r = 0.35	r = 0.61	r = 0.73	r = 0.60	r = 0.47	r = 0.48	r = 0.60	r = 0.65	r = 0.56	r = 0.65	r = 0.53
	p = 0.43	p = 0.11	p = 0.09	p = 0.33	p = 0.06	**p < 0.05**	p = 0.07	p = 0.17	p = 0.16	p = 0.07	**p < 0.05**	p = 0.09	**p < 0.05**	p = 0.12
MSA	r = 0.26	r = 0.25	r = 0.38	r = 0.44	r = 0.62	r = 0.73	r = 0.42	r = 0.52	r = 0.44	r = 0.47	r = 0.54	r = 0.45	r = 0.58	r = 0.49
	p = 0.47	p = 0.49	p = 0.28	p = 0.20	p = 0.05	**p < 0.05**	p = 0.23	p = 0.13	p = 0.20	p = 0.17	p = 0.11	p = 0.19	p = 0.08	p = 0.15
Cl^-	r = 0.41	r = 0.54	r = 0.47	r = 0.14	r = 0.42	r = 0.59	r = 0.45	r = 0.31	r = 0.30	r = 0.41	r = 0.59	r = 0.38	r = 0.45	r = 0.28
	p = 0.24	p = 0.11	p = 0.17	p = 0.70	p = 0.23	p = 0.07	p = 0.19	p = 0.38	p = 0.40	p = 0.24	p = 0.07	p = 0.28	p = 0.19	p = 0.43
Br^-	r = 0.03	r = 0.62	r = 0.67	r = 0.54	r = 0.56	**r = 0.78**	r = 0.68	r = 0.64	r = 0.61	r = 0.49	r = 0.62	r = 0.50	r = 0.67	r = 0.55
	p = 0.93	p = 0.05	**p < 0.05**	p = 0.11	p = 0.09	**p < 0.01**	**p < 0.05**	**p < 0.05**	p = 0.06	p = 0.15	p = 0.05	p = 0.14	**p < 0.05**	p = 0.10
NO_3^-	r = -0.24	**r = 0.76**	**r = 0.87**	**r = 0.79**	r = 0.66	r = 0.70	**r = 0.95**	**r = 0.82**	**r = 0.85**	r = 0.68	r = 0.62	r = 0.67	**r = 0.83**	**r = 0.78**
	p = 0.51	**p < 0.05**	**p < 0.01**	**p < 0.01**	**p < 0.05**	**p < 0.05**	**p < 0.01**	**p < 0.01**	**p < 0.01**	**p < 0.05**	p = 0.05	**p < 0.05**	**p < 0.01**	**p < 0.01**
SO_4^{2-}	r = 0.10	r = 0.61	r = 0.61	r = 0.31	r = 0.47	r = 0.58	r = 0.68	r = 0.45	r = 0.48	r = 0.48	r = 0.59	r = 0.44	r = 0.59	r = 0.47
	p = 0.78	p = 0.06	p = 0.06	p = 0.38	p = 0.17	p = 0.08	**p < 0.05**	p = 0.19	p = 0.16	p = 0.16	p = 0.07	p = 0.20	p = 0.07	p = 0.17
$nssSO4^{2-}$	r = -0.45	r = 0.24	r = 0.50	r = 0.68	r = 0.54	r = 0.38	r = 0.65	r = 0.61	r = 0.66	r = 0.50	r = 0.35	r = 0.47	r = 0.64	r = 0.72
	p = 0.19	p = 0.51	p = 0.14	**p < 0.05**	p = 0.11	p = 0.28	**p < 0.05**	p = 0.06	**p < 0.05**	p = 0.14	p = 0.33	p = 0.17	**p < 0.05**	**p < 0.05**

Table S3. Spearman correlation coefficients (r) and statistical significance (p) for correlations of PFOS, FBSA, FOSA and C_2 – C_{11} PFCAs with major ions in the Lomonosovfonna ice core. Moderate positive correlations (>0.50) and their statistically significant p-values are in bold ($p < 0.05$).

	FBSA	FOSA	PFOS	TFA	PFPrA	PFBA	PFPeA	PFHxA	PFHpA	PFOA	PFNA	PFDA	PFUnDA
K^+	r = -0.59	r = -0.17	r = -0.16	r = 0.01	**r = 0.57**	r = 0.40	r = 0.43	r = 0.30	r = -0.16	r = -0.01	r = 0.16	r = 0.23	r = 0.21
	p < 0.05	p = 0.51	p = 0.55	p = 0.96	**p < 0.05**	p = 0.11	p = 0.09	p = 0.24	p = 0.53	p = 0.96	p = 0.54	p = 0.38	p = 0.43
Mg^{2+}	**r = 0.62**	r = 0.04	r = 0.45	**r = 0.66**	r = -0.09	r = 0.07	r = 0.01	r = 0.14	r = -0.04	r = 0.19	r = -0.19	r = -0.28	r = -0.37
	p < 0.01	p = 0.88	p = 0.07	**p < 0.01**	p = 0.74	p = 0.79	p = 0.96	p = 0.59	p = 0.89	p = 0.47	p = 0.47	p = 0.27	p = 0.14
Ca^{2+}	r = -0.71	r = -0.16	r = -0.53	r = -0.59	r = 0.18	r = 0.04	r = 0.10	r = 0.02	r = -0.40	r = -0.26	r = -0.06	r = -0.06	r = 0.05
	p < 0.01	p = 0.54	p < 0.05	**p < 0.05**	p = 0.49	p = 0.87	p = 0.70	p = 0.93	p = 0.11	p = 0.31	p = 0.83	p = 0.82	p = 0.84
MSA	**r = 0.74**	r = 0.26	**r = 0.62**	**r = 0.78**	r = 0.02	r = 0.17	r = 0.10	r = 0.23	r = 0.18	r = 0.24	r = -0.12	r = -0.14	r = -0.27
	p < 0.01	p = 0.32	**p < 0.01**	**p < 0.01**	p = 0.94	p = 0.52	p = 0.71	p = 0.38	p = 0.49	p = 0.35	p = 0.65	p = 0.59	p = 0.29
Cl^-	r = 0.28	r = -0.34	r = -0.02	r = 0.23	r = -0.17	r = -0.10	r = -0.14	r = -0.04	r = -0.34	r = -0.01	r = -0.23	r = -0.37	r = -0.45
	p = 0.28	p = 0.19	p = 0.93	p = 0.37	p = 0.51	p = 0.72	p = 0.59	p = 0.87	p = 0.19	p = 0.96	p = 0.38	p = 0.15	p = 0.07
Br^-	**r = 0.55**	r = -0.13	r = 0.39	**r = 0.68**	r = -0.22	r = -0.05	r = -0.09	r = 0.06	r = 0.00	r = -0.04	r = -0.46	r = -0.49	r = -0.52
	p < 0.05	p = 0.62	p = 0.12	**p < 0.01**	p = 0.39	p = 0.86	p = 0.74	p = 0.83	p = 0.99	p = 0.89	p = 0.06	p < 0.05	p < 0.05
NO_3^-	r = -0.50	r = -0.39	r = -0.36	r = -0.10	r = 0.24	r = 0.15	r = 0.18	r = 0.10	r = -0.44	r = -0.23	r = -0.08	r = -0.08	r = -0.19
	p < 0.05	p = 0.12	p = 0.15	p = 0.69	p = 0.35	p = 0.57	p = 0.48	p = 0.71	p = 0.07	p = 0.38	p = 0.77	p = 0.76	p = 0.47
SO_4^{2-}	**r = 0.59**	r = -0.01	r = 0.26	**r = 0.56**	r = 0.01	r = 0.16	r = 0.12	r = 0.23	r = 0.00	r = 0.24	r = -0.07	r = -0.14	r = -0.33
	p < 0.05	p = 0.98	p = 0.31	**p < 0.05**	p = 0.96	p = 0.54	p = 0.65	p = 0.37	p = 1.00	p = 0.36	p = 0.79	p = 0.59	p = 0.19
$nssSO4^{2-}$	r = 0.43	r = 0.12	r = 0.25	**r = 0.51**	r = 0.14	r = 0.25	r = 0.24	r = 0.31	r = 0.03	r = 0.23	r = -0.02	r = -0.02	r = -0.22
	p = 0.08	p = 0.64	p = 0.34	**p < 0.05**	p = 0.60	p = 0.33	p = 0.36	p = 0.23	p = 0.90	p = 0.38	p = 0.95	p = 0.93	p = 0.39

Figure S1. The chemical melt proxy (log([Na^+]/[Mg^{2+}], grey points) and 3 point moving average (grey line) and effective melt layer thickness as a function of depth (cm weq).



Chapter 8

Discussion and Outlook

This chapter is a synopsis of the findings of this thesis and summarises possible avenues for future research.

8.1 Discussion and Conclusion 250
8.2 Outlook 252
8.3 References 257

8.1 Discussion and Conclusion

This thesis has four significant findings towards understanding PFAS in the Arctic. These are (i) establishing the atmospheric deposition fluxes of several PFAS in the remote European Arctic (Chapter 4), (ii) observing high seasonality in the atmospheric deposition of several PFAS and that it is likely linked to seasonal atmospheric photochemistry (Chapters 5 and 6), (iii) identifying a number of atmospheric precursors and possible precursors (Chapters 4 – 6), and (iv) finding that bromine radicals might provide a significant additional oxidant for the atmospheric degradation of precursors (Chapter 7).

From surface snow samples and a Lomonosovfonna ice core, Svalbard (Norwegian Arctic), 37 and 26 PFAS compounds were detected respectively, out of the 45 compounds targeted (Chapters 4 – 6). Alongside existing knowledge,[1] this show that PFAS contamination in the Arctic is widespread in the terrestrial cryosphere. Trifluoroacetic acid (TFA) was ubiquitously detected and was the highest concentration analyte in all samples. In the ice core the flux of TFA ranged from 290 – 8200 ng m^{-2} yr^{-1} (9.51 – 16,500 pg L^{-1}). High levels were also found at a remote site for TFA sampling in surface snow collected seasonally (January – August 2019) and its fluxes ranged from 22 – 1800 ng m^{-2} per precipitation event (7,300 – 270,000 pg L^{-1}). Indeed, TFA made up 71% and 95% of C_2 – C_{11} PFCAs in the Lomonosovfonna ice core and in surface snow from Foxfonna, respectively.

Sampling of surface snow at Foxfonna had the longest time series (January – August 2019), and the best possibility to represent a site receiving PFAS predominantly from long-range atmospheric process. No PFAS correlated with a marine aerosol proxy in surface snow from Foxfonna or the ice core from Lomonosovfonna (Chapters 5 and 6). This indicates that the long-range transport of PFAS to, and redistribution within, the Arctic by marine aerosols is insignificant.

However, snow sampling at Foxfonna showed that the deposition of many PFAS was highly seasonal. During 24-hour daylight, the median deposition fluxes of C_2 – C_{11} perfluoroalkyl carboxylic acids (PFCAs), perfluorohexane sulfonic acid (PFHxS), perfluorooctane sulfonic acid (PFOS) and hexafluoropropylene oxide dimer acid (HFPO-DA/GenX) were 2 – 38 times higher. Several of these PFAS compounds were correlated with solar radiation, which suggests that photochemistry is important to the atmospheric formation and consequential deposition of these PFAS.

Further investigations using the surface snow samples from Foxfonna and the Lomonosovfonna ice core suggested that bromine (Br) radicals were a significant additional atmospheric oxidant for the degradation of precursors in the Arctic atmosphere (Chapter 7). Br radicals are released during sea ice formation and their production is enhanced after polar sunrise during springtime in the Arctic. Br radicals are already known to be important for the input of mercury into the Arctic biosphere during atmospheric mercury depletion events (AMDEs).[2] The results from this thesis raise the possibility that a parallel mechanism for PFAS deposition might occur via 'atmospheric PFAS precursor depletion events' (APPDEs). This process could have a significant impact on the input of PFAS into Arctic ecosystem. The role of Br radicals in atmospheric precursor degradation, and the possible existence of atmospheric depletion events for PFAS (APPDEs), has not previously been considered.

The geographical extent of contamination from local sources of PFAS in Longyearbyen into surface snow in the terrestrial environment was found to be limited and Lomonosovfonna was found to predominantly receive PFAS input from long-range atmospheric processes (Chapter 6). On Lomonosovfonna, the distribution profile of PFCAs suggested that fluorotelomer alcohols (FTOHs) were the major atmospheric precursor to C_8 – C_{11} PFCAs, whereas C_2 – C_6 PFCAs had

alternative sources, such as hydrochlorofluorocarbons (HFCs) and other chlorofluorocarbon (CFC) replacement compounds (Chapter 4). High levels of TFA in the surface snow samples and ice core was attributed to the photochemical atmospheric degradation of these replacement products, indicating the impact of the Montreal Protocol on TFA levels in the environment.[3]

TFA and PFOS were found to correlate in the Lomonosovfonna ice core (Chapter 4). In addition, PFOS deposition in surface snow was found to correlate with solar radiation (Chapter 6). Together these observations provide some of the first empirically derived evidence for the photochemically dependent atmospheric formation of PFOS, but this thesis has been unable to chemically identify a precursor(s). Only one study has previously reported the radical-mediated formation of a PFSA from a precursor compound in a laboratory experiment.[4]

This thesis was unable to report trifluoromethane sulfonic acid (TFMS) levels in the Lomonosovfonna ice core due to contamination introduced during processing of the core (Chapter 4). In surface snow on Svalbard, TFMS was found to be ubiquitous, including on Lomonosovfonna and other high elevation remote glaciers (Chapter 5). However, this thesis has been unable to identify a source of this compound. HFPO-DA (GenX) was not detected in the ice core, but its detection was widespread in surface snow including at remote locations. Since its deposition correlated with solar radiation, this suggests that its formation is also dependent on the photochemical degradation of precursors in the atmosphere (Chapter 5). Nonetheless, a precursor could not be identified.

8.2 Outlook

In summary, future studies should aim to: (i) use new analytical techniques to understand the PFAS composition of the samples used in this thesis, (ii) look to retrieve and analyse ice core records at

new locations, (iii) undertake detailed atmospheric measurements to further confirm the presence of APPDEs in the Arctic atmosphere, (iv) undertake laboratory experiments to investigate APPDEs and the degradation of previously unconsidered precursors, (v) investigate further the atmospheric sources of TFMS and the precursors of PFOS and HFPO-DA (GenX) and, (vi) map out the extent of post-1930 glacier accumulation on Svalbard and elsewhere to assess the hazard posed by melting of this reservoir of PFAS from the terrestrial cryosphere. These suggestions for future work are here discussed in more detail.

Owing to the numerous PFAS that exist (see Chapter 1, section 1.2.1), it is unrealistic to use target methods to quantify them all individually (for example using mass spectrometry as this thesis has done). To overcome this, other methods can be used to quantify the total mass of all organofluorine in the samples. One such method is combustion ion chromatography (CIC).[5] This method combusts all extractable organofluorine (EOF), and converts it to fluoride to be measured by ion chromatography. Hence, a total mass of EOF per unit volume of melted snow/ice could be established. This could then be used to calculate the mass of EOF which has not been identified by targeted methods (for example, by using mass spectrometry). One study that used CIC found that in surface water, sediment and fish liver samples from a Norwegian lake and river, 84 – 99% of the EOF could not be assigned to the 37 targeted PFAS.[5] This demonstrates that a large proportion of the organofluorine in the environment is not being quantified by the current target methods.

Despite the high levels of TFA observed in snow and glacier ice in this thesis (Chapters 4 – 6), there has been limited research in the past 2 decades into the toxicology of TFA and other ultrashort perfluoroalkyl acids (C_1 – C_3 PFAAs).[6,7] For TFA, relatively high levels are thought to be safe, and their high polarity means that their ability to bioaccumulate is low. However, owing

to TFA's high environmental persistence and the high levels observed in precipitation (Chapters 4 – 6), it will likely accumulate in the aquatic environment. Hence, human exposure to high levels of TFA can be through drinking water. Future research needs to identify the safe levels of TFA (and ultrashort chain PFAAs) in drinking water for human consumption.

As consumer and industry requirements develop, and regulations on certain PFAS compounds come into force, new PFAS compounds are developed by industry. For example, GenX (HFPO-DA) was developed by DuPont in 2009 as an alternative to perfluorooctanoic acid (PFOA).[8] This thesis has been one of the first studies to report HFPO-DA in the remote Arctic environment.[9] Future studies should aim to keep up to date in the analysis of emerging PFAS compounds which have been recently developed by industry. In addition, owing to the range of CFC replacement products that exist, perfluorodicarboxylic acids ($HO_2C(CF)_nCO_2H$) could be considered for inclusion in targeted methods.

The results from this thesis have suggested that bromine radicals play a key role in the atmospheric degradation of precursors and the deposition of PFAS in the Arctic. The possibility for the existence of APPDEs needs to be investigated further by atmospheric sampling during Arctic springtime. This sampling would need to be highly resolved with respect to time and include all the relevant atmospheric species, such as BrO, precursors and degradation products i.e. PFAAs. The detection of AMDEs and ozone depletion events (ODEs) for mercury and ozone has relied on observing atmospheric depletion of gaseous elemental mercury and ozone on a precise time resolution of typically hours. However, existing atmospheric PFAS measurements rely on high volume air sampling which currently requires a single measurement to span approximately 1 week of air sampling.[10] Alternatively, daily snow sampling at, for example Foxfonna, could be used, alongside BrO atmospheric measurements to directly observed APPDEs. In addition, simulated

atmospheric conditions in laboratory-based experiments could be used to investigate APPDEs. This could be done by artificially recreating known atmospheric conditions for bromine during AMDEs, and observing the degradation products of precursors during these conditions.

This thesis could not identify the source of TFMS. To assist in this, future studies might attempt to separate the analysis of snow and glacier ice into particle bound and non-particle bound components to aid source elucidation. The ubiquitous detection of TFMS and high levels of TFA in the remote Arctic also merit themselves for inclusion as part of long-term atmospheric monitoring at the Zeppelin Observatory on Svalbard.

The widespread presence of PFAS in snow and glacier ice in the Arctic means that a large reservoir of ice containing PFAS contamination has been accumulating since around 1930. As the Arctic climate warms,[11] this ice will be more readily melt from glacier ablation surfaces. State of the art radiocarbon dating of ice,[12] could be used to map out the extent of post-1930 glacier ice on modern day ablation surfaces. This information could then be used to assess the potential hazard posed to downstream fjord and freshwater Arctic ecosystems, as this reservoir of contaminants melts with climate change. This secondary source could then provide a potentially important PFAS input to the Arctic biosphere.

Despite increasing mass loss from glaciers worldwide,[13] future ice cores could be used for monitoring the effectiveness of international regulations of PFAS (e.g. Stockholm Convention). This thesis has shown that ice cores provide an effective tool for understanding historical PFAS deposition and understanding PFAS atmospheric processes (Chapters 2 and 4). As such, new ice cores from sites with well-preserved records, should aim to establish the fluxes of PFAS deposition in other parts of the Arctic also (e.g., Alaska, Greenland, Franz Josef Land or Severnaya Zemlya) for a broader circum-Arctic monitoring overview. In addition, new ice core records from high

elevation sites in the Andes, New Zealand and Antarctica should be used to establish a baseline for the Southern Hemisphere. These new records should then be inspected to see if the onset of certain PFAS regulations have been effective in reducing the atmospheric deposition.

On 15th June 2022, the United States Environmental Protection Agency (EPA) released new drinking water health advisories for four PFAS: PFOA, PFOS, HFPO-DA (GenX) and perfluorobutane sulfonic acid (PFBS).[14] Whilst these advisories are non-regulatory, these levels were identified to protect human health. Previously, PFOA and PFOS had drinking water health advisories levels of 70 ng/L. However, these were recently revised to 4 pg/L for PFOA and 30 pg/L for PFOS. Advisories for PFBS (2000 ng/L) and HFPO-DA (10 ng/L) were also released. All snow and ice core samples in this thesis had concentrations significantly less than the health advisories for PFBS and HFPO-DA. However, concentrations of PFOA in the remote Lomonosovfonna ice core were consistently above the EPA drinking water health advisory (39.8 – 112 pg/L). In addition, for those subsections of the Lomonosovfonna ice core with detectable PFOS, these were similar to the EPA drinking water health advisory level (32.9 pg/L on average). The long-range atmospheric processes for the deposition of PFAS discussed in this thesis, will also occur outside of the Arctic. These processes will contribute, alongside several other mechanisms, towards PFAS contamination in drinking water globally. Clearly extensive regulation would be required by the Stockholm Convention, to bring global drinking water in line with the most recent EPA health advisories. Nonetheless, research, such as that presented in this thesis, is required to understand the processes of organic contaminants in the environment. This understanding ultimately contributes towards a wider body of evidence which informs the international regulation of organic contaminants through the Stockholm Convention.

8.3 References

1. Young, C. J. *et al.* Perfluorinated Acids in Arctic Snow: New Evidence for Atmospheric Formation. *Environ. Sci. Technol.* **41**, 3455–3461 (2007).
2. Schroeder, W. H. *et al.* Arctic springtime depletion of mercury. *Nature* **394**, 331–332 (1998).
3. Velders, G. J. M., Andersen, S. O., Daniel, J. S., Fahey, D. W. & McFarland, M. The importance of the Montreal Protocol in protecting climate. *Proc. Natl. Acad. Sci. U. S. A.* **104**, 4814–4819 (2007).
4. D'eon, J. C., Hurley, M. D., Wallington, T. J. & Mabury, S. A. Atmospheric chemistry of N-methyl perfluorobutane sulfonamidoethanol, C4F9SO2N(CH3)CH2CH2OH: kinetics and mechanism of reaction with OH. *Environ. Sci. Technol.* **40**, 1862–8 (2006).
5. Aro, R., Carlsson, P., Vogelsang, C., Kärrman, A. & Yeung, L. W. Fluorine mass balance analysis of selected environmental samples from Norway. *Chemosphere* **283**, 131200 (2021).
6. Berends, A. G., Boutonnet, J. C., De Rooij, C. G. & Thompson, R. S. Toxicity of trifluoroacetate to aquatic organisms. *Environ. Toxicol. Chem.* **18**, 1053–1059 (1999).
7. Boutonnet, J. C. *et al.* Environmental Risk Assessment of Trifluoroacetic Acid. *Hum. Ecol. Risk Assess.* **5**, 59–124 (1999).
8. Hogue, C. What's GenX still doing in the water downstream of a Chemours plant? *Chemical and Engineering News* vol. 96 (2018).
9. Joerss, H. *et al.* Transport of Legacy Perfluoroalkyl Substances and the Replacement Compound HFPO-DA through the Atlantic Gateway to the Arctic Ocean - Is the Arctic a Sink or a Source? *Environ. Sci. Technol.* **54**, 9958–9967 (2020).
10. Wong, F. *et al.* Assessing temporal trends and source regions of per- and polyfluoroalkyl substances (PFASs) in air under the Arctic Monitoring and Assessment Programme (AMAP). *Atmos. Environ.* **172**, 65–73 (2018).
11. Isaksen, K. *et al.* Exceptional warming over the Barents area. *Sci. Reports 2022 121* **12**, 1–18 (2022).
12. Fang, L., Jenk, T. M., Singer, T., Hou, S. & Schwikowski, M. Radiocarbon dating of alpine ice cores with the dissolved organic carbon (DOC) fraction. *Cryosphere* **15**, 1537–1550 (2021).
13. Zemp, M., Hoelzle, M. & Haeberli, W. Six decades of glacier mass-balance observations: a review of the worldwide monitoring network. *Ann. Glaciol.* **50**, 101–111 (2009).
14. U.S. EPA. *Drinking Water Health Advisories for PFAS Fact Sheet for Communities - June 2022*. (2022).